



2013

# BIOSYNTHETIC PATHWAY OF THE AMINORIBOSYL COMPONENT OF LIPOPEPTIDYL NUCLEOSIDE ANTIBIOTICS

Xiuling Chi

University of Kentucky, xchi22@gmail.com

**[Click here to let us know how access to this document benefits you.](#)**

---

## Recommended Citation

Chi, Xiuling, "BIOSYNTHETIC PATHWAY OF THE AMINORIBOSYL COMPONENT OF LIPOPEPTIDYL NUCLEOSIDE ANTIBIOTICS" (2013). *Theses and Dissertations--Pharmacy*. 23.  
[https://uknowledge.uky.edu/pharmacy\\_etds/23](https://uknowledge.uky.edu/pharmacy_etds/23)

This Doctoral Dissertation is brought to you for free and open access by the College of Pharmacy at UKnowledge. It has been accepted for inclusion in Theses and Dissertations--Pharmacy by an authorized administrator of UKnowledge. For more information, please contact [UKnowledge@lsv.uky.edu](mailto:UKnowledge@lsv.uky.edu).

**STUDENT AGREEMENT:**

I represent that my thesis or dissertation and abstract are my original work. Proper attribution has been given to all outside sources. I understand that I am solely responsible for obtaining any needed copyright permissions. I have obtained and attached hereto needed written permission statements(s) from the owner(s) of each third-party copyrighted matter to be included in my work, allowing electronic distribution (if such use is not permitted by the fair use doctrine).

I hereby grant to The University of Kentucky and its agents the non-exclusive license to archive and make accessible my work in whole or in part in all forms of media, now or hereafter known. I agree that the document mentioned above may be made available immediately for worldwide access unless a preapproved embargo applies.

I retain all other ownership rights to the copyright of my work. I also retain the right to use in future works (such as articles or books) all or part of my work. I understand that I am free to register the copyright to my work.

**REVIEW, APPROVAL AND ACCEPTANCE**

The document mentioned above has been reviewed and accepted by the student's advisor, on behalf of the advisory committee, and by the Director of Graduate Studies (DGS), on behalf of the program; we verify that this is the final, approved version of the student's dissertation including all changes required by the advisory committee. The undersigned agree to abide by the statements above.

Xiuling Chi, Student

Dr. Steven Van Lanen, Major Professor

Dr. Jim Pauly, Director of Graduate Studies

---

BIOSYNTHETIC PATHWAY OF THE AMINORIBOSYL COMPONENT OF  
LIPOPEPTIDYL NUCLEOSIDE ANTIBIOTICS

---

DISSERTATION

---

A dissertation submitted in partial fulfillment of the  
requirements for the degree of Doctor of Philosophy in the  
College of Pharmacy  
at the University of Kentucky

By  
Xiuling Chi

Lexington, Kentucky

Director: Dr. Steven Van Lanen, Professor of Pharmaceutical Science

Lexington, Kentucky

2013

Copyright © Xiuling Chi 2013

## ABSTRACT OF DISSERTATION

### BIOSYNTHETIC PATHWAY OF THE AMINORIBOSYL COMPONENT OF LIPOPEPTIDYL NUCLEOSIDE ANTIBIOTICS

Several lipopeptidyl nucleoside antibiotics that inhibit bacterial translocase I (MraY) involved in peptidoglycan cell wall biosynthesis contain an aminoribosyl moiety, an unusual sugar appendage in natural products. A-90289 and muraminomicin are the two representative antibiotics that belong to this family. Bioinformatic analysis of the biosynthetic A-90289 gene clusters revealed that five enzymes are likely involved in the assembly and attachment of the aminoribosyl unit. These enzymes of A-90289 are functionally assigned by *in vitro* characterization. The results reveal a unique ribosylation pathway that highlighted by uridine-5'-monophosphate as the source of the sugar, a phosphorylase strategy to generate a sugar-1-phosphate, and a primary amine-requiring nucleotidyltransferase that generates the NDP-sugar donor. Muraminomicin, which has a structure similar to A-90289, holds the distinction in that both ribose units are 2-deoxy sugars. The biosynthetic gene cluster of muraminomicin has been identified, cloned and sequenced, and bioinformatic analysis revealed a minimum of 24 open reading frames putatively involved in the biosynthesis, resistance, and regulation of muraminomicin. Similar to the A-90289 pathway, five enzymes are still likely involved in the assembly of the 2,5-dideoxy-5-aminoribose saccharide unit, and two are now functionally assigned and characterized: Mra20, a 5'-amino-2',5'-dideoxyuridine phosphorylase and Mra23, a UTP:5-amino-2,5-dideoxy- $\alpha$ -D-ribose-1-phosphate uridylyltransferase. The cumulative results are consistent with the incorporation of the ribosyl appendage of muraminomicin via the archetypical sugar biosynthetic pathway that parallels A-90289 biosynthesis.

**KEYWORDS:** Aminoribosyl unit, lipopeptidyl nucleoside antibiotics, peptidoglycan cell wall, biosynthetic gene cluster, ORF enzymes

XIULING CHI

Student's Signature

06.11.2013

Date

BIOSYNTHETIC PATHWAY OF THE AMINORIBOSYL COMPONENT OF  
LIPOPEPTIDYL NUCLEOSIDE ANTIBIOTICS

By

Xiuling Chi

Steven Van Lanen

---

Director of Dissertation

Jim Pauly

---

Director of Graduate Studies

06.11.2013

---

## ACKNOWLEDGMENTS

By completing this dissertation, I would like to express my sincere gratitude to my mentor, Dr. Steven Van Lanen, for his guidance, advice, inspiration and support throughout these several years. My special thanks for his always valuable knowledge, suggestions and wonderful ideas to help improve my natural product biosynthesis study and research. I am also thankful for my other committee members Dr. Jurgen Rohr, Dr. Chang-Guo Zhan, Dr. KyungBo Kim and Dr. Aardra Kachroo for their constantly support and helpful comments. I would like to thank Dr. Koichi Nonaka and Sankyo Co. Ltd. for supplying us with valuable strains, compounds as well as preliminary experiment results. Also, I would like to thank Dr. Pallab Pahari, Dr. Zhaoyong Yang, Dr. Nidhi Tibrewal, Dr. Madan K. Kharel, Dr. Guojun Wang and all the Van Lanen laboratory members for their help with research and suggestions. Last but not least, I would like to thank my family for their forever support to my career.

## TABLE OF CONTENTS

ACKNOWLEDGMENTS .....	iii
TABLE OF CONTENTS.....	iv
LIST OF TABLES .....	viii
LIST OF FIGURES .....	ix
LIST OF ABBREVIATIONS.....	xiii
Chapter one: Introduction .....	1
1.1. Significance of natural products .....	1
1.2. Discovery of new antibiotics.....	1
1.3. Biosynthesis of peptidoglycan cell wall.....	3
1.4. MraY - Translocase I .....	5
1.5. MraY – Translocase I Inhibitors.....	9
1.6. Glycosidic residues play a critical role in biological function of antibiotics ..	12
1.7. Traditional strategy for ribose and glucose incorporation into compounds..	13
Chapter two: Biosynthetic pathway of aminoribosyl moiety of A-90289.....	17
2.1. Background .....	17
2.2. Materials and methods.....	21
2.2.1. Chemicals and Reagents .....	21
2.2.2. Instrumentation .....	22
2.2.3. Bacterial Strains and Enzymes.....	23
2.2.4. Synthesis of uridine-5'-aldehyde, 1.....	23
2.2.5. Synthesis of 5'-amino-5'-deoxyuridine, 2 .....	25
2.2.6. Synthesis of 5'-amino-2',5'-dideoxyuridine, 7 .....	29
2.2.7. Cloning of genes for heterologous expression.....	31
2.2.8. <i>In vitro</i> characterization of LipP .....	33
2.2.9. Subcloning and expression in <i>S. lividans</i> TK-64 .....	34
2.2.10. <i>In vitro</i> characterization of LipM.....	35
2.2.11. OPA-modification and analysis of the LipM product .....	35
2.2.12. Production of the LipM product for mass and NMR spectroscopy...	36



2.2.13. <i>In vitro</i> characterization of LipO activity .....	37
2.2.14. Site-directed mutagenesis of LipO.....	37
2.2.15. <i>In vitro</i> characterization of LipN activity .....	38
2.2.16. Production of the LipN product for mass and NMR spectroscopy ...	38
2.3. Results: LipP Characterization .....	39
2.3.1. <i>In vitro</i> characterization of LipP activity.....	39
2.3.2. Kinetics characterization of LipP .....	42
2.3.3. <i>In vitro</i> characterization of <i>EcUdp</i> activity .....	44
2.3.4. Kinetics characterization of <i>EcUdp</i> .....	45
2.4. Results: LipM Characterization .....	46
2.4.1. <i>In vitro</i> characterization of LipM activity .....	46
2.4.2. <i>In vitro</i> characterization of OPA modified 5'-amino-5'-deoxyuridine (2) catalyzed by LipM .....	49
2.4.3. <i>In vitro</i> characterization of substrate 5'-amino-2',5'-dideoxyuridine (7) catalyzed by LipM .....	56
2.5. Results: LipO Characterization .....	63
2.5.1. <i>In vitro</i> characterization of LipO wild-type and mutant protein.....	63
2.5.2. LipO activity analyzed by HPLC and conversion efficiency with different amino donors .....	65
2.6. Results: LipN Characterization.....	68
2.6.1. <i>In vitro</i> characterization of LipN activity .....	68
2.7. Conclusion.....	77
2.8. Discussion .....	77
Chapter three: Biosynthetic pathway of 2'-deoxyaminoribosyl moiety of muraminomicin .....	81
3.1 Background .....	81
3.2. Materials and methods.....	83
3.2.1. Chemicals and instrumentation .....	83
3.2.2. Synthesis of substrates .....	83
3.2.3. Cloning of the muraminomicin gene cluster .....	85

3.2.4. Construction of genomic cosmid libraries .....	86
3.2.5. Inactivation of <i>mra20</i> gene by PCR targeting .....	86
3.2.6. Cloning of genes for heterologous expression.....	87
3.2.7. <i>In vitro</i> characterization of Mra20 .....	89
3.2.8. <i>In vitro</i> characterization of Mra23 .....	90
3.2.9. Subcloning and expression in <i>S. lividans</i> TK-64 .....	90
3.2.10. <i>In vitro</i> characterization of Mra21 .....	90
3.2.11. <i>In vitro</i> characterization of Mra22.....	91
3.2.12. <i>In vitro</i> characterization of Mra24 .....	91
3.3. Results: Identification of muraminomicin gene cluster .....	91
3.4. Results: Functional assignment of Mra20 as a low specificity pyrimidine nucleoside phosphorylase .....	97
3.4.1 <i>In vitro</i> characterization of Mra20 activity.....	97
3.4.2. Kinetics characterization of Mra20.....	99
3.5. Results: Bifunctional assignment of Mra20 as a potential nucleoside phosphorylase and cytidine deaminase. ....	101
3.5.1 <i>In vitro</i> characterization of Mra20 deaminase activity .....	101
3.5.2. Replacement of O <sup>16</sup> with O <sup>18</sup> in Mra20-catalyzed cytidine reaction .	104
3.6. Results: Functional assignment of Mra23 as a primary amine-requiring Nucleotidyltransferase.....	106
3.7. Results: <i>In vitro</i> characterization of Mra21 activity .....	111
3.8. Results: <i>In vitro</i> characterization of Mra22 activity .....	112
3.9. Results: <i>In vitro</i> characterization of Mra24 activity .....	116
3.9.1. <i>In vitro</i> characterization of Mra24 activity.....	116
3.9.2. Blast and alignment Mra24 with other dioxygenases .....	119
3.9.3. <i>Streptosporangium amethystogenes</i> genomic gene library construction .....	120
3.10. Development of a genetic system for <i>in vivo</i> muraminomicin studies .....	121
3.11. Conclusion .....	123
Chapter four: Summary .....	124

Bibliography .....	125
Vita .....	134

## LIST OF TABLES

Table 1. List of primers used in A-90289.....	33
Table 2. List of plasmids constructed/used in A-90289... ..	34
Table 3. Extracted kinetic constants for LipP and <i>EcUdp</i> .....	44
Table 4. Amino donor substrates for LipO .....	67
Table 5. List of primers used in muraminomicin.....	88
Table 6. List of plasmids constructed/used in muraminomicin .....	89
Table 7. Annotation of ORFs within the muraminomicin gene cluster.....	93
Table 8. Extracted kinetic constants for Mra20.....	100
Table 9. Growth mediums for <i>Streptosporangium</i> sp. SANK 60709.....	122

## LIST OF FIGURES

Figure 1.1. Structure of peptidoglycan .....	3
Figure 1.2. Biosynthesis of bacterial peptidoglycan cell wall mediated by twelve conserved enzymes .....	5
Figure 1.3. Reaction catalyzed by MraY.....	6
Figure 1.4. MraY structure and active site model .....	8
Figure 1.5. Inhibitors of MraY.....	10
Figure 1.6. Structure of representative lipopeptidyl nucleoside antibiotics containing an aminoribosyl moiety.....	11
Figure 1.7. Structure of vancomycin and bleomycin.....	13
Figure 1.8. Traditional strategies for glucose incorporation into a compound.....	14
Figure 1.9. Traditional strategies for ribose incorporation into a compound.....	15
Figure 1.10. Examples of incorporation of pentose units into acceptor molecules using 5-phospho- $\alpha$ -D-ribose-1-diphosphate (PRPP).....	15
Figure 2.1. <i>Streptomyces</i> sp. SANK 60405 wild-type and structure.....	18
Figure 2.2. The A-90289 biosynthetic gene cluster.....	18
Figure 2.3. Proposed biosynthetic pathway for the incorporation of the aminoribosyl moiety of A-90289.....	20
Figure 2.4. Proposed biosynthetic pathway for the incorporation of the aminoribosyl moiety of A-90289.....	39
Figure 2.5. Phosphorylase reaction catalyzed by LipP .....	40
Figure 2.6. SDS-PAGE analysis of purified His <sub>6</sub> - LipP .....	41
Figure 2.7. Characterization of LipP by HPLC.....	41
Figure 2.8. LC-MS analysis of the phosphorylase reaction.....	42
Figure 2.9. Kinetic characterization of LipP .....	43
Figure 2.10. In vitro characterization of EcUdp with hypothetical intermediates.....	45
Figure 2.11. Kinetics analysis of EcUdp.....	46
Figure 2.12. Proposed biosynthetic pathway for the incorporation of the aminoribosyl moiety of A-90289.....	47

Figure 2.13. Reaction catalyzed by LipM including in situ generation of the substrate and amine derivatization with <i>o</i> -phthalaldehyde (OPA).....	47
Figure 2.14. Characterization of LipM .....	48
Figure 2.15. In vitro characterization of LipM with alternative NTPs.....	49
Figure 2.16. OPA-modified substrate reaction catalyzed by HPLC.....	50
Figure 2.17. LC-MS analysis of the OPA-modified LipM product.....	51
Figure 2.18. Characterization of 5'-isoindolinine-5'-deoxy- $\alpha$ -D-ribose-1',2'-cyclic phosphate by 1D NMR.....	52
Figure 2.19. gCOSY NMR spectrum of 5'-isoindolinine-5'-deoxy- $\alpha$ -D-ribose-1',2'-cyclic phosphate.....	53
Figure 2.20. gHSQC NMR spectrum of 5'-isoindolinine-5'-deoxy- $\alpha$ -D-ribose-1',2'-cyclic phosphate.....	54
Figure 2.21. $^1\text{H}$ - $^{13}\text{C}$ gHMBC NMR spectrum of 5'-isoindolinine-5'-deoxy- $\alpha$ -D-ribose-1',2'-cyclicphosphate.....	55
Figure 2.22. $^1\text{H}$ - $^{31}\text{P}$ HMBC NMR spectrum of 5'-isoindolinine-5'-deoxy- $\alpha$ -D-ribose-1',2'- cyclicphosphate.....	56
Figure 2.23. HPLC and Kinetic analysis of LipP with 2'-deoxynucleosides.....	57
Figure 2.24. Characterization of LipM with substrate 5'-amino-2',5'-dideoxyuridine( <b>7</b> ) .....	58
Figure 2.25. LC-MS of the LipM product UDP-5''-amino-2'',5''-dideoxyribose ( <b>8</b> ) generated from surrogate substrate 5'-amino-2',5'-dideoxyuridine( <b>7</b> ).....	59
Figure 2.26. Characterization of UDP-5''-amino-2'',5''-dideoxyribose ( <b>8</b> ) by 1D NMR.....	60
Figure 2.27. gCOSY NMR spectrum of UDP-5''-amino-2'',5''-dideoxyribose ( <b>8</b> ).....	61
Figure 2.28. gHSQC NMR spectrum of UDP-5''-amino-2'',5''-dideoxyribose ( <b>8</b> ).....	62
Figure 2.29. Proposed biosynthetic pathway for the incorporation of the aminoribosyl moiety of A-90289.....	63
Figure 2.30. Putative biosynthesis of enamide-containing nucleoside antibiotics....	64
Figure 2.31 LipO wild-type and mutant protein expression and UV/Vis spectrum analysis.....	65

Figure 2.32. HPLC characterization of LipO .....	66
Figure 2.33. Proposed biosynthetic pathway for the incorporation of the aminoribosyl moiety of A-90289.....	68
Figure 2.34. LipN protein gel and HPLC analysis the degradation of UDP-5''-amino-2'',5''-dideoxyribose ( <b>8</b> ).....	69
Figure 2.35. <i>In vitro</i> characterization of LipN with substrate 5'-amino-5'-deoxyuridine ( <b>2</b> ).....	70
Figure 2.36. <i>In vitro</i> characterization of LipN with substrate 5'-amino-2',5'-dideoxy uridine( <b>7</b> ).....	71
Figure 2.37. LC-MS of the LipN product 5'-O-(5''-amino-5''-deoxy- $\beta$ -D-ribose)-uridine ( <b>9</b> ) starting form 5'-amino-5'-deoxyuridine ( <b>2</b> ) as the ultimate sugar donor and uridine ( <b>3</b> ) as a surrogate acceptor. ....	72
Figure 2.38. Characterization of 5'-O-(5''-amino-5''-deoxy- $\beta$ -D-ribose)-uridine ( <b>9</b> ) by 1D NMR.....	73
Figure 2.39. gCOSY NMR spectrum of 5'-O-(5''-amino-5''-deoxy- $\beta$ -D-ribose)-uridine ( <b>9</b> ).....	74
Figure 2.40. gHSQC NMR spectrum of 5'-O-(5''-amino-5''-deoxy- $\beta$ -D-ribose)-uridine ( <b>9</b> ).....	75
Figure 2.41. $^1\text{H}$ - $^{13}\text{C}$ gHMBC NMR spectrum of 5'-O-(5''-amino-5''-deoxy- $\beta$ -D-ribose)-uridine ( <b>9</b> ).....	76
Figure 2.42. Finalized biosynthetic pathway for the incorporation of the aminoribosyl moiety of A-90289.....	77
Figure 2.43. The conventional glycosylation mechanism with an NDP-sugar as the sugar donor.....	80
Figure 3.1. Structures of representative lipopeptidyl nucleoside antibiotics containing an aminoribofuranoside appendage (blue).....	82
Figure 3.2. Genetic architecture of the muraminomicin gene cluster.....	93
Figure 3.3. Resistance conferred by pMra02 upon heterologous expression in <i>Streptomyces lividans</i> TK21.....	96
Figure 3.4. <i>In vitro</i> characterization of Mra20.....	98

Figure 3.5. Activity of Mra20 with 2'-deoxynucleosides.....	98
Figure 3.6. Single-substrate kinetic analysis of Mra20.....	100
Figure 3.7. Proposed phosphorolysis reaction with cytidine catalyzed by Mra20...	101
Figure 3.8. Activity of Mra20 with cytidine.....	102
Figure 3.9. LC-MS of the Mra20 product with cytidine.....	103
Figure 3.10. Characterization product of Mra20-catalyzed cytidine reaction by 1D NMR.....	104
Figure 3.11. Characterization of Mra20-catalyzed reaction using O <sup>18</sup> .....	105
Figure 3.12. Characterization of NH <sub>3</sub> production.....	106
Figure 3.13. <i>In vitro</i> characterization of Mra23 with thymidine ( <b>12</b> ).....	108
Figure 3.14. Characterization of Mra23 with 5'-amino-5'-deoxythymidine ( <b>10</b> ).....	108
Figure 3.15. LC-MS of the Mra23 product UDP-5"-amino-2",5"-dideoxyribose ( <b>8</b> ) generated from substrate 5'-amino-5'-deoxythymidine ( <b>10</b> ).....	109
Figure 3.16. Proposed biosynthetic pathway of the disaccharide core of the muraminomicin.....	110
Figure 3.17. Proposed reaction catalyzed by Mra21.....	111
Figure 3.18. Characterization of Mra21.....	112
Figure 3.19. Proposed reaction catalyzed by Mra22.....	113
Figure 3.20. Characterization of Mra22.....	114
Figure 3.21. HPLC characterization of Mra22.....	115
Figure 3.22. Proposed reaction catalyzed by Mra24.....	117
Figure 3.23. Characterization of Mra24 with 2'-deoxyUMP.....	118
Figure 3.24. Characterization of Mra24 with UMP.....	119
Figure 3.25. Alignment Mra24 with similar dioxygenases from other strains.....	120
Figure 3.26. Colony Hybridization of <i>Streptosporangiummethystogenes</i> genomic gene library using dioxygenase gene probes.....	121
Figure 3.27. <i>Streptosporangium</i> sp. SANK 60709 strain.....	123



## LIST OF ABBREVIATIONS

amp	ampicillin
apr	apramycin
ATP	adenosine triphosphate
Asp	Aspartic acid
Asn	Asparagine
<i>B. Subtilis</i>	<i>Bacillus subtilis</i>
BLAST	basic local alignment search tool
bp	base pairs
CIP	calf intestinal phosphatase
CMP	cytidine monophosphate
COSY	correlation spectroscopy
CTP	cytidine triphosphate
DAP	diaminopimelic acid
DIG	digoxigenin
DNA	deoxyribonucleic acid
2D-NMR	two-dimensional nuclear magnetic resonance spectroscopy
DMF	dimethylformamide
DMSO	dimethylsulfoxide
EDTA	ethylenediaminetetraacetic acid
<i>E. coli</i>	<i>Escherichia coli</i>
FRT	flippase recognition target
GDP	guanosine diphosphate
GlcNAc	<i>N</i> -acetylglucosamine
GLDH	glutamate dehydrogenase
GMP	guanosine monophosphate
GTP	guanosine triphosphate
hr	hour
His <sub>6</sub>	hexahistidine

HMBC heteronuclear multiple-bond correlation spectroscopy  
 HPLC high performance liquid chromatography  
 HSQC heteronuclear single-quantum correlation spectroscopy  
 IPTG isopropyl- $\beta$ -D-thiogalactopyranoside  
 k kilo  
 Kan kanamycin  
 kb kilo base pairs  
 $k_{\text{cat}}$  turnover rate  
 kDa kilo Dalton  
 $\alpha$ -KG  $\alpha$ -ketoglutarate  
 $K_i$  inhibition constant  
 $K_m$  Michaelis-Menten constant  
 LB Luria broth  
 LC-MS Liquid chromatography–mass spectrometry  
 Lys Lysine  
 MDR multiple drug resistant  
 min minute  
 MraY phospho-MurNAc-pentapeptide translocase  
 MRSA Methicillin-resistant *Staphylococcus aureus*  
 MurNAc *N*-acetylmuramic acid  
 MW molecular weight  
 NADP<sup>+</sup> nicotinamide adenine dinucleotide phosphate  
 NADPH reduced form of NADP<sup>+</sup>  
 nm nanometer  
 NME new molecular entities  
 NMP monophosphate  
 NMR nuclear magnetic resonance spectroscopy  
 NTP nucleoside triphosphate  
 NDP nucleoside diphosphate  
 OD optical density

OPA o-phthalaldehyde  
 ORF open reading fram  
 PAGE polyacrylamide gel electrophoresis  
 PBPs penicillin binding proteins  
 PCR polymerase chain reaction  
 PEG polyethylene glycol  
 PEP phosphoenolpyruvic acid or phosphoenolpyruvate  
 PLP pyridoxal-phosphate  
 PRPP synthetase phosphoribosylpyrophosphate synthetase  
 RNA ribonucleic acid  
*S. aureus* *Staphylococcus aureus*  
*S. lividans* *Streptomyces. lividans*  
 sec second  
 SHMT Serine hydroxymethyltransferase  
 SDS sodium dodecyl sulfate  
 SDS-PAGE sodium dodecyl sulfate polyacrylamide gel electrophoresis  
 sp. Species  
*sp.* *Streptomyces*  
*TB* *tuberculosis*  
 TCA trichloroacetic acid  
 TMP thymidine monophosphate  
 TTP thymidine triphosphate  
 Udp uridine phosphorylases  
 UDP uridine-5'-diphosphate  
 UDP-GlcNAc5-diphospho-*N*-acetylglucosamine  
 UDP-MurNAcUDP-*N*-acetylmuramic acid  
 UMP uridine monophosphate  
 UTP uridine-5'-triphosphate  
 UV/Vis ultraviolet/visible

## **Chapter one: Introduction**

### **1.1. Significance of natural products**

The use of natural products has been the single most successful strategy in the discovery of novel medicines [1,2]. Not only have numerous medical breakthroughs been achieved based on compounds of natural origin, natural product compounds also represent a large share of the market [3]. The primary reasons why natural products have been always important for the pharmaceutical industry is: the ability to continue to inspire synthetic and analytical chemists [4,5]; remaining a major source of human medicines [6]; leading to important biological insights [7,8] and potentiality of many more natural products to discover [9,10,11]. Although the discovery of new natural products has been in decline over the past two decades, natural products still play an highly predominant role as sources of new drugs from 1981 to 2010 [12].

In general, among all drugs, almost half of new molecular entities in last 30 years were inspired from natural products, including the natural product itself, semi-synthetic modifications and pharmacophore-based synthesis [12]. Meanwhile, the other half of new molecular entities were from synthetic origin. As for the drugs to kill different kinds of bacteria, over 75% of antibacterial compounds were derived from natural products [12]. Therefore, based on the overview of the reported data hitherto, it turns out natural products play an even more crucial role to fight against infectious diseases.

### **1.2. Discovery of new antibiotics**

Although antibiotics have revolutionized medicine, new antibiotics have been in constant need over the past 70 years [13]. Many infectious and parasitic diseases have emerged and re-emerged with the worldwide environmental change and

migration. Therefore, a rapidly increasing death rate has been realized due to infectious bacterial diseases, which has also been correlated with the occurrence of multiple drug resistant (MDR) pathogens. MDR pathogens have become a critical public health problem in both hospital and community settings [14]. Almost 2 million Americans per year develop hospital-acquired Methicillin-resistant *Staphylococcus aureus* (MRSA) infections in the United States, resulting in ~16,000 annually. In total, nearly 100,000 deaths per year are due to infections disease, the majority of which are due to MDR pathogens [15]. As for community acquired MRSA, there has been an increase of 40% of new cases of resistance from 1999 to 2009 [16]. Similar problems are surfacing throughout the world. For example, *tuberculosis (TB)*, a disease primarily caused by *Mycobacterium tuberculosis*, has been reported to be the cause of 1.7 million deaths and 9.4 million new TB cases in 2009 alone, with the occurrence of drug resistance steadily increasing [17].

At the same time, new antibiotic development has slowed dramatically and even stopped due to market withdrawal and regulatory disincentives. Over the past 30 years there has been a dramatic decrease in FDA-approved systemic antibiotics and right now no new molecular entities (NME) are in phase III [13,18,19]. There is therefore, a seriously need to find new antibiotics with new structures and/or new targets to fight infectious disease.

Historically, antibiotics have been discovered based on whole-cell experiments examining cell growth inhibition, and the specific targets then identified. As a results, targets for antibiotic action have been classified into four major classes: bacterial cell wall biosynthesis; bacterial protein biosynthesis; DNA replication; and folate coenzyme biosynthesis [13][20]. Our lab focused on the activity-based approach which includes a high throughput enzyme assays with a target enzyme for the discovery of potential inhibitors. The main enzyme that we have focused on is bacteria translocase I, one of the key enzymes involved in peptidoglycan cell wall biosynthesis.

### 1.3. Biosynthesis of peptidoglycan cell wall

An essential process for bacterial cell survival and a well known targets for the design of antibiotics is the peptidoglycan biosynthetic pathway [21,22][23]. Bacterial peptidoglycan and its precursors were first identified and characterized in the 1940s [24]. This pathway results in the production of the cell wall peptidoglycan layer, which contains polymerized glycan chains with cross-linked peptides. The peptidoglycan layer is comprised of alternating *N*-acetylglucosamine (GlcNAc) and *N*-acetylmuramic acid (MurNAc) glycan moieties connected through  $\beta$ -1,4-linked polysaccharide peptidyl bonds. The general structure of pentapeptide attached to side chain of MurNAc is L-Ala- $\gamma$ -D-Glu-X-D-Ala-D-Ala where X is either L-Lys or meso-diaminopimelic acid (DAP). L-Lys is usually found in most Gram-positive bacteria, whereas DAP is often found in most Gram-negative bacteria. A 3-amino group of the Lys/DAP residue at position 3 and the D-Ala residue at position 4 of a second strand form the peptide linkage resulting in cross-links peptidoglycan of cell wall (**Fig 1.1**) [25,26]. The assembly of the cell wall occurs in three stages - 1) polymerization of the disaccharide and peptide side-chain within the cytosol, 2) the lipid cycle wherein the precursor is linked to a lipid carrier prior to leaving flipped to the outside, and 3) the cross-linking stage outside the cell leading to the rigid and essential cell wall structure [27].

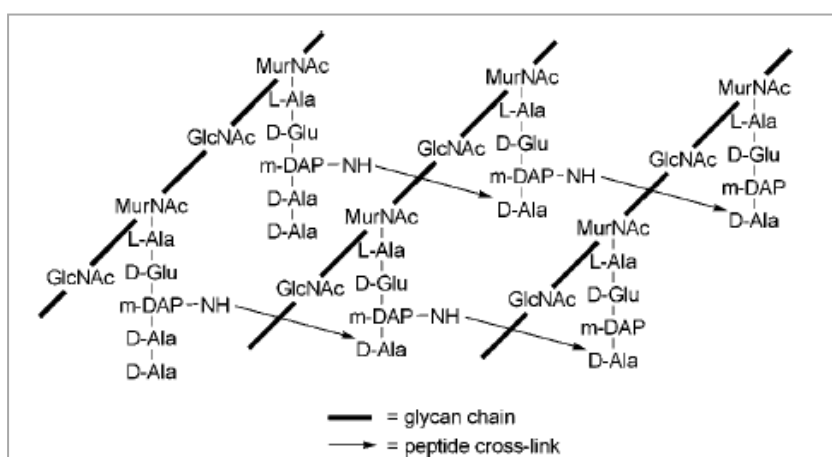


**Figure 1.1.** Structure of peptidoglycan.[26]

In the cytosolic stage, Uridine-5'-diphosphate (UDP)-sugars are the biosynthetic precursors for the biosynthesis of all cell wall components. The activated

monosaccharide uridine-5-diphospho-*N*-acetylglucosamine (UDP-GlcNAc) and UDP-*N*-acetylmuramic acid (UDP-MurNAc) are the starter of the building blocks for the polysaccharide backbone of peptidoglycan. UDP-MurNAc originates from UDP-GlcNAc by adding PEP catalyzed by MurA and MurB. A line of ATP-dependent ligases MurC–F catalyze the addition of L-Ala, D-Glu, L-Lys or m-DAP and D-Ala-D-Ala sequentially to UDP-MurNAc to generate UDP-MurNAc-pentapeptide, the final cytoplasmic precursor [21,22,25][28] (**Fig 1.2**). *MraY* (phospho-MurNAc-pentapeptide translocase), also known as translocase I, transfers the sugar-pentapeptide unit onto undecaprenyl phosphate (a lipid carrier) to generate lipid intermediate I [29]. Subsequently, lipid intermediate II is formed by adding GlcNAc sugar onto the 4'-hydroxyl of MurNAc, catalyzed by glycosyltransferase *MurG*. The precursor is then flipped from inside to outside of the cytoplasmic membrane by a "flippase" protein [29]. Lipid II further undergoes transglycosylation to generate a glycan polysaccharide by transpeptidation, catalyzed by penicillin binding proteins (PBPs) [30]. Undecaprenyl pyrophosphate is released from transglycosylation and recycled by dephosphorylation [29].

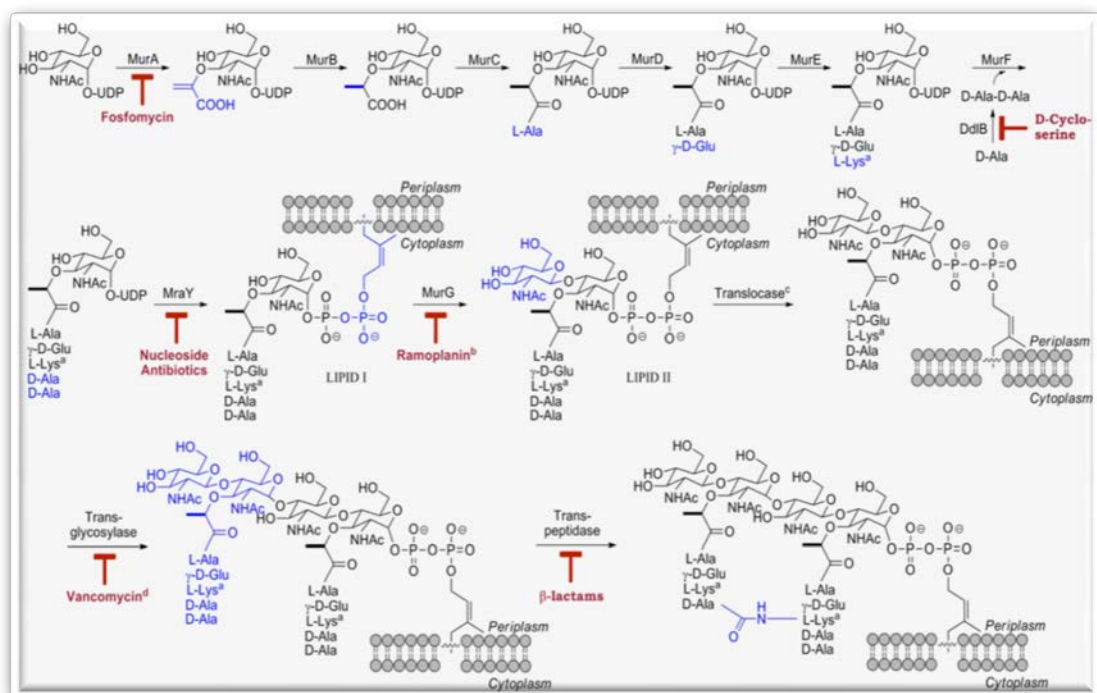


**Figure1.2. Biosynthesis of bacterial peptidoglycan cell wall mediated by twelve conserved enzymes.** The reaction catalyzed by each enzyme is highlighted in blue,

and natural products that inhibit the specified enzyme are highlighted in red. a. Diaminopimelic acid or L- $\alpha$ -Lys is found at this position. b. Ramoplanin also binds the product of MurG (Lipid II) and inhibits transglycosylases. c. Glycine ligases can precede translocase activity to yield branched peptidoglycan cell walls. d. Vancomycin inhibits the activity of transglycosylases by binding to the substrate, Lipid II.

Peptidoglycan cell walls are essential for the survival of all bacteria [29]. Twelve enzyme reactions are required for the biosynthesis of peptidoglycan cell wall, mechanisms of which haven't been completely characterized yet (**Fig. 1.2**). Most of these enzymes lack mammalian homologs, thus making cell wall biosynthesis an intriguing target for the discovery of new antibiotics. To date, natural enzyme inhibitors have been found for six of the biosynthetic steps. Two of the best examples vancomycin, that inhibit transglycosylation of lipid intermediate II outside the cytoplasmic membrane [31], and  $\beta$ -lactam antibiotics that inhibit the final transpeptidation step of cell wall biosynthesis [30] (**Fig. 1.2**). Among these six families of inhibitors, five of them have been clinically proven. Only the natural products, inhibiting bacterial translocase I, haven't been used in clinic yet, making it a unique target for new antibiotic discovery.

#### 1.4. MraY - Translocase I

MraY, which is also called translocase I, represents a novel target compared to currently marketed antibiotics. The catalytic reaction of MraY is transfer of MurNAc-pentapeptide from UDP-MurNAc-pentapeptide to undecaprenyl phosphate, releasing UMP to give undecaprenyl-disphospho-*N*-acetylmuramic acid-pentapeptide (also known as Lipid I) (**Fig 1.3**) [32,33]. Blast analysis of MraY shows that it has some sequence similarity with UDP-sugars transferase enzymes from prokaryotic and eukaryotic cell surface biosynthesis [34,35]. A mechanism of an active site nucleophile involved in either one-step or two-step reaction has been proposed. Isotope exchange experiments with *S. aureus* translocase I by Neuhaus and co-workers confirmed that the MraY-catalysed reaction is a two-step reaction, wherein



a nucleophile forms a covalent intermediate within the reaction[36]. This reaction starts the lipid cycle of cell wall biosynthesis and precedes translocation of the peptidoglycan cell wall component across the lipid membrane.

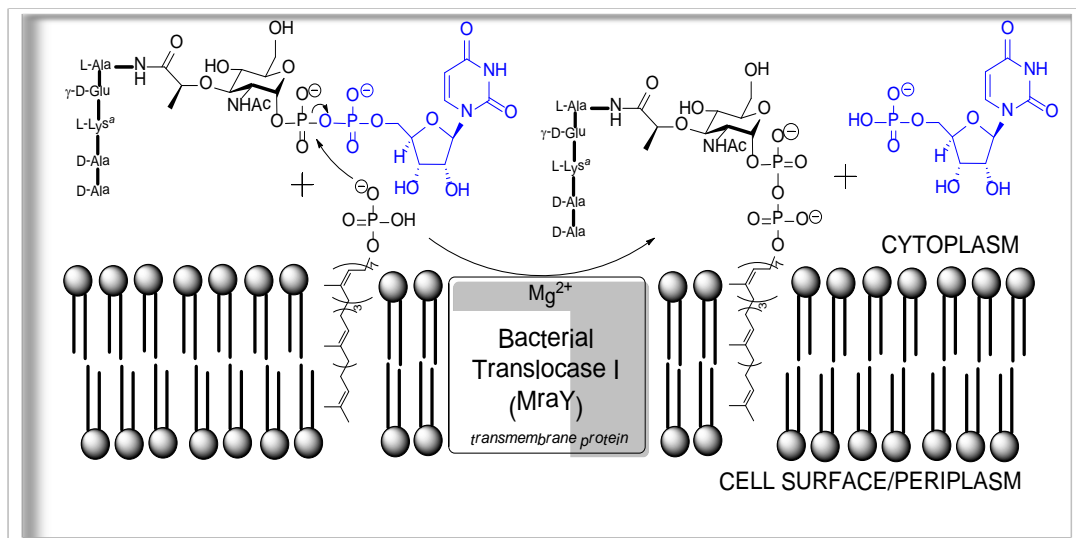


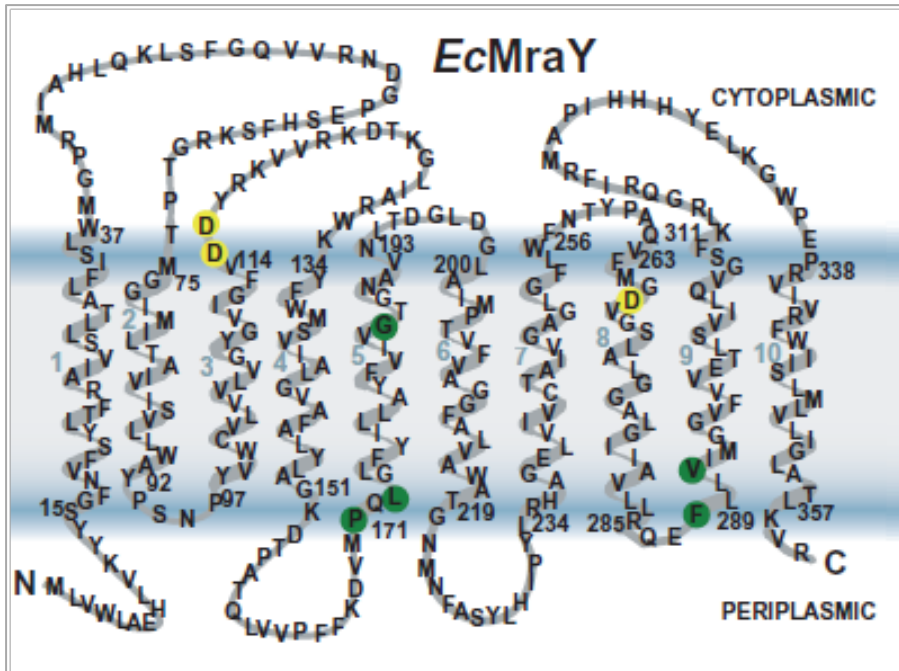
**Figure 1.3.** Reaction catalyzed by MraY. MraY, a transmembrane protein, catalyzes the formation of undecaprenyl-disphospho-*N*-acetylmuramic acid-pentapeptide as the first step in the lipid cycle of peptidoglycan cell wall biosynthesis. a: L- $\alpha$ -Lys or diaminopimelic acid.

The transferase activity catalyzed by MraY was first discovered in 1965 [37]. However, the gene for MraY was not identified until 1991 when over-expression of the *E. coli* gene resulted in increased transferase activity relative to the wild-type strain [33]. Subsequent insertional inactivation of the *mraY* gene in *E. coli* resulted in a lethal phenotype with early growth characteristics very similar to that of other mutant *E. coli* strains containing inactivated genes involved in peptidoglycan biosynthesis [38]. In addition to the gram-negative bacteria *E. coli*, the *mraY* gene was shown to be essential for the viability of the gram-positive bacteria *Streptococcus pneumonia* [39]. Based on bioinformatics analysis of the currently available 879 sequenced microbial genomes, a single copy of the essential *mraY* gene is readily identifiable by sequence similarity, and there are no reports of genetic redundancy of translocase activity [29].

It has been predicted that MraY is a trans-membrane protein with ten  $\alpha$ -helical regions, five cytoplasmic segments and six periplasmic segments. Ten  $\alpha$ -helices are

likely to form the hydrophobic tunnel that would correspond to the binding domain of undecaprenol phosphate. Five cytoplasmic segments are arranged like finger ends, bearing key amino acids required for both nucleotide substrate recognition and reaction catalysis (**Fig 1.4a**)[26]. Bouhss and co-workers identified MraY structure taking advantage of a  $\beta$ -lactamase fusion system with both enzymes purified from *E. coli* and *S. aureus* [40]. Due to the problems associated both with the preparation of substrates and the enzyme, biochemical characterization of MraY has been limited. However, preliminary biochemical characteristics from crude preparations of MraY from soluble membrane fractions have showed that  $Mg^{2+}$  is one of the crucial requirements for MraY activity [25]. Recently, recombinant *E. coli* MraY has been partially purified by using an engineered C-terminus His<sub>6</sub>-tag, but the activity was significantly reduced compared to crude preparations [41]. Furthermore, *Bacillus subtilis* MraY enzyme has been isolated to apparent homogeneity and shown to be active, however, similar to *E. coli* MraY, the specific activity and kinetic constants were inferior compared to crude preparations [42]. In spite of this reduced activity, site-directed mutagenesis was used to identify three Asp residues important for activity, Asp-115, Asp-116 and Asp-267. These three aspartic acid residues were very strictly conserved and might function as an active site nucleophile: Asp-115 and Asp-116 may form a binding site for  $Mg^{2+}$  and Asp-267 regarded as the active site residue used in the formation of a covalent enzyme-phospho-*N*-acetylmuramyl-pentapeptide intermediate (**Fig 1.4b**) [26,41]. Enzyme activity can be lost by replacing of each of three Asp residues by Asn [41,43]. These results were consistent with the earlier kinetic analysis with *S. aureus*, which suggested a double displacement mechanism [44].

(a)



(b)

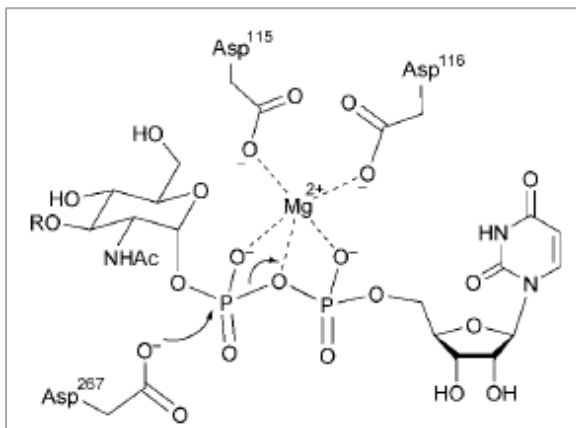


**Figure 1.4.** MraY structure and active site model.(a) Predicted catalytic aspartate residues are shown in yellow circles; amino acid mutations at specific sites in green circles are shown to have resistant activity to protein E.[45] (b) Model for active site and first chemical reaction of MraY.[26]

In addition, the two-dimensional membrane topology has been analysed by cross-linking to confirm bioinformatics prediction of membrane spanning regions shown in **Fig 1.4a**. This data is consistent with the conserved critical Asp loops within the active site of MraY being found on the cytoplasmic side of the lipid bilayer. However, the tertiary structure of MraY is still not known.

### 1.5. MraY – Translocase I Inhibitors

Since the identity of MraY was discovered, great efforts have been made to identify effective MraY inhibitors during the past two decades. This has led to the discovery of three different kinds of structural compounds that have the ability to inhibit MraY activity. They are: protein E, a helical protein composed of 93 amino acids; the lipopeptides amphomycin, fruilimicin & glycinocins; and nucleoside antibiotics (**Fig 1.5**) [25,32].

The first category of inhibitor is Protein E, an integral membrane protein encoded by DNA phage  $\Phi$ X-174 and leads to host cell lysis using an unclear mechanism [46,47]. Recently, Tanaka showed that the minimum requirements for lysis of host cells are a 18-residue peptides with the wild-type sequences of protein E. Also, the specific amino acids within and at the boundaries of this 18-membered helix were shown to be important for activity [45]. The second category of inhibitor is amphomycin, fruilimicin and glycinocins. They are cyclic lipopeptide compounds that inhibit MraY activity by formation of undecaprenyl phosphate complexes in the presence of  $\text{Ca}^{2+}$ , a mechanism analogous to the mode of action of vancomycin and teichoplanin [48,49]. The structures of friulimycins and glycinocins have been identified similar to amphomycin except minor modified residues [50,51]. Amphomycin is very active against Gram-positive bacteria *streptococci* and *enterococci* [52,53].

The last category of inhibitor, nucleoside antibiotics, is comprised of a large group of compounds that are categorized based on signature variations of the structure. More specifically, nucleoside antibiotics is classified into four families, including lipodisaccharyl nucleosides, lipopeptidyl nucleosides, peptidyl nucleosides, and glycosyl-peptidyl nucleosides (**Fig 1.5**). A uridine (or dihydrouridine) component can be found in all these classes of compounds. The variable structural components of each group of nucleoside antibiotics lead to slight variations in the specific mechanism of inhibitor. For example, the tunicamine residue of tunicamycin, one of members of

lipodisaccharyl nucleosides, is a structural mimic of disphospho-residue of UDP-MurNAc pentapeptide and it is a competitive inhibitor of MraY [21,34]. Mureidomycin, a lipopeptidyl nucleoside, have been shown to be competitive inhibitors against UDP-*N*-MurNAcpentapeptide [54,55]. On the other hand, the glycosyl-peptidyl-nucleoside antibiotic A-500359A has been shown to be a noncompetitive inhibitor against UDP-MurNAc pentapeptide residue [42]. Even though it is possible that the variations in mechanism of inhibition may be due to variability associated with the preparation and assay of MraY, it is certain that the nucleoside antibiotics described herein selectively inhibit the MraY- catalyzed reaction [25,32].

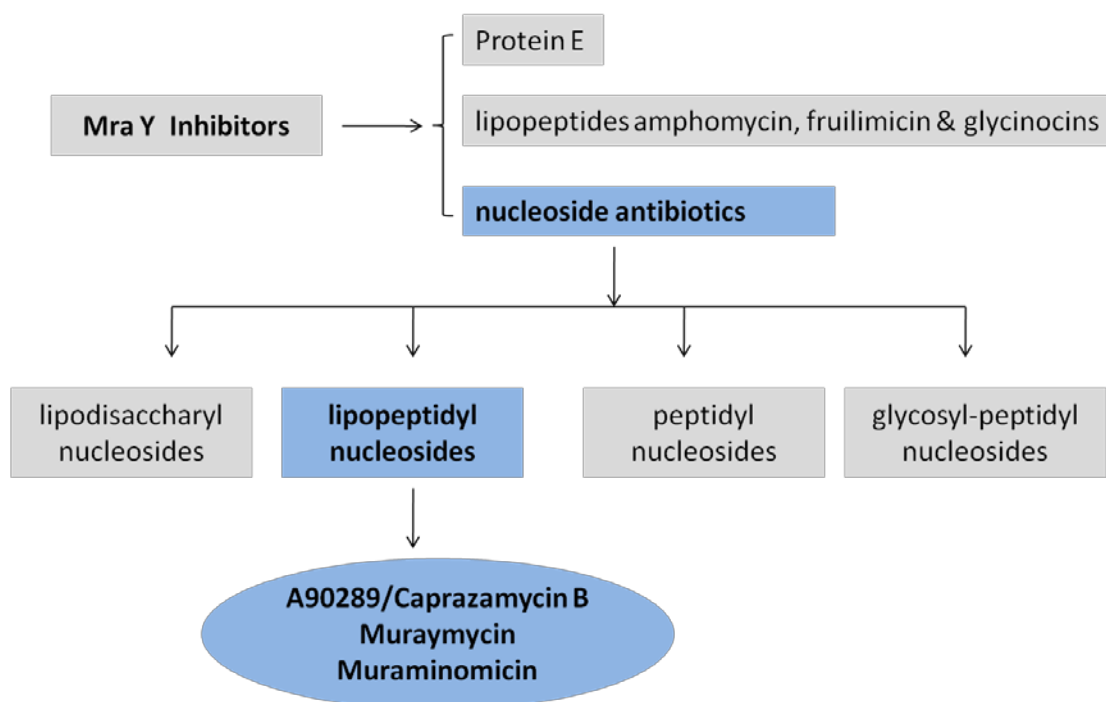


**Figure 1.5.** Inhibitors of MraY.

We have been studying the biosynthesis of several families of nucleoside antibiotics that inhibit the enzyme MraY involved in peptidoglycan cell wall biosynthesis [26], and all of these antibiotics contain unusual sugar appendages. The lipopeptidyl nucleoside family of MraY inhibitors, which includes A-90289s from *Streptomyces* sp.

SANK 60405 [56], caprazamycins from *Streptomyces* sp. MK739-62F [57], FR-900493 from *Bacillus cereus* No. 2045 [58][59], and muraymycins from *Streptomyces* sp. NRRL 30471 [60], contain an aminoribosyl moiety—a 5-amino-5-deoxyribose—attached via an O-glycosidic bond to a heptofuranose nucleoside component, 5'-C-glycyluridine (**Fig1.6**). We will focus on A-90289 and muraminomicin from *Streptosporangium* sp. lipopeptidyl nucleoside antibiotics biosynthesis in this thesis (**Fig 1.5**). Structure-activity relationship studies using simplified synthetic analogues of these compounds have revealed the aminoribosyl moiety [61], and specifically the primary amine functionality [62], is critical for optimal antibiotic activity.

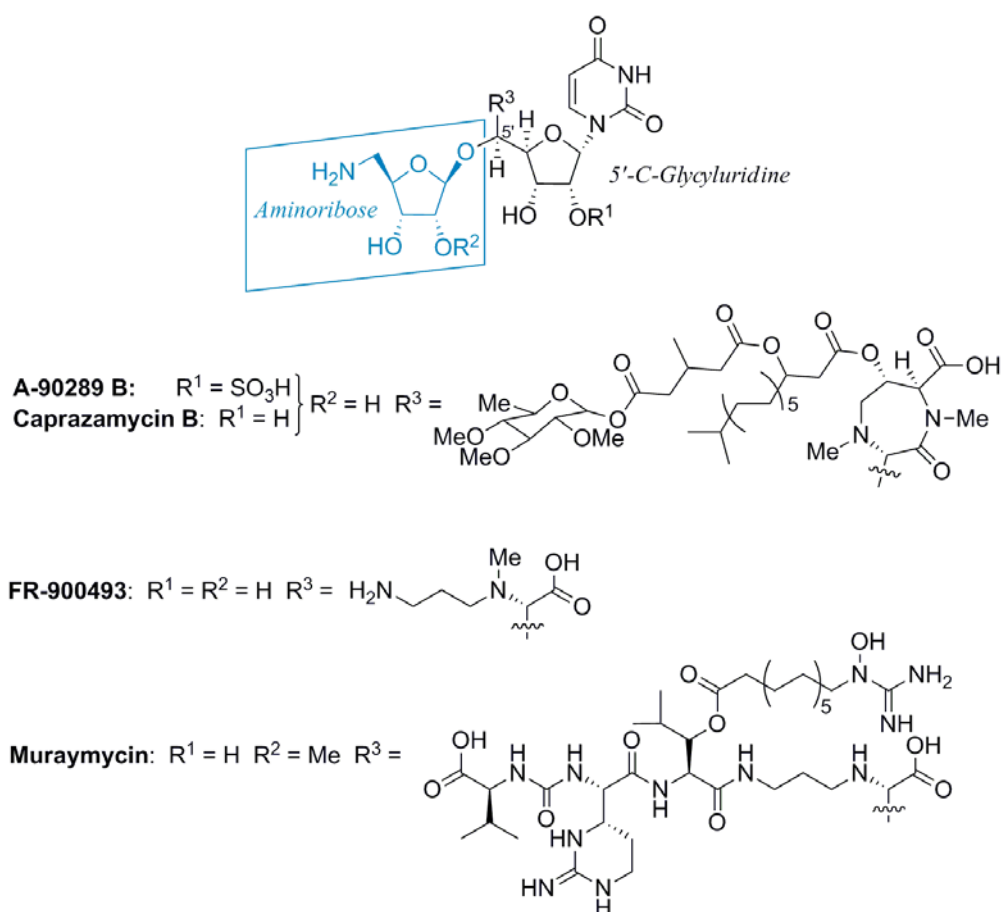


**Figure 1.6.** Structure of representative lipopeptidyl nucleoside antibiotics containing an aminoribosyl moiety.

## 1.6. Glycosidic residues play a critical role in biological function of antibiotics

Glycosylation is a common modification found in several microbial natural products of therapeutic value, and the sugar appendage typically has a profound effect on the biological activity [63,64]. The critical role of sugar residues in their activity opens up a large field for developing new glycosidic antibiotics, and vancomycin and bleomycin are two of the most illustrative examples (**Fig 1.7**)[65,66].

Vancomycin, the structure of which shown in **Fig 1.7**, is one of the glycopeptide antibiotics of last resort in the treatment of gram-positive bacterial infections. It consists of a core heptapeptide with attached saccharide moieties, one of which is the deoxyaminosugar vancosamine [67]. Sugar residues help to confer water solubility for the compounds with aromatic residues and the disaccharides are important in mediating back-to-back dimerization of glycopeptides [68][69]. With a disaccharide in the structure, the activity of vancomycin is increased by 50-100 times. Nevertheless, if an additional amino-sugar is added to vancomycin to generate a derivative, the activity will be promoted by 1000 times [70,71]. Bleomycin, used as an antitumor drug in the clinic, also exhibits antimicrobial activity against infections by both Gram-positive and Gram-negative bacteria [65,66]. It has been demonstrated that bleomycin works by cleavage of DNA and RNA strand under the effect of  $\text{Fe}^{2+}$  and oxygen reagents [72][73,74]. As for the disaccharide moieties in the structure of bleomycin, previous research revealed that they play an important role in activating bleomycin by binding of oxygen and the activation and protection (as a metal ligand) of the reactive iron-oxo or perferryl intermediate [75]. Furthermore, Natrajan proposed that the carbohydrate moiety is involved in cell surface recognition by bleomycin [76].

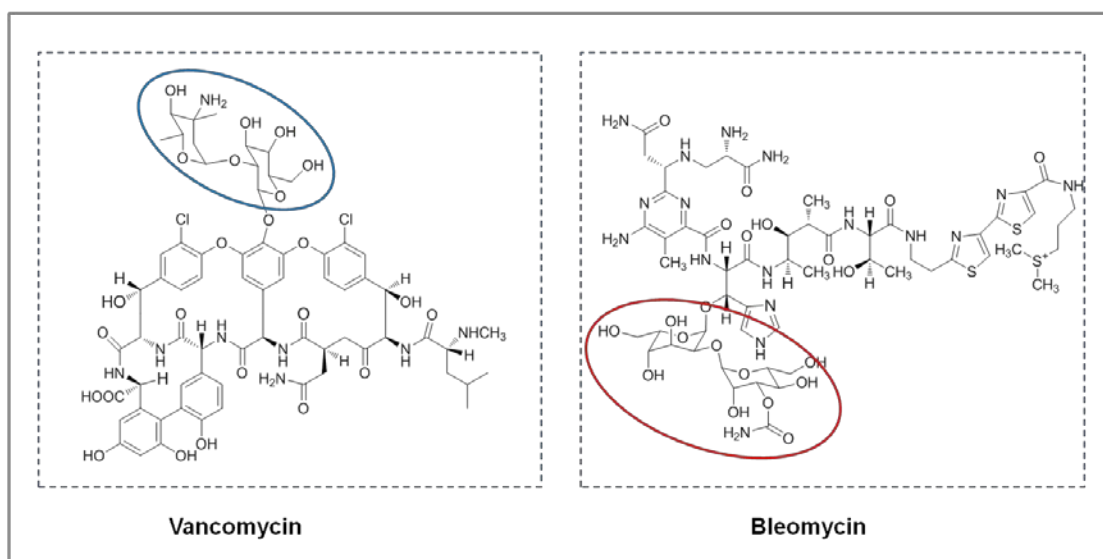


**Figure 1.7.** Structure of vancomycin and bleomycin. Glycosidic residues of both compounds are marked by blue and red circle respectively.

These unusual sugar appendages are crucial for the bioactivities of many bacterial natural products and they are typically modified resulting in many different kinds of formats inside the compounds, such as deoxysugars, aminosugars, etc [77]. As a result, alteration of sugar structures of these glycol conjugates via biosynthetic engineering approaches offers a platform for making and discovering novel natural product analogues [64]. In order to do so, it is absolutely necessary to find out how these sugar units are modified and assembled into compounds.

### 1.7. Traditional strategy for ribose and glucose incorporation into compounds

The modus operandi by which sugars are generally incorporated into molecular scaffolds such as natural products is (i) formation of a sugar-1-phosphate derived from a glycolytic intermediate or galactose, a catalytic process that requires either a phosphosugar mutase or an anomeric sugar kinase; (ii) conversion of the sugar-1-phosphate to usually an NDP-sugar (also called an activated sugar), a reaction catalyzed by a sugar-1-phosphate nucleotidyltransferase; and (iii) transfer of the sugar to an acceptor substrate by a glycosyltransferase to typically generate a new O-, N-, or aryl-C-glycosidic bond (**Fig 1.8**). A remarkable feature of glycosylated,



bacterial natural products is the high degree of variability and functionality that can be incorporated into the sugar moiety by reductases, epimerases, methyltransferases, and aminotransferases, among others—enzymatic modifications that generally occur at the level of the activated sugar prior to the glycosyltransferase-catalyzed reaction [63,64].

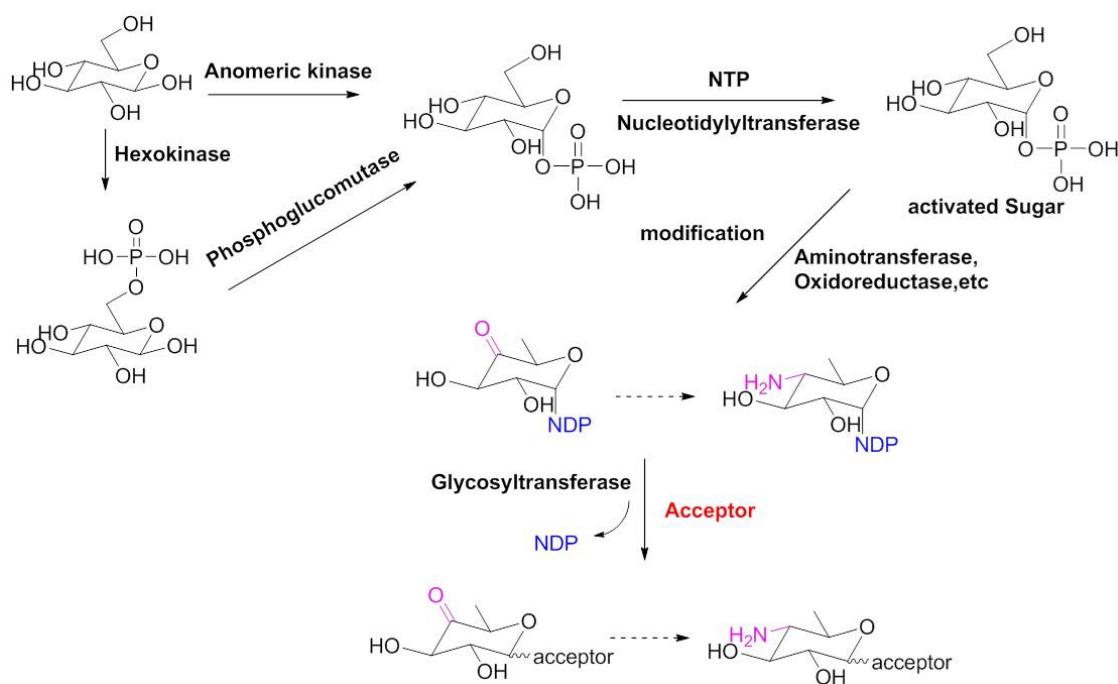


**Figure 1.8.** Traditional strategies for glucose incorporation into a compound.

The traditional strategy for ribose (five-membered ring sugar) is quite different from that of other hexoses and pentoses. It starts with ribose-5-phosphate, which is converted to 5-phospho- $\alpha$ -D-ribose-1-diphosphate (PRPP) by PRPP synthetase. This activated sugar is then used as a ribose-5-phosphate donor that is transferred to an acceptor by a phosphoribosyl transferase. Finally, the remaining phosphate group is hydrolyzed by phosphatase to generate a ribosylated compound (**Fig 1.9**). This strategy has recently been revealed for generating glycosidic bonds with ribose units in natural product biosynthesis. The ribosyl moiety of the aminoglycoside antibiotic butirosin was shown to be derived from PRPP [78], from which BtrL

transfers ribose-5-phosphate to the acceptor disaccharide neamine to generate an O-glycosidic bond and a second enzyme BtrP catalyses dephosphorylation to form the final trisaccharide scaffold (**Fig 1.10**). This tandem, enzyme-catalyzed process is also utilized during O-ribosylation of decaprenyl-phosphate to initiate the biosynthesis of mycobacterial arabinogalactan [79]. Along with the wealth of *N*- and *C*-ribosides that originate via phosphoribosyltransfer from 5-phospho- $\alpha$ -D-ribose-1-diphosphate (**Fig 1.10**) [26][80], it would appear that ribosylation is an exception to the typical glycosylation paradigm.

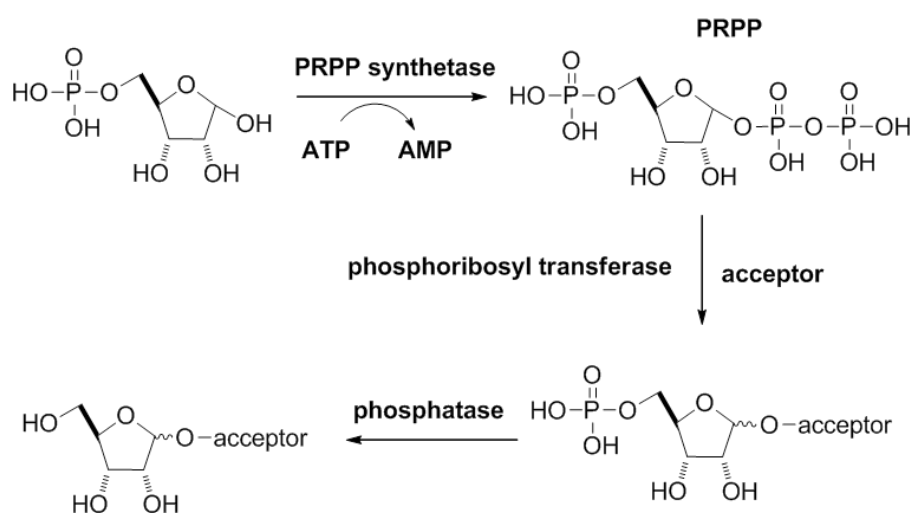


**Figure 1.9.** Traditional strategies for ribose incorporation into a compound.

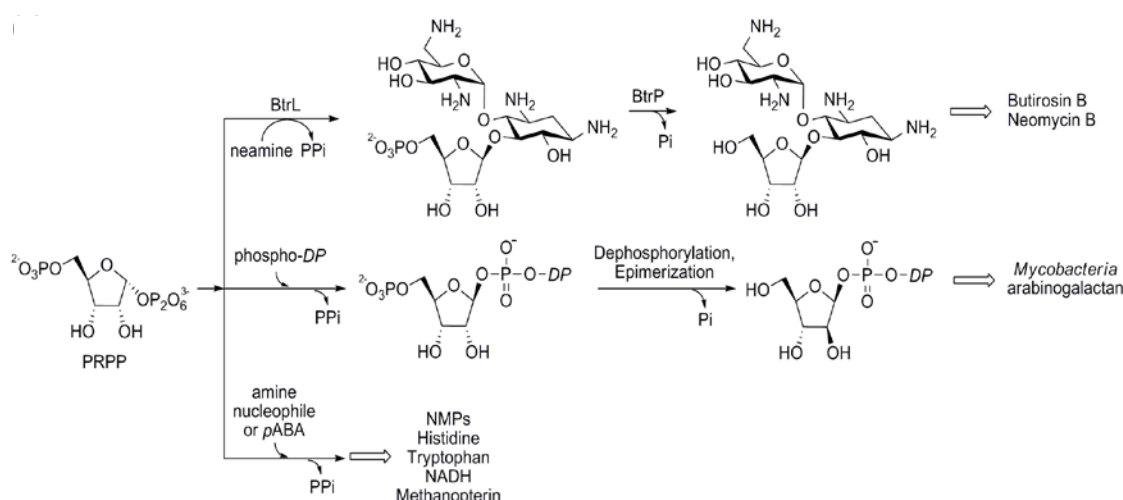


**Figure 1.10.** Examples of incorporation of pentose units into acceptor molecules using 5-phospho- $\alpha$ -D-ribose-1-diphosphate (PRPP).

Based on the two typical strategies for sugar units incorporation into a natural product discussed above, we aimed to determine how the glycosidic residues in lipopeptidyl nucleoside antibiotics are assembled. Like the clinically-used antibiotics, lipopeptidyl nucleoside antibiotics (A-90289 and muraminomicin) are structurally complex compounds that are normally difficult to be synthesized economically, and enzymatic biosynthesis offers a relatively efficient strategy to both produce and modify the scaffolds for preliminary testing as new drug candidates. It is envisioned that the information provided from or inspired from the sugar residue biosynthetic studies will have crucial importance to new antibiotics discovery and ultimately lead to therapeutic value clinically.

## Chapter two: Biosynthetic pathway of aminoribosyl moiety of A-90289

### 2.1. Background

Liposidomycins, the structure of which were first reported in 1988 [81], and caprazamycins isolated from *Streptomyces* sp. MK730-62F2 are prominent members of the peptidyl nucleoside antibiotics [57]. A-90289s, which also belong to the liposidomycin family of peptidyl nucleoside antibiotics, were initially identified and reported in 2010 [56]. A-90289, isolated from *Streptomyces* sp. SANK 60405, have a structure of which is very similar to caprazamycins (**Fig2.1**). They both share six core moieties in the structure: a 5'-glycyluridine, an aminoribose, a diazepanone, a 3-methyl-glutaric acid, a 6-deoxyglucose and a fatty acid. A-90289 is same as caprazamycins except that A-90289 containing sulfate group on the 2' position hydroxy group of 5'-glycyluridine moiety [56].

Recent studies have revealed that caprazamycin is very active against Gram-positive bacteria, in particular against the genus *Mycobacterium* including *Mycobacterium tuberculosis*, *Mycobacterium intracellulare* and *Mycobacterium avium* [82,83]. As for A-90289, it was reported that the inhibitory activity of A-90289 on bacterial translocase I was 36.5ng/ml ( $IC_{50}$ ). A-90289 is also very active against Gram-positive bacteria with a minimum inhibitory concentration (MIC) against *S. Aureus* ATCC 6538P, *Streptococcus pyogenes* and *Enterococcus faecium* of 8mg/ml, 4mg/ml and 16mg/ml, respectively[84].

(a)



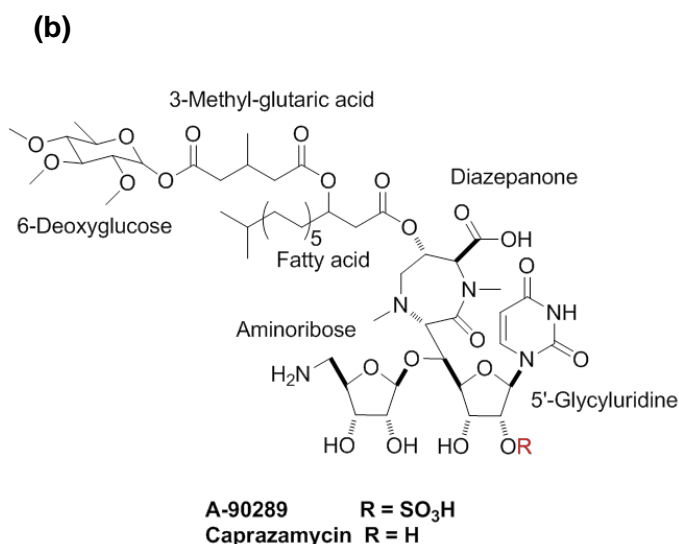


**Figure 2.1.** *Streptomyces* sp. SANK 60405 wild type and structure. (a) *Streptomyces* sp. SANK 60405 wild type strain grew on R2YE plates. (b) Structure of A-90289 and caprazamycin.

The biosynthetic gene cluster of caprazamycin has been cloned and characterized recently [85]. Shortly thereafter, the gene cluster of A-90289 was reported by M. Funabashi, et al in 2010 and demonstrated that there are 41 *orfs* that are responsible for the biosynthesis of A-90289 (**Fig2.2**) [56]. The sequence comparison of A-90289 gene cluster and caprazamycin gene cluster showed very high similarity (ORFs having between 80-91% sequence identities). However, there are clear differences within the boundary regions, and of particular interest is the gene for a sulfotransferase (LipB) that is found at the upstream boundary of the A-90289 gene cluster and not found within the caprazamycin gene cluster, which is expected based on structural comparisons of these two compounds.

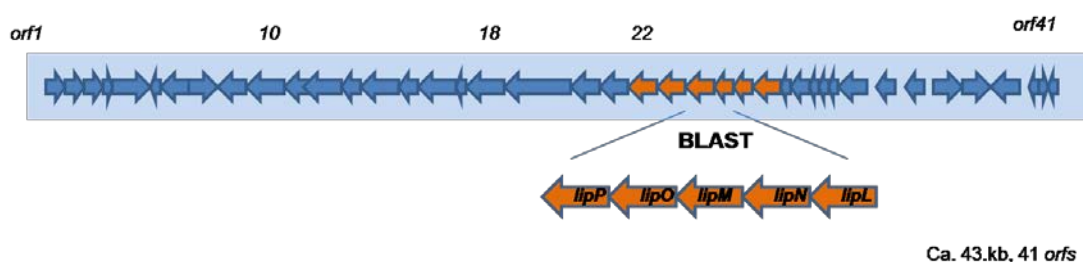


**Figure 2.2.** The A-90289 biosynthetic gene cluster. All the *orfs* in A-90289 gene cluster is shown in blue. The five *orfs* (*lipP-L*) that are involved in aminoribosyl moiety incorporation is highlighted in yellow.

The first insight into how the disaccharide core is assembled was unveiled upon cloning of the biosynthetic gene clusters for these lipopeptidyl nucleoside antibiotics along with liposidomycin and muraymycin [56,85,86,87], which revealed six-shared genes encoding a putative serine hydroxymethyltransferase (*shmt* for the A-90289 gene cluster), a non-heme, Fe(II)-dependent dioxygenase (*lipL*), a putative nucleotidyltransferase (*lipM*), glycosyltransferase (*lipN*), aminotransferase (*lipO*), and uridine phosphorylase (*lipP*). We initially demonstrated that LipL is a non-heme, Fe(II)-dependent  $\alpha$ -ketoglutarate:UMP dioxygenase that catalyzes the conversion UMP to uridine-5'-aldehyde (**1**) during A-90289 biosynthesis (**Fig 2.3**)[88]. In turn we proposed that uridine-5'-aldehyde (**1**) serves as the substrate for a putative SHMT LipK (Serine hydroxymethyltransferase), catalyzing an aldol-type reaction using glycine as a co-substrate to generate 5'-C-glycyluridine. We have subsequently shown uridine-5'-aldehyde (**1**) is a substrate for LipK along with L-threonine to form 5'-C-glycyluridine [89]. Based on the conjecture that the most efficient overall biosynthetic pathway will be employed, we subsequently hypothesized uridine-5'-aldehyde (**1**) is also an intermediate in the pathway leading to the aminoribosyl moiety, which would necessitate aminotransfer, phosphorolysis, ribose activation, and ribosyltransfer by LipO, LipP, LipM and LipN, respectively (**Fig 2.3**).

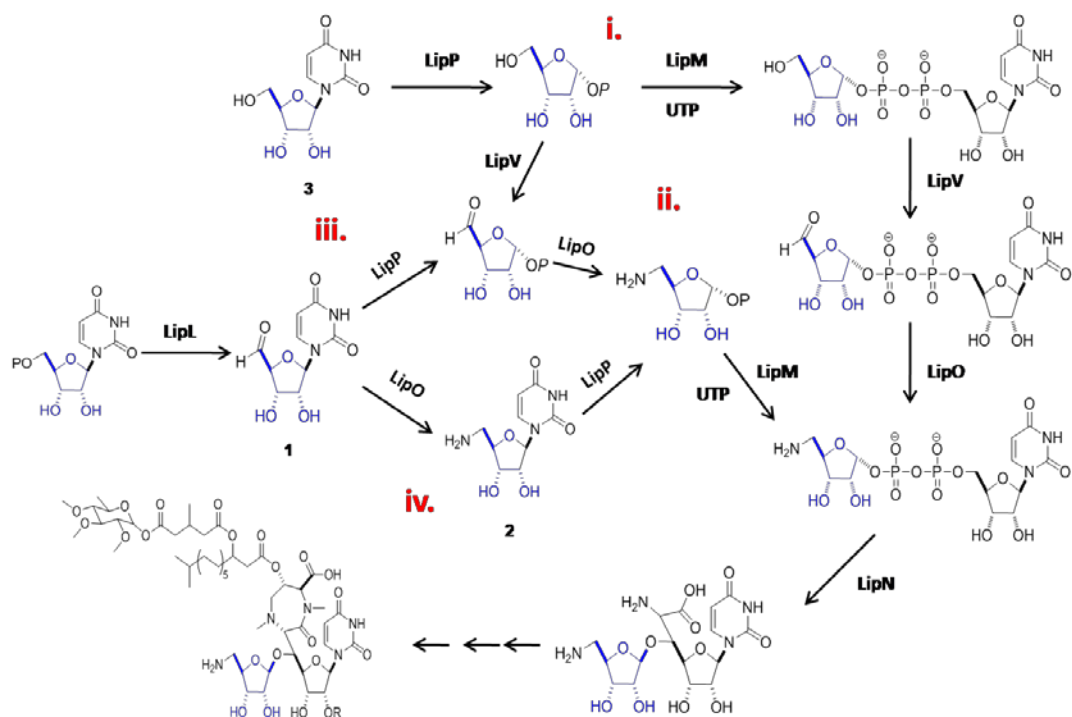


**Figure 2.3.** Proposed biosynthetic pathway for the incorporation of the aminoribosyl moiety of A-90289.

The apparent involvement of a nucleotidyltransferase and glycosyltransferase suggested the pathway leading to the aminoribosyl moiety does not parallel the known ribosylation pathways that are PRPP-dependent but instead utilizes an NDP-sugar as the activated, sugar donor. Thus, the original biosynthetic pathway for amino-ribose moiety incorporation into A-90289 was proposed (**Fig 2.3**), a pathway that follows the archetypical sugar biosynthetic paradigm described in section 1.7.

We envisioned 4 potential routes leading to the final aminoribosyl moiety attachment based on bioinformatics analysis catalyze. Two routes would start from uridine, wherein a phosphorylase (LipP) catalyzed the formation of a ribose-1-phosphate intermediate. In one route: the nucleotidyltransferase (LipM) catalyses formation of the activated NDP-sugar, which is followed by oxidation of the primary hydroxyl group by a putative dehydrogenase (LipV) to give the aldehyde. The ribose then undergoes transamination by aminotransferase (LipO). The second route starting from uridine is catalysis by the dehydrogenase (LipV) to generate the 5'-aldehyde of

ribose-1-phosphate, and an amine group is introduced in a reaction catalyzed by the aminotransferase (LipO). This aminoribosyl moiety is then transferred to NTP (nucleoside triphosphate) to form the activated sugar counterpart catalyzed by the nucleotidylyltransferase (LipM). Finally this activated NDP (nucleoside diphosphate)-sugar could be finally transferred to an acceptor to complete the ribose incorporation by glycosyltransferase (LipN). Another two hypothetical routes would start with UMP, which is oxidized by dioxygenase (LipL) to form uridine-5'-aldehyde, and then converted to the ribose-1-phosphate derivative by the uridine phosphorylase. Following transamination, the nucleotidylyltransferase (LipM) catalyzes the formation of the amino-ribosyl-NDP sugar, which serves as the activated sugar for transfer by the glycosyltransferase (LipN) to the acceptor to form the final disaccharide. Alternatively, transamination could occur prior to formation of the ribose-1-phosphate, which is then processed by LipM and LipN.

We now present the delineation of the biosynthetic pathway for incorporating this moiety by functionally assigning four enzymes, LipP-N. Our results define a new sugar-like pathway for ribose incorporation that does not originate from PRPP. These results also reveal a unique O-ribosylation pathway that indeed parallels the typical glycosylation paradigm yet with significant distinctions that are disclosed herein.

## **2.2. Materials and methods**

### **2.2.1. Chemicals and Reagents**

Uridine, uracil, UTP, UDP, UMP, TTP, CTP, GTP, TMP, CMP, GMP, o-phthalaldehyde (OPA), L-Methionine, L-glutamate, L-aspartate and other amino donors were purchased from Sigma-Aldrich (St. Louis, MO) or Promega (Madison, WI). Buffers, salts, and media components were purchased from Fisher Scientific (Pittsburgh, PA). Synthetic oligonucleotides were purchased from Integrated DNA Technologies



(Coralville, IA). Wizard® *Plus* SV Minipreps DNA Purification Systems, Wizard® SV Gel and PCR Clean-Up System were purchased from Promega (Madison, WI, USA). pET-30 Xa/LIC Vector Kit was purchased from Calbiochem (San Diego, CA, USA). InstaGene Matrix was purchased from Bio-Rad (Hercules, CA). Ni-NTA agarose was purchased from Qiagen (Valencia, CA). Amicon Ultra 10000 MWCO centrifugal filter was purchased from Millipore (Billerica, MA). PD-10 desalting column was purchased from GE Healthcare (Pittsburgh, PA). DNA sequencing was performed using the BigDye™ Terminator version 3.1 Cycle Sequencing kit from Applied Biosystems, Inc. (Foster City, CA) and analyzed at the University of Kentucky Advanced Genetic Technologies Center.

### **2.2.2. Instrumentation**

UV/Vis spectroscopy was performed with a Bio-Tek  $\mu$ Quant microplate reader using Microtest™ 96-well plates (BD Biosciences) or a Shimadzu UV/Vis-1800 Spectrophotometer. HPLC was performed with a Waters Alliance 2695 separation module (Milford, MA) equipped with a Waters 2998 diode array detector and an analytical Apollo C-18 column (250 mm x 4.6 mm, 5  $\mu$ m) or a semi-preparative Apollo C-18 column (250 mm x 10 mm, 5  $\mu$ m) purchased from Grace (Deerfield, IL). Electrospray ionization-MS was performed using an Agilent 6120 Quadrupole MSD mass spectrometer (Agilent Technologies, Santa Clara, CA) equipped with an Agilent 1200 Series Quaternary LC system and an Eclipse XDB-C18 column (150mm x 4.6 mm, 5  $\mu$ m, 80Å). High-resolution MS was obtained at the University of Minnesota, Department of Chemistry Mass Spectrometry Facility. NMR data were collected using a Varian Unity Inova 300, 400 or 500 MHz Spectrometer (Varian, Inc., Palo Alto, CA). <sup>31</sup>P chemical shifts were assigned relative to phosphoric acid standard.

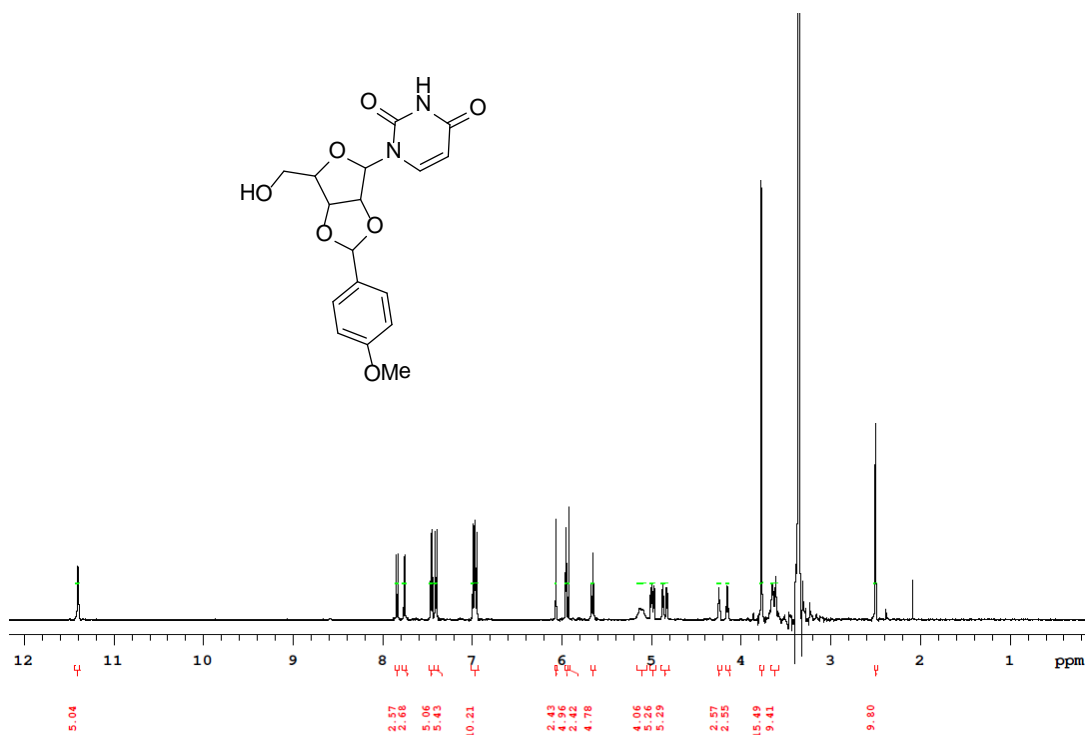
### 2.2.3. Bacterial Strains and Enzymes

NovaBlue GigaSingles™ Competent Cells was purchased from Calbiochem (San Diego, CA, USA). One Shot® BL21 (DE3) Chemically Competent *E. coli* was purchased from Invitrogen (Camarillo, CA). TaKaRa LA Taq® DNA polymerase with GC Buffer was purchased from Takara Bio Inc (Otsu, Shiga, Japan), T4 DNA ligase, NdeI, and Hind III were purchased from New England Biolabs (Ipswich, MA). Expand long template PCR system was purchased from Roche Applied Science (Indianapolis, IN).

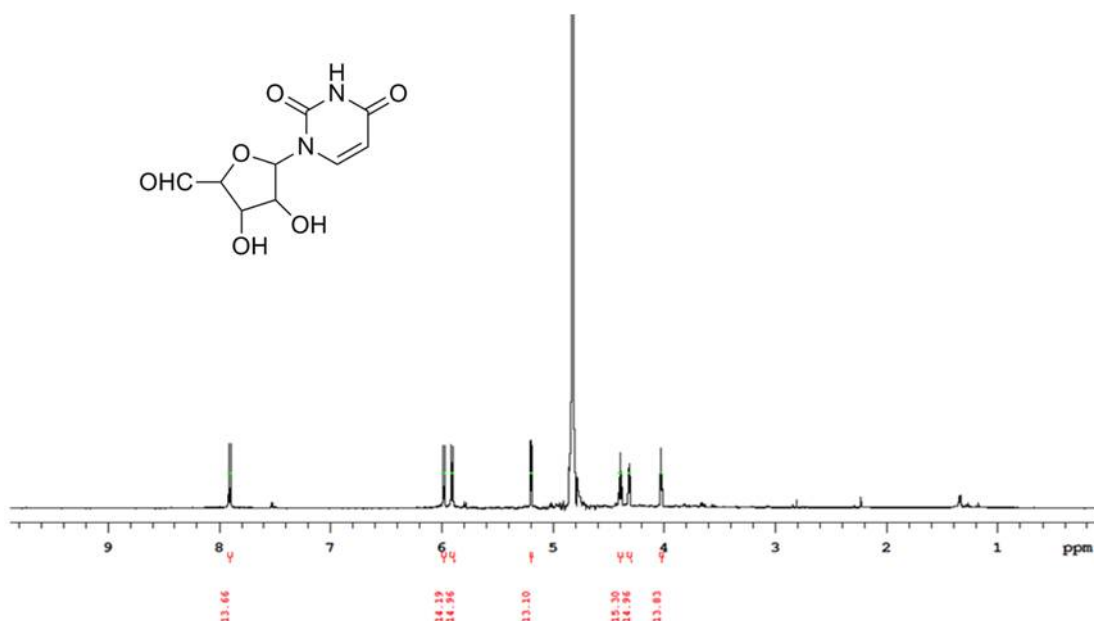
### 2.2.4. Synthesis of uridine-5'-aldehyde, 1

The synthesis of uridine-5'-aldehyde (1) followed a previously described procedure [88].

*2',3'-O-p-Methoxybenzylideneuridine*. To a solution of uridine (2.0 g, 8.2 mmol) in dry THF (30 mL), ZnCl<sub>2</sub> (1.1 g, 8.2 mmol) and *p*-methoxybenzaldehyde (4 mL, 32.8 mmol) was added. The turbid mixture was stirred for 2 days at room temperature and THF was removed. The product was precipitated by the addition of diethyl ether (50 mL), which was filtered, washed with water (2 × 25 mL) and diethyl ether (2 × 25 mL). Crystallization from hot water containing a little ethanol provided *2',3'-O-p*-methoxybenzylideneuridine (2.1 g, 71%) as white solid. Mp: 205-206 °C (lit: 207-208 °C) (1). <sup>1</sup>H-NMR (DMSO-*d*<sub>6</sub>, 500 MHz) (2): δ 11.40 (brs, 1H), 7.83 and 7.75 (2 × d, 1H, *J* = 8.0 Hz), 7.45 and 7.40 (2 × d, 2H, *J* = 8.5 Hz), 6.98 and 6.96 (2 × d, 2H *J* = 9.0 Hz), 6.06 and 5.92 (2 × s, 1H), 5.95 (2 × d, 1H, *J* = 3.0 Hz), 5.65 (2 × dd, 1H, *J* = 8.0, 2.0 Hz), 5.13 and 5.09 (2 × brs, 1H), 4.99 and 4.97 (2 × dd, 1H, *J* = 6.5, 2.5 Hz), 4.87 and 4.82 (2 × dd, 1H, *J* = 6.5, 3.0 Hz), 4.24 and 4.15 (2 × dd, 1H, *J* = 4.5, 3.5 Hz), 3.78 and 3.77 (2 × s, 3H), 3.65 and 3.61 (2 × m, 2H).



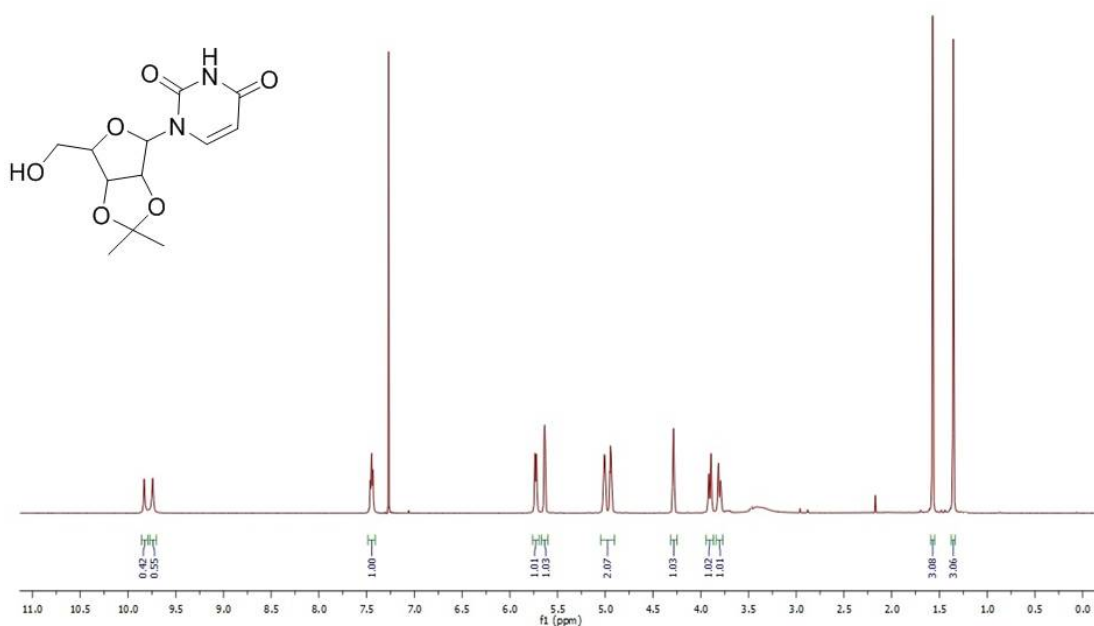
*Uridine-5'-aldehyde*, **1**. Trifluoroacetic acid (0.2 mL, 2.5 mmol) was added to an ice-cooled solution of 2',3'-*O*-*p*-methoxybenzylideneuridine (1.0 g, 2.76 mmol), *N,N'*-dicyclohexylcarbodiimide (3.1 g, 15 mmol), and pyridine (0.04 mL, 5 mmol) in anhydrous dimethyl sulfoxide (13 mL), and the resulting mixture was stirred at room temperature for 16 h. Ethyl acetate (50 mL) was added to the reaction mixture and precipitated *N,N'*-dicyclohexylurea was filtered off while washing with another portion of ethyl acetate (50 mL). Combined filtrates were washed with water (2 × 50 mL), dried (Na<sub>2</sub>SO<sub>4</sub>), and concentrated to give crude 2',3'-*O*-*p*-methoxybenzylideneuridine 5'-aldehyde as a white solid. Without further purification, the compound was dissolved in a solution of 90% trifluoroacetic acid (20 mL) and stored at 37 °C for 16 h and then concentrated. An aqueous solution (30 mL) of the residue was washed with chloroform (2 × 15 mL) and ethyl acetate (20 mL). Removal of the water afforded compound uridine-5'-aldehyde (**1**) (360 mg, 54% in two steps) as off-white foam. The compound is extremely hygroscopic in nature and exists mostly in hydrated form. <sup>1</sup>H-NMR (D<sub>2</sub>O, 500 MHz)(3): δ 7.88 (d, 1H, *J* = 8.0 Hz), 5.96 (d, 1H, *J* = 6.0 Hz), 5.88 (d, 1H, *J* = 8.0 Hz), 5.17 (d, 1H, *J* = 4.0 Hz), 4.37 (dd, 1H, *J* = 6.0, 5.5 Hz), 4.32-4.26 (1H, m), 4.00 (dd, 1H, *J* = 4.0, 3.5 Hz); <sup>13</sup>C-NMR (D<sub>2</sub>O, 125 MHz): δ 166.05, 151.74, 141.88, 102.44, 88.53, 86.17, 73.26, 69.60.



### 2.2.5. Synthesis of 5'-amino-5'-deoxyuridine, **2**

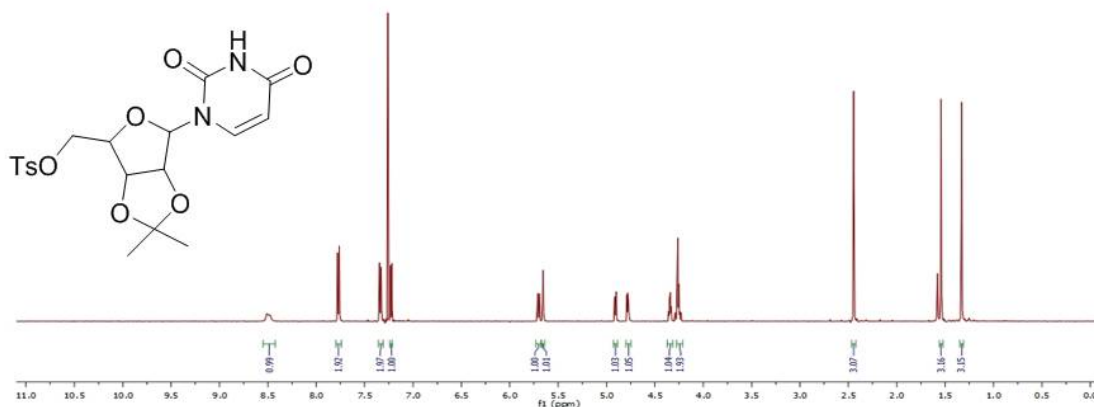
The synthesis of 5'-amino-5'-deoxyuridine (**2**) followed a previously described five-step procedure with minor modifications [90]. Lithium azide was prepared from sodium azide and lithium sulfate as previously described [91].

**2',3'-O-Isopropylideneuridine.** To a solution of uridine (**3**) (10 g; 41 mmol) and *p*-toluenesulfonic acid monohydrate (1.2 g; 7 mmol) in anhydrous DMF containing 4 Å molecular sieves was added 2,2-dimethoxypropane (20 mL, 164 mmol), and the mixture heated at 40 °C until completion (3 hr) as monitored using TLC (CHCl<sub>3</sub>:MeOH, 12:1). DMF was removed by rotary evaporation and the solid re-dissolved in ethyl acetate (100 mL) and washed with water (2 × 40 mL) and saturated sodium bicarbonate in water (2 × 40 mL). The ethyl acetate extract was dried and the product purified by silica gel chromatography (CHCl<sub>3</sub>:MeOH, 12:1) to yield 6.3 g (56 %) of 2',3'-O-isopropylideneuridine. <sup>1</sup>H-NMR (CDCl<sub>3</sub>, 500 MHz): δ 9.83 (s, 1H), 9.74 (s, 1H), 7.45 (t, 1H, *J* = 7.0 Hz), 5.73 (d, 1H, *J* = 8.0 Hz), 5.68-5.60 (m, 1H), 5.05-4.97 (m, 1H), 4.96-4.91 (m, 1H), 4.28 (brs, 1H), 3.90 (d, 1H, *J* = 11.0 Hz), 3.80 (d, 1H, *J* = 11.0 Hz), 1.57 (s, 3H), 1.35 (s, 3H).



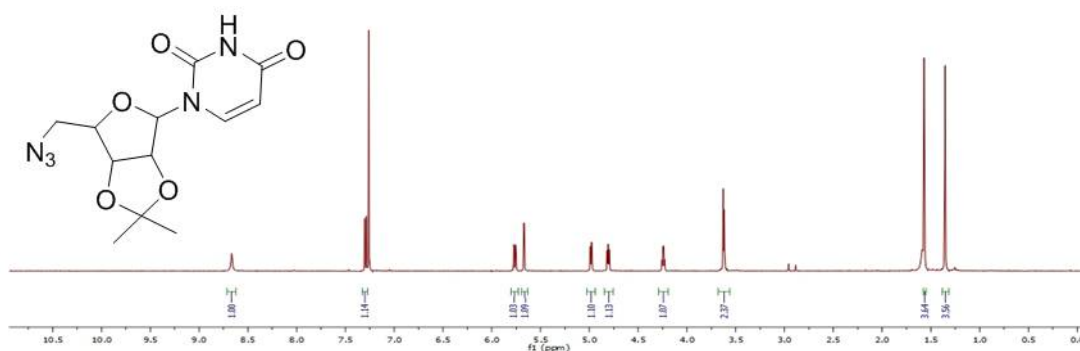
*2',3'-O-Isopropylidene-5'-O-toluenesulfonyluridine.*

To a solution of 2',3'-O-Isopropylideneuridine (6.25 g, 21 mmol) in dichloromethane (90 mL) was added pyridine (5.4 mL, 63 mmol) and *p*-toluenesulfonyl chloride (16.8 g, 84 mmol), and the solution stirred at room temperature until completion (24 hr) as monitored by TLC (CHCl<sub>3</sub>:MeOH, 25:1). Following the addition of water (50 mL), the product was extracted with chloroform (2 x 50 mL) and washed with saturated sodium bicarbonate in water (2 x 50 mL). After removal of chloroform and dichloromethane by rotary evaporation, the product was purified by silica gel chromatography (CHCl<sub>3</sub>:MeOH, 25:1) to yield 7.54 g (78 %) of 2',3'-O-Isopropylidene-5'-O-toluenesulfonyluridine. <sup>1</sup>H-NMR (CDCl<sub>3</sub>, 500 MHz):  $\delta$  8.51 (s, 1H), 7.77 (d, 2H, *J* = 8.0 Hz), 7.34 (d, 2H, *J* = 8.0 Hz), 7.22 (d, 1H, *J* = 8.0 Hz), 5.70 (dd, 1H, *J* = 8.0, 2.0 Hz), 5.66 (d, 1H, *J* = 2.0 Hz), 4.91 (dd, 1H, *J* = 6.0, 2.0 Hz), 4.78 (dd, 1H, *J* = 6.0, 3.5 Hz), 4.39-4.30 (m, 1H), 4.28-4.21 (m, 2H), 2.44 (s, 3H), 1.54 (s, 3H), 1.33 (s, 3H).



*5'-Azido-5'-deoxy-2',3'-O-isopropylideneuridine.*

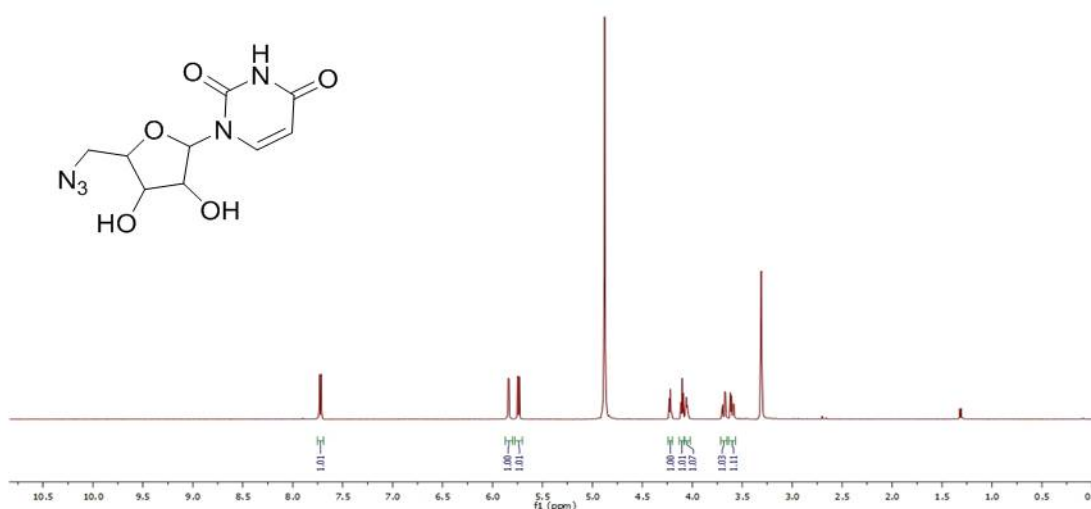
To a solution of 2',3'-O-Isopropylidene-5'-O-toluenesulfonyluridine (6.5 g, 14.8 mmol) in DMF (30 mL) was added lithium azide (3.7 g, 75.5 mmol), and the solution heated at 45 °C until completion (16 hr) as monitored using TLC (hexanes:ethyl acetate, 1:1). After removal of DMF by rotary evaporation, the product was purified by silica gel chromatography (CHCl<sub>3</sub>:MeOH, 25:1) to yield 4.2 g (92 %) of 5'-azido-5'-deoxy-2',3'-O-isopropylideneuridine. <sup>1</sup>H-NMR (CDCl<sub>3</sub>, 500 MHz):  $\delta$  8.67 (s, 1H), 7.29 (d, 1H,  $J$  = 8.5 Hz), 5.76 (dd, 1H,  $J$  = 8.0, 2.0 Hz), 5.67 (d, 1H,  $J$  = 2.0 Hz), 4.98 (dd, 1H,  $J$  = 6.5, 2.0 Hz), 4.81 (dd, 1H,  $J$  = 6.5, 4.0 Hz), 4.30-4.20 (m, 1H), 3.62 (d, 2H,  $J$  = 4.0 Hz), 1.57 (s, 3H), 1.35 (s, 3H).



*5'-Azido-5'-deoxyuridine.*

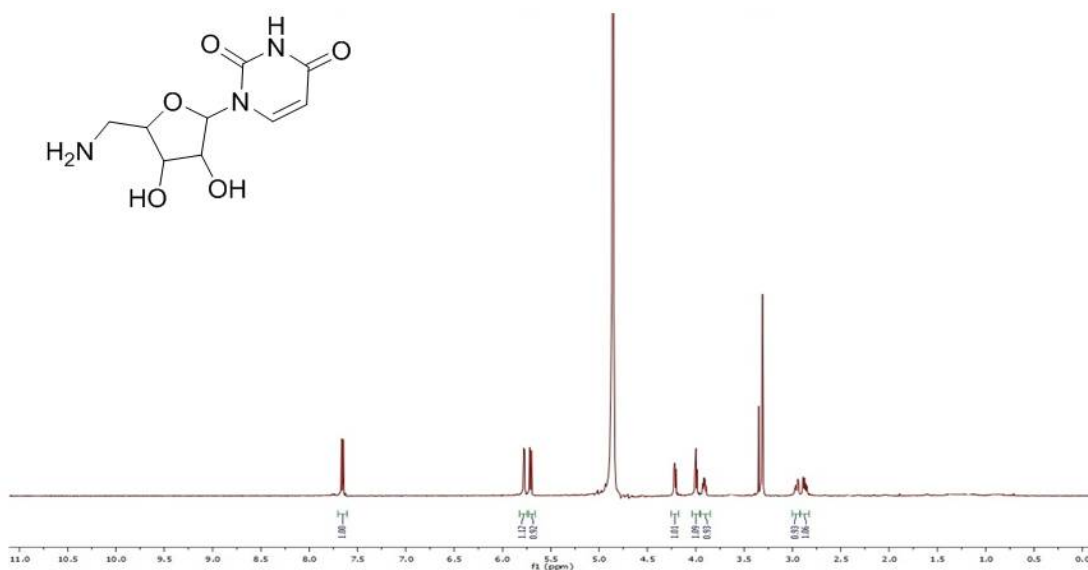
2',3'-O-Isopropylidene-5'-O-toluenesulfonyluridine (4.1 g, 13.3 mmol) was added to 90% TFA in water (75 mL) and the solution stirred at room temperature until

completion (10 min) as monitored by TLC ( $\text{CHCl}_3$ :MeOH, 6:1). After drying by rotary evaporation, the product was purified by silica gel chromatography ( $\text{CHCl}_3$ :MeOH, 6:1) to yield 2.9 g (81 %) of 5'-azido-5'-deoxyuridine.  $^1\text{H}$ -NMR ( $\text{CD}_3\text{OD}$ , 500 MHz):  $\delta$  7.72 (d, 1H,  $J$  = 8.0 Hz), 5.84 (d, 1H,  $J$  = 4.5 Hz), 5.74 (d, 1H,  $J$  = 8.0 Hz), 4.22 (t, 1H,  $J$  = 5.5 Hz), 4.10 (t, 1H,  $J$  = 5.5 Hz), 4.08-4.02 (m, 1H), 3.68 (dd, 1H,  $J$  = 13.0, 3.0 Hz), 3.60 (dd, 1H,  $J$  = 13.0, 4.5 Hz).



#### ***5'-Amino-5'-deoxyuridine, 2.***

5'-azido-5'-deoxyuridine (2 g, 7.43 mmol) was suspended in anhydrous methanol (48 mL) and purged with  $\text{N}_2$ . Following the addition of 10% Pd/C (0.4 g),  $\text{H}_2$  gas was bubbled through and the solution was stirred for at room temperature until completion (3 hr) as monitored by TLC ( $\text{CHCl}_3$ :MeOH:acetic acid 1:1:1). After filtration and drying by rotary evaporation, the product was purified by silica gel chromatography ( $\text{CHCl}_3$ :MeOH:acetic acid 1:1:1) to yield 1.7 g (96 %) of 5'-amino-5'-deoxyuridine (**2**).  $^1\text{H}$ -NMR ( $\text{CD}_3\text{OD}$ , 500 MHz):  $\delta$  7.66 (d, 1H,  $J$  = 8.5 Hz), 5.77 (d, 1H,  $J$  = 4.5 Hz), 5.71 (d, 1H,  $J$  = 8.5 Hz), 4.22 (dd, 1H,  $J$  = 6.0, 5.0 Hz), 3.99 (dd, 1H,  $J$  = 6.0, 5.0 Hz), 3.95-3.88 (m, 1H), 2.96 (dd, 1H,  $J$  = 13.5, 4.5 Hz), 2.88 (dd, 1H,  $J$  = 13.5, 7.0 Hz).

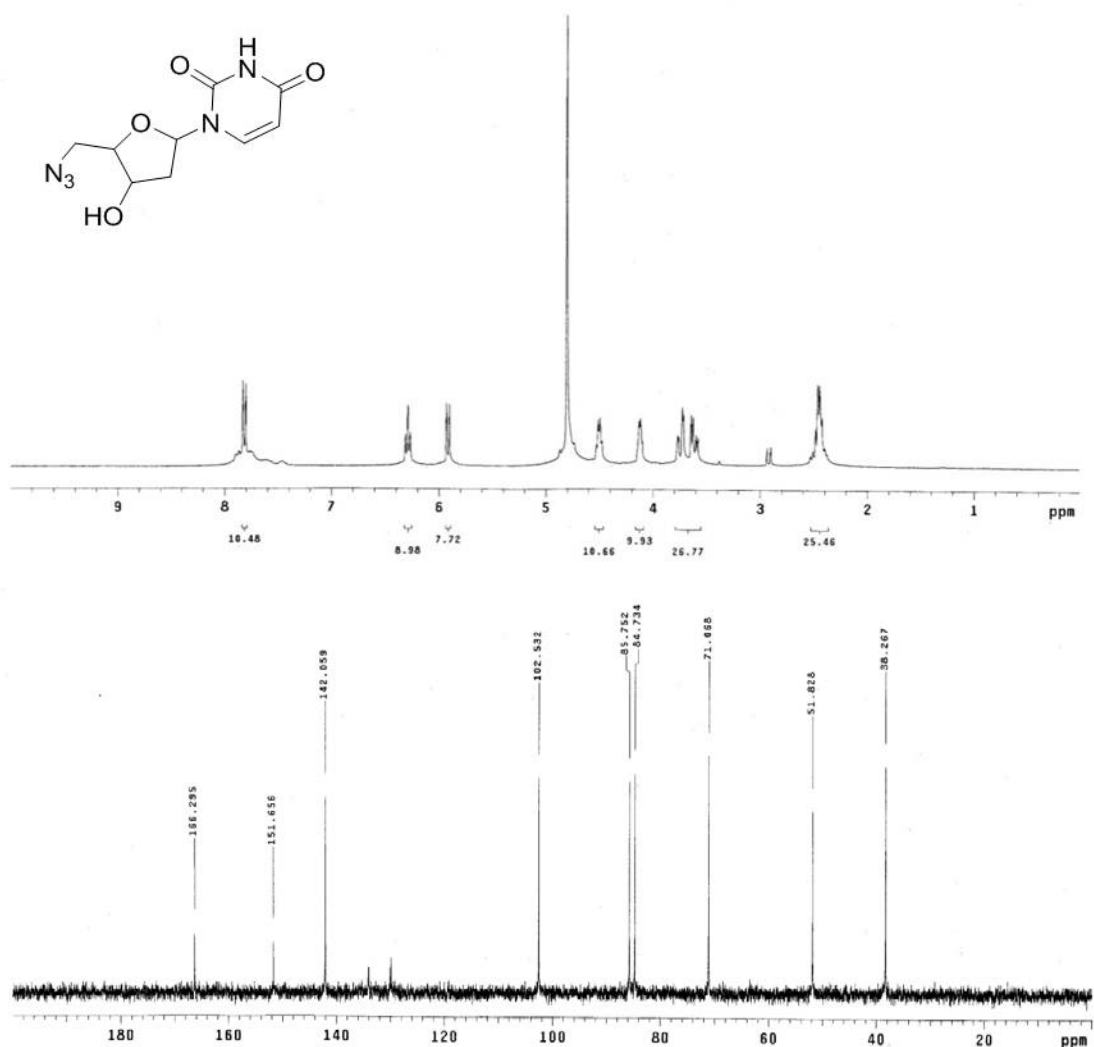


### 2.2.6. Synthesis of 5'-amino-2',5'-dideoxyuridine, 7

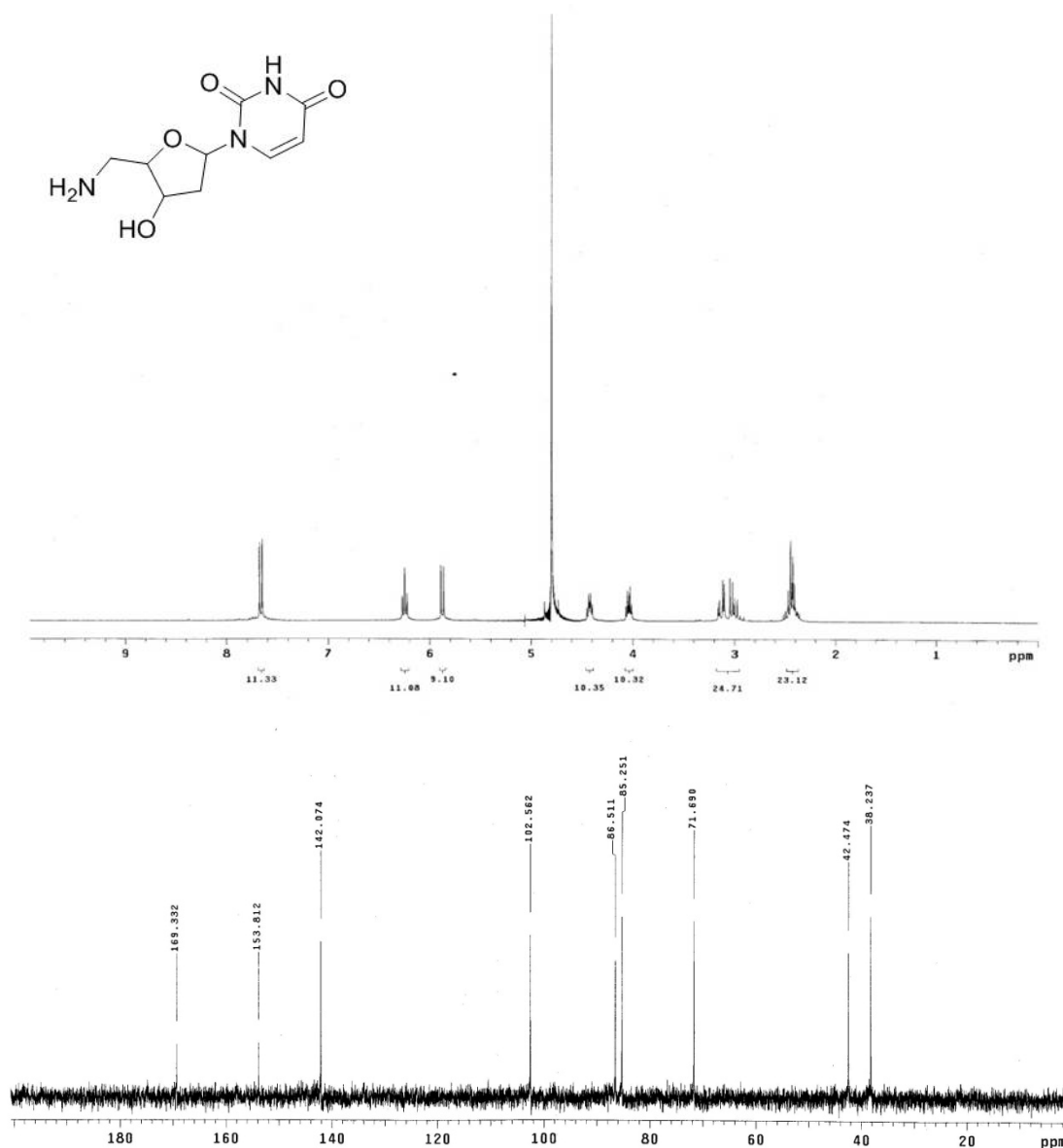
The synthesis of 5'-amino-2',5'-dideoxyuridine(**7**) followed a previously described two-step procedure with minor modifications [79]. Lithium azide was prepared from sodium azide and lithium sulfate as previously described [78].

**5'-Azido-2',5'-dideoxyuridine.** To a solution of 2'-deoxyuridine (0.95 g, 4.2 mmol) in dry DMF (20 mL) was sequentially added triphenylphosphine (1.2 g, 4.6 mmol), lithium azide (1.07 g, 22 mmol), and carbon tetrabromide (1.5 g, 4.6 mmol), and the solution stirred vigorously at room temperature until completion (16 hr) as monitored by TLC (CHCl<sub>3</sub>:MeOH, 15:1). After drying by rotary evaporation, the product was purified by silica gel chromatography (CHCl<sub>3</sub>:MeOH, 15:1) to yield 0.74 g (70 %) of 5'-azido-2',5'-dideoxyuridine. <sup>1</sup>H-NMR (300MHz, D<sub>2</sub>O): δ 7.82 (d, 1H, *J* = 13.5 Hz), 6.29 (t, 1H, *J* = 11.5Hz), 5.92 (d, 1H, *J* = 14.0Hz), 4.53-4.45 (m, 1H), 4.15-4.07 (m, 1H), 3.76-3.55 (m, 2H), 2.46-2.39 (m, 2H); <sup>13</sup>C-NMR (75MHz, D<sub>2</sub>O): δ 166.3 (C), 151.7 (C), 142.1 (CH), 102.5 (CH), 85.8 (CH), 84.7 (CH), 71.1 (CH), 51.8 (CH<sub>2</sub>), 38.3 (CH<sub>2</sub>).





5'-Amino-2',5'-dideoxyuridine, 7.5'-azido-5'-deoxyuridine (0.5 g, 2.0 mmol) was suspended in anhydrous methanol (12 mL) and purged with N<sub>2</sub>. Following the addition of 10% Pd/C (0.1 g), H<sub>2</sub> gas was bubbled through and the solution was stirred for at room temperature until completion (3 hr) as monitored by TLC (CHCl<sub>3</sub>:MeOH:acetic acid 1:1:1). After filtration and drying by rotary evaporation, the product was purified by silica gel chromatography (CHCl<sub>3</sub>:MeOH:acetic acid 1:1:1) to yield 0.38 g (84 %) of 5'-amino-2',5'-dideoxyuridine(7). <sup>1</sup>H-NMR (300 MHz, D<sub>2</sub>O): δ 7.67 (d, 1H, *J* = 13.5 Hz), 6.25 (t, 1H, *J* = 11.5 Hz), 5.88 (d, 1H *J* = 13.5 Hz), 4.55-4.35 (m, 1H), 4.08-4.00 (m, 1H), 3.20-2.90 (m, 2H), 2.50-2.38 (m, 2H); <sup>13</sup>C-NMR (75 MHz, D<sub>2</sub>O): δ 169.3 (C), 153.8 (C), 142.1 (CH), 102.6 (CH), 86.5 (CH), 85.2 (CH), 71.7 (CH), 42.5 (CH<sub>2</sub>), 38.2 (CH<sub>2</sub>).



### 2.2.7. Cloning of genes for heterologous expression

Genes were amplified by PCR using Expand Long Template PCR System with supplied Buffer 2, 200  $\mu$ M dNTPs, 5% DMSO, 10 ng DNA template, 5 U DNA polymerase, and 200 nM each of the separate primer pairs (**Table 1**). DNA templates for PCR cloning were *E. coli* DH5 $\alpha$  genomic DNA (*Ecudp*) or cosmid pN1 (*lipP*, *M*, *O* and *N* genes). The PCR program included an initial hold at 94  $^{\circ}$ C for 2 min, followed by 30 cycles of 94  $^{\circ}$ C for 10 s, 56  $^{\circ}$ C for 15 s, and 68  $^{\circ}$ C for 50 s. The gel-purified

PCR product was inserted into pET-30 Xa/LIC using ligation-independent cloning as described in the provided protocol to yield pET30-*LipP*, pET30-*Ecudp*, pET30-*LipM*, etc (**Table 2**). The genes were sequenced to confirm PCR fidelity.

**Table 1.** List of primers used in A-90289.

Primers	Oligonucleotide sequence
<i>lipP_for</i>	5'-GGTATTGAGGGTTCGCATGAACGAGACAATCGGGGTTG-3'
<i>lipP_rev</i>	5'-AGAGGAGAGTTAGAGCCCTAGACATGGATCATCCCCG-3'
<i>Ecudp_for</i>	5'-GGTATTGAGGGTTCGCATGTCCAAGTCTGATGTTTTTCATC-3'
<i>Ecudp_rev</i>	5'-AGAGGAGAGTTAGAGCCTTACAGCAGACGACGCGCCG-3'
<i>lipO_for</i>	5'-GGTATTGAGGGTTCGCATGTCCGTGCTGGGGCGG-3'
<i>lipO_rev</i>	5'-AGAGGAGAGTTAGAGCCTCATGAGGGCTTCTTCGGTG-3'
<i>lipO(K282A)_for</i>	5'-GACCTGACCGCCTTCAGC <u>GCG</u> GGCCTGACCAACGGCGTG-3'
<i>lipO(K282A)_rev</i>	5'-CACGCCGTTGGTCAGGCC <u>GCG</u> GCTGAAGGCGGTCAGGTC-3'
<i>lipM_for</i>	5'-GGTATTGAGGGTTCGCATGAAGGTGTCCGTCATCATC-3'
<i>lipM_rev</i>	5'-AGAGGAGAGTTAGAGCCTCAGCACTCCGGGCATCG-3'
<i>lipN_for</i>	5'-GGTATTGAGGGTTCGCATGCCCGGAG-3'
<i>lipN_rev</i>	5'-AGAGGAGAGTTAGAGCCTCATCGTCC-3'

Plasmids were introduced into *E. coli* BL21 (DE3) cells, and the transformed strains were grown in LB supplemented with 50 µg/mL kanamycin. Following inoculation of 500 mL of LB with 50 µg/mL kanamycin, the cultures were grown at 18°C until the cell density reached an OD<sub>600</sub> ~ 0.5 when expression was induced with 0.1 mM IPTG. Cells were harvested after an overnight incubation at 18 °C and lysed using a French Press with one pass at 15000 psi. Following centrifugation the protein was purified using affinity chromatography with Ni-NTA agarose, and the recombinant proteins were desalted into 50 mM Tris-HCl (pH 8), 100 mM NaCl, and 5 % glycerol using a PD-10 desalting column. The purified protein was concentrated using an Amicon Ultra 10000 MWCO centrifugal filter and stored as glycerol stocks (40%) at -20 °C. Protein purity was assessed as by 12% acrylamide SDS-PAGE; His<sub>6</sub>-tagged proteins were utilized without further modifications.

**Table 2. List of plasmids constructed/used in A-90289.**

Strain/Plasmid	Characteristics and Relevance	References
<i>E.coli</i> Nova-Blue	host for routine cloning works	Novagen
<i>E.coli</i> BL21 (DE3)	host for protein expression	Novagen
pET30	expression vector	Novagen
pET30- <i>lipP</i>	<i>lipP</i> gene cloned to pET30	This study
pET30- <i>Ecudp</i>	<i>Ecudp</i> gene cloned to pET30	This study
pET30- <i>lipO</i>	<i>lipO</i> gene cloned to pET30	This study
pET30- <i>lipM</i>	<i>lipM</i> gene cloned to pET30	This study
pET30- <i>lipN</i>	<i>lipN</i> gene cloned to pET30	This study
pUWL201pw	expression vector	This study
pUWL201pw- <i>lipM</i>	<i>lipM</i> gene cloned to pUWL201pw	This study
pUWL201pw- <i>lipO</i>	<i>lipO</i> gene cloned to pUWL201pw	This study
pUWL201pw- <i>lipO</i> (K282A)	<i>lipO</i> (K282A) gene cloned to pUWL201pw	This study
pUWL201pw- <i>lipN</i>	<i>lipN</i> gene cloned to pUWL201pw	This study

### 2.2.8. *In vitro* characterization of LipP

Reactions consisted of 25 mM potassium phosphate pH 7.5, 2 mM uridine (**3**) or analogue, and 100 nM LipP at 30 °C, and terminated by the addition of cold TCA to 5% (w/v) or by ultrafiltration using a Microcon YM-3. Following centrifugation to remove protein, the reaction components were analyzed by HPLC using a C-18 reverse-phase column. A series of linear gradients was developed from 0.1 % TFA in 5 % acetonitrile (A) to 0.1 % TFA in 90% acetonitrile (B) in the following manner (beginning time and ending time with linear increase to % B): 0-4 min, 100% B; 4-24 min, 50% B; 24-26 min, 100% B; 26-32 min, 100% B; and 32-35 min, 0% B. The flow rate was kept constant at 1.0 mL/min, and elution was monitored at 260 nm. LC-MS was performed using a linear gradient from 0.1% formic acid in water to 0.1% formic acid in acetonitrile over 20 min. The flow rate was kept constant at 0.4 mL/min, and elution was monitored at 254 nm.

The effect of pH on LipP activity was carried out in 50 mM indicated buffer, 2.5 mM potassium phosphate, 2.5 mM uridine (**3**), and 1  $\mu$ M LipP for 5 min at 30 °C. The

reactions were terminated with 0.1 M sodium hydroxide, and uracil (**4**) formation was determined by UV/Vis spectroscopy with  $\Delta\epsilon_{290\text{ nm}} = 5,700\text{ M}^{-1}$  at pH 13. To determine the kinetic constants with respect to the co-substrate nucleoside, reactions were carried out in 50 mM Tris-HCl pH 9.0 consisting of saturating phosphate (1.5 mM) and variable nucleoside (10 - 4,700 M uridine, 10 – 10,000 M 2'-deoxy-uridine (**11**), 8 - 800 M 5'-amino-5'-deoxyuridine (**2**), or 30 - 3000 M uridine-5'-aldehyde (**1**), and 100 nM LipP at 30 °C under initial velocity conditions. Single substrate kinetics at pH 7.5 was carried out using identical conditions except with increased LipP (730 nM). Kinetic analysis with *Ec*Udp was carried out with final enzyme concentrations of 100 nM at pH 9.0 and 200 nM at pH 7.5.

#### **2.2.9. Subcloning and expression in *S. lividans* TK-64**

Plasmids pET30-*lipM*, pET30-*lipO*, pET30-*lipO*(K282A) and pET30-*lipN* were digested with *Nde*I-*Hind*III and the DNA fragment of the expected size was purified and ligated to the identical sites of pUWL201pw to yield pUWL201pw-*lipM*, pUWL201pw-*lipO*, pUWL201pw-*lipO*(K282A), and pUWL201pw-*lipN*, respectively. The resulting plasmids were transformed into *S. lividans* TK-64 using PEG-mediated protoplast transformation and plated on R2YE. After 14 hr at 28 °C, the plates were overlaid with 1 mL of water supplemented with 200 µg of thiostrepton. Single colonies were transferred to fresh R2YE plates supplemented with 10 µg/mL thiostrepton, and after 4 days at 28 °C positive transformants were confirmed by colony PCR using InstaGene Matrix from Bio-Rad and LA-Taq polymerase with GC buffer II. A single colony was utilized to inoculate 50 mL R2YE containing 10 µg/mL thiostrepton, grown for 2 days at 28 °C at 250 rpm, and 2 mL transferred to fresh 50 mL containing 10 µg/mL thiostrepton. Following growth for 3 days at 28 °C at 250 rpm, the cells were collected by centrifugation and washed with 10% glycerol prior to lysis by French press and protein purification as described above.

### 2.2.10. *In vitro* characterization of LipM

Reactions consisted of 50 mM potassium phosphate pH 7.5, 5 mM MgCl<sub>2</sub>, 2 mM uridine (**3**) or analogue, 5 mM nucleotide triphosphate, 5 μM LipP, and 1 μM LipM at 30 °C, and the reaction terminated by the addition of cold TCA to 5% (w/v) or by ultrafiltration using a Microcon YM-3. The activity of LipM was tested with sugar-1-phosphates generated in situ from synthetic uridine (**3**), 2'-deoxy-uridine (**11**), 5'-amino-5'-deoxyuridine (**2**), or 5'-amino-2',5'-dideoxyuridine (**7**) and the cosubstrate nucleotide UTP, dUTP, TTP, rCTP, dCTP, dGTP, rGTP, dATP, or rATP. Following centrifugation to remove protein, the reaction components were analyzed by HPLC using a C-18 reverse-phase analytical column. A series of linear gradients was developed from 40 mM phosphoric acid-triethylamine pH 6.5 (C) to 20% methanol (D) in the following manner (beginning time and ending time with linear increase to % D): 0-8 min, 100% D; 8-18 min, 60% D; 18-25 min, 95% D; 25-32 min, 95% D; and 32-35 min, 0% D. The flow rate was kept constant at 1.0 mL/min, and elution was monitored at 260 nm. LC-MS and NMR were performed as above.

### 2.2.11. OPA-modification and analysis of the LipM product

Amine-containing compounds were detected by precolumn modification with o-phthalaldehyde (OPA). Following the enzyme reaction, LipM was removed by ultrafiltration and an equal volume of OPA solution (to 4 mg of OPA was sequentially added 50 μL ethanol, 4.5 mL 0.1 M sodium borate pH 9.5, and 11 μL β-mercaptoethanol) was added. The modified reaction components were analyzed by HPLC using a C-18 reverse-phase analytical column. A series of linear gradients was developed from 50 mM sodium acetate pH 6.0 in 5% acetonitrile (A) to 50 mM sodium acetate pH 6.0 in 50% acetonitrile and 40% methanol (B) in the following manner (beginning time and ending time with linear increase to % B): 0-4 min, 0% B; 4-24 min, 50% B; 24-26 min, 100% B; 26-32 min, 100% B; and 32-35 min, 0% B. The flow rate was kept constant at 1.0 mL/min, and elution was monitored at 335 nm.

LC-MS was performed using a linear gradient from 0.1% formic acid in water to 0.1% formic acid in acetonitrile over 20 min. The flow rate was kept constant at 0.4 mL/min, and elution was monitored at 335 nm.

#### 2.2.12. Production of the LipM product for mass and NMR spectroscopy

Large scale production and isolation of the OPA-modified product was identical to the reactions described above using 5'-amino-5'-deoxyuridine (**2**) and UTP as the starting substrates with the following modifications: sodium acetate was substituted with ammonium acetate for HPLC and a semipreparative HPLC column was used with a flow rate of 3.5 mL/min. The peak corresponding to the product (5'-isoindoline-5'-deoxyribose-1',2'-cyclic phosphate) was collected and freeze-dried prior to spectroscopic analysis. <sup>1</sup>H-NMR (500MHz, D<sub>2</sub>O):  $\delta$  7.72 (d, 1H,  $J=7.5$  Hz, H-7), 7.62 (t, 1H,  $J=7.5$  Hz, H-5), 7.54 (d, 1H,  $J=7.5$  Hz, H-4), 7.50 (t, 1H,  $J=7.5$  Hz, H-6), 5.90 (dd, 1H,  $J=4.5, 17.5$  Hz, H-'), 4.95-4.80 (m, 1H, H-2'), 4.65 (d, 1H,  $J=18.0$  Hz, H-3), 4.53 (d, 1H,  $J=18.0$  Hz, H-3), 4.32-4.29 (m, 1H, H-4'), 3.99-3.93 (m, 2H, H-3', H-5'), 3.87 (d, 1H,  $J=15.0$  Hz, H-5'); <sup>13</sup>C-NMR (125 MHz, D<sub>2</sub>O):  $\delta$  171.1 (C-1), 142.3 (C-1a), 132.2 (CH-5), 130.6 (C-3a), 127.9 (CH-6), 122.9 (CH-4), 122.8 (CH-7), 100.9 (CH-1'), 78.3 (CH-2'), 78.1 (CH-4'), 71.7 (CH-3'), 52.1 (CH<sub>2</sub>-3), 42.8 (CH<sub>2</sub>-5'); <sup>31</sup>P-NMR (202.5 MHz, D<sub>2</sub>O):  $\delta$ 19.05.

Large scale isolation of the LipM product starting from 5'-amino-2',5'-dideoxyuridine(**7**) was carried out with HPLC using a C-18 reverse-phase semipreparative column. A series of linear gradients was developed from 50 mM acetic acid-triethylamine pH 6.5 (C) to 50 mM acetic acid-triethylamine pH 6.5 containing 20 % methanol (D) in the following manner (beginning time and ending time with linear increase to % H): 0-8 min, 0% D; 8-18 min, 60% D; 18-25 min, 95% D; 25-32 min, 95% D; and 32-35 min, 0% D. The flow rate was kept constant at 3.5 mL/min, and elution was monitored at 260 nm. The peak corresponding to the

product UDP-5"-amino-2",5"-dideoxyribose (**8**) was collected and freeze-dried prior to spectroscopic analysis. <sup>1</sup>H-NMR (500MHz, D<sub>2</sub>O): δ 7.95 (d, 1H, *J* = 8.0 Hz, H-5), 6.00-5.88 (m, 3H, H-4, H-1', H-1"), 4.45-4.33 (m, 3H, H-4', H-3', H-2'), 4.30-4.17 (m, 4H, H-5', H-4", H-3"), 3.33 (d, 1H, *J* = 13.0 Hz, H-5"), 2.98 (dd, 1H, *J* = 12.5, 10.5 Hz, H-5"), 2.53-2.45 (m, 1H, H-2"), 2.24-2.15(m, 1H, H-2"); <sup>13</sup>C-NMR (125 MHz, D<sub>2</sub>O): δ 166.1 (C-3), 151.7 (C-1), 141.6 (CH-5), 102.5 (CH-1"), 100.9 (CH-4), 88.3 (CH-1'), 83.2 (CH-4"), 81.8 (CH-3'), 73.7 (CH-2'), 71.7 (CH-3"), 69.5 (CH<sub>4</sub>'), 64.7 (CH<sub>2</sub>-5'), 41.0 (2 × CH<sub>2</sub>, 2" & 5"); <sup>31</sup>P-NMR (202.5 MHz, D<sub>2</sub>O): δ -11.66 (d, *J* = 20.4 Hz), -13.67 (d, *J* = 17.8 Hz).

### 2.2.13. *In vitro* characterization of LipO activity

Reactions consisted of 50 mM potassium phosphate pH 7.5, 2 mM uridine-5'-aldehyde (**1**), 2 mM amine donor, 200 μM PLP, and 1 μM LipO at 30 °C, and the reaction terminated by the addition of cold TCA to 5% (w/v) or by ultrafiltration using a Microcon YM-3. Alternatively, PLP was eliminated from the reaction mixture to give comparable results. HPLC analysis of the reaction was similar to that described for LipM.

### 2.2.14. Site-directed mutagenesis of LipO

A K282A point mutation of LipO was generated by PCR amplification using pET30-*LipO* as a template and the Expand Long Template PCR system. Reactions were performed using the manufacturer's provided Buffer 2 with 5% DMSO, primers (**Table 2**) and the reverse complement (the engineered Ala codon is underlined), and a PCR program consisting of an initial hold at 94 °C for 2 min followed by 20 cycles of 94 °C for 10 s, 56 °C for 20 s, and 68 °C for 7 min. The template DNA was digested with 10 units of *DpnI* for 1 h at 37 °C and transformed into *E. coli* DH5α competent cells. The introduction of the correct point mutation and the sequence of



the entire gene including 200 bp upstream and downstream were confirmed by DNA sequencing to yield pET30-*lipO*(K282A).

#### **2.2.15. *In vitro* characterization of LipN activity**

Reactions consisted of 50 mM potassium phosphate pH 7.5, 2 mM 5'-amino-5'-deoxyuridine (**2**), 2.8  $\mu$ M LipP at 30 °C for 2 hours. LipP was removed by ultrafiltration, and 86 $\mu$ L of the filtrate was added to a solution of 5 mM MgCl<sub>2</sub>, 2 mM UTP, 1 mM uridine (**3**), 12  $\mu$ M LipM, and 7  $\mu$ M LipN (final volume of 100  $\mu$ L) and incubated at 30 °C for the indicated time points. HPLC analysis was performed using a TFA mobile phase as described above.

#### **2.2.16. Production of the LipN product for mass and NMR spectroscopy**

Large scale isolation of the LipN product starting from 5'-amino-5'-deoxyuridine (**2**) was carried out with HPLC using a C-18 reverse-phase semipreparative column using the above conditions for OR25 starting from 5'-amino-2',5'-dideoxyuridine (**7**) except acetic acid-triethylamine was substituted with TFA. The peak corresponding to the product 5'-O-(5''-amino-5''-deoxyribose)-uridine (**9**) was collected and freeze-dried prior to spectroscopic analysis. <sup>1</sup>H-NMR (500MHz, D<sub>2</sub>O):  $\delta$  7.73 (d, 1H,  $J$  = 8.5 Hz, H-5), 5.89 (d, 1H,  $J$  = 8.5 Hz, H-4), 5.86 (d, 1H,  $J$  = 3.0 Hz, H-1'), 5.11 (s, 1H, H-1''), 4.38-4.34 (m, 1H, H-2'), 4.29-4.07 (m, 6H, H-2'', H-3', H-3'', H-4', H-4'', H-5'), 3.80-3.71 (m, 1H, H-5'), 3.38 (d, 1H,  $J$  = 13.0 Hz, H-5''), 3.04 (dd, 1H,  $J$  = 10, 13.0 Hz, H-5''), <sup>13</sup>C NMR (125 MHz, D<sub>2</sub>O):  $\delta$  166.0 (C-3), 151.3 (C-1), 141.7 (CH-5), 107.8 (CH-1''), 101.9 (CH-4), 90.1 (CH-1'), 81.9 (CH-3'), 78.3 (CH-3''), 73.9 (CH-4'), 73.2 (CH-2'), 72.5 (CH-4''), 69.1 (CH-2''), 68.1 (CH<sub>2</sub>-5'), 43.2 (CH<sub>2</sub>-5'').

## 2.3. Results: LipP Characterization

### 2.3.1. *In vitro* characterization of LipP activity

Our previous results have demonstrated that a non-heme, Fe(II)-dependent  $\alpha$ -KG:UMP dioxxygenase generates uridine-5'-aldehyde (**1**) from UMP to initiate the biosynthesis of the modified uridine (**3**) component, 5'-C-glycyluridine, of A-90289 [88]. Thus, the aminoribosyl moiety was potentially derived from uridine (**3**), uridine-5'-aldehyde (**1**) or 5'-amino-5'-deoxyuridine (**2**) (**Fig 2.4**). These hypothetical intermediate were therefore synthesized with the expectation that one of these would serve as a substrate for the phosphorylase LipP.

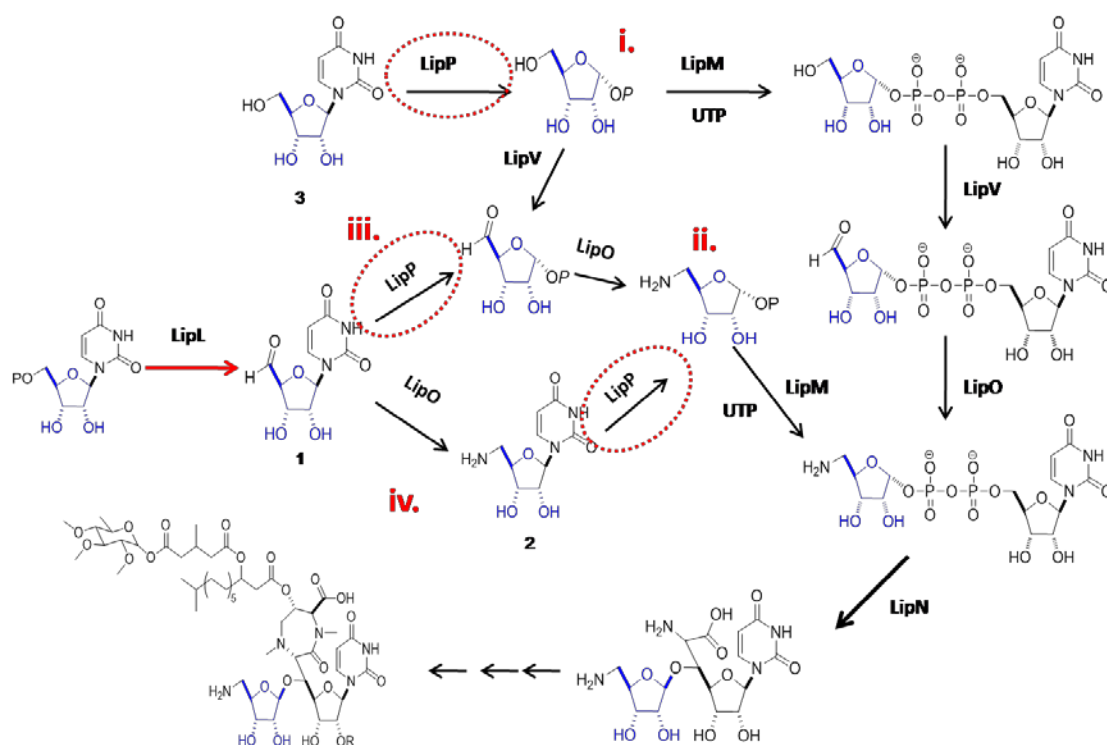


**Figure 2.4.** Proposed biosynthetic pathway for the incorporation of the aminoribosyl moiety of A-90289.

Bioinformatics analysis revealed LipP has sequence similarity to proteins annotated as uridine phosphorylases (Udp), an enzyme family that catalyzes the

phosphorolysis of uridine (**3**) or—less efficiently—thymidine nucleosides to generate  $\alpha$ -D-ribose-1-phosphate and uracil (**4**) or thymine, respectively, to initiate nucleotide salvage pathways (**Fig 2.5**)[92]. Although inactive with the 5'-monophosphorylated nucleotide, both human and mouse Udp have been shown to have modest activity with unnatural 5'-deoxynucleosides [93,94]. However, the potential activity of Udp with the 5'-modifications under investigation has not been reported, so it remained unclear as to the chemical identity of the LipP substrate.

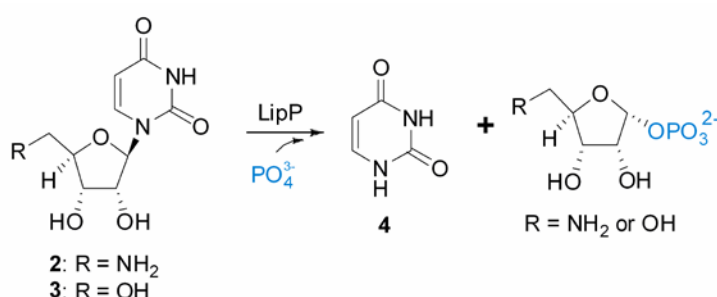


**Figure 2.5.** Phosphorylase reaction catalyzed by LipP.

The *lipP* gene was cloned and expressed in *E. coli* to yield soluble protein with the expected size (**Fig 2.6**). Initial activity tests using HPLC revealed uridine (**3**) is rapidly converted to uracil (**4**) and  $\alpha$ -D-ribose-1-phosphate by LipP (**Fig 2.7 a**) as expected. In addition to the formation of the pyrimidine base, LC-MS analysis of the reaction revealed an (M - H)<sup>-</sup> ion at  $m/z = 228.7$  that was absent in the control (**Fig 2.8 c**), a mass that is consistent with the molecular formula C<sub>5</sub>H<sub>9</sub>NO<sub>8</sub>P of the expected product  $\alpha$ -D-ribose-1-phosphate. Further activity tests revealed the hypothetical pathway intermediates uridine-5'-aldehyde (**1**) and 5'-amino-5'-deoxyuridine (**2**) were also converted to uracil (**4**) and the respective sugar-1-phosphate by LipP (**Fig 2.7 b,c**), thus warranting further kinetic investigation for LipP.

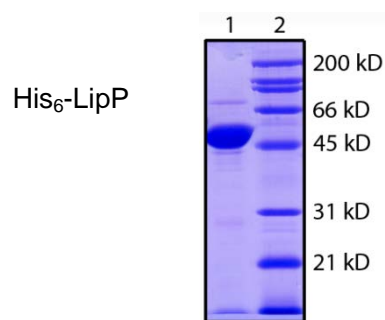


**Figure 2.6.** SDS-PAGE analysis of purified His<sub>6</sub>-LipP (expected MW of 52.9 kD).

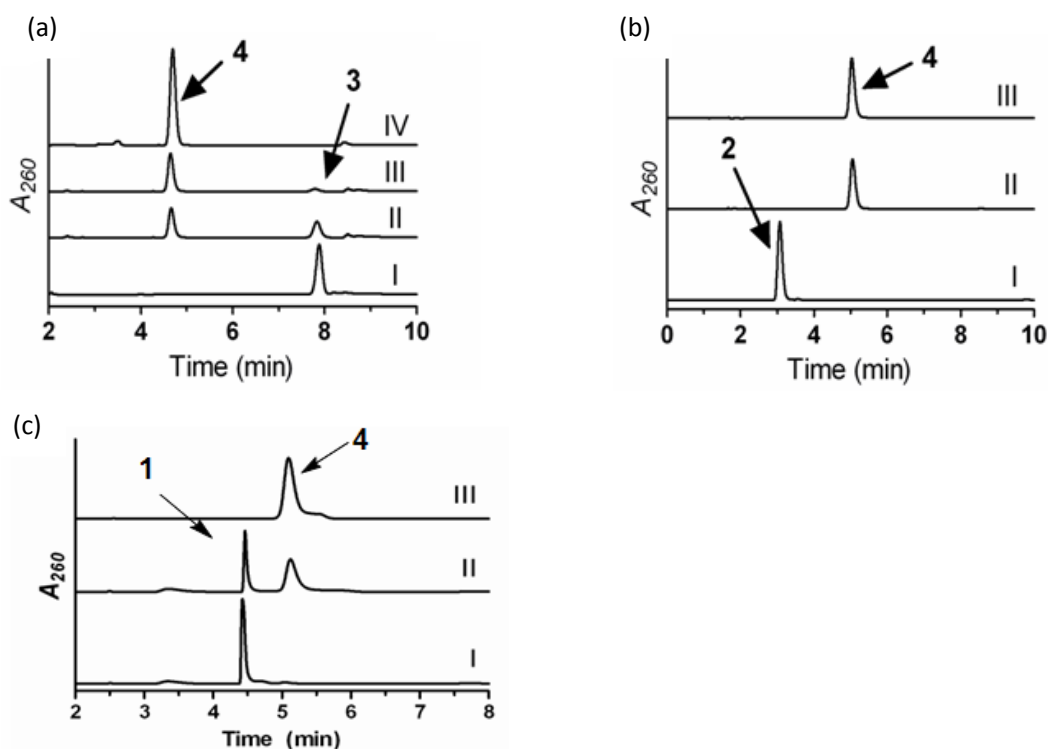


**Figure 2.7.** Characterization of LipP by HPLC. (a) HPLC analysis using uridine (**3**) after (I) 30 min without LipP, (II) 5 min reaction, (III) 30 min reaction, and (IV) authentic uracil (**4**). (b) HPLC analysis using 5'-amino-5'-deoxyuridine (**2**) after (I) 30 min without LipP, (II) 30 min reaction, and (III) authentic uracil (**4**). (c) HPLC analysis of the reaction using substrate uridine-5'-aldehyde (**1**) after (I) 3 hr without LipP, (II) 3 hr reaction, and (III) authentic uracil (**4**).  $A_{260}$ , absorbance at 260 nm.

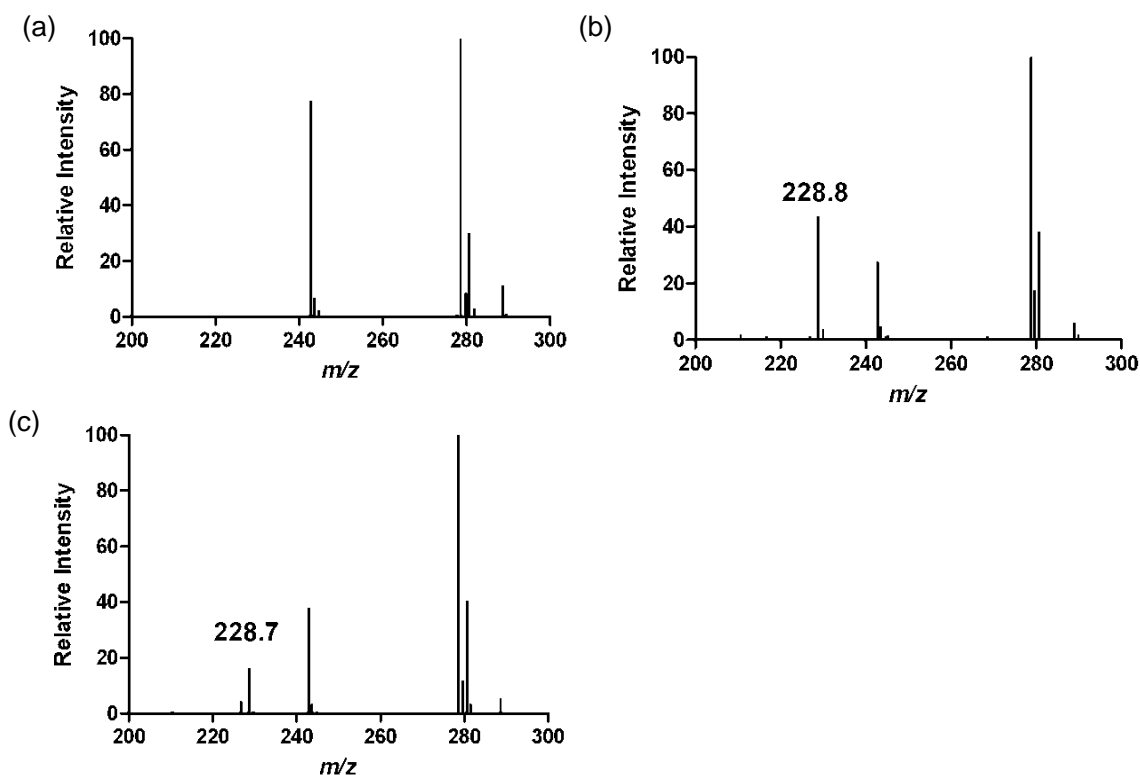


**Figure 2.8.** LC-MS analysis of the phosphorylase reaction. (a) Mass spectrum for the ion peak eluting at time  $t = 2.852$  min of the reaction mixture without enzyme. (b) Mass spectrum for the ion peak eluting at time  $t = 2.852$  min of the *EcUdp* reaction. (c) Mass spectrum for the ion peak eluting at time  $t = 2.852$  min of the LipP reaction.

### 2.3.2. Kinetics characterization of LipP

The pH profile for LipP was initially examined using 5'-amino-5'-deoxyuridine (**2**) or uridine (**3**) as a substrate and detection of uracil (**4**) by UV/Vis spectroscopy (**Fig 2.9 a**) [95], revealing an apparent optimal activity for LipP at pH = 9.0, which is moderately higher than reported for *EcUdp* (pH ~ 7.5) (**Fig 2.9 b**) [96]. As a result, single substrate kinetic analysis was performed at both pH 9.0 and 7.5 with all hypothetical pathway intermediates (**Fig 2.9 c-f**). The extracted kinetic constants (**Table 3**) revealed that LipP has comparable efficiency with 5'-amino-5'-deoxyuridine (**2**) and uridine (**3**) at pH 9.0, thus both appear to be viable substrates *in vivo*. Saturation kinetics could not be reached with uridine-5'-aldehyde (**1**) (**Fig 2.9g**), and the relatively low first-order rate constant of  $k = (3.0 \pm 0.5) \times 10^{-2} \text{ min}^{-1}$  suggests that uridine-5'-aldehyde (**1**) is less probable as the *in vivo* substrate.

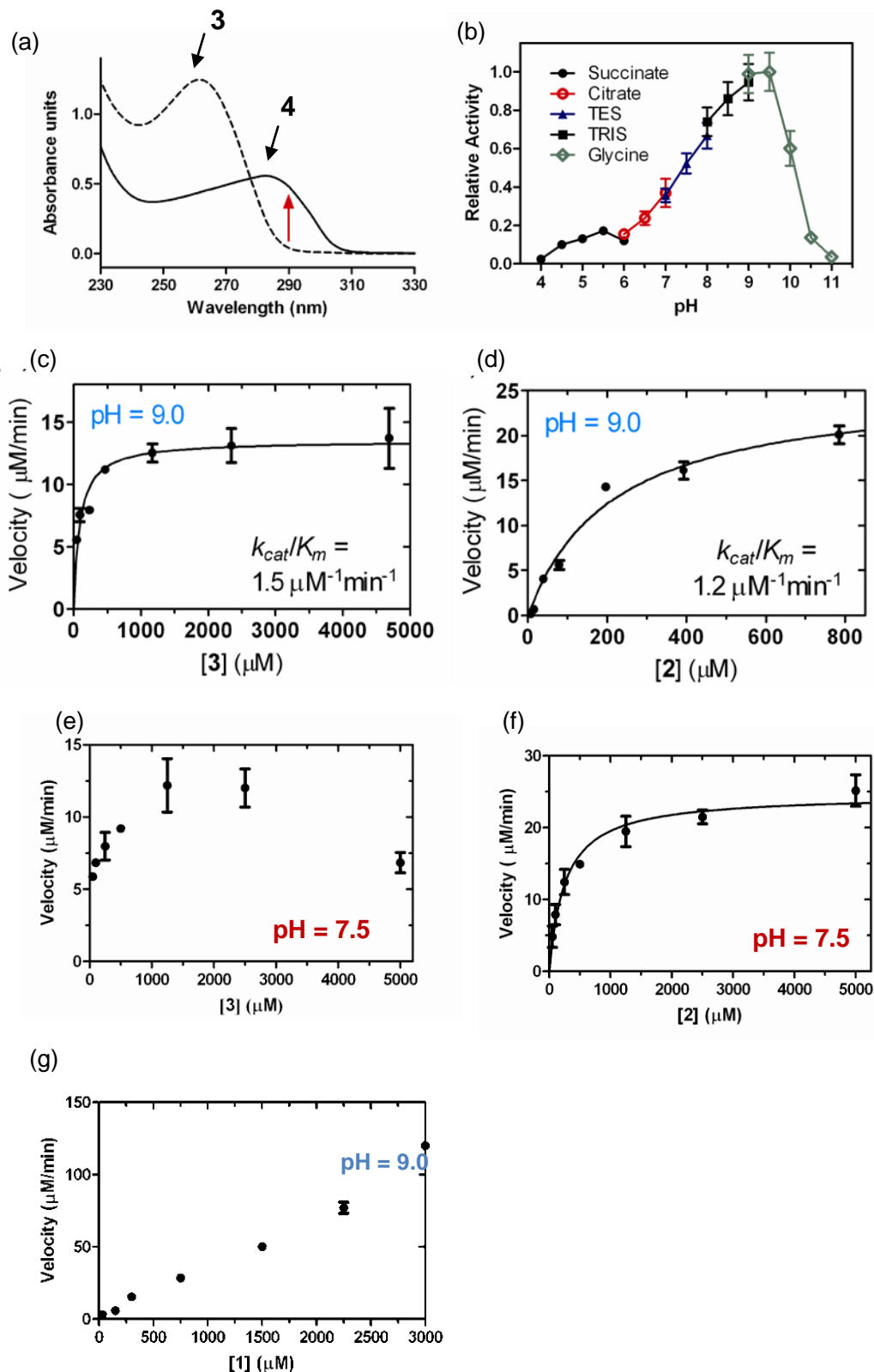


**Figure 2.9.** Kinetic characterization of LipP. a) Assay by UV/Vis spectroscopy by taking advantage of the different absorption profiles of uridine (3) and uracil (4) at alkaline pH. Shown are spectra of standards at pH ~ 13. (b) pH profile using the indicated buffers. (c) Single-substrate kinetic analysis with variable uridine (3) at pH

9.0. (d) Single-substrate kinetic analysis with variable 5'-amino-5'-deoxyuridine (**2**) at pH 9.0. (e) Single-substrate kinetic analysis with variable uridine (**3**) at pH 7.5. (f) Single-substrate kinetic analysis with variable 5'-amino-5'-deoxyuridine (**2**) at pH 7.5. (g) Single-substrate kinetic analysis with variable uridine-5'-aldehyde (**1**) at pH 9.0.

**Table 3.** Extracted kinetic constants for LipP and *EcUdp*.

Enzyme	pH	Substrate <sup>a</sup>	$K_m$ ( $\mu\text{M}$ )	$k_{cat}$ ( $\text{min}^{-1}$ )	$k_{cat}/K_m$ ( $\mu\text{M}^{-1}\text{min}^{-1}$ )	Relative efficiency
LipP	9.0	Uridine ( <b>3</b> )	$87 \pm 21$	$(1.3 \pm 0.1) \times 10^2$	1.5	100
		Thymidine	$(2.8 \pm 0.2) \times 10^3$	$5.3 \pm 0.2$	$1.9 \times 10^{-3}$	0.13
		ADU ( <b>2</b> )	$(2.1 \pm 0.3) \times 10^2$	$(2.6 \pm 0.2) \times 10^2$	1.2	80
		2'-deoxyU( <b>1</b> )	$(3.1 \pm 0.4) \times 10^3$	$(2.1 \pm 0.8) \times 10^2$	$6.8 \times 10^{-2}$	4.5
	7.5	Uridine ADU ( <b>2</b> )	NA <sup>b</sup> $(2.6 \pm 0.5) \times 10^2$	NA <sup>b</sup> $34 \pm 1.6$	$1.3 \times 10^{-1}$	8.7
<i>EcUdp</i>	9.0	Uridine ( <b>3</b> )	$(1.3 \pm 0.2) \times 10^3$	$(2.6 \pm 0.1) \times 10^3$	2	100
		ADU ( <b>2</b> )	$(1.0 \pm 0.2) \times 10^3$	$(9.7 \pm 0.7) \times 10^2$	1.0	49
	7.5	Uridine ( <b>3</b> )	$(1.5 \pm 0.1) \times 10^3$	$(1.6 \pm 0.1) \times 10^3$	1.1	55
		ADU ( <b>2</b> )	$(2.0 \pm 0.5) \times 10^3$	$(3.2 \pm 0.4) \times 10^2$	$1.6 \times 10^{-1}$	8

<sup>a</sup>ADU, 5'-amino-5'-deoxyuridine; 2'-deoxyU, 2'-deoxyuridine.

<sup>b</sup>not applicable, non-Michaelis-Menten kinetics was observed.

### 2.3.3. *In vitro* characterization of *EcUdp* activity

Initial activity tests using HPLC revealed uridine (**3**) is rapidly converted to uracil (**4**) and  $\alpha$ -D-ribose-1-phosphate by *EcUdp* (**Fig 2.10 b**) as expected. This enzyme was characterized *in vitro* with hypothetical intermediates in the biosynthesis of the 5-amino-5-deoxyribosyl moiety of A-90289. For comparisons the *udp* gene from *E. coli* was also cloned and expressed to yield recombinant *EcUdp* (**Fig 2.10 a**). In addition to the formation of the pyrimidine base, LC-MS analysis of the reaction

revealed an  $(M - H)^-$  ion at  $m/z = 228.7$  that was absent in the control (**Fig 2.8b**), a mass that is consistent with the molecular formula  $C_5H_9NO_8P$  of the expected product  $\alpha$ -D-ribose-1-phosphate. Further activity tests revealed the hypothetical pathway intermediates uridine-5'-aldehyde (**1**) and 5'-amino-5'-deoxyuridine (**2**) were also converted to uracil (**4**) and the respective sugar-1-phosphate by *EcUdp* (**Fig 2.10 c,d**), thus warranting further kinetic investigation for *EcUdp*.

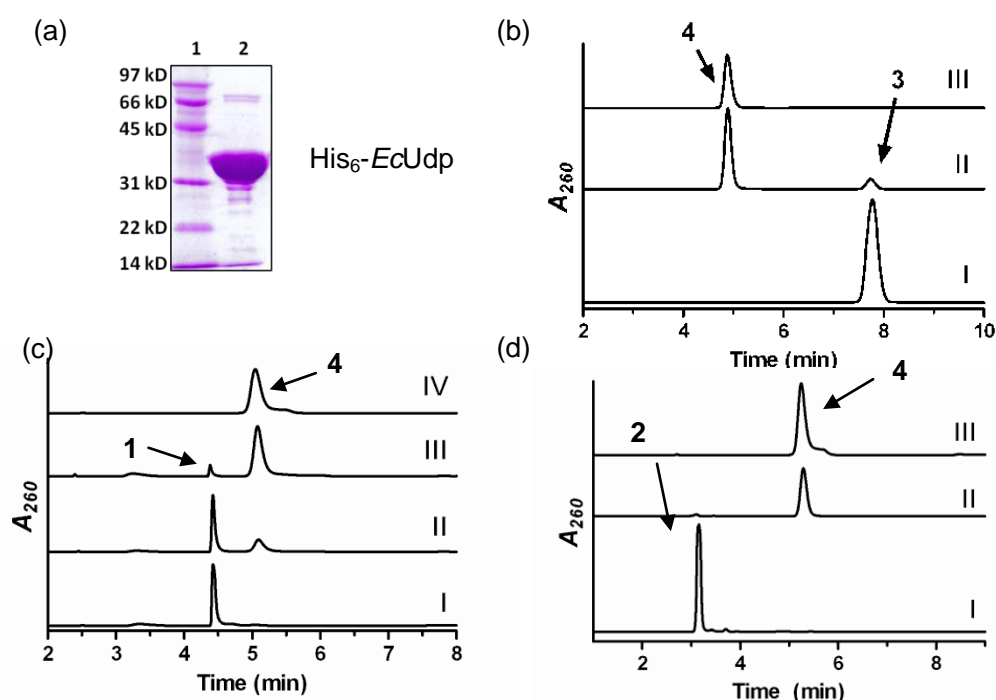


**Figure 2.10** *In vitro* characterization of *EcUdp* with hypothetical intermediates. (a) SDS-PAGE analysis of purified His<sub>6</sub>-*EcUdp* (expected MW of 32.2 kD). (b) HPLC analysis using substrate uridine (**3**) after (I) 30 min without *EcUdp*, (II) 30 min reaction, and (III) authentic uracil (**4**). (c) HPLC analysis using substrate **1** after (I) 30 min without *EcUdp*, (II) 30 min reaction, (III) 3 hr reaction and (IV) authentic uracil (**4**). (d) HPLC analysis using substrate 5'-amino-5'-deoxyuridine (**2**) after (I) 30 min without *EcUdp*, (II) 30 min reaction, and (III) authentic uracil (**4**).

### 2.3.4. Kinetics characterization of *EcUdp*

Single substrate kinetic analysis for *EcUdp* was performed at both pH 9.0 and 7.5 with all hypothetical pathway intermediates (**Fig 2.11a**). The extracted kinetic constants (**Table 3**) revealed that *EcUdp* has comparable efficiency with



5'-amino-5'-deoxyuridine (**2**) and uridine (**3**) at pH 9.0. Although the  $K_m$  and  $k_{cat}$  for each respective substrate were lower for LipP relative to *EcUdp*, the efficiencies and kinetic trends for both enzymes were quite comparable

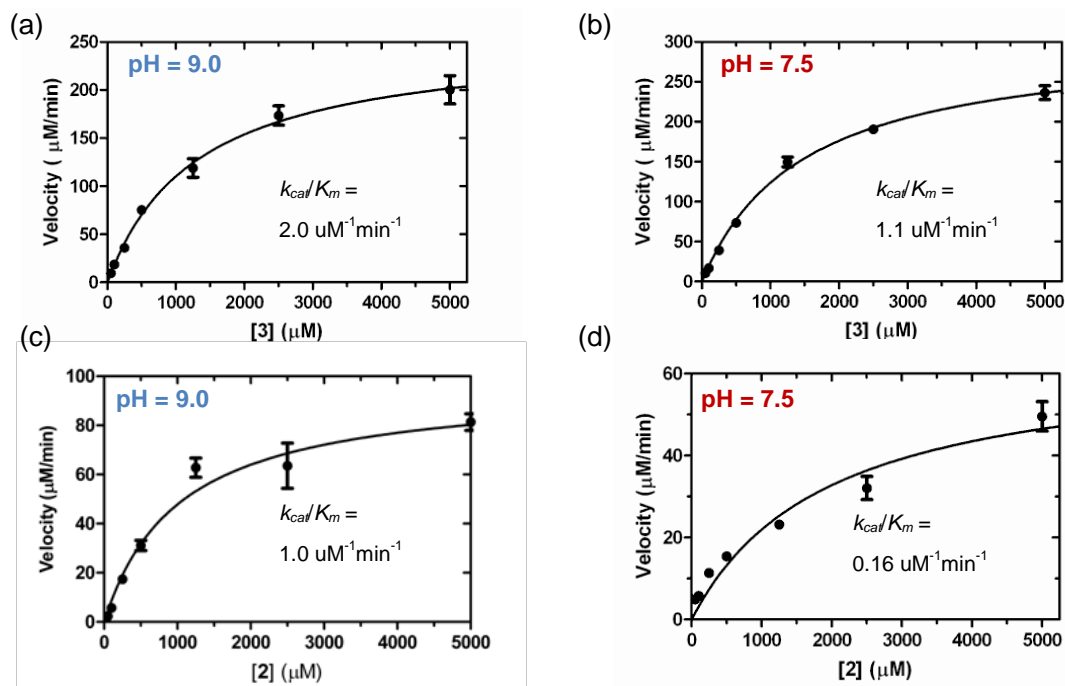


**Figure 2.11. Kinetics analysis of *EcUdp*.** (a) Single-substrate kinetic analysis with variable uridine (**3**) at pH 9.0. (b) Single-substrate kinetic analysis with variable uridine (**3**) at pH 7.5. (c) Single-substrate kinetic analysis with variable 5'-amino-5'-deoxyuridine (**2**) at pH 9.0. (d) Single-substrate kinetic analysis with variable 5'-amino-5'-deoxyuridine (**2**) at pH 7.5.  $A_{260}$ , absorbance at 260 nm.

## 2.4. Results: LipM Characterization

### 2.4.1. *In vitro* characterization of LipM activity

Since the kinetic analysis revealed both 5'-amino-5'-deoxyuridine (**2**) and uridine (**3**) are good substrates for LipP, while uridine-5'-aldehyde (**1**) is not, we eliminated one potential biosynthetic pathway leaving three potential pathways (**Fig 2.12**). The downstream enzyme LipM was characterized next to further define the pathway (**Fig 2.12**). Bioinformatics analysis of LipM revealed sequence similarity to proteins annotated as putative nucleotidyltransferases. The potential reaction catalyzed by

LipM is shown in **Fig 2.13**. To interrogate the activity in detail, *lipM* was expressed in *E. coli*, however the recombinant protein was insoluble using a variety of growth and induction conditions. Therefore, we turned to *S. lividans* TK64 as a host, which resulted in the successful preparation of soluble, recombinant LipM (**Fig 2.14 a**).

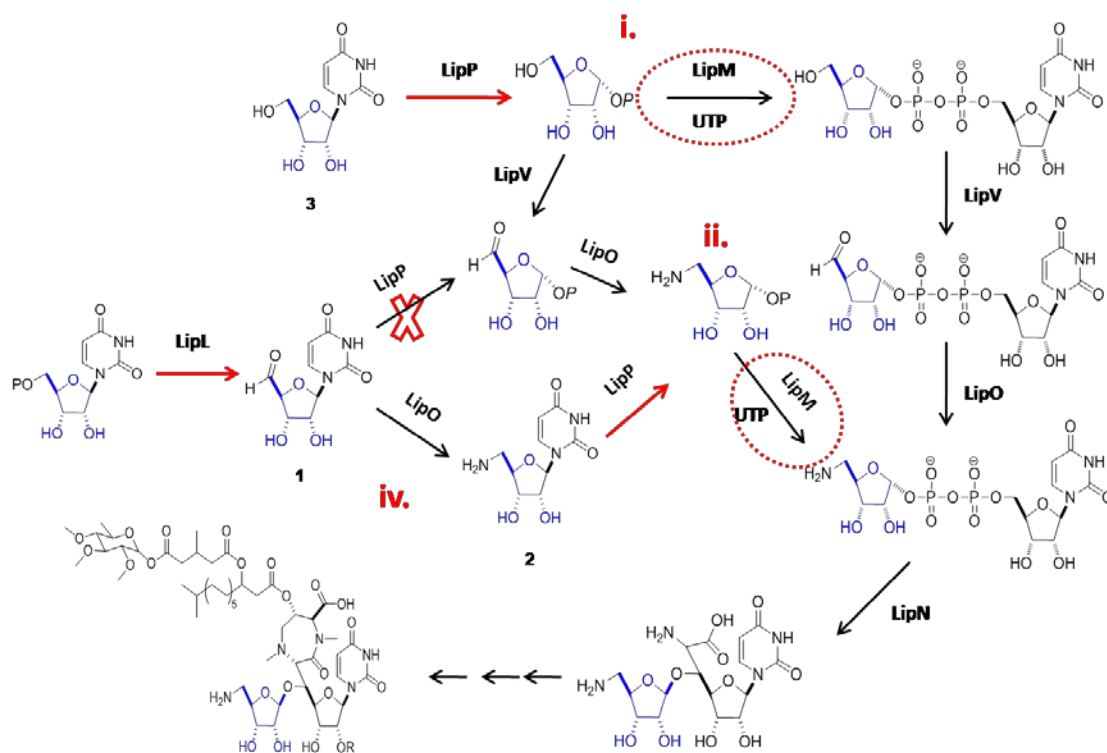


**Figure 2.12.** Proposed biosynthetic pathway for the incorporation of the aminoribosyl moiety of A-90289.

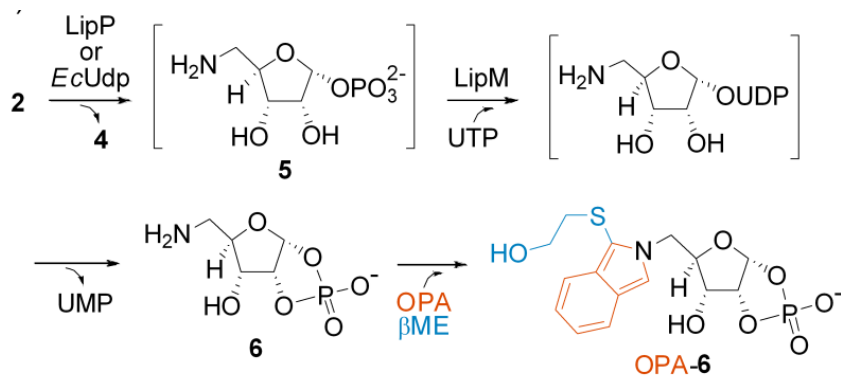


**Figure 2.13.** Reaction catalyzed by LipM including in situ generation of the substrate and amine derivatization with o-phthalaldehyde (OPA).

The activity of LipM was tested with  $\alpha$ -D-ribose-1-phosphate or 5-amino-5-deoxy- $\alpha$ -D-ribose-1-phosphate (**5**) generated in situ by LipP, and analysis of these reactions revealed a new peak was formed only in the presence of 5-amino-5-deoxy- $\alpha$ -D-ribose-1-phosphate (**5**) and UTP or - to a lesser extent - TTP, CTP, or GTP (**Fig 2.14 b** and **Fig 2.15**). Unexpectedly, the new peak derived from activity tests with 5-amino-5-deoxy- $\alpha$ -D-ribose-1-phosphate (**5**) and the different NTPs had the same retention time and UV/Vis spectrum as the respective nucleotide monophosphate (NMP), and co-injections with authentic material and LC-MS revealed this to be the case.

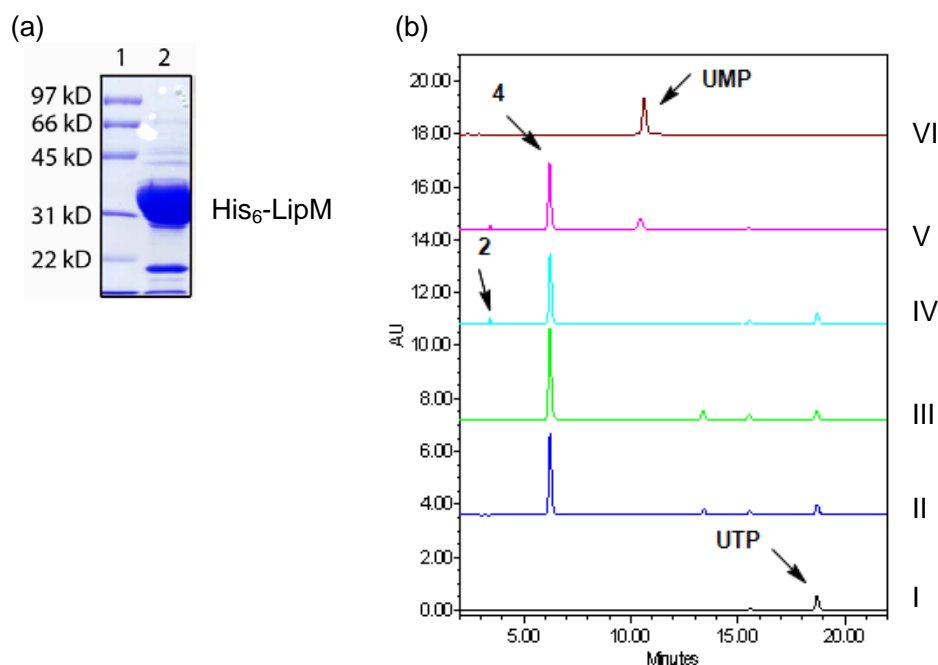


**Figure 2.14.** Characterization of LipM. (a) SDS-PAGE analysis of purified His<sub>6</sub>-LipM (expected MW of 31.3 kD). (b) HPLC analysis starting with 5'-amino-5'-deoxyuridine (**2**) or uridine (**3**). (I) authentic UTP, (II) 3 hr reaction with substrate uridine (**3**), with LipP, (III) 3 hr reaction with substrate uridine (**3**), with LipP and LipM, (IV) 3 hr reaction with substrate 5'-amino-5'-deoxyuridine (**2**), with LipP, (V) 3 hr reaction with substrate 5'-amino-5'-deoxyuridine (**2**), with LipP and LipM, and (VI) authentic UMP.  $A_{260}$ , absorbance at 260 nm.

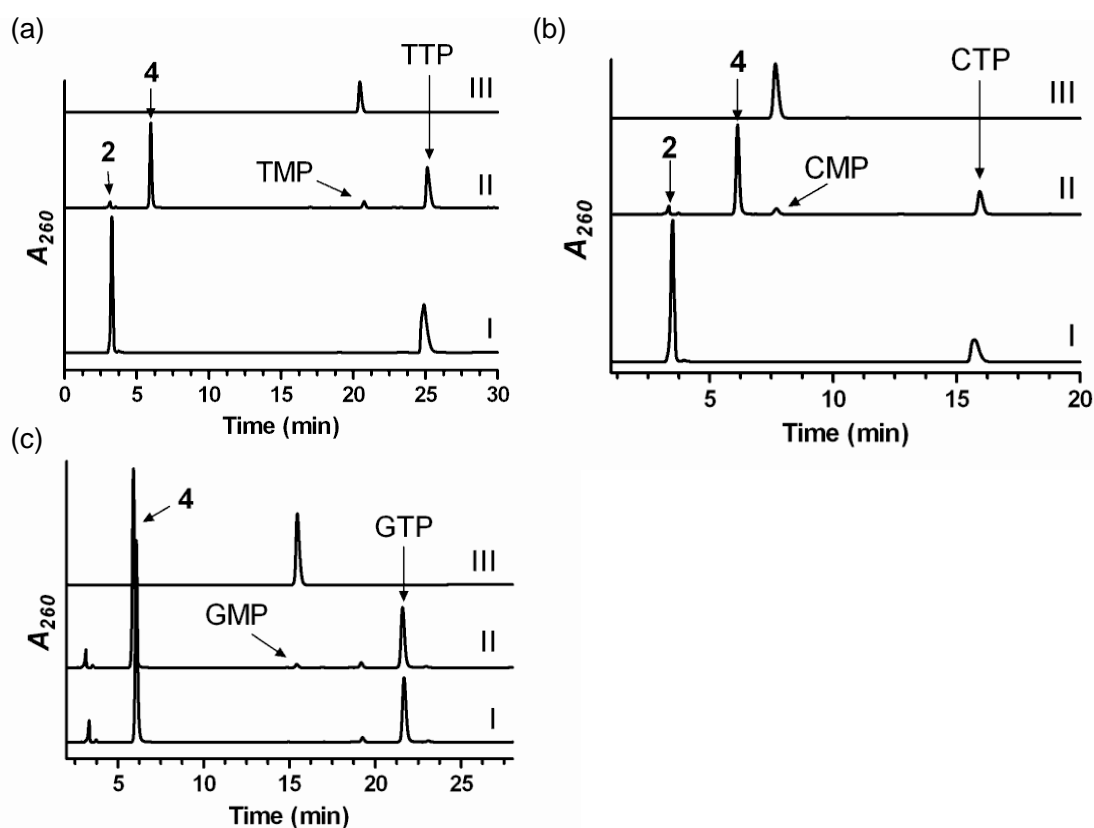


**Figure 2.15.** *In vitro* characterization of LipM with alternative NTPs. (a) HPLC analysis after (I) 3 hr without LipP, (II) 3 hr reaction, and (III) authentic TMP. (b) HPLC analysis after (I) 3 hr without LipP, (II) 3 hr reaction, and (III) authentic CMP. (c) HPLC analysis after (I) 3 hr without LipP, (II) 3 hr reaction, and (III) authentic GMP.  $A_{260}$ , absorbance at 260 nm.

#### 2.4.2. *In vitro* characterization of OPA modified 5'-amino-5'-deoxyuridine (2) catalyzed by LipM

We hypothesized that the NMP was generated by the degradation of the product via intramolecular attack of the 2-hydroxy group of the aminoribosyl unit on the proximal phosphate, a phenomenon that was previously observed upon characterization of apiofuranosyl-1,2-cyclic phosphate as the product of the plant bifunctional UDP-apiose/UDP-xylose synthase that catalyzes decarboxylation of UDP-glucuronic acid[97]. To detect any potential amine-containing product, the reaction components were first modified with OPA prior to injection, and two new peaks were identified by HPLC (**Fig 2.16**).

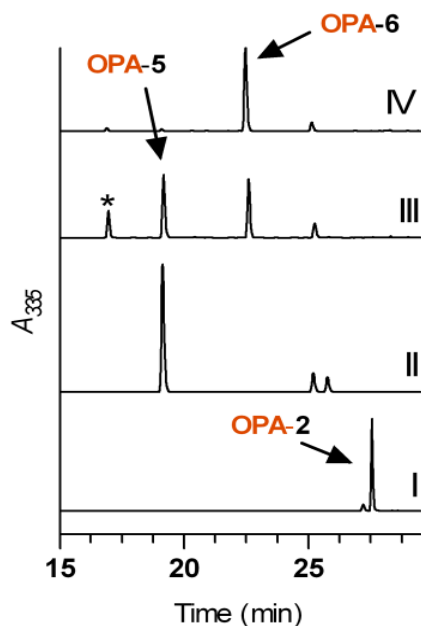


**Figure 2.16.** OPA-modified substrate reaction catalyzed by HPLC. HPLC analysis of reaction mixtures with OPA derivatization starting with 5'-amino-5'-deoxyuridine (**2**) after (I) 30 min without LipP, (II) 30 min without LipM (II), 30 min reaction (III), and 3 hr reaction (IV).  $A_{335}$ , absorbance at 335 nm.

The first peak was identified as residual OPA-modified 5-amino-5-deoxy- $\alpha$ -D-ribose-1-phosphate (OPA-5), while LC-MS analysis of the remaining peak yielded an  $(M - H)^-$  ion at  $m/z = 385.6$ , consistent with the molecular formula  $C_{15}H_{18}NO_7PS$  of an OPA-modified 5-amino-5-deoxy- $\alpha$ -D-ribose-1,2-cyclicphosphate (OPA-6) (expected  $m/z = 386.1$ ) (**Fig 2.13** and **Fig 2.17 a,b**). Large-scale purification of OPA-6 and subsequent LC-MS and 1D and 2D NMR spectroscopic characterization (**Fig 2.15 c,d-2.21**)—notably the  $^1H$ - $^{31}P$  HMBC data that was consistent with the very recently discovered metabolite  $\alpha$ -D-ribose-1,2-cyclicphosphate[98] (**Fig 2.22**)—revealed the expected degradation product (an isoindol-1-one) for OPA-6[99]. Although the genuine identity of the product of the LipM-catalyzed reaction remained elusive at this stage, the results did reveal that LipM only utilizes a sugar-1-phosphate containing a primary amine functionality.

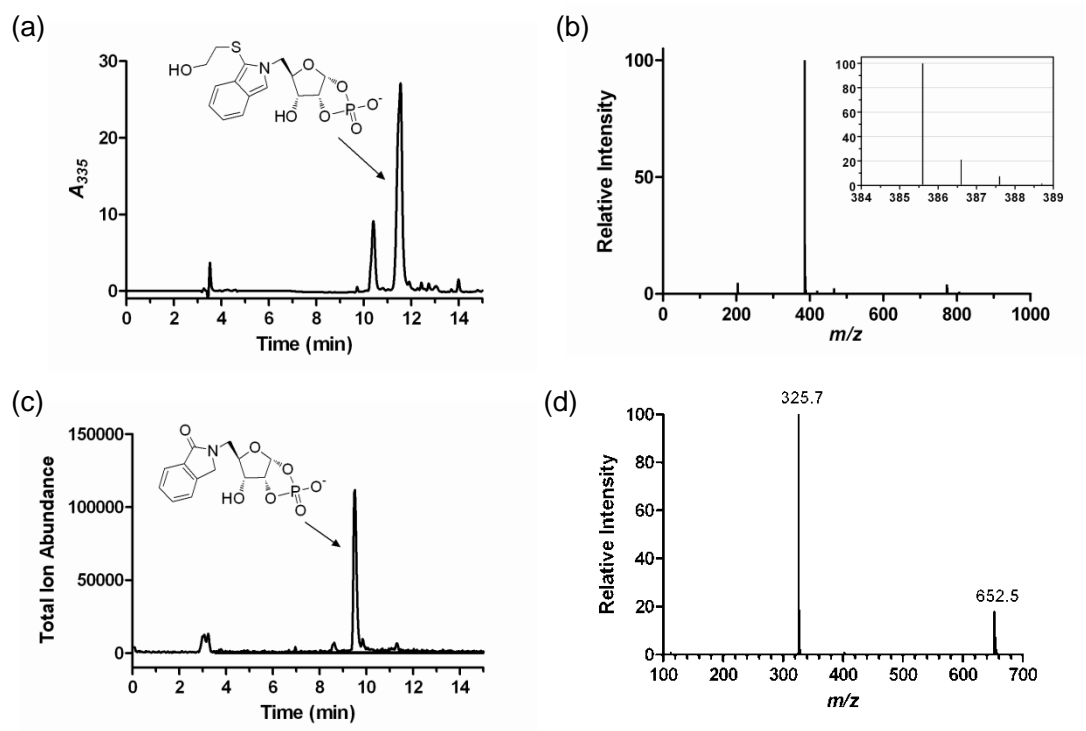


**Figure 2.17.** LC-MS analysis of the OPA-modified LipM product. (a) LC analysis of the LipM product prior to purification. (b) Mass spectrum for the peak at elution time  $t = 11.4$  min displaying the expected isotopic distribution (inset). (c) LC-MS analysis of the LipM product following purification using total negative ion current for detection. (d) Mass spectrum for the peak eluting at time  $t = 9.6$  min.  $A_{335}$ , absorbance at 335 nm.

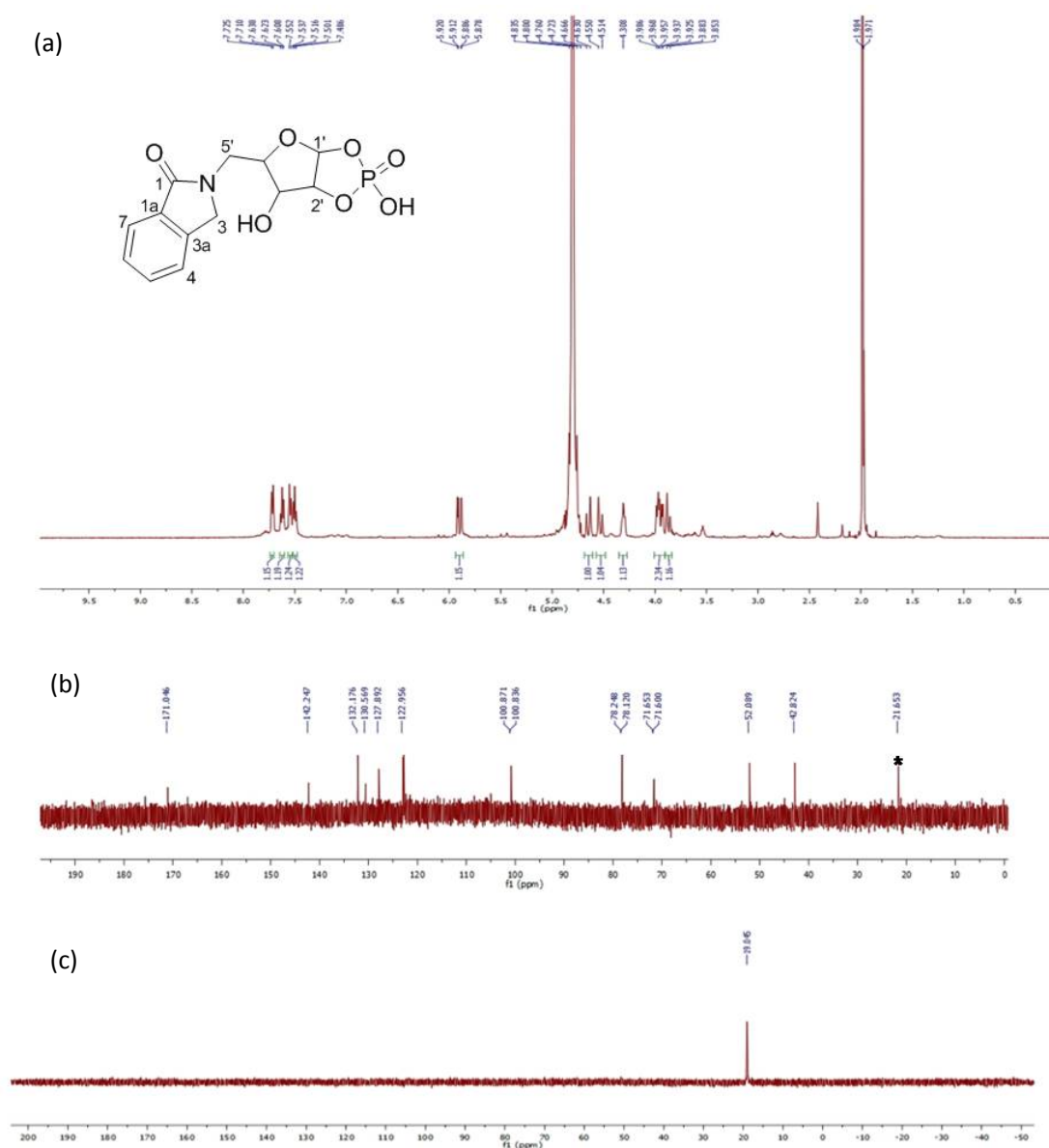


**Figure 2.18.** Characterization of 5'-isoindoline-5'-deoxy- $\alpha$ -D-ribose-1',2'-cyclic phosphate by 1D NMR. (a)  $^1\text{H}$ -NMR spectrum. (b)  $^{13}\text{C}$ -NMR spectrum. (c)  $^{31}\text{P}$ -NMR spectrum. \*Acetic acid

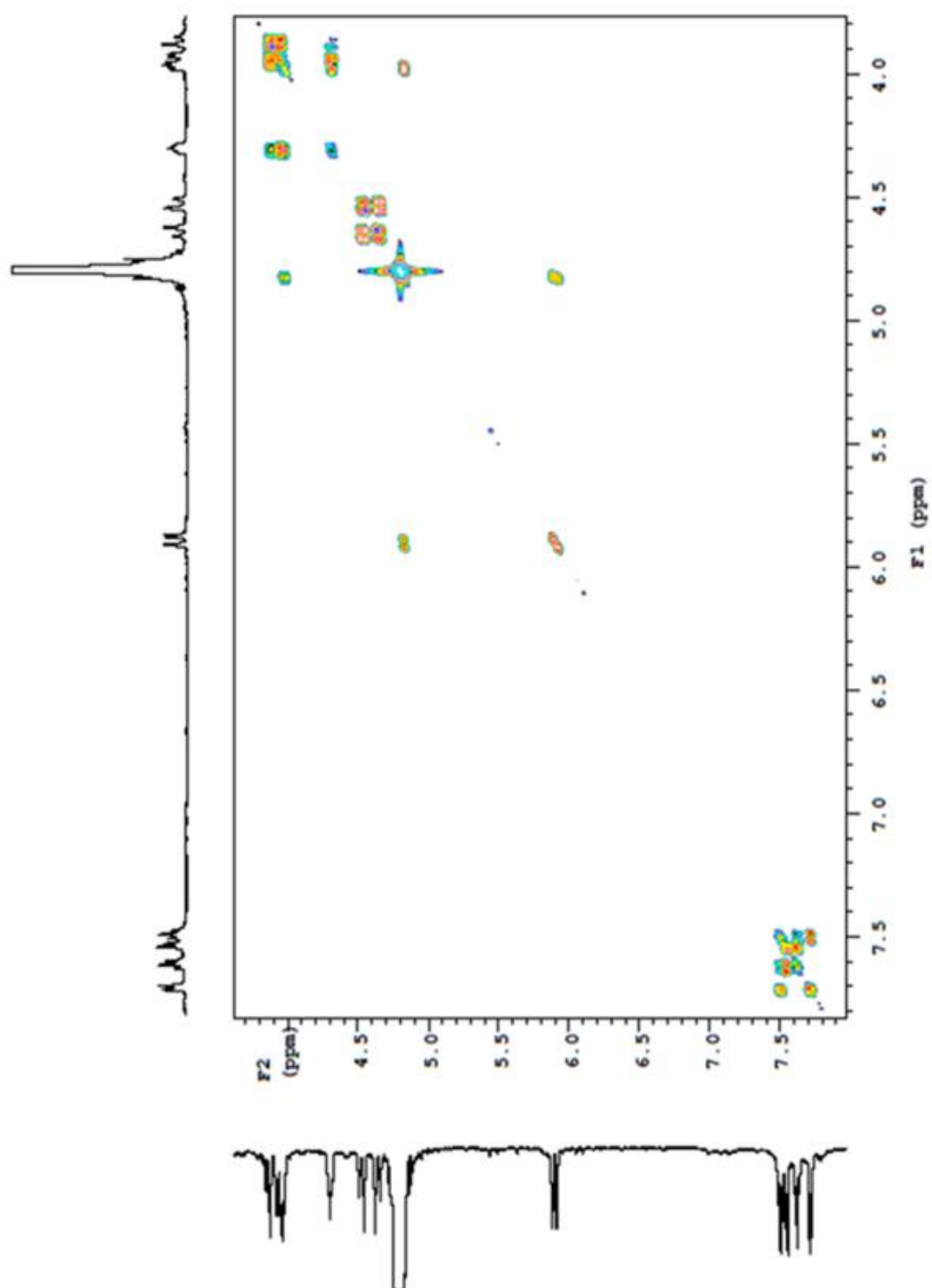


**Figure2.19.** gCOSY NMR spectrum of 5'-isoindoline-5'-deoxy- $\alpha$ -D-ribose-1',2'-cyclicphosphate.



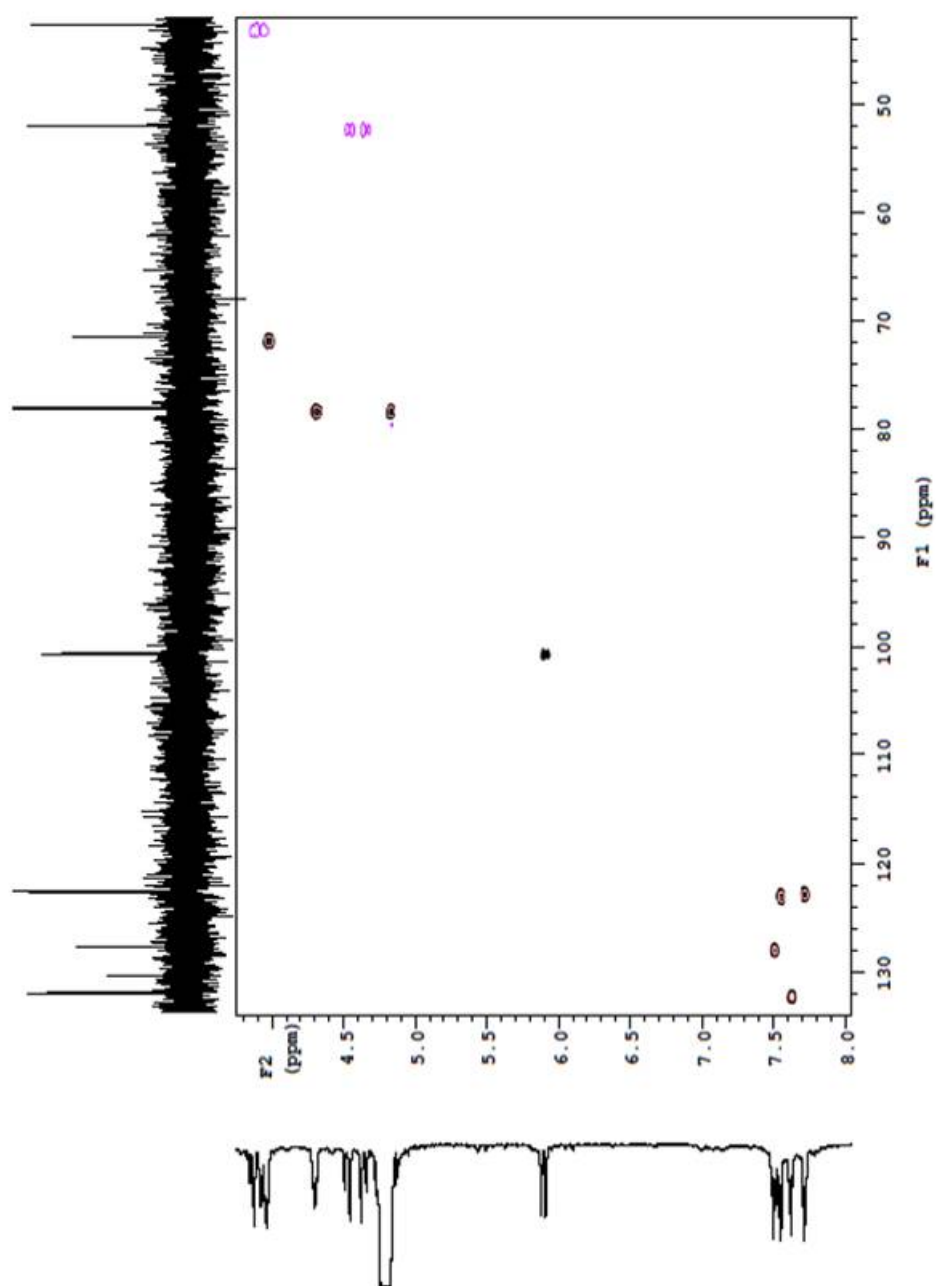


**Figure 2.20.** gHSQC NMR spectrum of 5'-isoindoline-5'-deoxy- $\alpha$ -D-ribose-1',2'-cyclicphosphate.

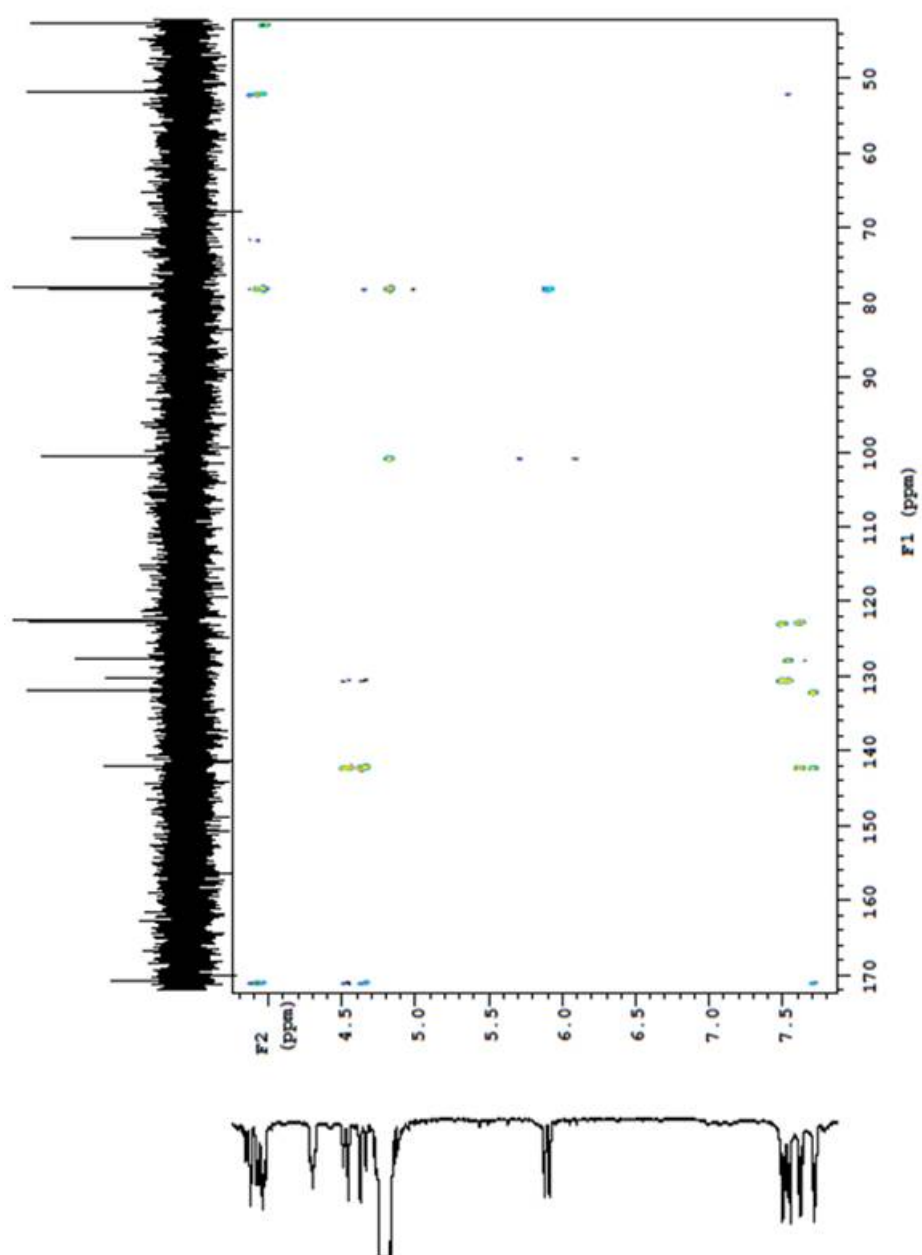


**Figure 2.21.**  $^1\text{H}$ - $^{13}\text{C}$  gHMBC NMR spectrum of 5'-isoindoline-5'-deoxy- $\alpha$ -D-ribose-1',2'-cyclicphosphate.

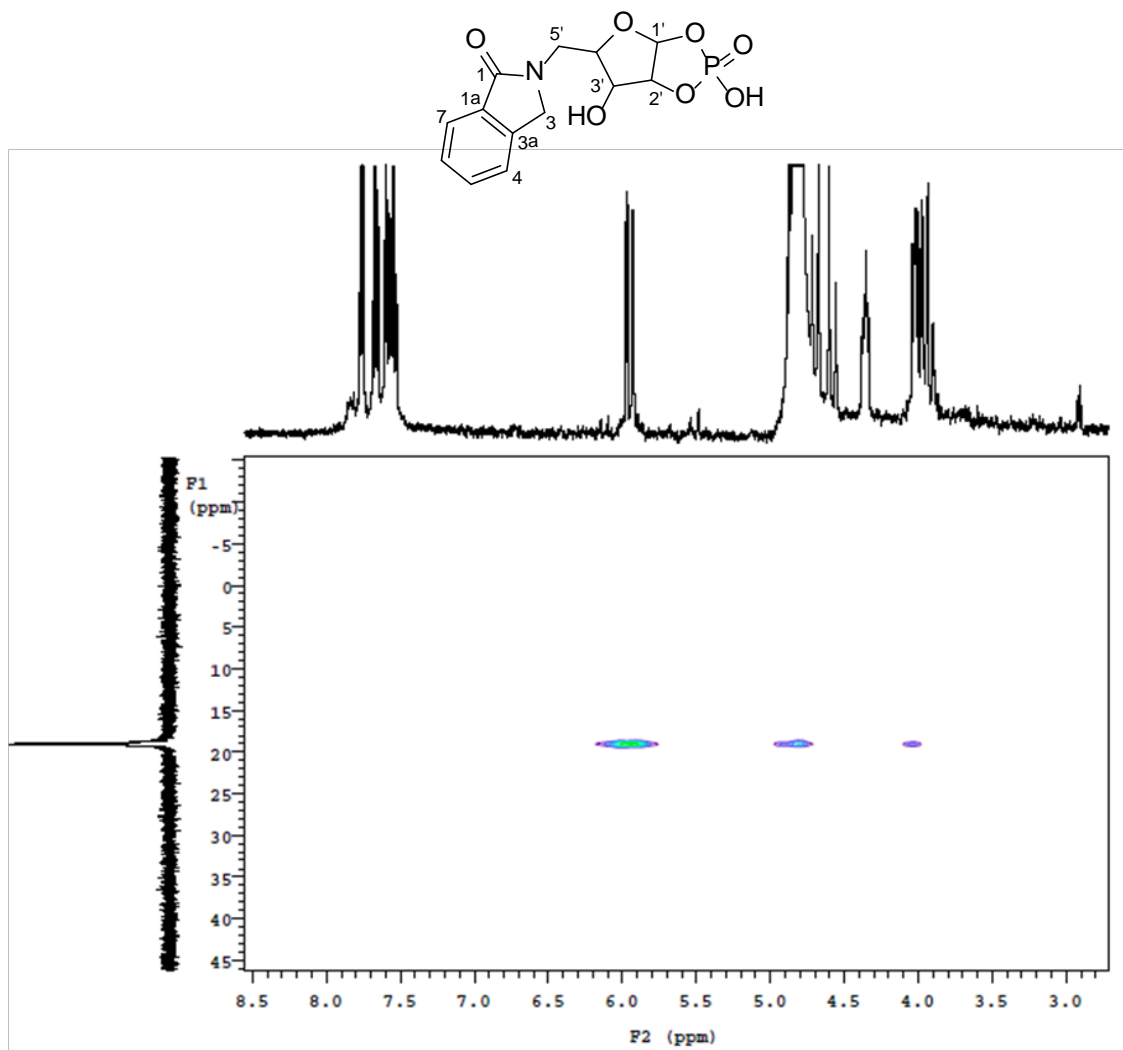


**Figure 2.22.**  $^1\text{H}$ - $^{31}\text{P}$  HMBC NMR spectrum of 5'-isoindoline-5'-deoxy- $\alpha$ -D-ribose-1',2'-cyclicphosphate

#### 2.4.3. *In vitro* characterization of substrate 5'-amino-2',5'-dideoxyuridine (7) catalyzed by LipM

We rationalized that a stable LipM product would be attainable by using a 2-deoxyribose-containing surrogate substrate. *EcUdp* as well as other UDPs are known to catalyze phosphorolysis using thymidine (12) or 2'-deoxyuridine (11)[96,100], and similarly LipP catalyzed the reaction with either substrate (Fig 2.24 a,b), although the latter was determined to be nearly 35-fold more efficient (Table 3 and Fig 2.23 c,d). Identical to the results utilizing 5'-hydroxy nucleosides (i.e. uridine 3), in situ generation of 2-deoxy- $\alpha$ -D-ribose-1-phosphate did not yield a product when

tested with LipM. Subsequently, the potential substrate 5'-amino-2',5'-dideoxyuridine (**7**) was synthesized from 2'-deoxyuridine (**11**), and the reaction catalyzed by LipM was tested in **Fig 2.24 a**. HPLC analysis with this surrogate substrate revealed it was processed by both LipP and LipM, generating two new peaks with uridine (**3**)-like chromophores ( $UV_{max} \sim 260$  nm) (**Fig 2.24 b**). While the minor peak was identified as UDP, the major peak did not co-elute with any known uracil (**4**)-containing metabolite. LC-MS analysis of the purified new peak revealed an  $(M - H)^-$  ion at  $m/z = 517.6$ , consistent with the molecular formula  $C_{14}H_{23}N_3O_{14}P_2$  of UDP-5"-amino-2",5"-dideoxyribose (**8**) (expected  $m/z = 518.1$ ) (**Fig2.25**). NMR analysis, including  $^1H$ -,  $^{13}C$ -, and  $^{31}P$ -NMR,  $^1H$ - $^1H$  COSY, and  $^1H$ - $^{13}C$  HMBC (**Figs 2.26-28**), confirmed the identity of the product as UDP-5"-amino-2",5"-dideoxyribose (**8**), thus consistent with the function of LipM as a UTP:5-amino-5-deoxy- $\alpha$ -D-ribose-1-phosphate uridylyltransferase.

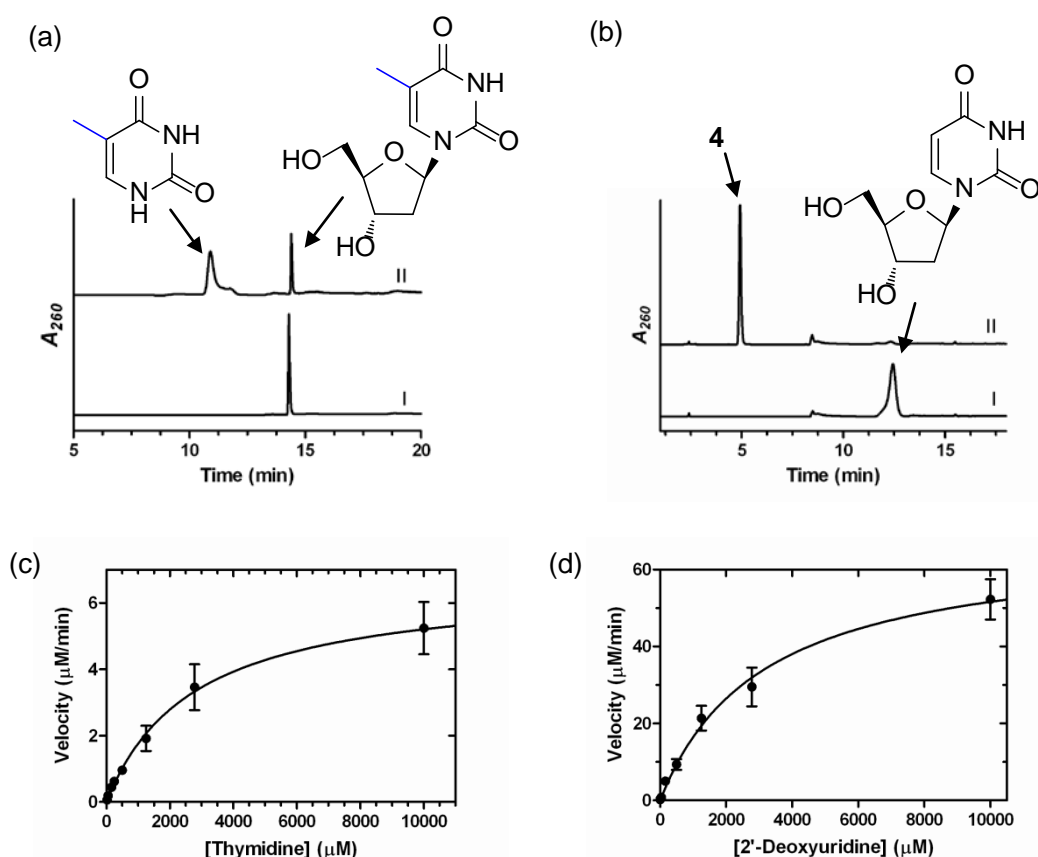


**Figure 2.23.** HPLC and Kinetic analysis of LipP with 2'-deoxynucleosides.(a) HPLC analysis using thymidine (**12**)after (I) 3 hr without LipP and (II) 3 hr reaction. (b)

HPLC analysis using 2'-deoxyuridine (**11**) after (I) 3 hr without LipP and (II) 3 hr reaction. (c) Single-substrate kinetic analysis with variable thymidine (**12**) at pH 9.0. (d) Single-substrate kinetic analysis with variable 2'-deoxyuridine (**11**) at pH 9.0.  $A_{260}$ , absorbance at 260 nm.

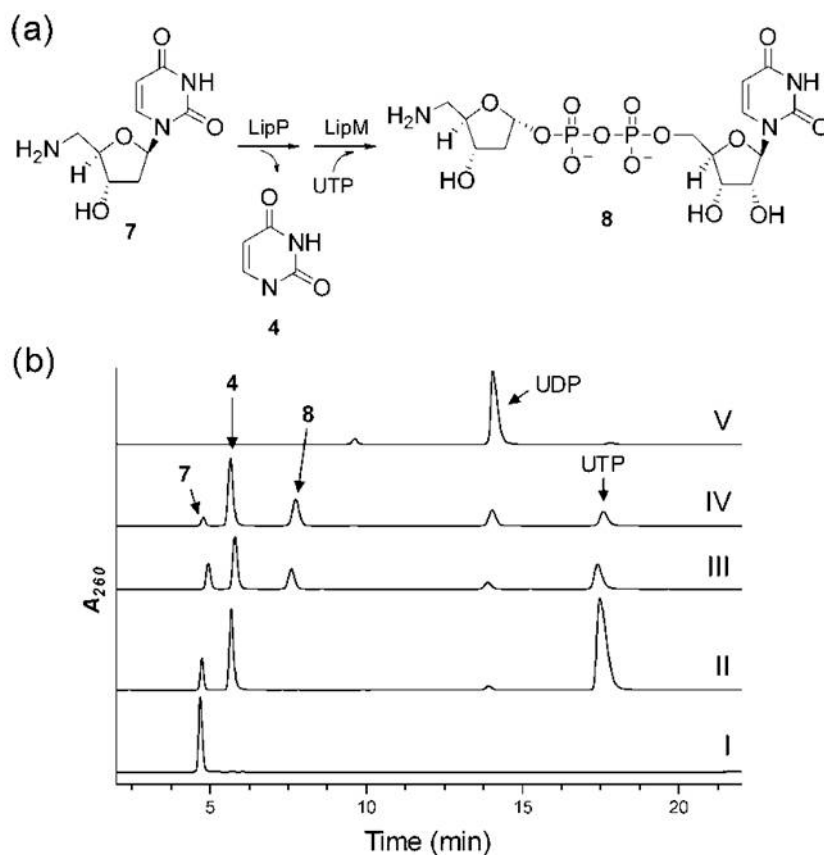


**Figure 2.24.** Characterization of LipM with substrate 5'-amino-2',5'-dideoxyuridine(**7**). (a) Enzymatic preparation of the substrate using LipP and the dideoxyuridine analogue 5'-amino-2',5'-dideoxyuridine(**7**) and the reaction catalyzed by LipM to generate UDP-5'-amino-2',5'-dideoxyribose (**8**). (b) HPLC analysis of the reaction starting with 5'-amino-2',5'-dideoxyuridine(**7**) after (I) 3 hr without UTP and LipP, (II) 3 hr without LipM, (III) 1 hr reaction, (IV) 3 hr reaction, and (V) authentic UDP.  $A_{260}$ , absorbance at 260 nm.

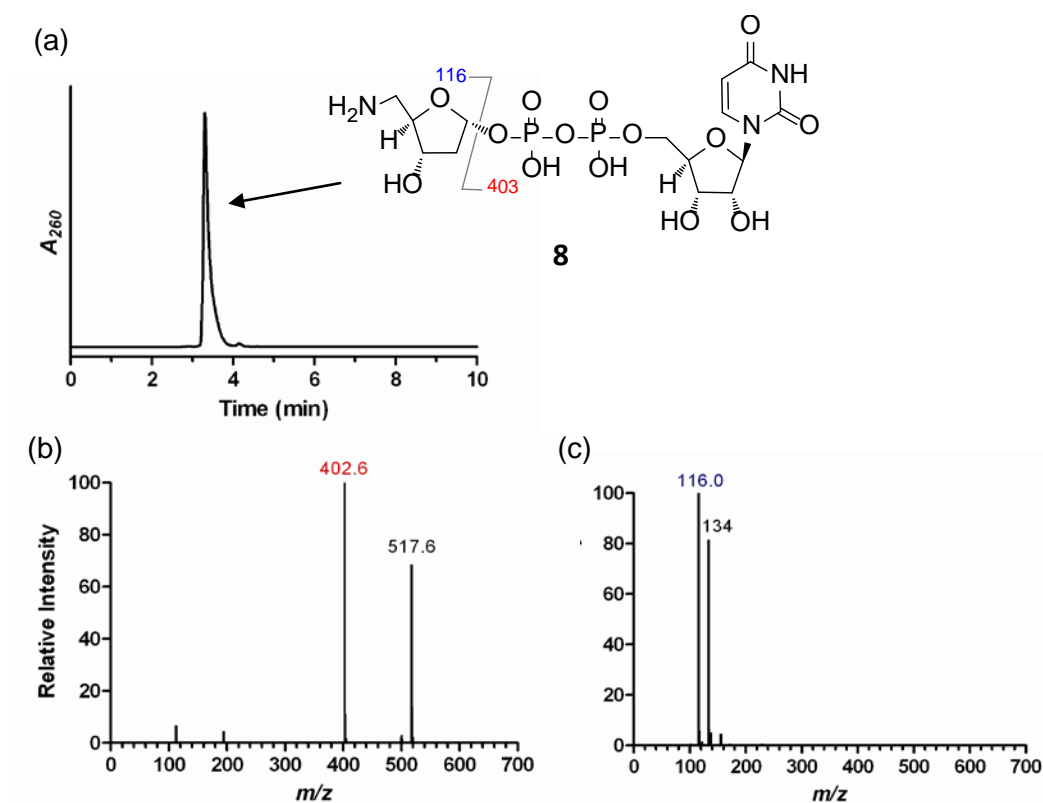


**Figure 2.25.** LC-MS of the LipM product UDP-5''-amino-2'',5''-dideoxyribose (**8**) generated from surrogate substrate 5'-amino-2',5'-dideoxyuridine(**7**). (a) LC analysis of UDP-5''-amino-2'',5''-dideoxyribose (**8**) following purification. (b) Negative ion mass spectrum for the peak at elution time  $t = 3.3$  min. (c) Positive ion mass spectrum for the peak at elution time  $t = 3.3$  min.  $A_{260}$ , absorbance at 260 nm.

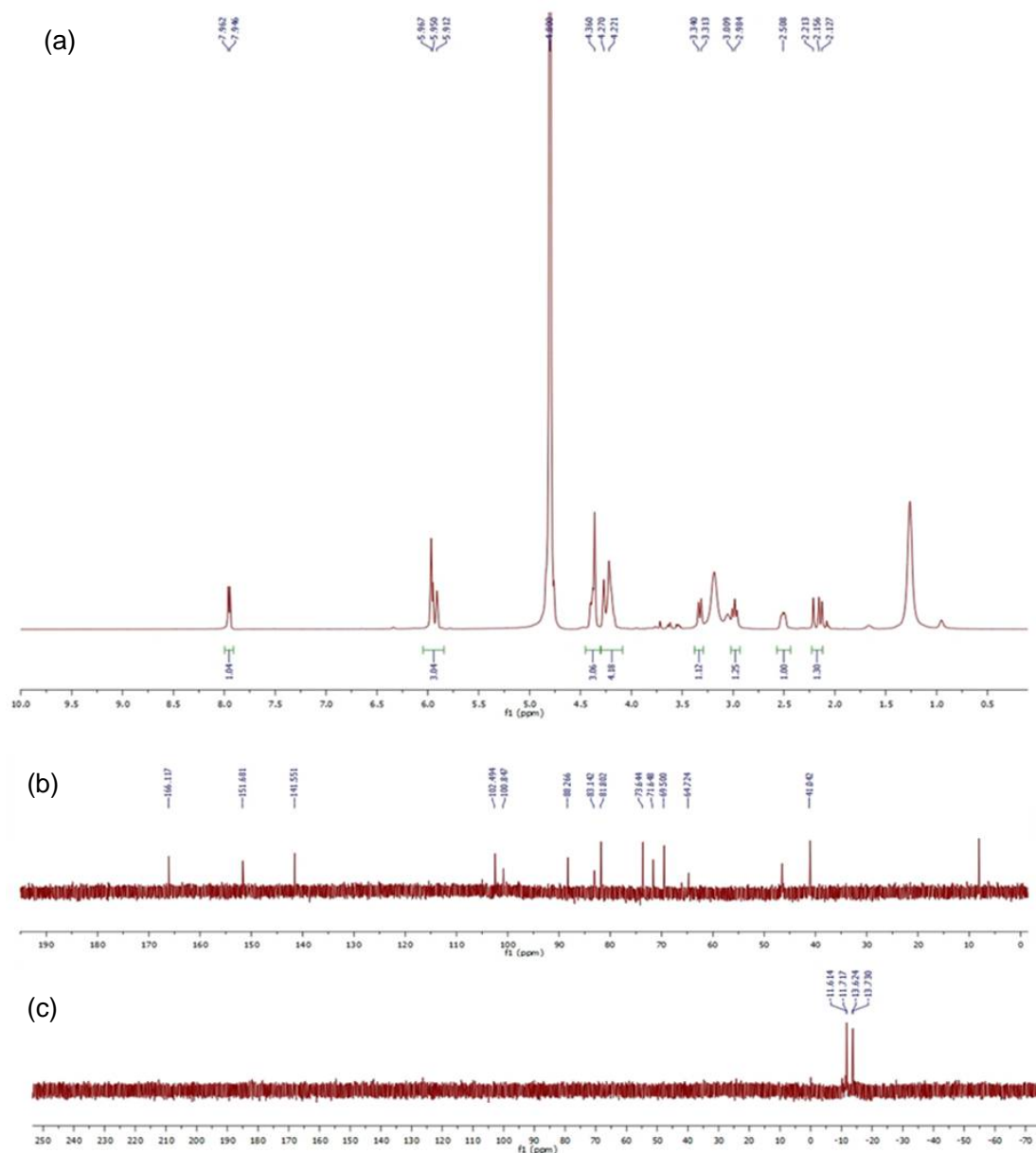


**Figure 2.26.** Characterization of UDP-5''-amino-2'',5''-dideoxyribose (**8**) by 1D NMR. (a)  $^1\text{H}$ -NMR spectrum. (b)  $^{13}\text{C}$ -NMR spectrum. (c)  $^{31}\text{P}$ -NMR spectrum.  $^*\text{Et}_3\text{N}$

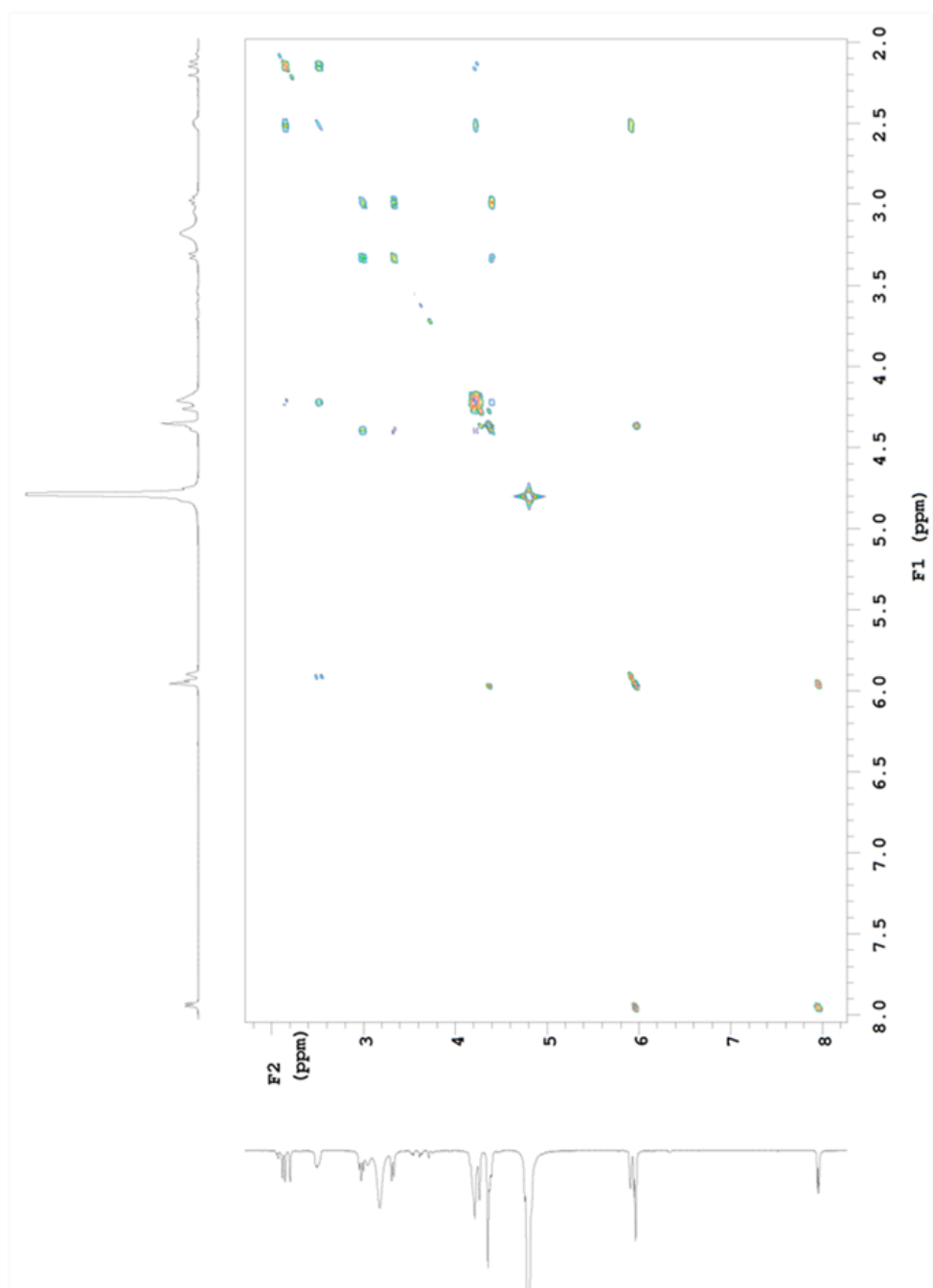


**Figure 2.27.** gCOSY NMR spectrum of UDP-5'-amino-2',5'-dideoxyribose (**8**).



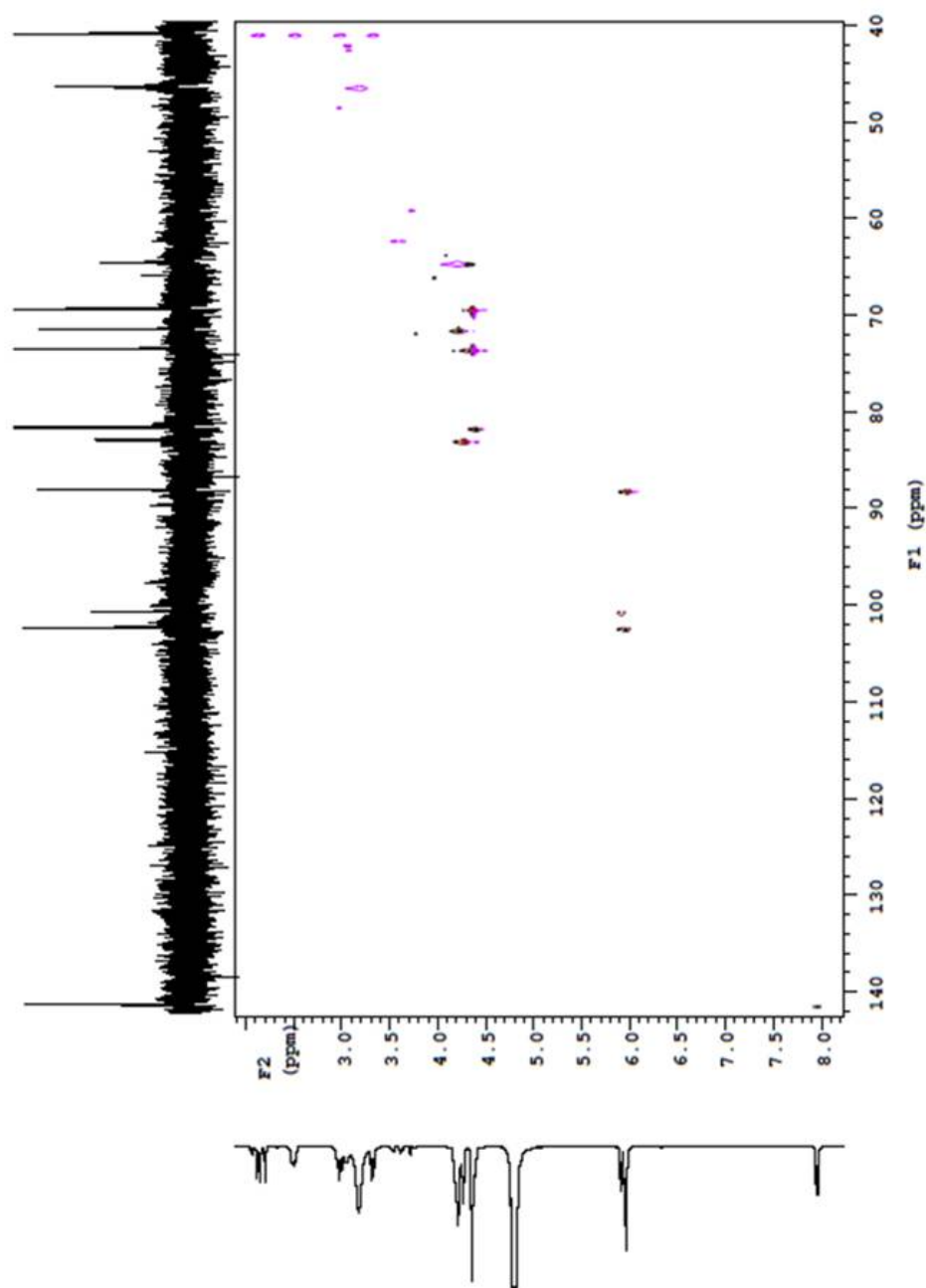


**Figure 2.28.** gHSQC NMR spectrum of UDP-5'-amino-2',5'-dideoxyribose (**8**).

## 2.5. Results: LipO Characterization

### 2.5.1. *In vitro* characterization of LipO wild-type and mutant protein

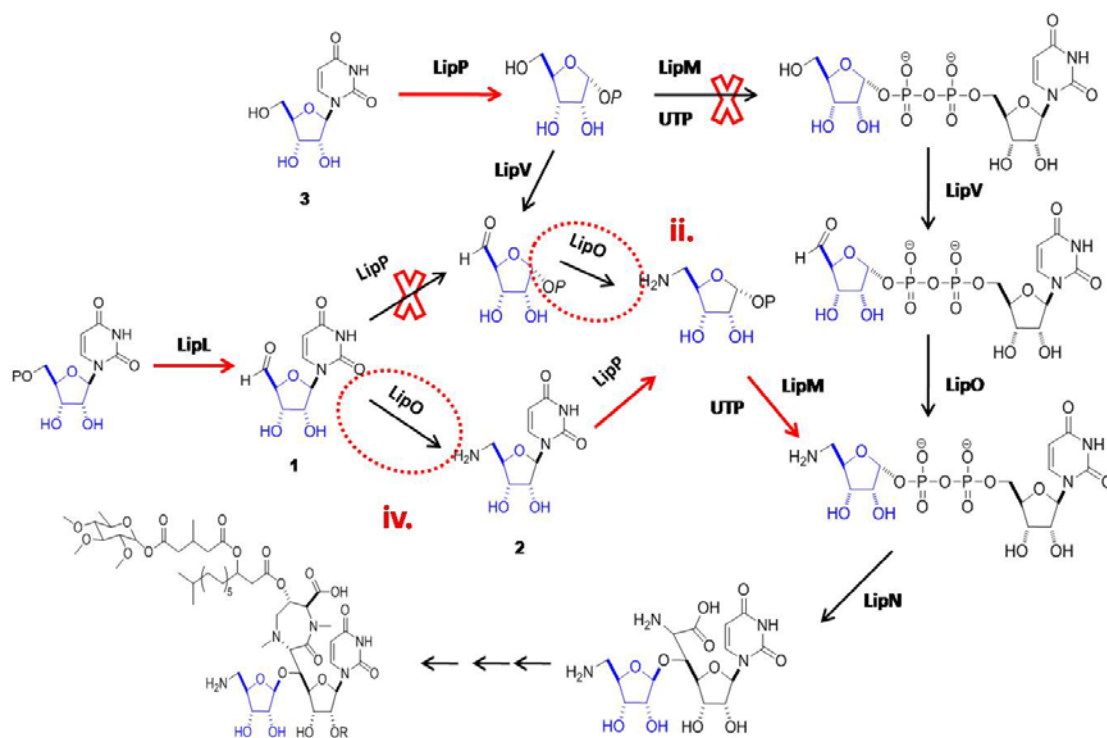


**Figure 2.29.** Proposed biosynthetic pathway for the incorporation of the aminoribosyl moiety of A-90289.

After confirming that LipM only utilized the amine-containing ribose-1-phosphate to produce the activated UDP sugar, a second hypothetical pathway was eliminated (**Fig 2.29**). Thus, there were only two pathways left. To differentiate between these two, we next turned our attention to the remaining enzyme, LipO. LipO has modest sequence similarity to several proteins predicted to belong to the pyridoxal-phosphate (PLP)-dependent aspartate aminotransferase (Type I) superfamily [101][102]. Of note is the sequence similarity of LipO to PacE (37 % identity / 51 % similarity) involved in the biosynthesis of the pacidamycin family of antibiotics. The pacidamycins consist of an enamide-containing nucleoside with a 5'-amine functionality as the sole ribose-derived unit, which we and others have previously speculated proceeds through uridine-5'-aldehyde (**1**) as an intermediate

[88,103,104,105] (**Fig2.30**), which would necessitate transamination at the nucleoside level to yield the nucleoside building block. Thus, we envisioned an analogous biosynthetic pathway such that LipO catalyzes aminotransfer utilizing the corresponding nucleoside uridine-5'-aldehyde (**1**).

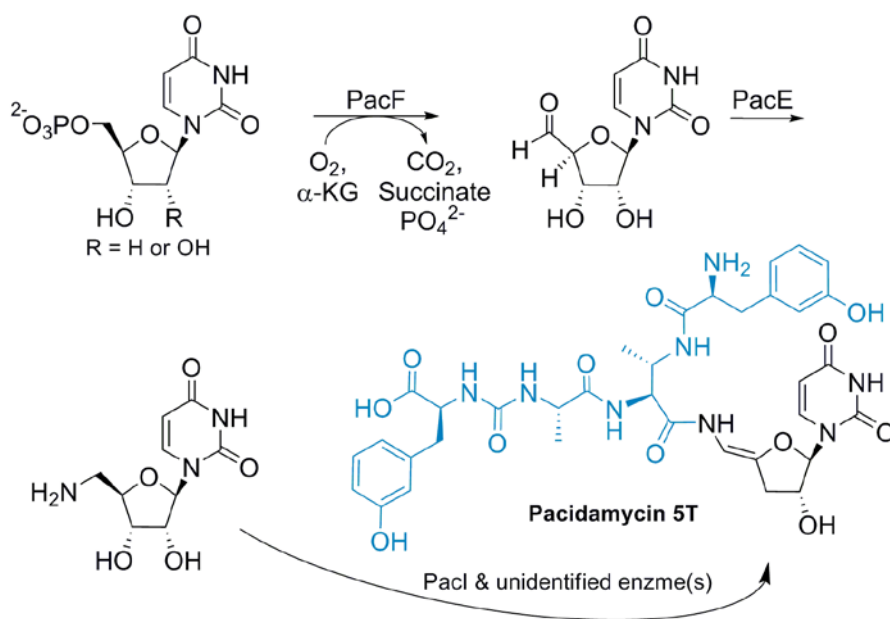


**Figure 2.30.** Putative biosynthesis of enamide-containing nucleoside antibiotics. Putative pathway and intermediates leading to the enamide-containing nucleoside moiety found in pacidamycins.

Similarly to LipM, the gene product of *lipO* was only soluble when expressed in *S. lividans* TK64 (**Fig 2.31 a**) and was shown by UV/Vis spectroscopy to co-purify with the cofactor PLP (**Fig 2.31 b**). The mutant LipO(K282A), expected to be unable to form an internal aldimine with Lys and hence be inactive, was also produced in *S. lividans* TK64 to yield a purified protein devoid of bound PLP (**Fig 2.31 a,b**).

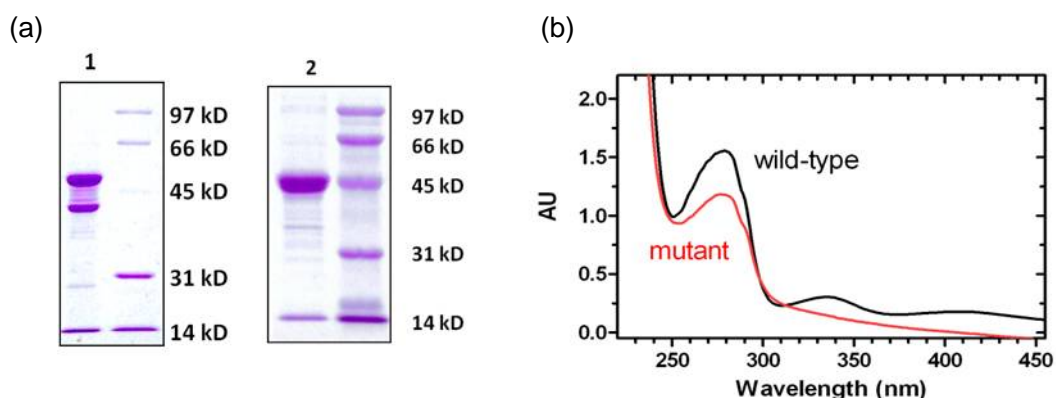


**Figure 2.31** LipO wild-type and mutant protein expression and UV/Vis spectrum analysis. (a) SDS-PAGE analysis of purified His<sub>6</sub>-LipO (lane 1) and His<sub>6</sub>-LipO (K282A) (lane 2, expected MW of 50.7 kD). Several attempts to purify the wild-type enzyme yielded the same contaminating protein band, which is currently under investigation to resolve this issue. (b) UV/Vis spectrum of LipO (wild-type) and LipO(K282A) (mutant).

### 2.5.2. LipO activity analyzed by HPLC and conversion efficiency with different amino donors

The activity of LipO was next monitored by HPLC using diode array for detection, and to simplify the analysis, the putative product 5'-amino-5'-deoxyuridine (**2**) was synthesized and used as a standard. When LipO was incubated with uridine-5'-aldehyde (**1**) and L-glutamate or L-aspartate, two common amine donors for the Type 1 aminotransferase superfamily, a small peak representing < 1 % conversion appeared in both cases, which was confirmed as 5'-amino-5'-deoxyuridine (**2**) by LC-MS and co-injections with authentic 5'-amino-5'-deoxyuridine (**2**) (**Fig 2.32 a**); in contrast, no new peak was observed with LipO (K282A) (**Fig 2.32 b**). Further analysis revealed several potential amine donors were substrates—findings similar to many other characterized aminotransferases [102], however, the highest specific activity was obtained with L-methionine followed by *N*-acetylcysteine, L-arginine, and *S*-adenosyl-L-methionine (**Table 4**). Finally, the reverse reaction of LipO using 5'-amino-5'-deoxyuridine (**2**) and 4-methylthio-2-oxobutanoate or other amine acceptors as substrates was not observed, suggesting that the equilibrium of aminotransfer favors formation of

5'-amino-5'-deoxyuridine (**2**). The results are consistent with the functional assignment of LipO as a methionine: uridine-5'-aldehyde (**1**) aminotransferase and, importantly, that 5'-amino-5'-deoxyuridine (**2**) is the likely intermediate in the biosynthesis of the aminoribosyl moiety of A-90289.

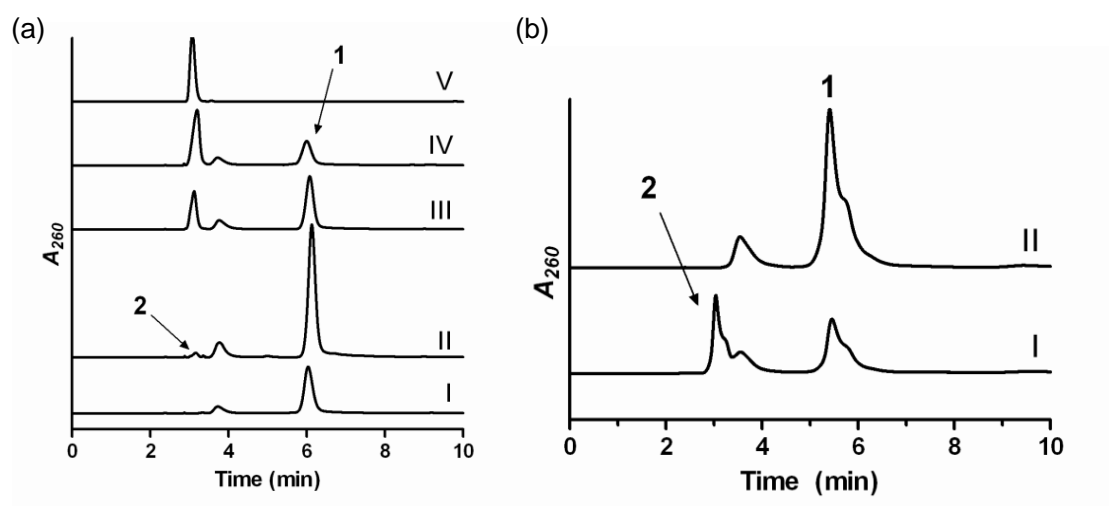


**Figure 2.32.** HPLC characterization of LipO. (a) HPLC analysis starting with uridine-5'-aldehyde (**1**) after (I) 4 hr without LipO, (II) 4 hr reaction with glutamate as an amine donor, (III) 4 hr reaction with L-methionine as an amine donor, (IV) 4 hr reaction with L-methionine as an amine donor spiked with authentic 5'-amino-5'-deoxyuridine (**2**), and (V) authentic 5'-amino-5'-deoxyuridine (**2**). (b) HPLC analysis of 4 hr reaction with (I) wild-type LipO and (II) LipO(K282A).  $A_{260}$ , absorbance at 260 nm.

**Table 4.** Amino donor substrates for LipO.

Amino Donor	Relative Specific Activity <sup>a</sup>
L-methionine	100
<i>N</i> -acetyl- L-cysteine	58
L -arginine	58
S-adenosyl- L-methionine	55
L-ornithine	50
L-isoleucine methylester	47
L-histidine	47
O-phospho- L-serine	47
L-glutamine	44
L-proline	44
L-asparagine	21
L-phenylalanine	19
L-lysine	16
L-histidine	13
DL-alanine	13
L-cysteine	11
S-adenosyl- L-homocysteine	9.4
glycine	7.1
L-tyrosine	7.1
L-isoleucine	5.0
L-serine	5.0
L-threonine	3.8
L-valine	3.5
L-serine	2.9
L-glutamate	2.3
DL-isoleucine	1.8
L-tryptophan	1.5
β-alanine	1.5
D-cysteine	1.2
D-alanine	0.9
NH <sub>4</sub> OH	0.9
L-aspartate	0.6

<sup>a</sup>The specific activity of LipP with L-methionine is 0.12 μmol min<sup>-1</sup> mg<sup>-1</sup> at 30 °C and pH = 7.5, which is comparable to the specific activity of methionine-glyoxylate transaminase from *Brassica* sp [106].

## 2.6. Results: LipN Characterization

### 2.6.1. *In vitro* characterization of LipN activity

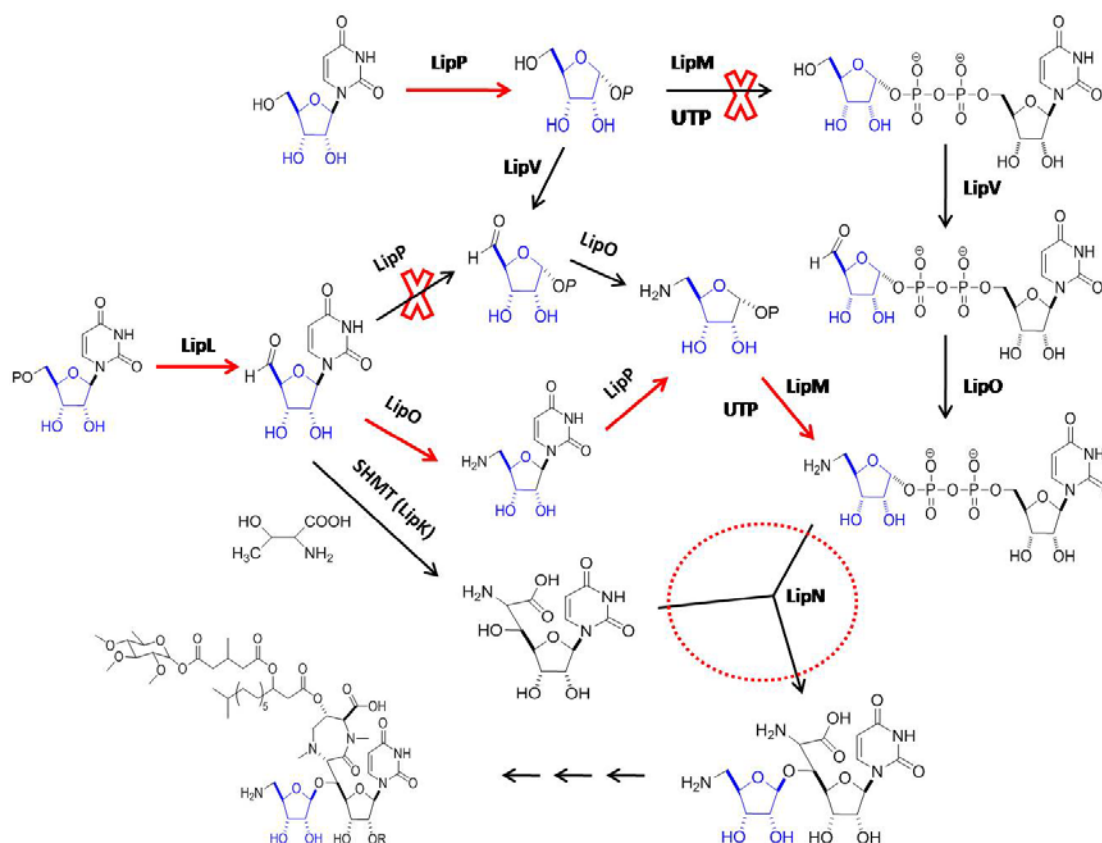


**Figure 2.33.** Proposed biosynthetic pathway for the incorporation of the aminoribosyl moiety of A-90289.

After the activity of LipO was confirmed, the biosynthetic pathway for the aminoribose was revealed to start with UMP with sequential catalysis by LipL, LipO, LipP and LipM. We finally turned our attention to LipN, which has low sequence identity to a small number of proteins annotated as putative glycosyltransferases. We hypothesized that LipN utilized UDP-5"-amino-2",5"-dideoxyribose (**8**) as a sugar donor. Once again, soluble protein was only obtained upon heterologous expression in *S. lividans* TK64 (**Fig 2.34 a**). Unfortunately UDP-5"-amino-2",5"-dideoxyribose (**8**) was not stable upon storage, in this case degrading to UDP and an undetermined product likely by hydrolysis of the anomeric bond (**Fig 2.34 b**). Thus we again relied

on the in situ generation of substrate beginning with 5'-amino-5'-deoxyuridine (**2**) or 5'-amino-2',5'-dideoxyuridine(**7**). While no glycosyltransferase activity was observed with PRPP or ribose-1-phosphates generated with LipP, HPLC analysis of LipN reactions using surrogate acceptor uridine (**3**) revealed a new, small peak starting from either 5'-amino-5'-deoxyuridine (**2**)(**Fig 2.35**) or 5'-amino-2',5'-dideoxyuridine(**7**) (**Fig 2.36**) as the ultimate sugar donor generated from LipP and LipM. Our pilot experiments suggested higher yields were obtained with the genuine sugar donor UDP-5-amino-5-deoxy- $\alpha$ -D-ribose, and thus no further experiments were undertaken with UDP-5''-amino-2'',5''-dideoxyribose (**8**). Following large-scale purification of the LipN - product generated from 5'-amino-5'-deoxyuridine (**2**) and uridine (**3**), mass and complete NMR spectroscopic analysis (**Fig 2.37-40**)—notably the  $^1\text{H}$ - $^{13}\text{C}$  HMBC demonstrating the H-1''and C-5' correlation (**Fig 2.41**)—revealed the identity of the new product as 5'-O-(5''-amino-5''-deoxy- $\alpha$ -D-ribose)-uridine (**9**) (**Fig 2.35**). Thus, the function of LipN is assigned as a 5-amino-5-deoxy- $\alpha$ -D-ribosyltransferase that catalyzes the terminal step in the biosynthesis of the aminoribosyl moiety.

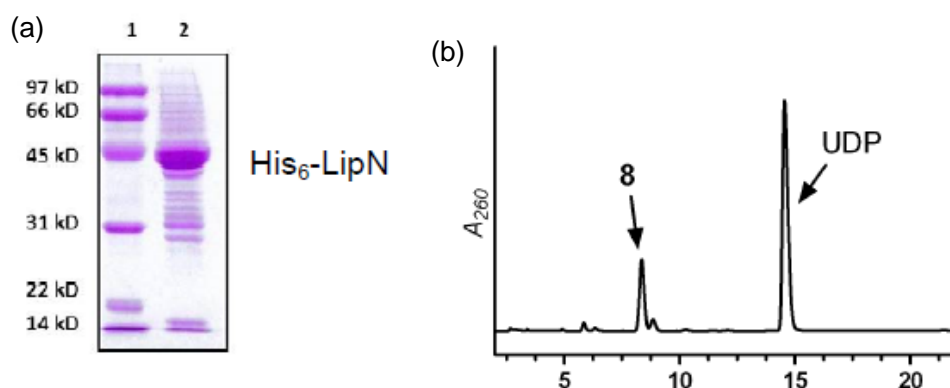


**Figure 2.34.** LipN protein gel and HPLC analysis the degradation of UDP-5''-amino-2'',5''-dideoxyribose (**8**). (a) SDS-PAGE of partially purified His<sub>6</sub>-LipN (expected MW of 42.3 kD). (b) HPLC analysis using ion-pairing chromatography revealing the degradation of UDP-5''-amino-2'', 5''-dideoxyribose (**8**) to UDP following storage at -20 °C for one week.



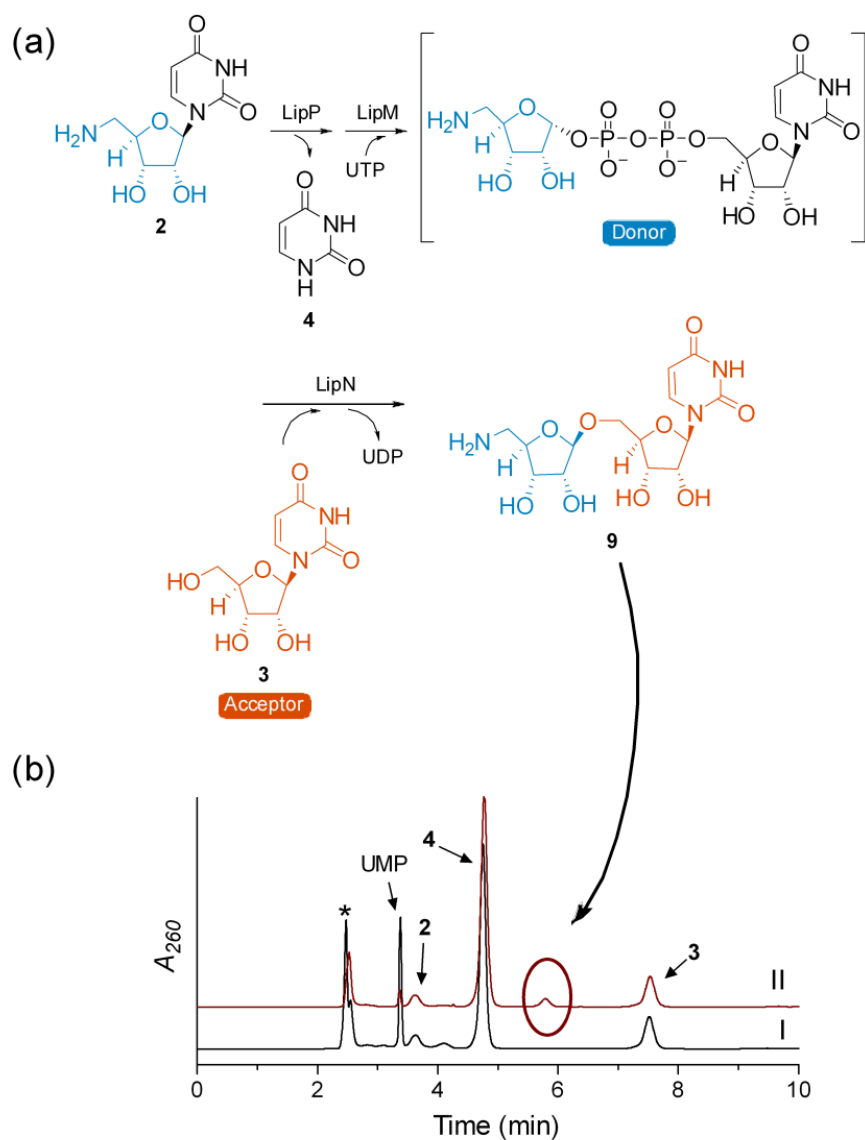


**Figure 2.35.** *In vitro* characterization of LipN with substrate 5'-amino-5'-deoxyuridine (**2**). (a) Enzymatic preparation of the sugar donor substrate using LipP and LipM, and the reaction catalyzed by LipN using the surrogate acceptor substrate **3** to generate 5'-O-(5''-amino-5'-deoxy-β-D-ribose)-uridine (**9**). (b) HPLC analysis of the reaction starting with 5'-amino-5'-deoxyuridine (**2**) after (I) 3 hr without LipN and (II) 3 hr reaction. \*indicates expected retention time for residual UTP and co-product UDP.  $A_{260}$ , absorbance at 260 nm.

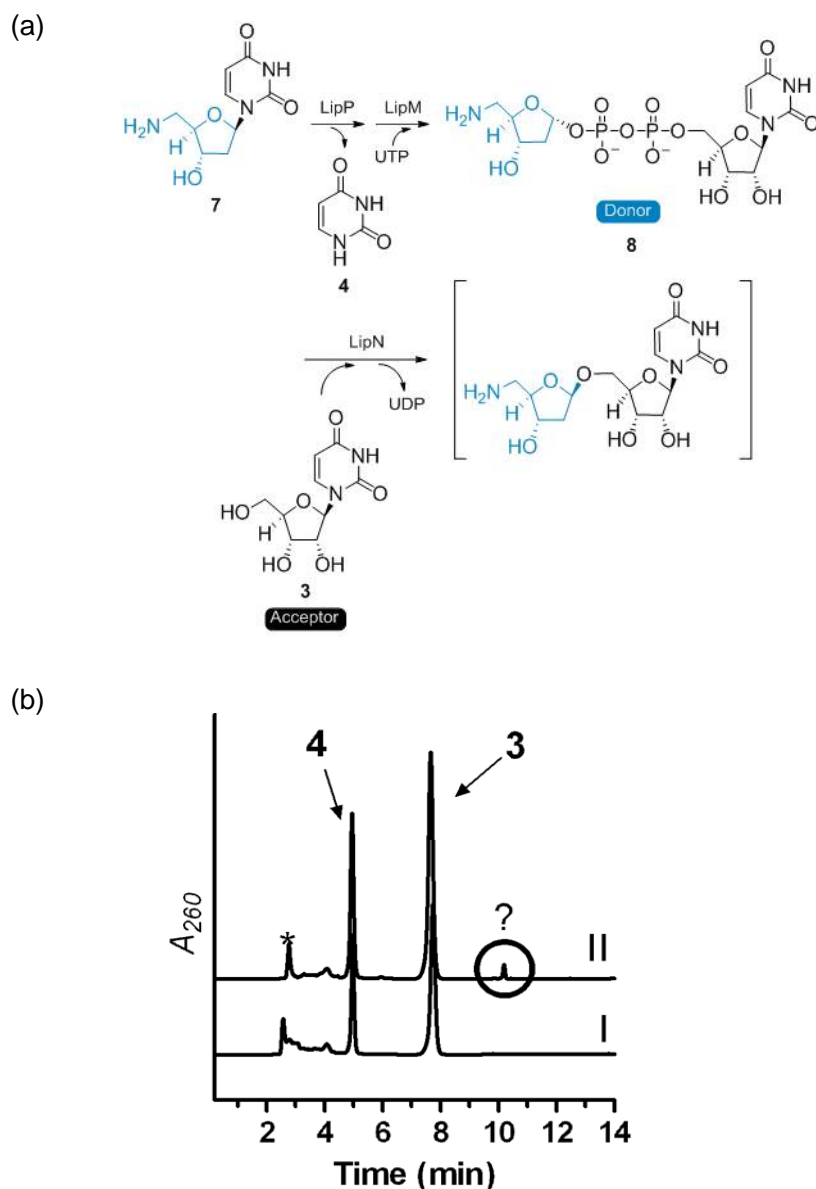


**Figure 2.36.** *In vitro* characterization of LipN with substrate 5'-amino-2',5'-dideoxyuridine (7). (a) Enzymatic preparation of the sugar donor substrate using LipP and LipM, and the reaction catalyzed by LipN using the surrogate acceptor substrate uridine (3) to generate the putative product shown. (b) HPLC analysis using uridine (3) as the acceptor substrate and UDP-5''-amino-2'', 5''-dideoxyribose (8) as the donor substrate (generated in situ starting from 5'-amino-2',5'-dideoxyuridine (7) after (I) 3 hr without LipN and (II) 3 hr reaction. \* indicates expected retention time for residual substrate UTP and product UDP.  $A_{260}$ , absorbance at 260 nm.

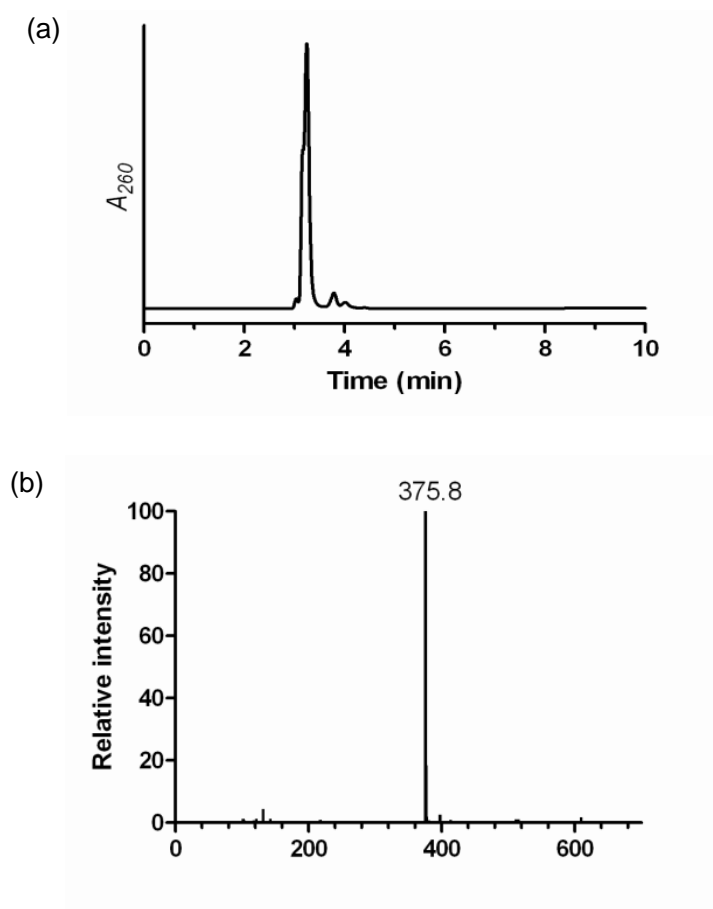


**Figure 2.37.** LC-MS of the LipN product 5'-O-(5''-amino-5''-deoxy- $\beta$ -D-ribose)-uridine (**9**) starting from 5'-amino-5'-deoxyuridine (**2**) as the ultimate sugar donor and uridine (**3**) as a surrogate acceptor. (a) LC analysis of 5'-O-(5''-amino-5''-deoxy- $\beta$ -D-ribose)-uridine (**9**) following purification. (b) Positive ion mass spectrum for the peak at elution time  $t = 3.2$  min.  $A_{260}$ , absorbance at 260 nm.

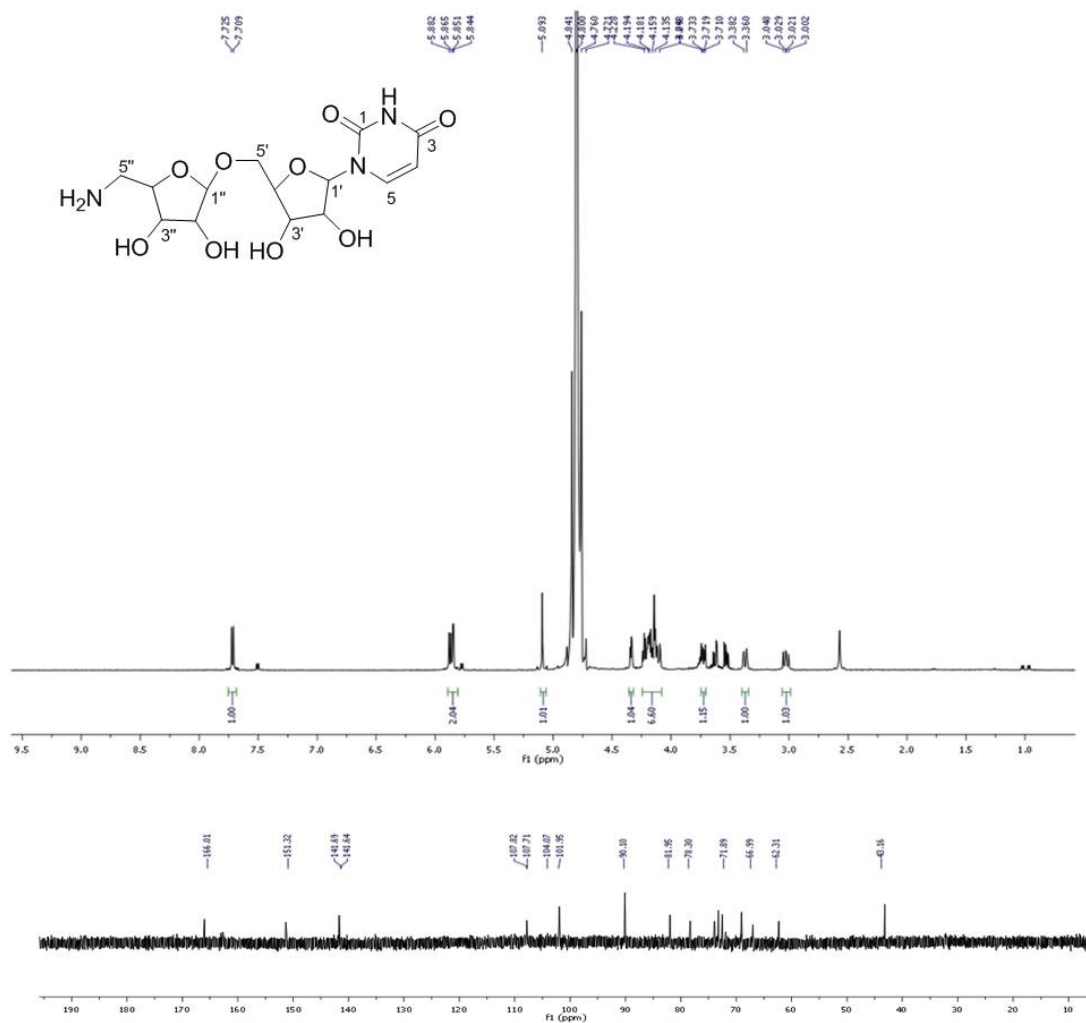


**Figure 2.38.** Characterization of 5'-O-(5''-amino-5''-deoxy-β-D-ribose)-uridine (**9**) by 1D NMR. (a) <sup>1</sup>H-NMR spectrum. (b) <sup>13</sup>C-NMR spectrum. \*unidentified impurity

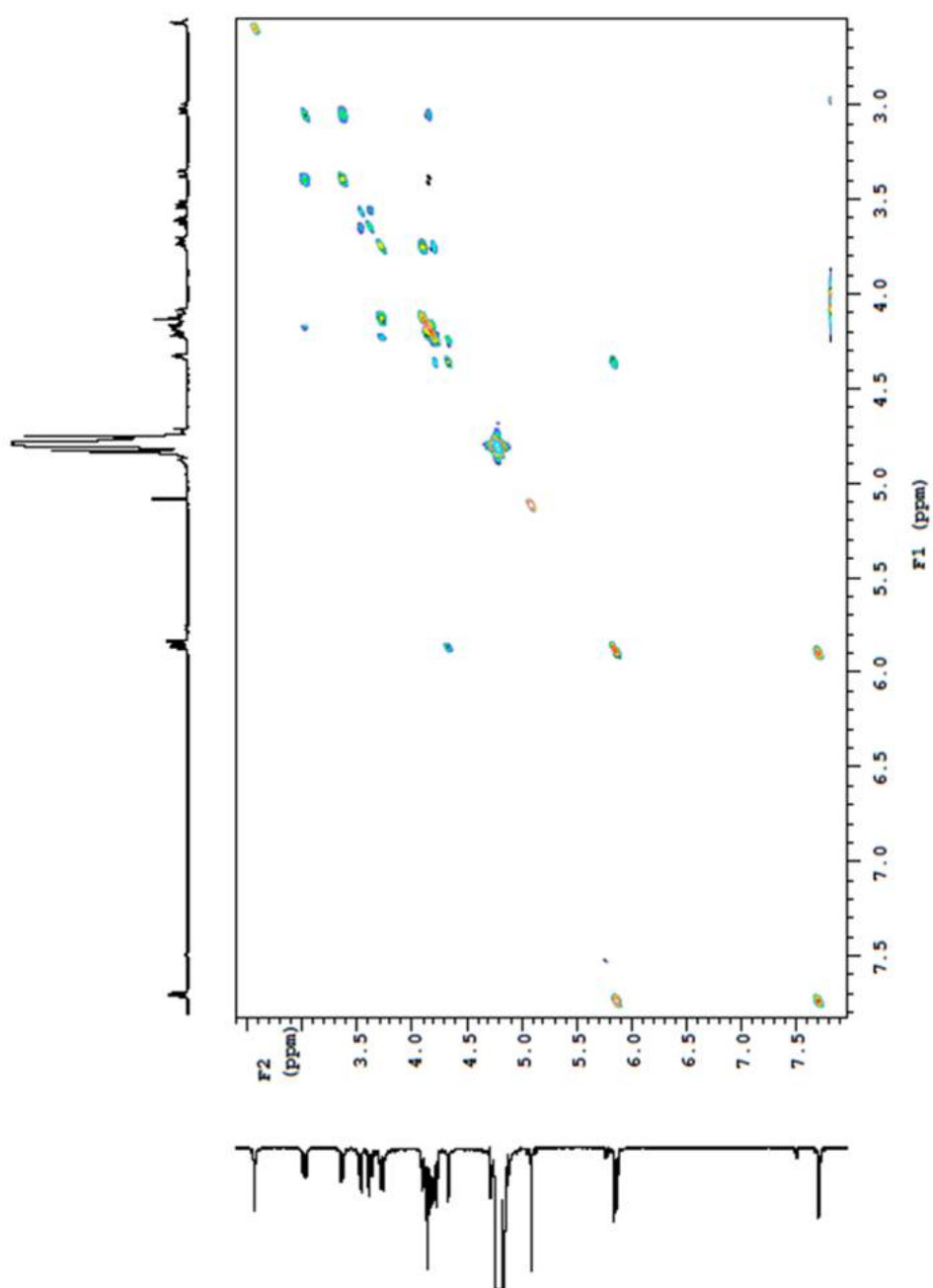


**Figure 2.39.** gCOSY NMR spectrum of 5'-O-(5''-amino-5''-deoxy- $\beta$ -D-ribose)-uridine (9).

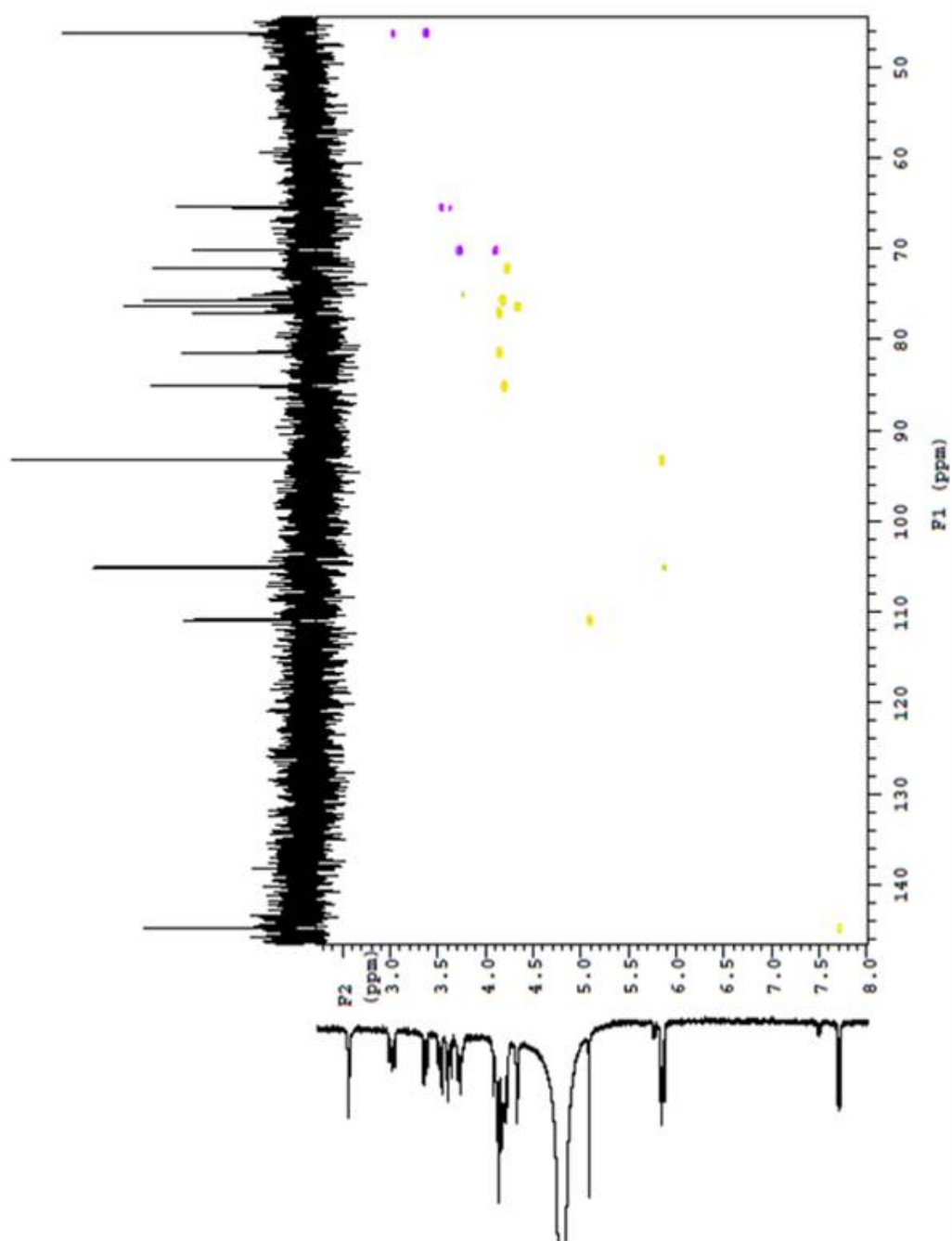


**Figure 2.40.** gHSQC NMR spectrum of 5'-O-(5''-amino-5''-deoxy- $\beta$ -D-ribose)-uridine (9).

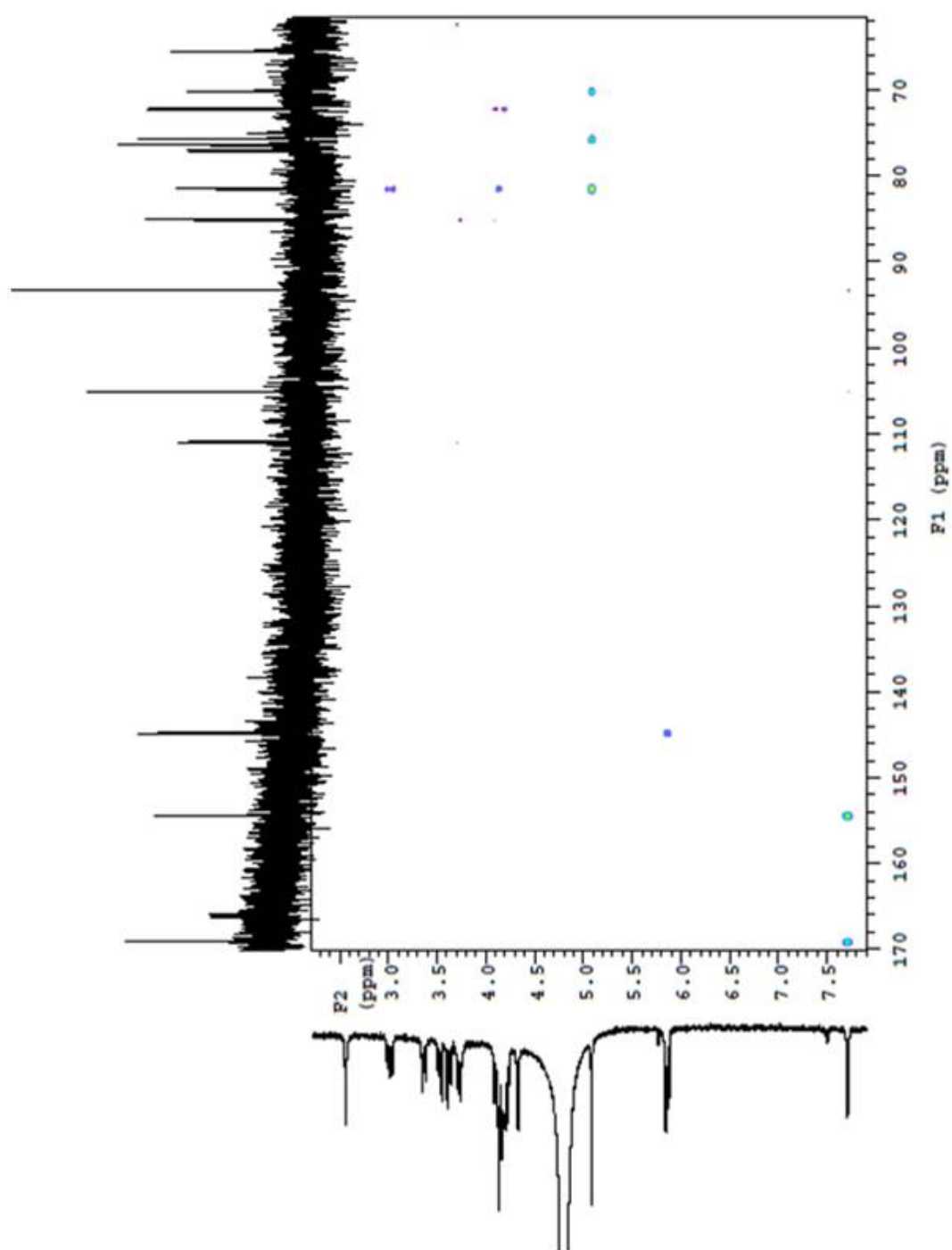


**Figure 2.41.**  $^1\text{H}$ - $^{13}\text{C}$  gHMBC NMR spectrum of 5'-O-(5''-amino-5''-deoxy- $\beta$ -D-ribose)-uridine (**9**).

## 2.7. Conclusion

In summary, we have completed the functional assignment of five enzymes involved in the modification and incorporation of the aminoribosyl moiety of A-90289 antibiotics. The pathway is initiated by the LipL-catalyzed conversion of a novel ribosyl donor UMP to form the aldehyde uridine-5'-aldehyde (**1**) [88]. Following introduction of the amine by LipO, LipP catalyzes phosphorolysis to initiate “salvage” of the modified sugar and LipM subsequently catalyzes the formation of an activated pentofuranose that serves as the final sugar donor. Finally, the ribosyltransferase LipN completes the pathway by incorporation of the aminoribosyl moiety, the identity of which is apparently dictated by the specificity of the pathway-initiating enzyme LipL and the penultimate enzyme LipM. The end result is a sugar biosynthetic pathway highlighted in **Fig 2.42** that not only establishes an alternative mechanism for ribosylation but also features intriguing variations of the established paradigm for glycosylation.

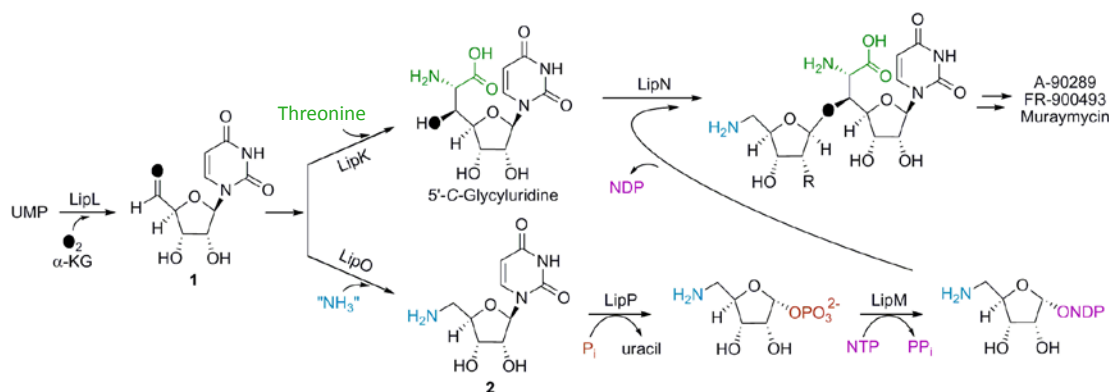


**Figure 2.42.** Finalized biosynthetic pathway for the incorporation of the aminoribosyl moiety of A-90289.

## 2.8. Discussion

Bacterial natural products are notorious for their diverse array of sugar modifications that are typically critical for their biological activity. As a result there has been a significant effort toward understanding the molecular details behind incorporation of



these sugars, in part with the expectation that the results will ultimately enable rationale manipulation of sugar biosynthetic pathways as a strategy to produce novel glycosylated compounds [63,64]. Undoubtedly, the identification and characterization of new pathways will afford more tools for applying such a structural diversification approach, and thus we initiated studies toward delineating the biosynthetic mechanism of a unique pentofuranose—an aminoribosyl moiety found in several lipopeptidyl nucleosides of potential therapeutic significance as antibiotics. Our strategy to unravel the pathway was to reconstitute the enzyme activities *in vitro*, which ultimately required the use of the heterologous host *S. lividans* TK64 to obtain three of the four enzymes in soluble form. Our prior results with LipL demonstrated this enzyme had strict specificity for the substrate UMP to initiate the pathway [88], an attribute that was not reciprocated by the four enzymes assigned in this study. LipO utilized a variety of amine donors with L-methionine as the slightly preferred amine source, the biological relevance of which is currently under investigation. Likewise, the phosphorylase LipP was equally efficient with hypothetical pathway intermediates 5'-amino-5'-deoxyuridine (**2**) and uridine (**3**). Sequence analysis of the whole genomes of the Actinomycetales has revealed minimally one 5'-nucleosidase is encoded within the chromosomal DNA suggesting these organisms have the capability to convert the nucleic acid building block UMP to uridine (**3**). Thus, based solely on the results with LipP, the identity of the *in vivo* substrate could not be established. However, the realization that the amine needs to be incorporated prior to formation of activated sugar would necessitate an additional, unidentified enzyme to oxidize  $\alpha$ -D-ribose-1-phosphate prior to LipO catalysis if uridine (**3**) was indeed the pathway precursor. Thus, we currently prefer a pathway originating from UMP without the involvement of uridine (**3**) as shown in **Figure 2.42**.

While we were initially disheartened by the lack of substrate specificity of LipP, this low specificity turned out to be critical for discovering the function of LipM by enabling the preparation of a surrogate substrate that was converted to a less unstable product for structural elucidation. Similarly, we took advantage of the

promiscuity of LipN with respect to the sugar acceptor to define its function as a ribosyltransferase. Interestingly, although the genuine sugar donor UDP-5-amino-5-deoxy- $\alpha$ -D-ribose was initially only indirectly identified as the LipM-product based on the identification of UMP and OPA modified 5-amino-5-deoxy- $\alpha$ -D-ribose-1,2-cyclicphosphate (OPA-6) and—despite exhaustive attempts—could not be directly observed by MS, our successful analysis of LipN with in situ generated UDP-5-amino-5-deoxy- $\alpha$ -D-ribose suggests that this activated sugar is formed yet is refractive to direct characterization using the conditions employed here. Although it remains a possibility that 5-amino-5-deoxy- $\alpha$ -D-ribose-1,2-cyclicphosphate (**6**) is generated enzymatically by a contaminating protein, several activated sugars are known to be unstable; for instance, it has recently been reported that the expected product of UDP-apiose/UDP-xylose synthase can be transiently detected by high-field NMR prior to degrading to the isolable apiofuranosyl-1,2-cyclic phosphate [97] and the activated carbocycle NDP-valienol can only be detected by MS within the crude reaction mixture [107].

Although the glycosylation process predominantly involves the incorporation of hexoses, it is not limited to these sugars: several pentose units, for example, are derived from this glycosylation mechanism that typically proceeds with decarboxylation of an NDP-glucuronic acid (**Fig 2.43**) [97,108,109,110,111,112]. Alternatively, sugar salvage pathways from plants [113,114][115], and the thermophilic bacterium *Thermus caldophilus* GK24 [116] have been characterized that utilize broad-specificity nucleotidyltransferases capable of activating the pentopyranosyl phosphates of D-xylose and L-arabinose albeit with lower efficiencies than the  $\alpha$ -D-hexopyranosyl phosphates of glucose and galactose. Furthermore, a nucleotidyltransferase from *Salmonella enterica typhimurium* LT2 ( $E_p$ ) has been extensively studied and shown to utilize  $\alpha$ -D-xylose-1-phosphate along with dozens of  $\alpha$ -D-hexopyranosyl phosphates [117,118,119]. Although a more in depth investigation is underway, our results identified LipM as an unusual

$\alpha$ -D-pentofuranosyl-1-phosphate-activating enzyme with an apparently more refined specificity and hence well-defined role in A-90289 biosynthesis. Furthermore, LipM was shown to have an absolute requirement for the primary amine functionality, which is likewise unusual relative to other bacterial nucleotidyltransferases that have been demonstrated to activate unnatural aminohexoses although with equal or less efficiency relative to the hydroxylated counterpart [118,119,120,121,122].

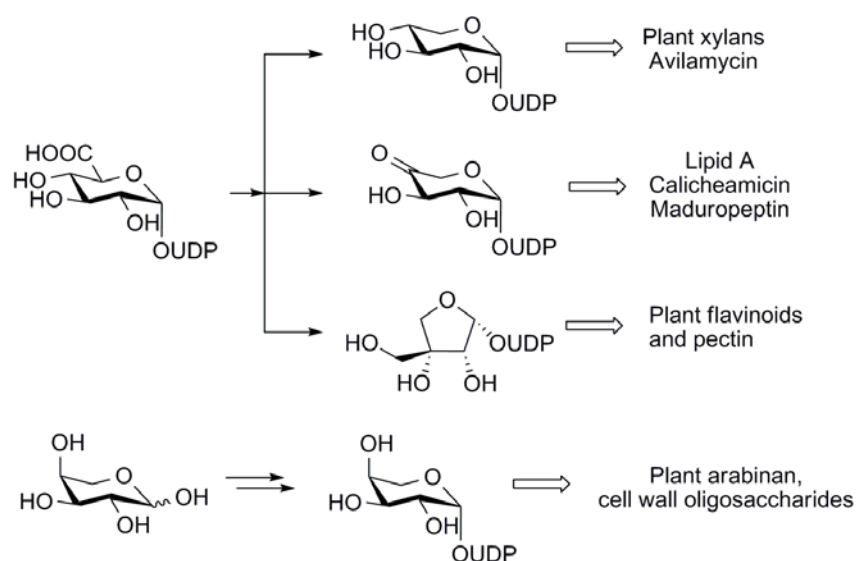
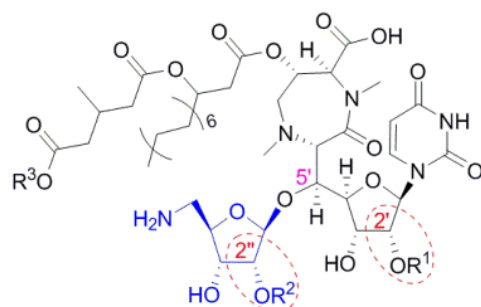


**Figure 2.43.** The conventional glycosylation mechanism with an NDP-sugar as the sugar donor.

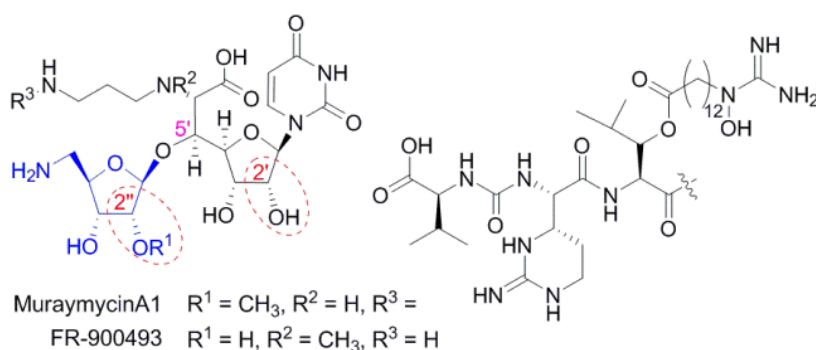
## Chapter three: Biosynthetic pathway of 2'-deoxyaminoribosyl moiety of muraminomicin

### 3.1. Background

Muraminomicin, which is isolated from *Streptosporangium amethystogenes* SANK 60709, was discovered based on its potent inhibitory activity on bacterial translocase I ( $IC_{50}=12.8$  ng/ml)[84]. Subsequently, muraminomicin was shown to have excellent anti Gram-positive bacteria activity against strains like *S. aureus* & *B. subtilis* [123]. Structural determination revealed muraminomicin belonged to the peptidyl nucleoside antibiotics family (**Fig 3.1**). However, unlike A-90289 and caprazamycins, a few unique structural features were uncovered. These included a deoxyheptose in place of the permethylated rhamnose, an appended succinyl moiety, and the incorporation of 2-deoxyribosyl. The structure-activity relationship of muraminomicin is still not defined, and nothing is known about how this molecule is assembled. In order to pinpoint the factors controlling the incorporation of these and other structural variations observed in muraminomicin, the biosynthetic gene cluster of muraminomicin has been identified and five 2-deoxyfuranoses biosynthetic related enzymes (Mra20-Mra24) were uncovered, all with sequence similarity to those identified within the A-90289 gene cluster. Thus, it appeared that the 2-deoxyribose followed the unusual paradigm revealed from analysis of the A-90289 biosynthetic pathway.



A-90289 A  $R^1 = \text{SO}_3\text{H}$ ,  $R^2 = \text{H}$ ,  $R^3 = \text{permethylated rhamnose}$   
 Caprazamycin A  $R^1 = \text{H}$ ,  $R^2 = \text{H}$ ,  $R^3 = \text{permethylated rhamnose}$   
 Liposidomycin C  $R^1 = \text{H}$ ,  $R^2 = \text{SO}_3\text{H}$ ,  $R^3 = \text{H}$



Significantly natural product with a similar 2-deoxyfuranose structure are rare, and thus by unraveling the biochemical events in muraminomicin biosynthesis is expected to provide us novel and valuable information that can be used to prepare new compounds. We have now successfully defined the function of the two of the enzymes to provide insight into how this deoxy furanose is assembled de novo.

## 3.2. Materials and methods

### 3.2.1. Chemicals and instrumentation

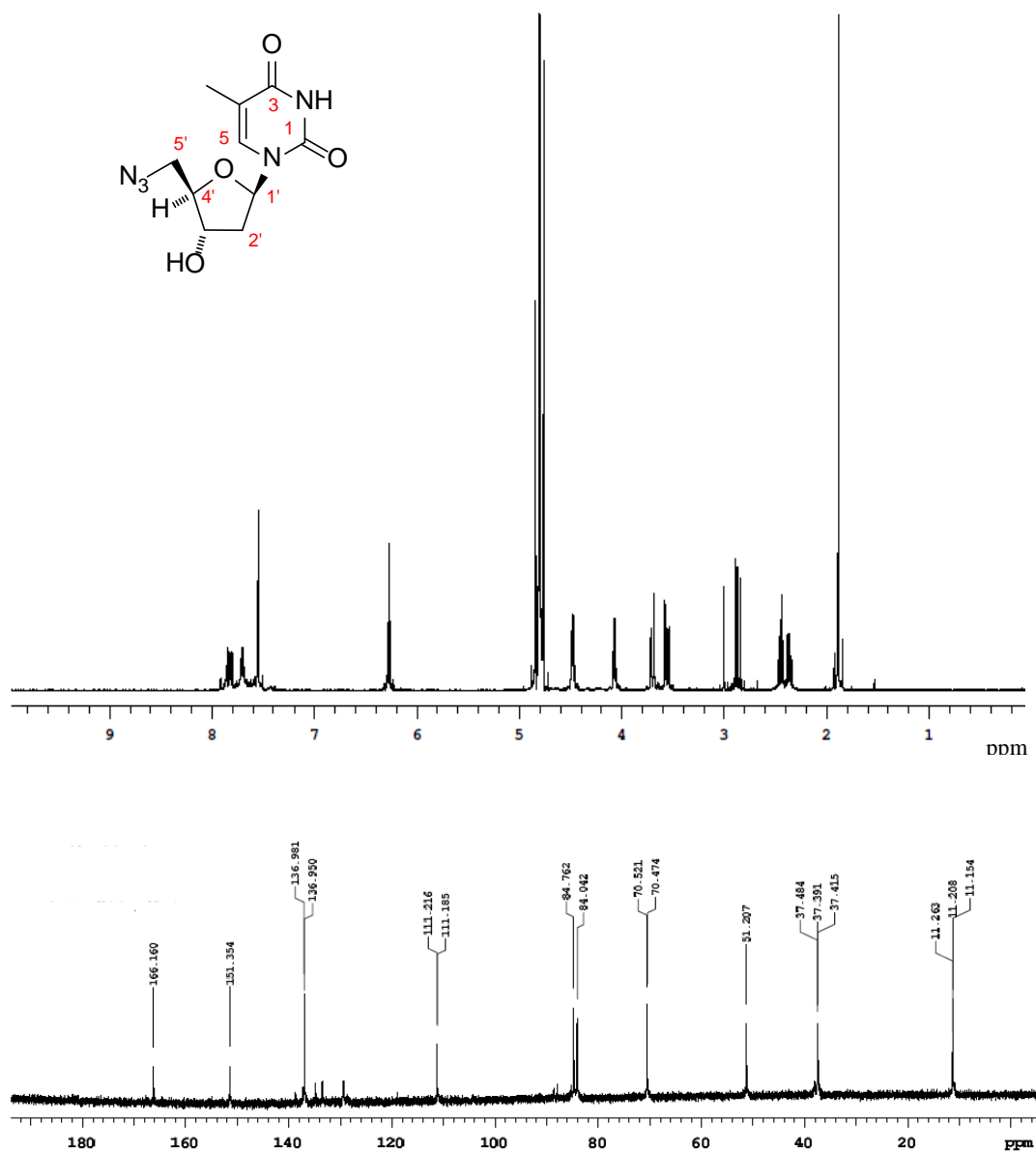
Nucleoside bases, nucleosides, and nucleotides were purchased from Sigma or Promega. Buffers, salts, and media components were purchased from Fisher Scientific. UV/Vis spectroscopy was performed with a Bio-Tek  $\mu$ Quant microplate reader using Microtest™ 96-well plates or a Shimadzu UV/Vis-1800 Spectrophotometer. Synthetic oligonucleotides were purchased from Integrated DNA Technologies. DNA sequencing was performed using the BigDye™ Terminator version 3.1 Cycle Sequencing kit from Applied Biosystems, Inc. and analyzed at the University of Kentucky Advanced Genetic Technologies Center. HPLC was performed with a Waters Alliance 2695 separation module (Milford, MA) equipped with a Waters 2998 diode array detector and an analytical Apollo C-18 column (250 mm x 4.6 mm, 5  $\mu$ m) or a semi-preparative Apollo C-18 column (250 mm x 10 mm, 5  $\mu$ m) purchased from Grace. Electrospray ionization-MS was performed using an Agilent 6120 Quadrupole MSD mass spectrometer equipped with an Agilent 1200 Series Quaternary LC system and an Eclipse XDB-C18 column (150mm x 4.6 mm, 5  $\mu$ m, 80Å). NMR data were collected using a Varian Unity Inova 300, 400 or 500 MHz Spectrometer.

### 3.2.2. Synthesis of substrates

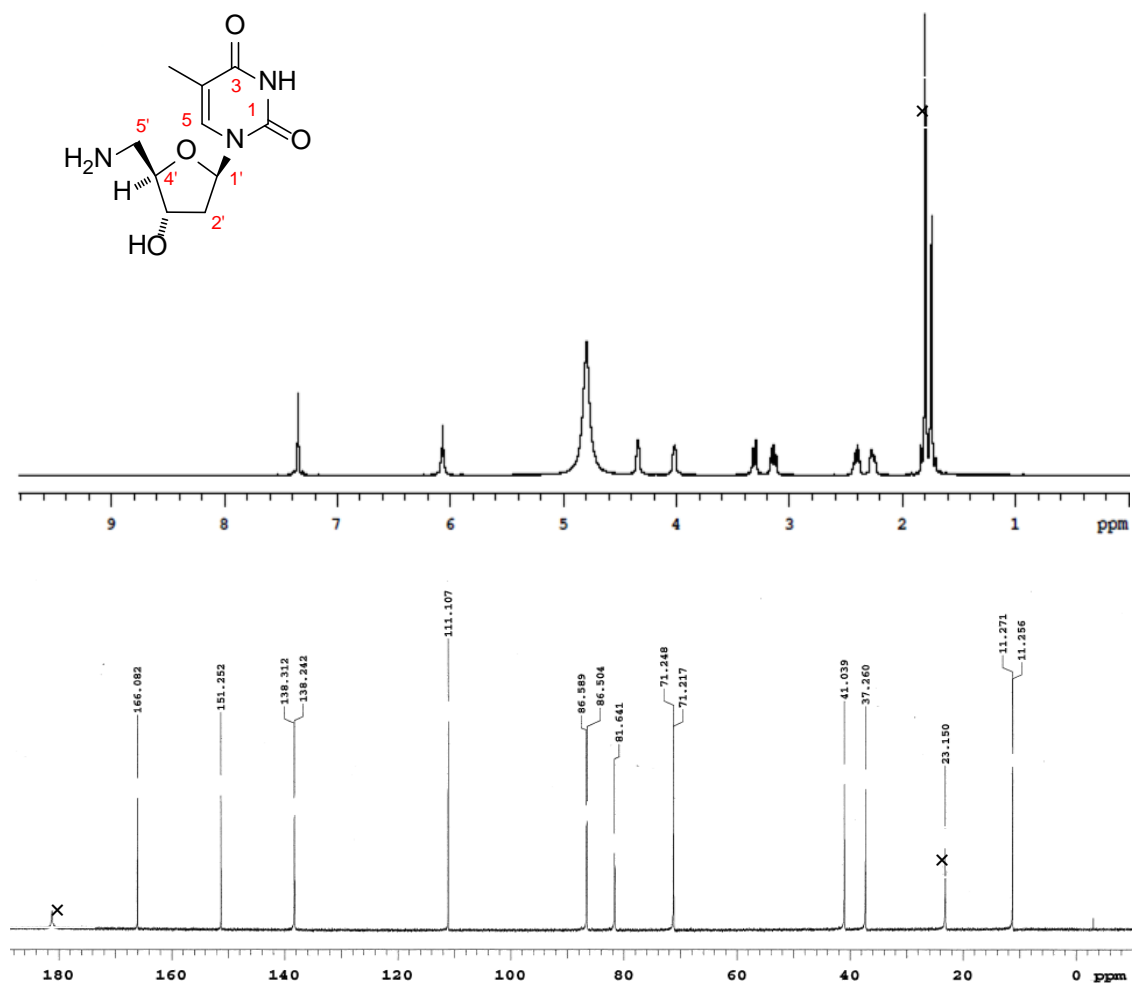
The synthesis of 5'-amino-5'-deoxyuridine (**2**) and 5'-amino-2',5'-dideoxyuridine (**7**) was described in section 2.2.5 and 2.2.6 [124]. The identical two-step procedure for the latter was used to synthesize 5'-amino-5'-deoxythymidine (**10**) (see below).

*Step 1: 5'-Azido-5'-deoxythymidine.*  $^1\text{H}$ -NMR (500MHz,  $\text{D}_2\text{O}$ ):  $\delta$  7.55 (s, 1H), 6.27 (t, 1H,  $J = 7$  Hz), 4.51-4.45 (m, 1H), 4.08-4.04 (m, 1H), 3.72-3.51 (m, 2H), 2.50-2.31 (m, 2H), 1.89-1.82 (s, 3H);  $^{13}\text{C}$ -NMR (100MHz,  $\text{D}_2\text{O}$ ):  $\delta$  166.2 (C), 151.4 (C), 136.97 (CH), 111.2 (CH), 84.8 (CH), 84.1 (CH), 70.5 (CH), 51.2 ( $\text{CH}_2$ ), 37.4 ( $\text{CH}_2$ ), 11.2

(CH<sub>3</sub>).



Step 2: 5'-Amino-5'-deoxythymidine, **2**. <sup>1</sup>H-NMR (500 MHz, D<sub>2</sub>O): δ 7.36 (s, 1H), 6.07 (t, 1H, J = 7 Hz), 4.38-4.30 (m, 1H), 4.08-3.95 (m, 1H), 3.35-3.08 (m, 2H), 2.45-2.22 (m, 2H), 1.78-1.70 (s, 3H); <sup>13</sup>C-NMR (125 MHz, D<sub>2</sub>O): δ 166.1 (C), 151.3 (C), 138.3 (CH), 111.2 (CH), 86.5 (CH), 81.6 (CH), 71.2 (CH), 41.0 (CH<sub>2</sub>), 37.3 (CH<sub>2</sub>), 11.3 (CH<sub>3</sub>). (x: acetate)



### 3.2.3. Cloning of the muraminomicin gene cluster

*Streptosporangium amethystogenes* sp. SANK 60709 genomic DNA was partially digested with *Sau3AI* to give ~40-kb DNA fragments that were dephosphorylated with bacterial alkaline phosphatase (BAP) and ligated into *Bam*HI-digested cosmid vector SuperCos1-P that contains the loxP site in SuperCos1 and was dephosphorylated by BAP after *Xba*I digestion. The ligation products were packaged with Gigapack III Gold packaging extract as described by the manufacturer, and the resulting recombinant phage was used to transfect *E. coli* XL-1 Blue MR. Approximately 10,000 colonies from the obtained genomic library were screened by colony hybridization using digoxigenin (DIG)-labeled DNA obtained by PCR using degenerate primers as previously described[125]. Hybridization was carried out using DIG easy hyb at 42 °C



and the resulting filter was washed under high stringency conditions (0.1 X SSC including 0.1 % SDS, 68 °C). Detection was performed using CDP-Star according to the manufacturer's procedures.

Based on restriction digest analysis, four positive cosmids, pMra01-04, were isolated and sequenced using a Roche GS FLX system. Potential open reading frames were defined using Frameplot 4.0, and database comparison for sequence homology was performed with BLAST search tools using the National Center for Biotechnology Information. The sequence has been deposited at GenBank under accession no. AB746937.

#### **3.2.4. Construction of genomic cosmid libraries**

Genomic DNA of muraminomycin was isolated following a standard instruction [126]. Then the genomic DNA was packaged using BigEasy<sup>®</sup> v2.0 Linear Cloning Kits [127]. Firstly, the genomic DNA was partially digested with *NotI* to generate restriction fragments. Then the produced fragments were ligated to the pJAZZ<sup>®</sup> vector and transformed into BigEasy TSA<sup>™</sup> electrocompetent cells. More than 5000 colonies were obtained as positive clones. Degenerate primers (*mra24\_probe\_for* and *mra24\_probe\_rev*) (**Table 5**) were designed to amplify the internal nucleotide sequences of dioxygenase from the genomic DNA of *Streptosporangium amethystogenes* sp. The amplified fragments were labeled with DIG and preceded with hybridization and finally used for screening. The colony hybridization and southern blot analyses revealed four different cosmid clones.

#### **3.2.5. Inactivation of *mra20* gene by PCR targeting**

The double crossover inactivation experiment was carried out using a modified PCR-targeting REDIRECT protocol [128]. Briefly, a chloramphenicol resistance gene with engineered flanking flippase recognition target (FRT) was used as a template to

amplify disruption cassette using the primer pair (*mra20\_inact\_for*, *mra20\_inact\_rev*) (**Table 5**). *E. coli* BW25141/pKD78 (amp<sup>r</sup>) cell was transferred with pMra02 cosmid. The resulting chloramphenicol inactivation cassettes were then introduced into *E. coli* BW25141/pKD78 (amp<sup>r</sup>) by electroporation. The incubation temperature was increased from 30°C to 37°C to eliminate the temperature sensitive cosmid, and the resulting amp and apr resistant colonies were harvested for further use. A control primer pair (*mra20\_con\_for* + *mra20\_con\_rev*) was created from nearly upstream of *mra20* and was used to confirm the replacement of the targeted gene with the chloramphenicol cassette (**Table 5**). The final mutated cosmid (*pMra02-mra20-*) was transformed into *E. coli* ET12567/pUZ8002 and conjugated into muraminomicin producing strain following the standard protocol procedure.

### 3.2.6. Cloning of genes for heterologous expression

Genes were amplified by PCR using Expand Long Template PCR System from Roche with supplied Buffer 2, 200 µM dNTPs, 5% DMSO, 10 ng DNA pMra02, 5 U DNA polymerase, and 200 nM each of the following primer pairs (**Table 5**). The PCR program included an initial hold at 94 °C for 2 min, followed by 30 cycles of 94 °C for 10 s, 56 °C for 15 s, and 68 °C for 60 s. The gel-purified PCR product was inserted into pET-30 Xa/LIC using ligation-independent cloning as described in the provided protocol to yield pET30-*mra20* to pET30-*mra24* (**Table 6**). The genes were sequenced to confirm PCR fidelity.

**Table 5.** List of primers used in muraminomycin.

Primers	Oligonucleotide sequence
<i>mra20_for</i>	5'- GGTATTGAGGGTCGCATGAACGAGAT -3'
<i>mra20_rev</i>	5'- AGAGGAGAGTTAGAGCCTCACCCGG -3'
<i>mra23_for</i>	5'- GGTATTGAGGGTCGCATGTCGGTCG -3'
<i>mra23_rev</i>	5'- AGAGGAGAGTTAGAG CCTCAGCCGA -3'
<i>mra21_for</i>	5'- GGTATTGAGGGTCGCATGAGCGGGA-3'
<i>mra21_rev</i>	5'- AGAGGAGAGTTAGAGCCTCATCCGAC-3'
<i>mra22_for</i>	5'- GGTATTGAGGGTCGCATGGCACCCG -3'
<i>mra22_rev</i>	5'- AGAGGAGAGTTAGAGCCTCACTCTGA-3'
<i>mra24_for</i>	5'- GGTATTGAGGGTCGCATGAGCCAATT -3'
<i>mra24_rev</i>	5'- AGAGGAGAGTTAGAGCCTCAAGCGG-3'
<i>mra20_inact_for</i>	5'-CCTGGACGCGCTCGATACGGCGGGAAGGCACGTCGGA TGATTCCGGGGATCCGT CGACC-3'
<i>mra20_inact_rev</i>	5'-CTCTGTTACCGGCGGGAAGACGCCGCCAACGGGTGTTC A TGTAGGCTGGAGCTGCTTC-3'
<i>mra20_con_for</i>	5'-GCCGGCGTCGCCGACGT-3'
<i>mra20_con_rev</i>	5'-TTCACGCGCGGATTACG-3'
<i>mra24_probe_for</i>	5'-GAACGGCACACAGACCGAAC-3'
<i>mra24_probe_rev</i>	5'-ATCTTGTCGCAGACGCCGAG-3'

Plasmids were introduced into *E. coli* BL 21(DE3) cells, and the transformed strains were grown in LB supplemented with 50 µg/mL kanamycin. Following inoculation of 500 mL of LB with 50 µg/mL kanamycin, the cultures were grown at 18°C until the cell density reached an OD<sub>600</sub> ~ 0.5 when expression was induced with 0.1 mM IPTG. Cells were harvested after an overnight incubation at 18 °C and lysed using a French Press with one pass at 15000 psi. Following centrifugation the protein was purified using affinity chromatography with Ni-NTA agarose from Qiagen, and the recombinant proteins were desalted into 50 mM Tris-HCl (pH 8), 100 mM NaCl, and 5 % glycerol using a PD-10 desalting column. The purified protein was concentrated using an Amicon Ultra 10000 MWCO centrifugal filter and stored as glycerol stocks (40%) at -20 °C. Protein purity was assessed as by 12% acrylamide SDS-PAGE; His<sub>6</sub>-tagged proteins were utilized without further modifications.

**Table 6.** List of plasmids constructed/used in muraminomicin.

Strain/Plasmid	Characteristics and Relevance	References
<i>E.coli</i> Nova-Blue	Host for routine cloning works	Novagen
<i>E.coli</i> BL21 (DE3)	Host for protein expression	Novagen
pET30	Expression vector	Novagen
pET30- <i>mra20</i>	<i>mra20</i> gene cloned to pET30	This study
pET30- <i>mra23</i>	<i>mra23</i> gene cloned to pET30	This study
pET30- <i>mra21</i>	<i>mra21</i> gene cloned to pET30	This study
pET30- <i>mra22</i>	<i>mra22</i> gene cloned to pET30	This study
pET30- <i>mra24</i>	<i>mra24</i> gene cloned to pET30	This study
pUWL201pw	Expression vector	This study
pUWL201pw- <i>mra21</i>	<i>mra21</i> gene cloned to pUWL201pw	This study
pUWL201pw- <i>mra22</i>	<i>mra22</i> gene cloned to pUWL201pw	This study
pUWL201pw- <i>mra24</i>	<i>mra24</i> gene cloned to pUWL201pw	This study

### 3.2.7. *In vitro* characterization of Mra20

Reactions consisted of 25 mM potassium phosphate pH 7.5, 2 mM 5'-amino-5'-deoxyuridine (**2**) or analogue, and 100 nM Mra20 at 30 °C, and terminated by the addition of cold TCA to 5% (w/v) or by ultrafiltration using a Microcon YM-3. Following centrifugation to remove protein, the reaction components were analyzed by HPLC using a C-18 reverse-phase column. A series of linear gradients was developed from 40 mM phosphoric acid-triethylamine pH 6.5 (A) to 20% methanol (B) in the following manner (beginning time and ending time with linear increase to % B): 0-8 min, 0% B; 8-18 min, 60% B; 18-25 min, 95% B; 25-32 min, 95% B; and 32-35 min, 0% B. The flow rate was kept constant at 1.0 mL/min, and elution was monitored at 260 nm.

To determine the kinetic constants with respect to the co-substrate nucleoside, reactions were carried out in 50 mM Tris-HCl pH 9.0 consisting of saturating phosphate (1.5 mM) and variable nucleoside (25 – 5,000  $\mu$ M), and 100 nM Mra20 at 30 °C under initial velocity conditions. The reactions were terminated with 0.1 M

sodium hydroxide, and nucleobase formation was determined by UV/Vis spectroscopy with  $\Delta\epsilon_{300\text{ nm}} = 3,700\text{ M}^{-1}$  at pH 13 for thymine (**13**) and  $\Delta\epsilon_{290\text{ nm}} = 5,700\text{ M}^{-1}$  at pH 13 for uracil (**4**).

### 3.2.8. *In vitro* characterization of Mra23

Reactions consisted of 50 mM potassium phosphate pH 7.5, 5 mM  $\text{MgCl}_2$ , 2 mM thymidine (**12**) or analogue, 5 mM UTP, 5  $\mu\text{M}$  Mra20, and 1  $\mu\text{M}$  Mra23 at 30 °C, and the reaction terminated by the addition of cold TCA to 5% (w/v) or by ultrafiltration using a Microcon YM-3. The activity of Mra23 was tested with sugar-1-phosphates generated in situ from synthetic 5'-amino-2',5'-dideoxyuridine(**7**), thymidine (**12**), 5'-amino-5'-deoxythymidine (**10**) or 2'-deoxyuridine (**11**) with co-substrate UTP. Following centrifugation to remove protein, the reaction components were analyzed by HPLC using a phosphoric acid-triethylamine mobile phase as described above. LC-MS was performed using a linear gradient from 0.1% formic acid in water to 0.1% formic acid in acetonitrile over 20 min. The flow rate was kept constant at 0.4 mL/min, and elution was monitored at 254 nm.

### 3.2.9. Subcloning and expression in *S. lividans* TK-64

Plasmids pET30-*mra21*, pET30-*mra22* and pET30-*mra24* were digested with *NdeI-HindIII* and the DNA fragment of the expected size was purified and ligated to the identical sites of pUWL201pw to yield pUWL201pw-*mra21*, pUWL201pw-*mra22* and pUWL201pw-*mra24*, respectively (**Table 6**). The detailed procedures were described in section **2.2.8**.

### 3.2.10. *In vitro* characterization of Mra21

Reactions consisted of 50 mM potassium phosphate pH 7.5, 2 mM

uridine-5'-aldehyde (**1**), 2 mM amine donor, 200  $\mu$ M PLP, and 1  $\mu$ M Mra21 at 30 °C, and the reaction terminated by the addition of cold TCA to 5% (w/v) or by ultrafiltration using a Microcon YM-3. Different amino acids were used as amine donors to test Mra21 activity. HPLC analysis of the reaction was similar to that described for LipM.

#### **3.2.11. *In vitro* characterization of Mra22**

Reactions consisted of 50 mM potassium phosphate pH 7.5, 2 mM 5'-amino-2',5'-dideoxyuridine(**7**) or 5'-amino-5'-deoxythymidine (**10**), 2.8  $\mu$ M Mra20 at 30 °C for 2 hours. Mra20 was removed by ultrafiltration, and 86  $\mu$ L of the filtrate was added to a solution of 5 mM MgCl<sub>2</sub>, 2 mM UTP, 1 mM 2'-deoxyuridine (**11**), 12  $\mu$ M Mra23, and 7  $\mu$ M Mra22 (final volume of 100  $\mu$ L) and incubated at 30 °C for the indicated time points. HPLC analysis was performed using a TFA mobile phase as described above.

#### **3.2.12. *In vitro* characterization of Mra24**

Reactions consisted of 50 mM Tris-HCl (pH 7.5), 0.5 mM UMP or 2'-deoxy UMP, 1 mM  $\alpha$ -KG, 0.2 mM ascorbate, 0.1 mM FeCl<sub>2</sub>, and 3  $\mu$ M Mra24 at 30 °C. Control reactions were performed with or without the addition of corresponding components or enzyme. The reaction terminated by the addition of cold TCA to 5% (w/v) or by ultrafiltration using a Microcon YM-3. HPLC analysis of the reaction was similar to that described for LipM.

### **3.3. Results: Identification of muraminomicin gene cluster**

The structural similarity to liposidomycin, caprazamycin, and A-90289 suggested the muraminomicin gene cluster shares most of the biosynthetic genes. We recently

reported the utility of using degenerate primers for a gene annotated as aserine hydroxymethyltransferase (described in section 2.1) to specifically identify the genetic locus involved in the biosynthesis of these related nucleosides, and this strategy was employed here to amplify DNA fragments with the expected size from *Streptosporangium amethystogenes* sp. SANK 60709 genomic DNA. The amplified DNA was utilized as a probe to ultimately identify 4 cosmids (pMra01-04) that were sequenced and analyzed, yielding 53 complete *orfs* within 73.6 kb of contiguous DNA (**Fig 3.2a and Table 7**). Of these *orfs*, 22 were shared amongst all of the aforementioned clusters and a minimum of 2 *orfs* were unique to the muraminomicin gene cluster: *mra3* encoding a hypothetical membrane protein and *mra3* encoding a putative C-methyltransferase of the radical SAM superfamily and *mra4* encoding a hypothetical membrane protein. These *orfs* are inserted within a subcluster of genes responsible for the biosynthesis of the permethylated rhamnose, and the gene encoding a 3'-O-methyltransferase involved in A-90289 and caprazamycin biosynthesis (**Fig3.2b**) is missing from the muraminomicin gene cluster. Thus, it is proposed that Mra3 catalyzes C-methylation at C-6 of rhamnose to generate the unusual heptose found in muraminomicin while Mra4 functions as a 3-O-succinyltransferase (**Fig3.1**).

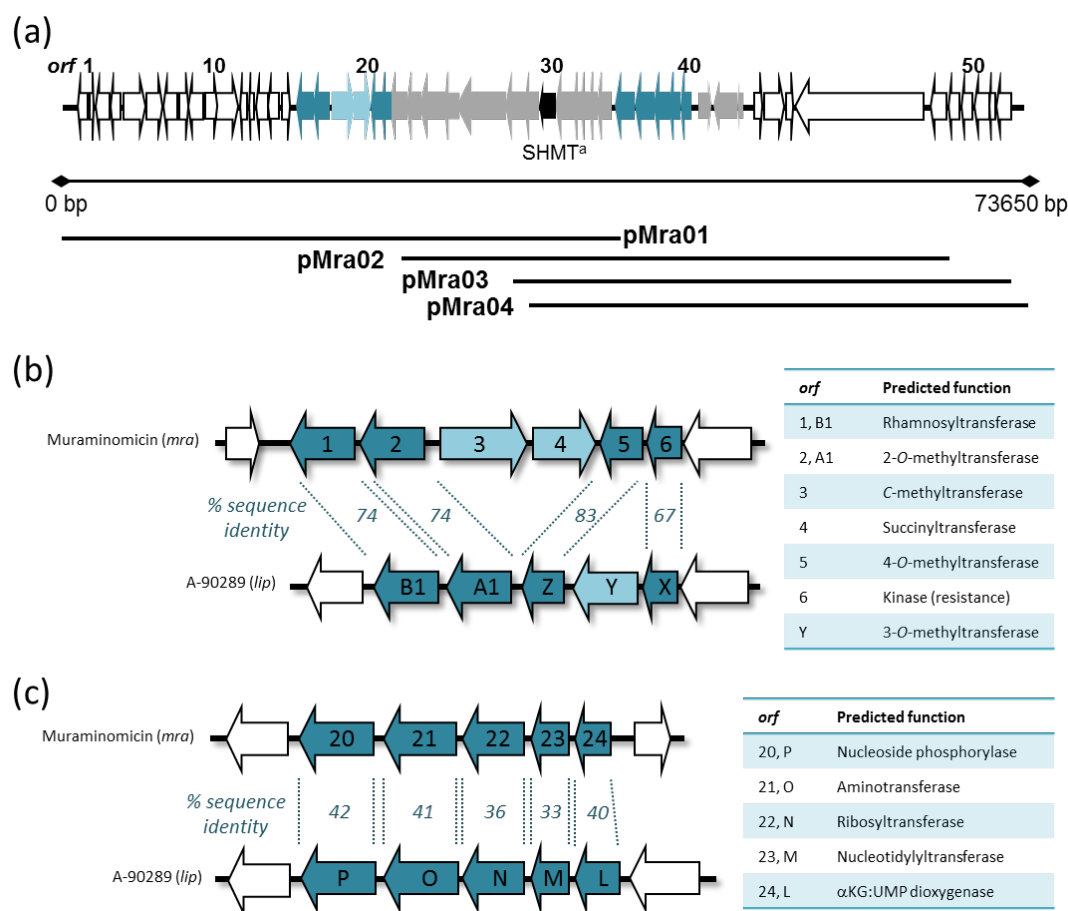


**Figure 3.2.** Genetic architecture of the muraminomicin gene cluster. (a) Organization of the ~74-kb of sequenced DNA. (b) Comparison of the subcluster of genes involved in the biosynthesis of the rhamnosyl moiety. (c) Comparison of the subcluster of genes involved in the biosynthesis of the aminoribosyl moiety.

**Table 7.** Annotation of ORFs within the muraminomicin gene cluster.

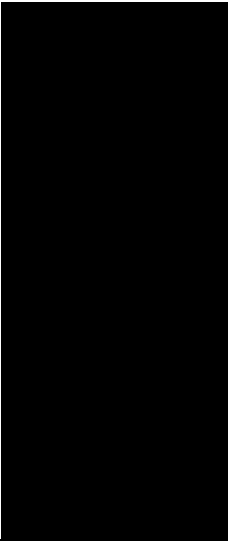
Protein <i>a</i>	Size <i>b</i>	Proposed function	Sequence similarity (protein, accession no., origin)	Identity / similarity <sup>c</sup>	A-90289 <i>d</i>	Identity %
ORF-1	25	RNA polymerase, sigma	SrosDRAFT_47470	93/97		
ORF-1	12	anti-anti-sigma factor	SrosDRAFT_47460	89/94		
ORF-1	35	hypothetical protein	SghaA1_010100033943	62/72		
ORF-1	23	response regulator	SrosDRAFT_47450	89/94		
ORF-1	56	PAS domain S-box protein	SrosDRAFT_47440	89/95		
ORF-1	39	glycosyltransferase	SrosDRAFT_47420	83/92		
ORF-1	32	hypothetical protein	SrosDRAFT_47400	74/82		
ORF-9	24	hypothetical protein	FRAAL6120 (YP_716259)	49/65		
ORF-8	36	sugar diacid utilization	SrosDRAFT_47390	79/84		
ORF-7	30	L-proline dehydrogenase	SrosDRAFT_47380	83/89		



Table 7 (continued)

ORF-6	56	delta-1-pyrroline-5-carbox	SrosDRAFT_47370 (ZP_04474156)	92/95		
ORF-5	18	hypothetical protein	SrosDRAFT_40310 (ZP_04473452)	84/90		
ORF-4	15	DNA-binding protein	SrosDRAFT_40320 (ZP_04473453)	70/79		
ORF-3	29	hypothetical protein	SGR_1524 (YP_001823036)	49/62		
ORF-2	30	NmrA family protein	Franean1_1468 (YP_001505814)	65/76		
ORF-1	19	tetR-family transcriptional	Franean1_1469 (YP_001505815)	72/80		
Mra1	39	rhamnosyltransferase	Cpz31 (ACQ63639)	78/88	LipB1	74
Mra2	39	sugar	Cpz30 (ACQ63638)	78/82	LipA1	74
Mra3	52	radical SAM	CalU22 (AAM94801)	67/81		
Mra4	38	predicted membrane	NdasDRAFT_4699 (ZP_04335569)	55/67		
Mra5	26	sugar	Cpz29 (ACQ63637)	81/89	LipZ	83
Mra6	21	TmrB-like protein	Cpz27 (ACQ63635)	71/80	LipX	67
Mra7	39	SAM-dependent	Cpz26 (ACQ63634)	74/84	LipW	72
Mra8	32	alcohol dehydrogenase	Cpz25 (ACQ63633)	88/93	LipV	86
Mra9	60	hypothetical protein	Cpz24 (ACQ63632)	69/78	LipU	68
Mra10	34	lipase	Cpz23 (ACQ63631)	78/88	LipT	79
Mra11	12	ABC multidrug resistance	Cpz22 (ACQ63630)	77/84	LipS	76
Mra12	49	acyltransferase	Cpz21 (ACQ63629)	75/85	LipR	76
Mra13	35	acyl-CoA synthase	Cpz20 (ACQ63628)	87/90	LipQ	84
Mra14	42	SHMT-like	Cpz14 (ACQ63622)	81/87	LipK	83
Mra15	44	aminotransferase	Cpz13 (ACQ63621)	77/86	LipJ	76
Mra16	18	TmrB-like protein	Cpz12 (ACQ63620)	72/81	LipI	71
Mra17	21	SAM-dependent	Cpz11 (ACQ63619)	75/86	LipH	78
Mra18	17	beta-hydroxylase	Cpz10 (ACQ63618)	84/91	LipG	80
Mra19	32	AraC family transcriptional	Cpz9 (ACQ63617)	65/72	LipF	61
Mra20	45	pyrimidine-nucleoside	DealDRAFT_0710 (ZP_03728855)	46/63	LipP	42
	5	phosphorylase	<i>Dethiobacter alkaliphilus</i> AHT 1			
Mra21	43	aminotransferase	CetH (ACH85568)	52/64	LipO	41
Mra22	36	glycosyltransferase	Orf13 (BAI23321)	39/57	LipN	36
Mra23	23	nucleotidyltransferase	Amir_3895 (YP_003101615)	40/51	LipM	33
Mra24	21	dioxygenase	Orf7 (BAI23315)	41/56	LipL	40
ORF1	32	DNA polymerase beta	Mpop_3269 (YP_001925955)	29/43		
ORF2	61	glucose-methanol-choline	SACE_4301 (YP_001106495)	46/58		
ORF3	16	hypothetical protein	N9414_23023 (ZP_01630686)	33/48		

Table 7 (continued)

ORF4	19	hypothetical protein	SrosDRAFT_27630 (ZP_04472191)	74/83	
ORF5	50	hydrolase	Svir_18520 (YP_003133702)	62/72	
ORF6	18	NADPH-dependent FMN	Pat9bDRAFT_2775 (ZP_05729459)	43/65	
ORF7	33	amino acid adenylation	Sare_4562 (YP_001539321)	49/62	
ORF8	39	acyl-CoA dehydrogenase	TcurDRAFT_15750 (ZP_04030556)	73/84	
ORF9	28	hypothetical protein	hyg24 (ABC42561)	43/56	
ORF10	30	Short-chain	Bxe_B2739 (YP_552606)	57/71	
ORF11	38	hypothetical protein	Plav_2009 (YP_001413280)	63/78	
ORF12	14	hypothetical protein	Veis_2934 (YP_997688)	57/73	
ORF13	38	acyl-CoA dehydrogenase	TcurDRAFT_39460 (ZP_04032895)	50/65	

<sup>a</sup>Sequences are deposited at NCBI (accession no. AB746937).<sup>b</sup>Numbers are in amino acids.<sup>c</sup>% sequence identity and similarity for the entire length of the proteins.<sup>d</sup>Sequences are deposited at NCBI (accession no. AB530986).

In contrast to the obvious differences within the genetic architecture of the locus involved in the biosynthesis of the rhamnosyl moiety, the five gene subcluster required for aminoribose formation appeared essentially the same for theA-90289 and muraminomicin gene clusters (**Fig3.2c**). However, minimally two differences were uncovered upon closer bioinformatics analysis: (i) the sequence identity between LipP-L and Mra20-24 were considerably lower compared to the remaining shared ORFs and (ii) the LipL homologue, Mra24, is lacking ~60 amino acids at the C-terminus that contains a His residue that is part of the HX(D/E)<sub>n</sub>H motif (X is any amino acid), which is essential for Fe(II) binding and hence activity. Therefore, it is highly likely that Mra24 does not encode a functional non-heme Fe(II),  $\alpha$ -KG-dependent dioxygenase.

To provide initial evidence that the correct genetic locus was identified prior to completion of the sequencing, we introduced cosmid pMra02 into the heterologous host *Streptomyces lividans* TK21 with the expectation that this cosmid contains a genetic element involved in muraminomicin resistance. In contrast to controls using the empty vector, *S. lividans* TK21/pMra02 was resistant to muraminomicin at 100 mg

mL<sup>-1</sup> on solid media (**Fig 3.3**). Retrospective analysis of this cosmid sequence reveals two potential resistance candidates *mra11* and *mra16* that encode a putative ABC-transporter and a protein with similarity to tunicamycin-resistance protein TmrB, respectively [129]. Although muraminomicin was not produced by the recombinant strain, a red phenotype was observed upon introduction of pMra02 and muraminomicin selection, suggesting the cosmid and antibiotic likely up regulate additional host genes such as those potentially involved in actinorhodin biosynthesis. Encoded within pMra02 is a protein with similarity to AraC positive regulatory protein, which may be partially responsible for this phenotypic output. The identity of the individual genes involved in resistance and regulation is currently under investigation, nevertheless, the results are consistent with the role of the genetic locus in muraminomicin production.

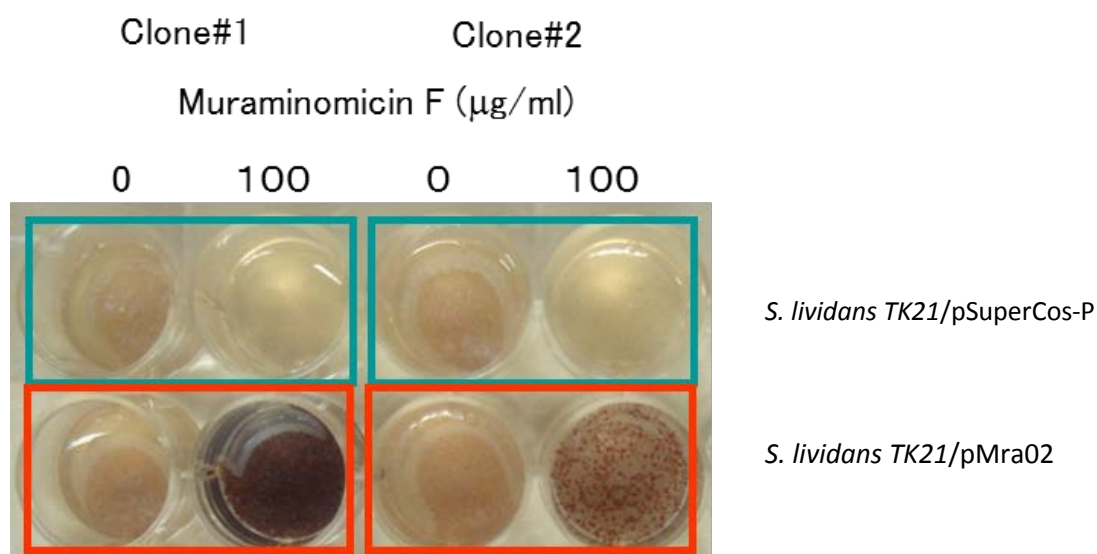


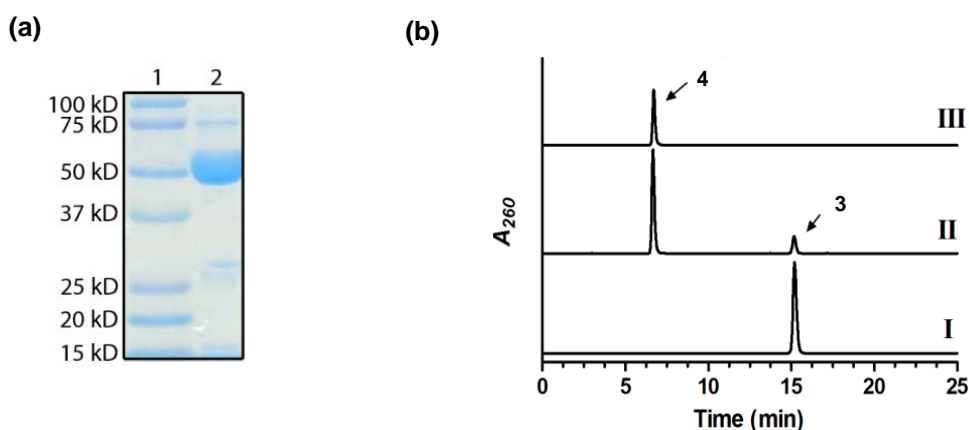
**Figure 3.3.** Resistance conferred by pMra02 upon heterologous expression in *Streptomyces lividans* TK21.

### 3.4. Results: Functional assignment of Mra20 as a low specificity pyrimidine nucleoside phosphorylase

#### 3.4.1 *In vitro* characterization of Mra20 activity

Pyrimidine nucleoside phosphorylases catalyze the phosphorolysis of thymidine or uridine nucleosides to generate 2-deoxy- $\alpha$ -D-ribose-1-phosphate and thymine or  $\alpha$ -D-ribose-1-phosphate and uracil as described for LipP, respectively [130,131]. Although thymidine phosphorylases from several organisms are highly specific for the 2'-deoxyribosyl moiety, some are reported to have very little discrimination at this position. LipP was slightly specific for the hydroxylated ribose; additionally, efficiency with 5'-amino-5'-deoxyuridine (**2**) was comparable to that of uridine (**3**) [124].

The *mra20* gene, which is homologous to *lipP*, was cloned and expressed in *E. coli* to yield soluble protein (**Fig 3.4a**). Using HPLC for detection, initial activity tests with Mra20 revealed uridine (**3**) was converted to uracil (**4**) and  $\alpha$ -D-ribose-1-phosphate (**Fig 3.4b**), and identically to LipP [124], the Mra20-catalyzed reaction also proceeded with 5'-amino-5'-deoxyuridine (**2**) (**Fig3.4c**). Additional activity tests revealed hypothetical pathway intermediates 2'-deoxyuridine (**11**), 5'-amino-2',5'-dideoxyuridine (**7**), thymidine (**12**) and 5'-amino-5'-deoxythymidine (**10**) were also converted to uracil (**4**) or thymine (**13**) and the respective sugar-1-phosphate by Mra20 (**Fig 3.5**), thus warranting further kinetic investigation.



(c)

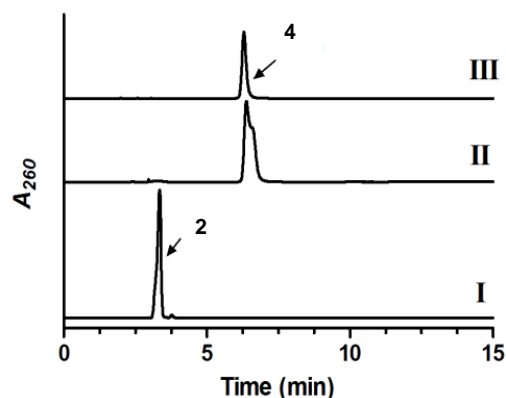
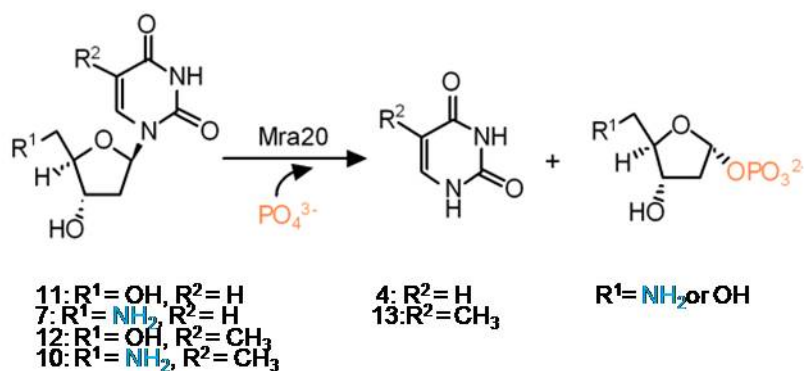
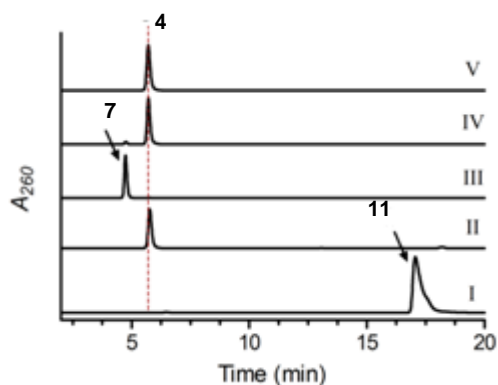


**Figure 3.4.** *In vitro* characterization of Mra20. (a) SDS-PAGE analysis of partially purified His<sub>6</sub>-Mra20 (expected MW of 52.5 kD). (b) HPLC analysis using uridine (**3**) after 1 hr without Mra20 (I), 1 hr reaction (II) and authentic uracil (**4**) (III). (c) HPLC analysis using 5'-amino-5'-deoxyuridine (**2**) after 1 hr without Mra20 (I), 1 h reaction (II) and authentic uracil (**4**) (III).  $A_{260}$ , absorbance at 260 nm.

(a)



(b)



(c)

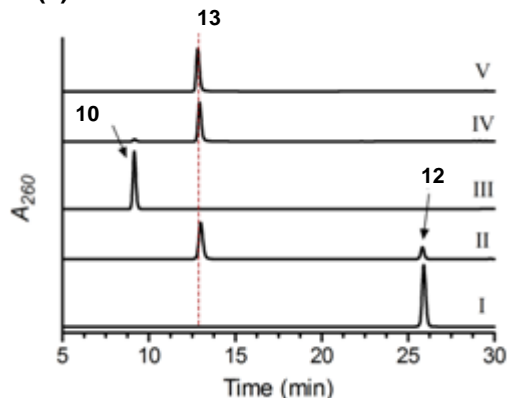


**Figure 3.5.** Activity of Mra20 with 2'-deoxynucleosides. (a) Phosphorolysis reaction catalysed by Mra20. (b) HPLC analysis following a 1 h reaction using 2'-deoxyuridine

(11) without Mra20 (I), 2'-deoxyuridine (11) with Mra20 (II), 5'-amino-2',5'-dideoxyuridine(7) without Mra20 (III), 5'-amino-2',5'-dideoxyuridine(7) with Mra20 (IV), and authentic uracil (4). (c) HPLC analysis following a 1 hr reaction using thymidine (12) without Mra20 (I), thymidine (12) with Mra20 (II), 5'-amino-5'-deoxythymidine (10) without Mra20 (III), 5'-amino-5'-deoxythymidine (10) with Mra20(IV), and authentic thymine (13).

### 3.4.2. Kinetics characterization of Mra20

For comparative purposes, single substrate kinetic analysis was performed under the optimized conditions for LipP using UV/Vis spectroscopy for detection of the free nucleobase under alkaline conditions. All of the tested substrates displayed typical Michaelis–Menten kinetics (**Fig 3.6**), and the extracted kinetic constants revealed that Mra20 is most efficient with thymine containing nucleosides with little preference for the C-5' functional group (**Table 8**). Although the  $K_m$  and  $k_{cat}$  were both significantly increased, the efficiency with 2'-deoxyuridinederivatives was quite comparable to the respective thymine containing nucleoside. Similar to LipP, these kinetic results suggest that Mra20 has little preference toward any hypothetical pathway intermediates, and thus cannot be utilized to delineate the timing of the biochemical events. However, in contrast to LipP, Mra20 has a modest specificity toward the 2'-deoxynucleosides relative to the hydroxylated counterpart, which is consistent with the observed 5-amino-2,5-dideoxyribosyl moiety that is found in the muraminomicins.

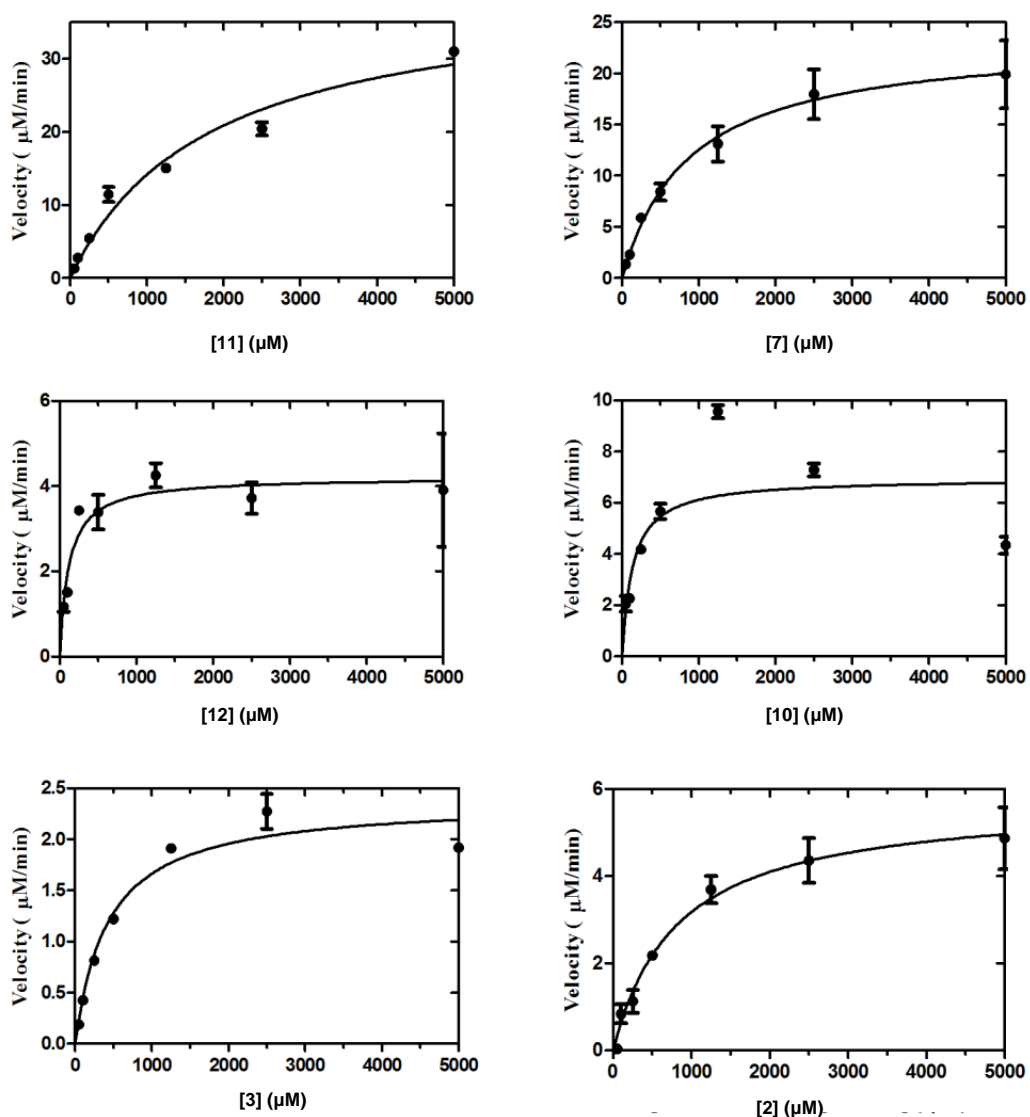


**Figure 3.6.** Single-substrate kinetic analysis of Mra20. Data were fitted to the Michaelis-Menten equation and extracted kinetic constants are given in **Table 8**.

**Table 8.** Extracted kinetic constants for Mra20.

Substrate	$K_m$ (mM)	$k_{cat}$ (min <sup>-1</sup> )	Relative efficiency (%)
11	$1.8 \pm 0.3$	$28 \pm 2$	61
7	$0.87 \pm 0.24$	$16 \pm 2$	75
12	$0.12 \pm 0.04$	$2.9 \pm 0.2$	100
10	$0.13 \pm 0.05$	$3.1 \pm 0.3$	93
3	$0.43 \pm 0.07$	$0.9 \pm 0.1$	8
2	$0.82 \pm 0.21$	$4.0 \pm 0.3$	19

### 3.5. Results: Bifunctional assignment of Mra20 as a potential nucleoside phosphorylase and cytidine deaminase.

#### 3.5.1 *In vitro* characterization of Mra20 deaminase activity

Mra20 is most efficient with thymine containing nucleosides as described above (**Table 8**). This suggests Mra20 has some specificity for a 2'-deoxy nucleoside. During our screen of potential substrates, we unexpectedly observed an activity with cytidine. This observation was unusual since pyrimidine nucleosides phosphorylases that use uridine or thymidine cannot turnover cytidine. This Mra20 was first confirmed to catalyze phosphorolysis of cytidine to generate ribose-1-phosphate and a UV-active base as shown by HPLC (**Fig 3.7**). Interestingly, the base counterpart generated from cytidine had the same retention time with uracil instead of cytosine (**Fig 3.8**).

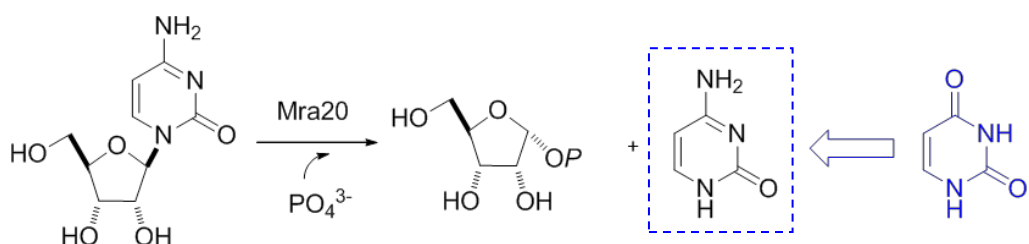


**Figure 3.7.** Proposed phosphorolysis reaction with cytidine catalyzed by Mra20.



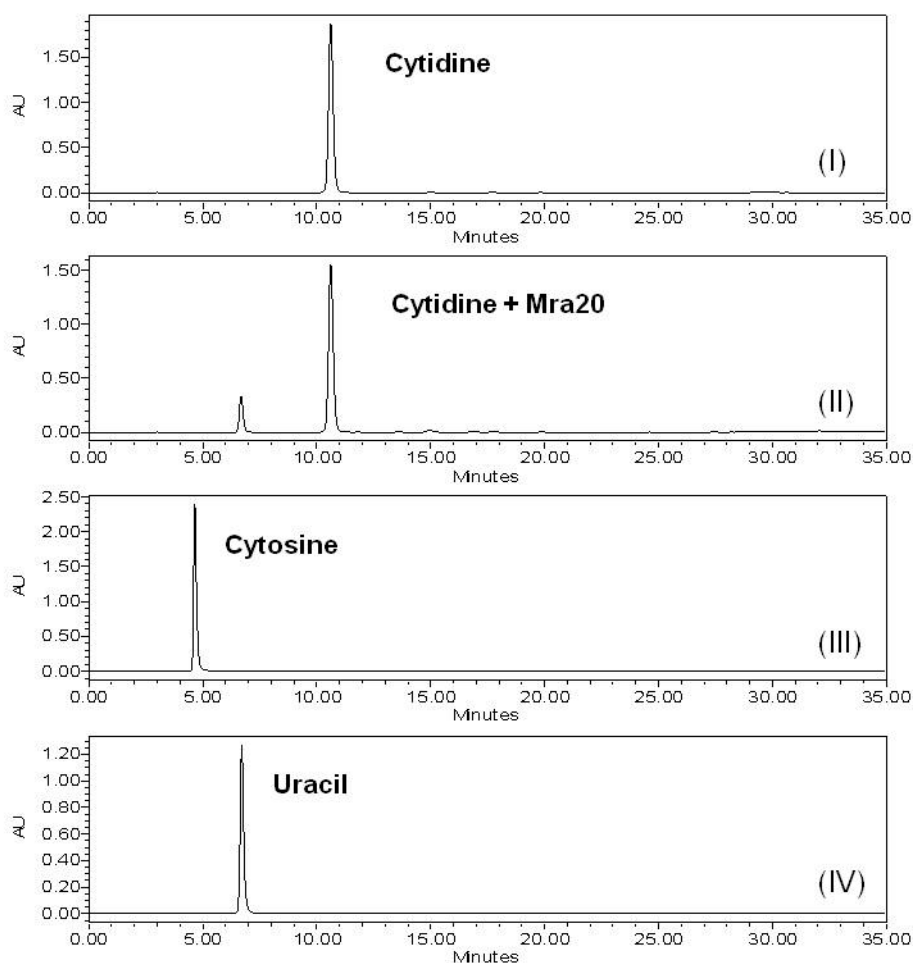


**Figure 3.8.** Activity of Mra20 with cytidine. HPLC analysis following a 1 hr reaction using cytidine without Mra20 (I), cytidine with Mra20 (II), authentic cytosine (III) and authentic uracil (IV).

To confirm the product was uracil rather than cytosine, LC-MS was performed to analyze and distinguish the substrate cytidine and product using authentic uracil and cytosine as controls. LC-MS analysis of cytosine revealed the expected  $(M - H)^-$  ion at  $m/z = 110.0$  and uracil revealed the expected  $(M - H)^-$  ion at  $m/z = 111.0$ . The product of Mra20 reaction starting from cytidine yielded an  $(M - H)^-$  ion at  $m/z = 110.9$ , which was consistent with uracil and not cytosine (**Fig 3.9**).  $^1\text{H-NMR}$  analysis of the Mra20 product demonstrated that the proton signal shift of the product was identical to the proton signal of uracil compare to cytosine (**Fig 3.10**). Thus, both LC-MS and  $^1\text{H-NMR}$  confirmed that this product is uracil.

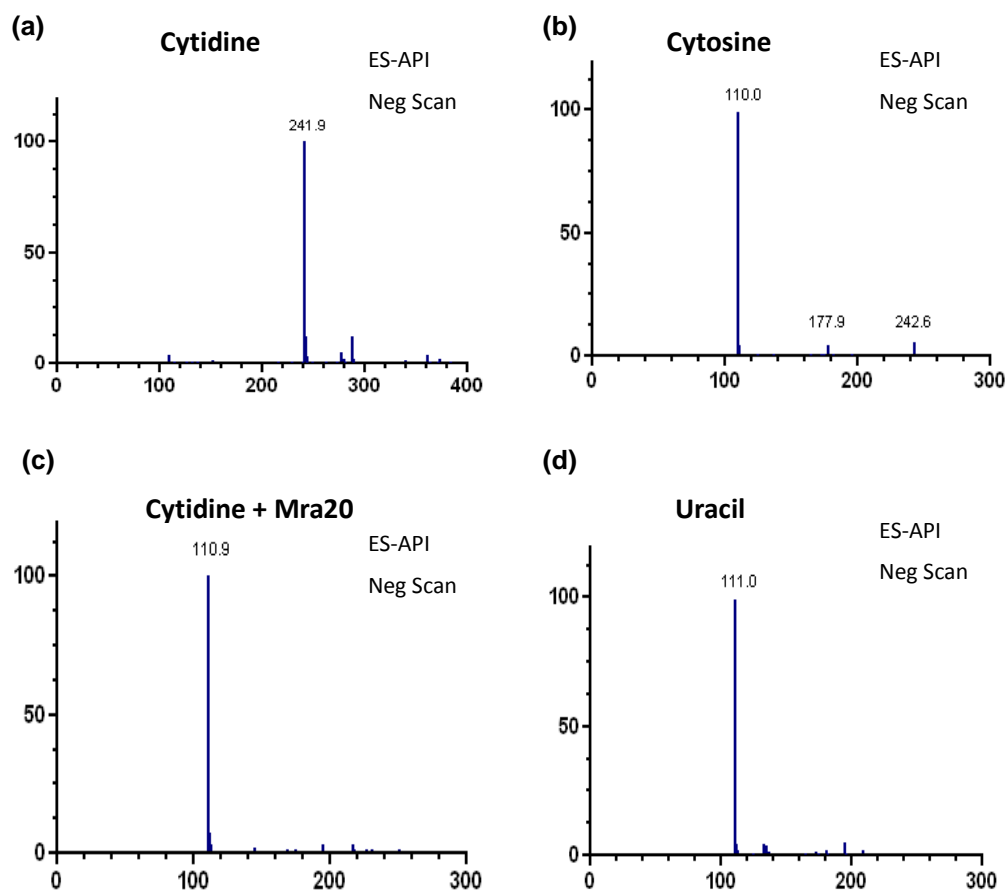


**Figure 3.9.** LC-MS of the Mra20 product with cytidine. (a) Negative ion mass spectrum for the peak of cytidine. (b) Negative ion mass spectrum for the peak of cytosine. (c) Positive ion mass spectrum for the peak of the product of cytidine with Mra20. (d) Negative ion mass spectrum for the peak of uracil.

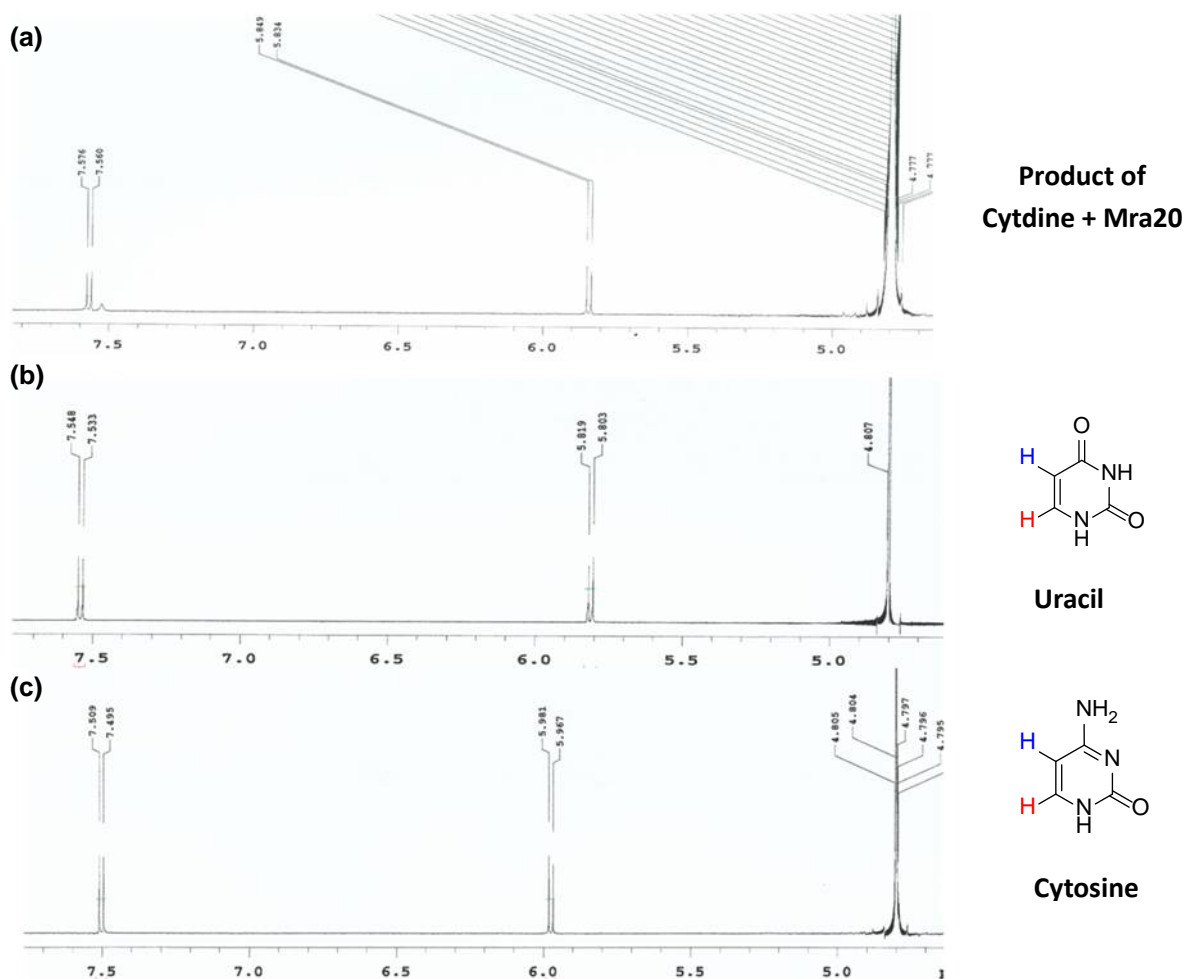


**Figure 3.10.** Characterization product of Mra20-catalyzed cytidine reaction by 1D NMR. (a)  $^1\text{H}$ -NMR spectrum of the product of cytidine with Mra20. (b)  $^1\text{H}$ -NMR spectrum of uracil. (c)  $^1\text{H}$ -NMR spectrum of cytosine.

### 3.5.2. Replacement of $\text{O}^{16}$ with $\text{O}^{18}$ in Mra20-catalyzed cytidine reaction

To further confirm uracil as the product and to explore the deamination mechanism of cytosine to uracil,  $\text{O}^{18}$  was used to replace the  $\text{H}_2\text{O}$  ( $\text{O}^{16}$ ) in the Mra20-catalyzed cytidine reaction. The product was analyzed by LC-MS revealing an  $(\text{M} - \text{H})^-$  ion at  $m/z = 112.9$ , a 2 unite increase compared to uracil,  $(\text{M} - \text{H})^-$  ion at  $m/z = 111.0$ . This result indicated that the origin of new oxygen atom on the 4-carbonyl of uracil originates from  $\text{H}_2\text{O}$  (**Fig 3.11**).

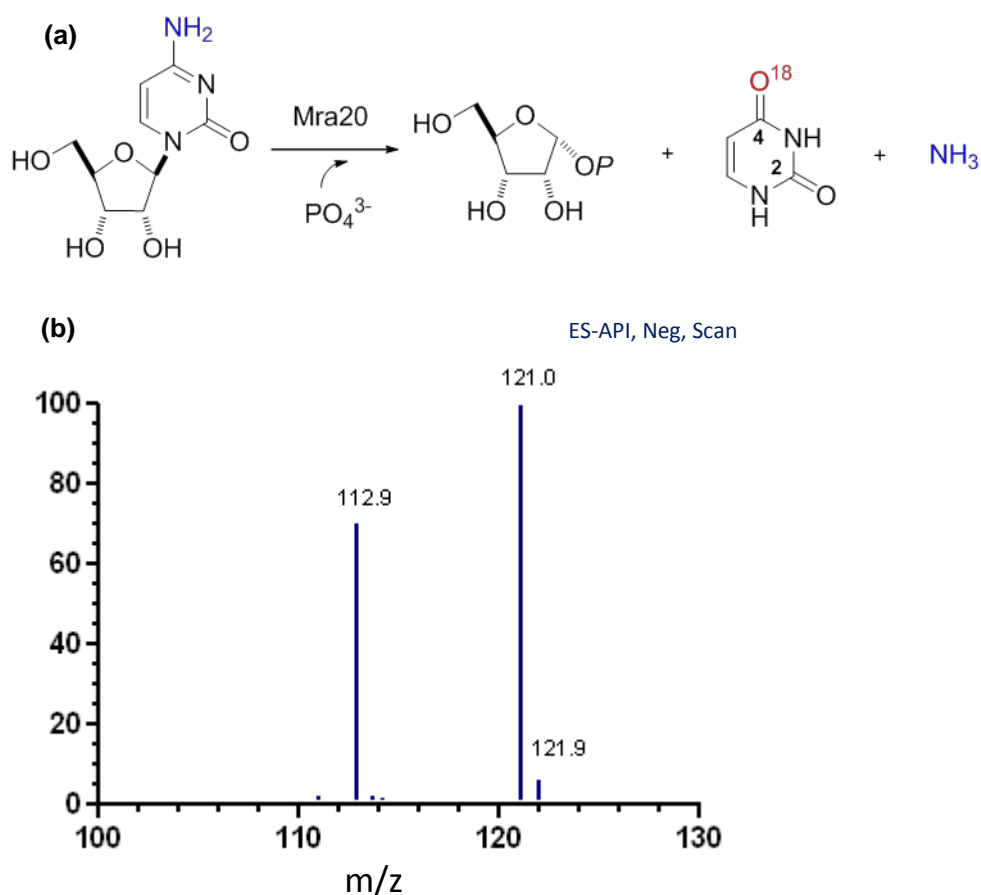


**Figure 3.11.** Characterization of Mra20-catalyzed reaction using O<sup>18</sup>. (a) Proposed reaction of cytidine catalyzed by Mra20 using O<sup>18</sup>. (b) LC-MS analysis of the product from the reaction of Mra20 with cytidine (Negative ion mass spectrum ).

### 3.5.3. Characterization of NH<sub>3</sub> production in Mra20-catalyzed cytidine reaction

The results above suggest ammonia is also produced during the conversion of cytidine to uracil. To confirm that free ammonia (NH<sub>3</sub>) was produced from this reaction, glutamate dehydrogenase (GLDH), α-ketoglutarate (α-KG) and NADPH was used in a coupled enzyme assay. The GLDH catalyzes the reductive conversion of α-KG to glutamate using NH<sub>3</sub> as the source of amine as shown in **Fig 3.12a**. Since NADPH has a UV absorption maximum at 340 nm, the reaction was monitored by UV-Vis spectroscopy by monitoring the decrease in absorbance over a 1 hr reaction. As time increased, a linear decrease in absorbance was observed indicating the α-KG-glutamate interchange reaction happened and confirms the existence of free NH<sub>3</sub> (**Fig 3.12b**).

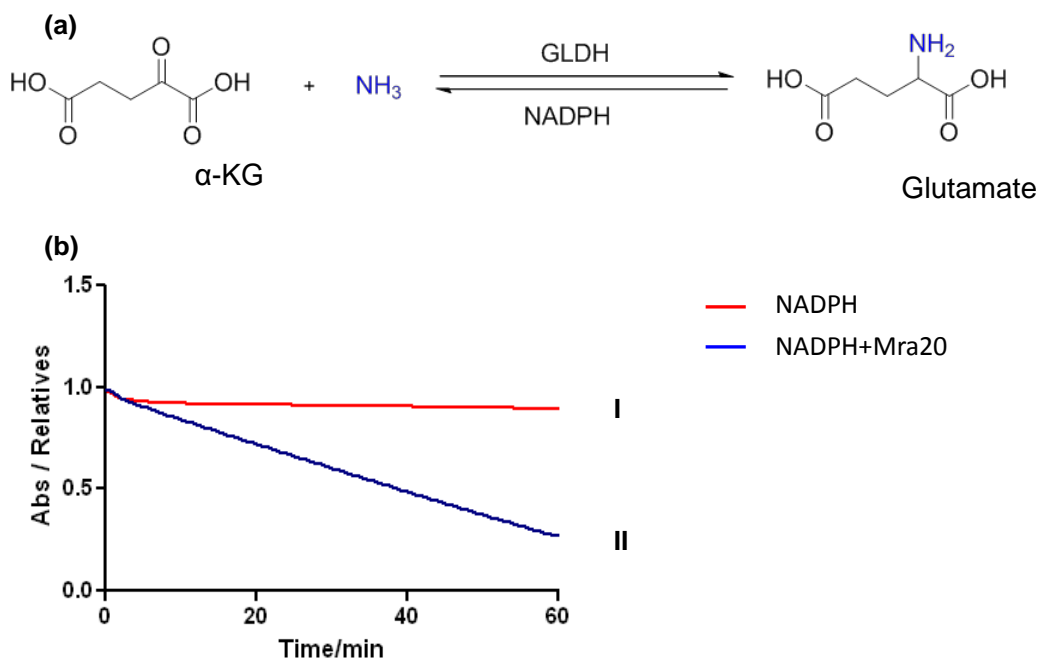


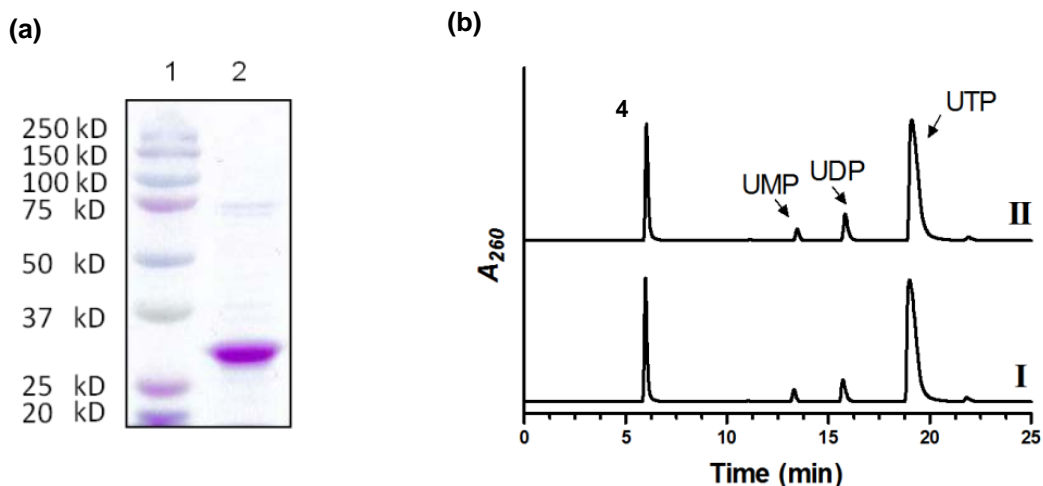
**Figure 3.12.** Characterization of  $\text{NH}_3$  production. (a) Reaction of  $\alpha\text{-KG}$  and  $\text{NH}_3$  catalyzed by GLDH to generate glutamate. (b) change of NADPH monitored by UV-Vis. (I) Control reaction with NADPH,  $\alpha\text{-KG}$ , cytidine and GLDH added, without adding Mra20; (II) Reaction with NADPH,  $\alpha\text{-KG}$ , cytidine and GLDH added, adding Mra20.

### 3.6. Results: Functional assignment of Mra23 as a primary amine-requiring Nucleotidyltransferase

Bioinformatic analysis revealed Mra23 has sequence similarity to LipM and other nucleotidyltransferases, enzymes that utilize a sugar-1-phosphate and nucleotide-5'-triphosphate to generate NDP-sugars [132]. The Mra23 homologue from the A-90289 pathway (LipM) has already been demonstrated to function as a nucleotidyltransferase, using 5-amino-5-deoxy- $\alpha\text{-D}$ -ribose-1-phosphate and UTP to generate the activated sugar, and, interestingly, is only able to turn over ribose-1-phosphate with a 5-amine functionality.

Similarly to Mra20, the gene product of *mra23* was soluble when produced in *E. coli* (Fig 3.13a). The activity of Mra23 was tested with 2-deoxy- $\alpha\text{-D}$ -ribose-1-phosphate or 5-amino-2,5-dideoxy- $\alpha\text{-D}$ -ribose-1-phosphate generated in situ by Mra20 from

2'-deoxyuridine (**11**) and nucleosides 5'-amino-2',5'-dideoxyuridine(**7**), 5'-amino-5'-deoxythymidine (**10**), thymidine (**12**), and analysis of these reactions revealed a new peak was formed only in the presence of 5-amino-2,5-dideoxy- $\alpha$ -D-ribose-1-phosphate from 5'-amino-2',5'-dideoxyuridine(**7**) or 5'-amino-5'-deoxythymidine (**10**) and UTP (**Fig 3.14, Fig 3.13b,c**). LC-MS analysis of the purified new peak revealed an (M-H)<sup>-</sup> ion at  $m/z = 517.6$ , consistent with the molecular formula  $C_{14}H_{23}N_3O_{14}P_2$  of UDP-5-amino-2,5-dideoxyribose UDP-5"-amino-2",5"-dideoxyribose (**8**)(expected  $m/z = 518.1$ ) (**Fig 3.14a, Fig 3.15**). We had previously characterized UDP-5"-amino-2",5"-dideoxyribose (**8**) by HR-MS and complete NMR analysis using LipP and LipM starting from 5'-amino-2',5'-dideoxyuridine(**7**), and thus co-injections were utilized to confirm the product of Mra20 and Mra23 (**Fig 3.14**). In total, the data is consistent with the function of Mra23 as a UTP:5-amino-2,5-dideoxy- $\alpha$ -D-ribose-1-phosphateuridylyltransferase as the penultimate catalyst for formation of the disaccharide of muraminomycin.



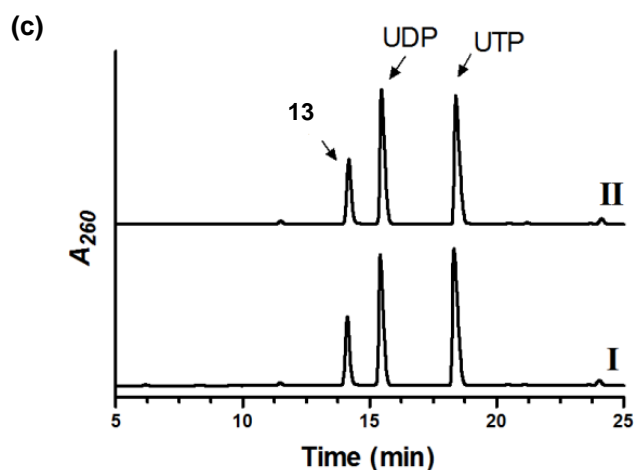


**Figure 3.13.** *In vitro* characterization of Mra23 with thymidine (**12**). (a) SDS-PAGE analysis of purified His<sub>6</sub>-Mra23 (expected MW of 29.6 kD). (b) HPLC analysis of the reaction starting with uridine after 3 hr without Mra23 (I) and 3 hr reaction (II). (c) HPLC analysis of the reaction starting with thymidine (**12**) after 3 hr without Mra23 (I) and 3 hr reaction (II).  $A_{260}$ , absorbance at 260 nm.

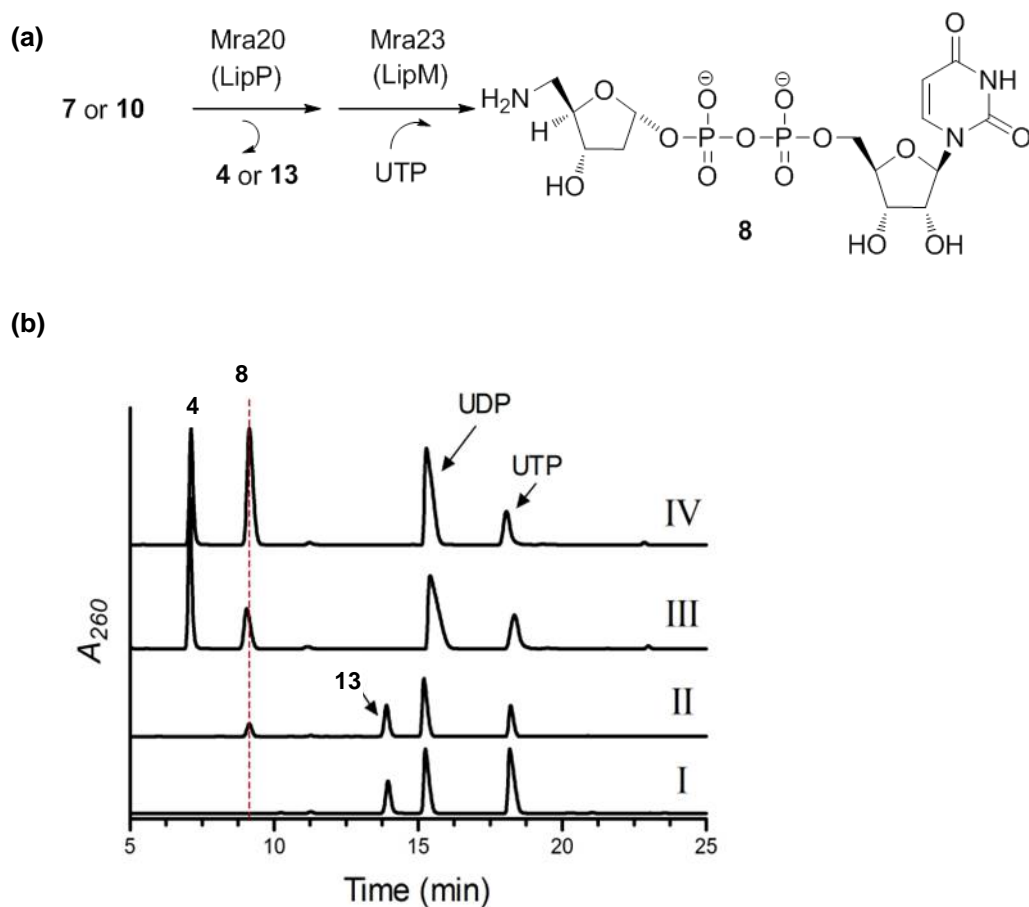


**Figure 3.14.** Characterization of Mra23 with 5'-amino-5'-deoxythymidine (**10**). (a) Enzymatic preparation of the substrate using Mra20, and the reaction catalyzed by

Mra23 to generate UDP-5''-amino-2'',5''-dideoxyribose (**8**). (b) HPLC analysis following a 3 hr reaction starting from 5'-amino-5'-deoxythymidine (**10**) without Mra23 (I), 5'-amino-5'-deoxythymidine (**10**) with Mra23 (II), a 12 hr reaction starting from 5'-amino-2',5'-dideoxyuridine (**7**) with LipM from the A-90289 biosynthetic pathway replacing Mra23 (III), and a 12 hr reaction starting from 5'-amino-2',5'-dideoxyuridine (**7**) with LipM coinjected with purified UDP-5''-amino-2'',5''-dideoxyribose (**8**) generated by Mra23 (IV).

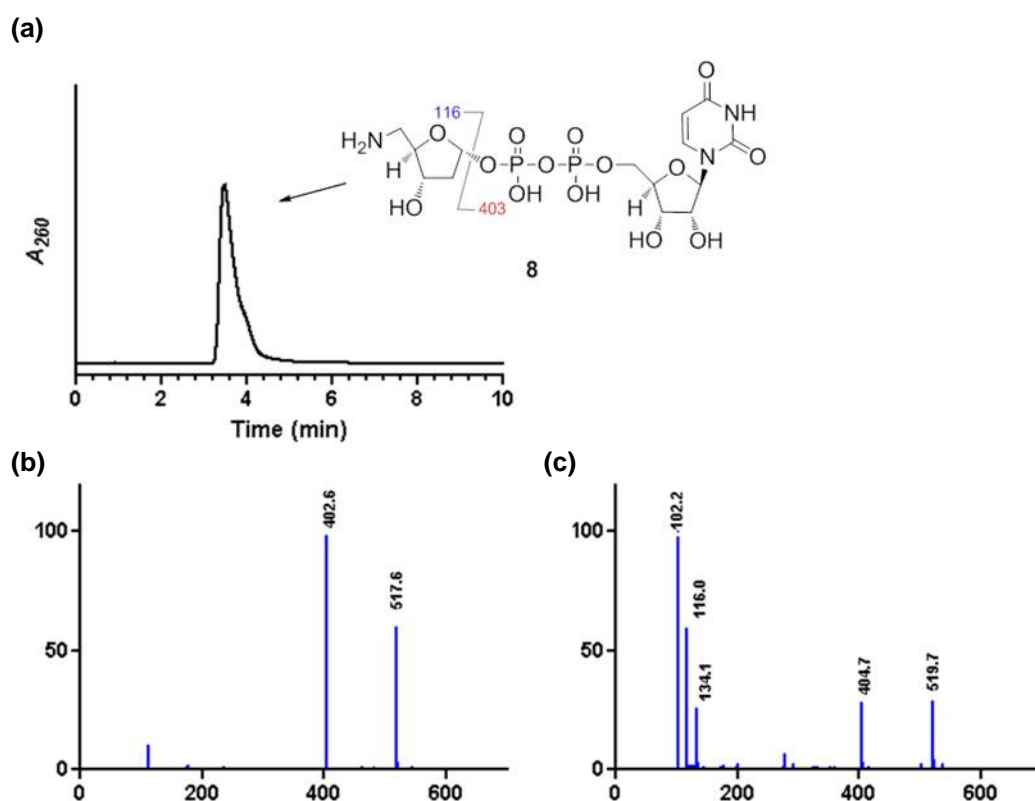


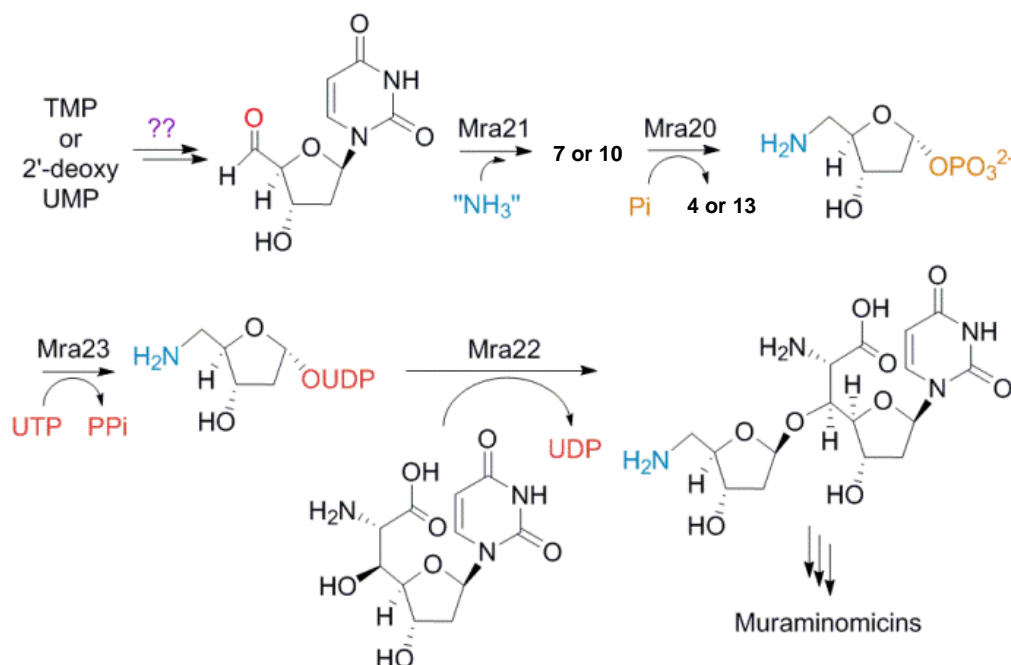
**Figure 3.15.** LC-MS of the Mra23 product UDP-5''-amino-2'',5''-dideoxyribose (**8**) generated from substrate 5'-amino-5'-deoxythymidine (**10**). (a) LC analysis of UDP-5''-amino-2'',5''-dideoxyribose (**8**) following purification. (b) Negative ion mass spectrum for the peak at elution time  $t = 3.5$  min. (c) Positive ion mass spectrum for the peak at elution time  $t = 3.5$  min.  $A_{260}$ , absorbance at 260 nm.

The substrate specificity of Mra23 is intriguing for a couple of reasons. Firstly, the transfer of ribosyl units onto acceptor molecules typically occurs with 5-phosphoribosyl-1-pyrophosphate, and the characterization of Mra23 and LipM has revealed a ribosyl transfer paradigm using NDP-sugars [124]. This realization may ultimately provide an opportunity to diversify structures by incorporating unnatural ribosyl units in place of the native sugar via a combinatorial biosynthetic strategy.



Secondly, several characterized nucleotidyltransferases are known or have been engineered by mutagenesis to accept aminosugar-1-phosphates; however, these enzymes in general have little discrimination between the amine or hydroxyl group[118,120,121,122]. Both Mra23 and LipM now establish a nucleotidyltransferase family whose activity is absolutely dependent upon the amine functionality, and on-going structural efforts will undoubtedly establish the molecular details behind this unusual specificity.

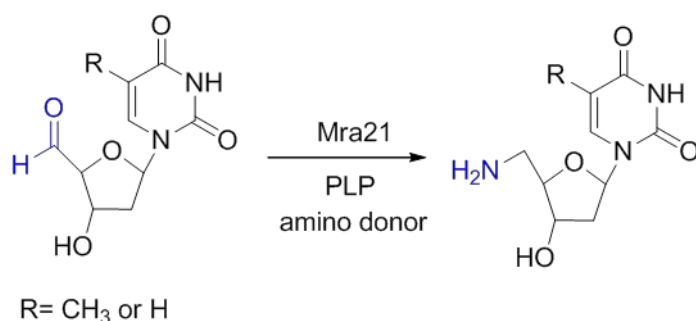
The combined results now allow us to define a probable pathway leading to the disaccharide core starting from either TMP or 2'-deoxyUMP (**Fig 3.16**). Through an as of yet unclear mechanism, the 5'-aldehyde is installed to serve as the substrate for the putative aminotransferase Mra21 to generate 5'-amino-2',5'-dideoxyuridine (**7**) or 5'-amino-5'-deoxythymidine (**10**). Following phosphorolysis of the glycosidic bond by Mra20, the aminosugar-1-phosphate is activated as the UDP-sugar by Mra23 prior to transfer to the acceptor molecule, which is most likely 2'-deoxy-5'-C-glycyluridine.



**Fig. 3.16.** Proposed biosynthetic pathway of the disaccharide core of the muraminomycins.

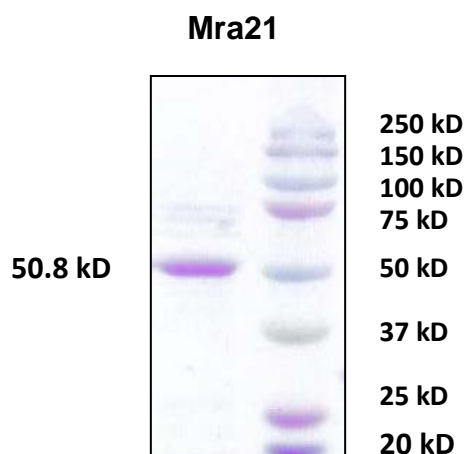
### 3.7. Results: *In vitro* characterization of Mra21 activity

Similar to LipO, bioinformatics analysis of Mra21 revealed sequence similarity to proteins annotated as putative aminotransferase. The potential reaction catalyzed by Mra21 was shown in **Fig 3.17**. To interrogate the mechanism of amine group incorporation, *mra21* was first expressed in *E. coli*, however the recombinant protein was insoluble using a variety of growth and induction conditions. Therefore, we turned to *Streptomyces lividans* TK64 as a host, which resulted in the successful preparation of soluble, recombinant Mra21 (**Fig 3.18a**).



**Figure 3.17.** Proposed reaction catalyzed by Mra21.

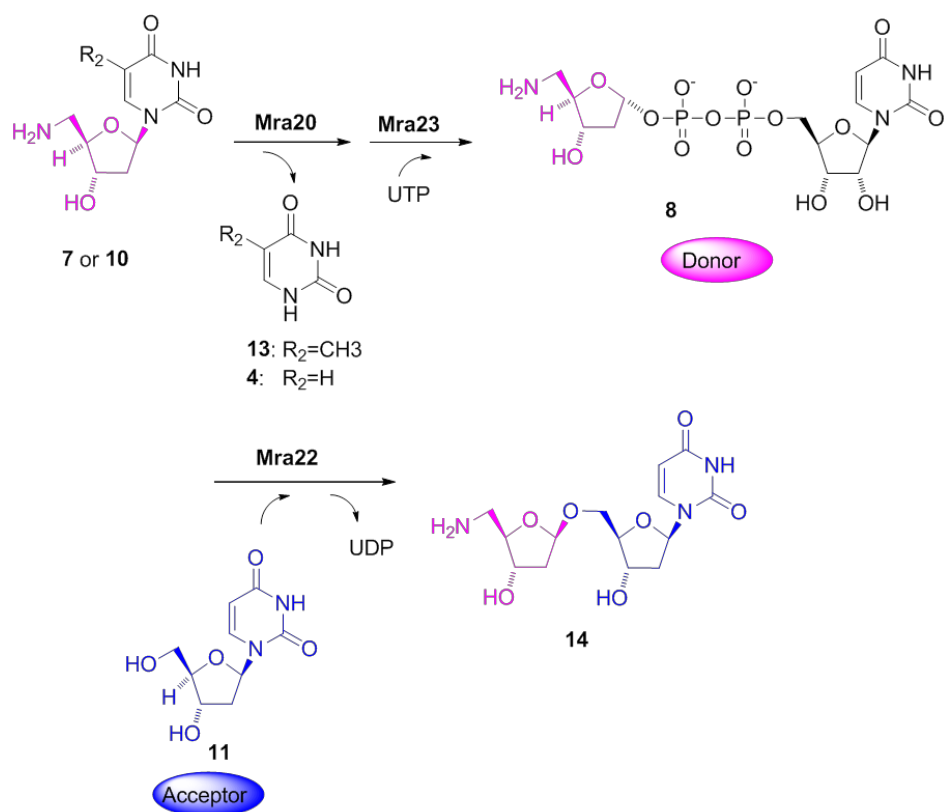
Since the true substrate for Mra21 was not available, 5'-aldehyde-uridine (**1**) was used as a substitute substrate to test the activity of Mra21 (**Fig 3.18b**). Unexpectedly, no new peak was detected after Mra21 incubated with 5'-aldehyde-uridine (**1**) and different amino donors, even though several different buffer conditions were tested. This result suggests Mra21 has specificity for the 2'-deoxynucleoside or, alternatively, the wrong amino donors were used. Hence further characterization with Mra21 is needed to verify the activity, and efforts are underway to synthesize the potential substrate 2'-deoxythymidine-5'-aldehyde.



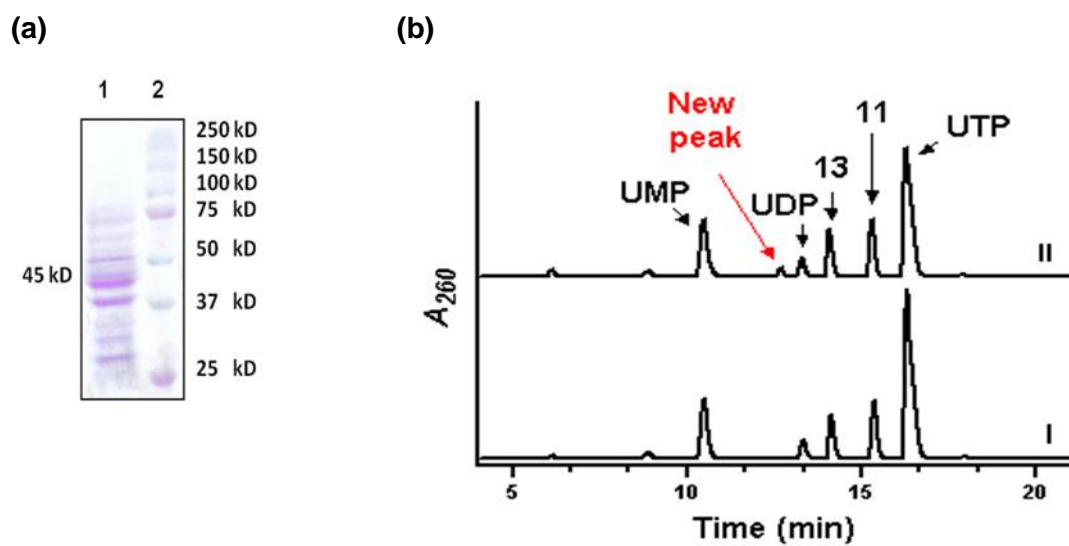
**Figure 3.18.** Characterization of Mra21. SDS-PAGE analysis of purified His<sub>6</sub>-Mra21 (expected MW of 50.8 kD).

### 3.8. Results: *In vitro* characterization of Mra22 activity

We then turned our attention to Mra22, which has sequence identity to a small number of proteins annotated as putative glycosyltransferases by bioinformatics analysis. Similar to LipN, Mra22 was predicted to transfer a 2'-deoxysugar to the sugar acceptor to generate the final glycoside as shown in **Fig 3.19**. To test the activity of Mra22, *mra22* was first tried to express in *E. coli*, however, same as Mra21, the recombinant protein was insoluble using a variety of growth and induction conditions. Therefore, Mra22 was tried to express from *Streptomyces lividans* TK64, which resulted in the soluble, recombinant Mra22 (**Fig 3.20a**).



**Figure 3.19.** Proposed reaction catalyzed by Mra22.



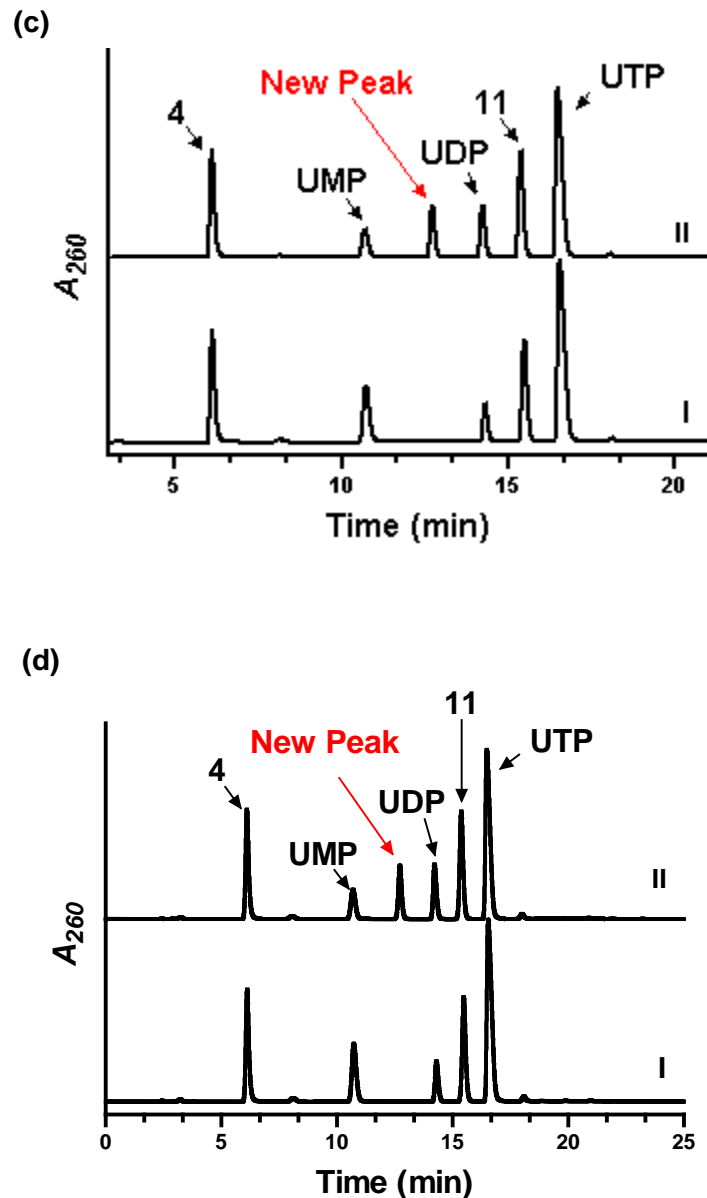


**Figure 3.20.** Characterization of Mra22. (a) SDS-PAGE analysis of purified His<sub>6</sub>-Mra22 (expected MW of 45 kD). (b) HPLC analysis of the reaction with 2'-deoxyuridine (**11**) starting with 5'-amino-5'-deoxythymidine (**10**) after (I) 3 hr without Mra22 and (II) 3 hr reaction. (c) HPLC analysis of the reaction starting with 5'-amino-2',5'-dideoxyuridine(**7**) after (I) 3 hr without Mra22 and (II) 3 hr reaction. (d) HPLC analysis of the reaction starting with 5'-amino-5'-deoxyuridine (**2**) after (I) 3 hr without Mra22 and (II) 3 hr reaction.  $A_{260}$ , absorbance at 260 nm.

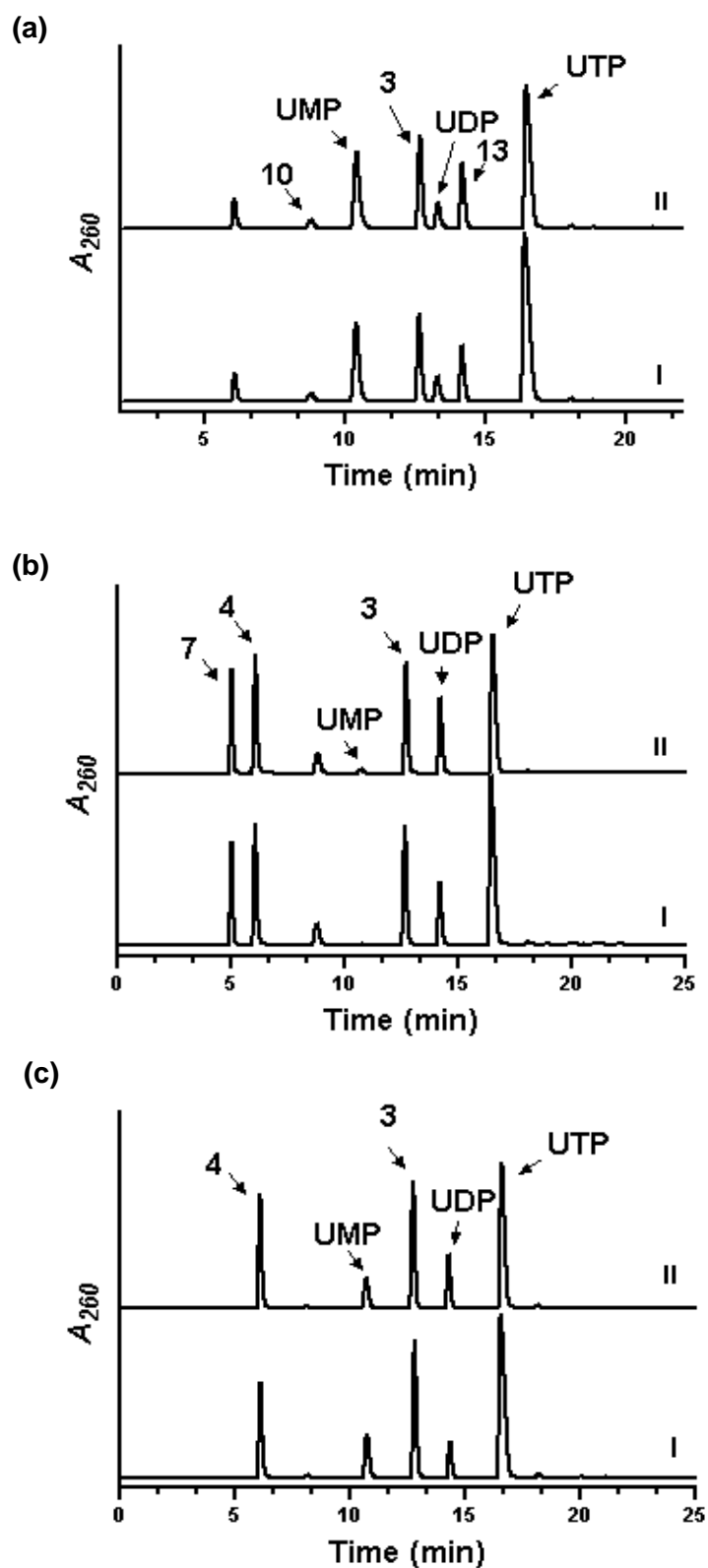


**Figure 3.21.** HPLC characterization of Mra22. (a) HPLC analysis of the reaction with uridine (3) starting with 5'-amino-5'-deoxythymidine (10) after (I) 3 hr without Mra22 and (II) 3 hr reaction. (c) HPLC analysis of the reaction starting with 5'-amino-2',5'-dideoxyuridine(7) after (I) 3 hr without Mra22 and (II) 3 hr reaction. (d)

HPLC analysis of the reaction starting with 5'-amino-5'-deoxyuridine (**2**) after (I) 3 hr without Mra22 and (II) 3 hr reaction.  $A_{260}$ , absorbance at 260 nm.

With the soluble protein in hand, the activity of Mra22 was tested with in situ generation of substrate beginning from 5'-amino-5'-deoxyuridine (**2**), 5'-amino-2',5'-dideoxyuridine (**7**) and 5'-amino-5'-deoxythymidine (**10**). HPLC analysis of Mra22 reactions revealed a new peak while using 2'-deoxyuridine (**11**) as surrogate acceptor (**Fig 3.20 b, c, d**). However, no new peak was detected while using uridine (**3**) as surrogate acceptor (**Fig 3.21 a, b, c**). Although the yield for the new peak was very low, the product of the peak was purified and finally analyzed by NMR. However,  $^1\text{H}$  and  $^{13}\text{C}$  NMR analysis of this new peak shown that it was uridine, rather than the expected compound (data not shown). Thus the true function of Mra22 needs further investigation.

### **3.9. Results: *In vitro* characterization of Mra24 activity**

#### **3.9.1. *In vitro* characterization of Mra24 activity**

Similar to LipL, Mra24 has sequence similarity to proteins annotated as putative a non-heme Fe(II) and  $\alpha$ -ketoglutarate ( $\alpha$ -KG)-dependent dioxygenase based on bioinformatics analysis. Previous results have demonstrated that LipL from A-90289 gene cluster is Fe(II)- and  $\alpha$ -ketoglutarate ( $\alpha$ -KG)-dependent dioxygenase, and UMP was the only substrate for LipL [88]. Based on this, we hypothesized that 2'-deoxyUMP might be the substrate for Mra24 as shown in **Fig 3.22**. To investigate the potential of oxidization process, *mra24* was first tried to express in *E. coli*, and a soluble protein was obtained (**Fig 3.23 a**).

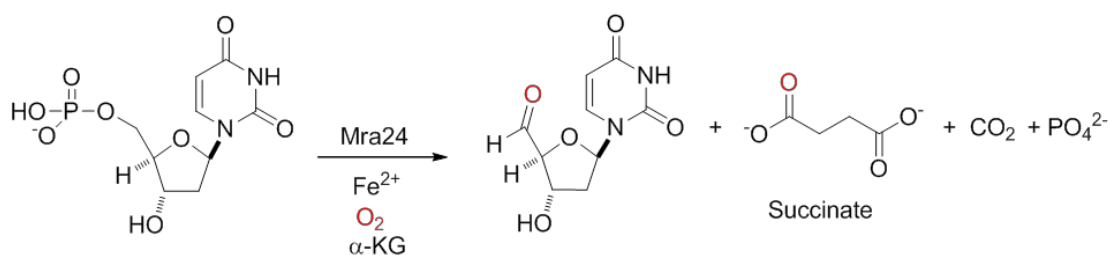


**Figure 3.22.** Proposed reaction catalyzed by Mra24.

The potential activity of Mra24 was analyzed by HPLC using 2'-deoxyUMP and UMP as substrates. Unexpectedly, the formation of 2'-deoxyuridine (**11**) and uridine (**3**) was detected instead of an oxidized product after incubation with enzyme (**Fig 3.23b**, **3.24**). This result suggested that Mra24 functioned as a phosphatase instead of dioxygenase. To confirm these results, we expressed the *mra24* gene in *S. lividans* TK64, and soluble protein was also obtained. The same reaction was repeated with the newly purified Mra24 enzyme. Unfortunately, the same results were obtained as the reaction catalyzed by the enzyme purified from *E. coli*. Thus, regardless of the source, it appeared Mra24 functions as a phosphatase, and kinetic studies are ongoing to ascertain the significance of this activity.

**(a) Mra24**





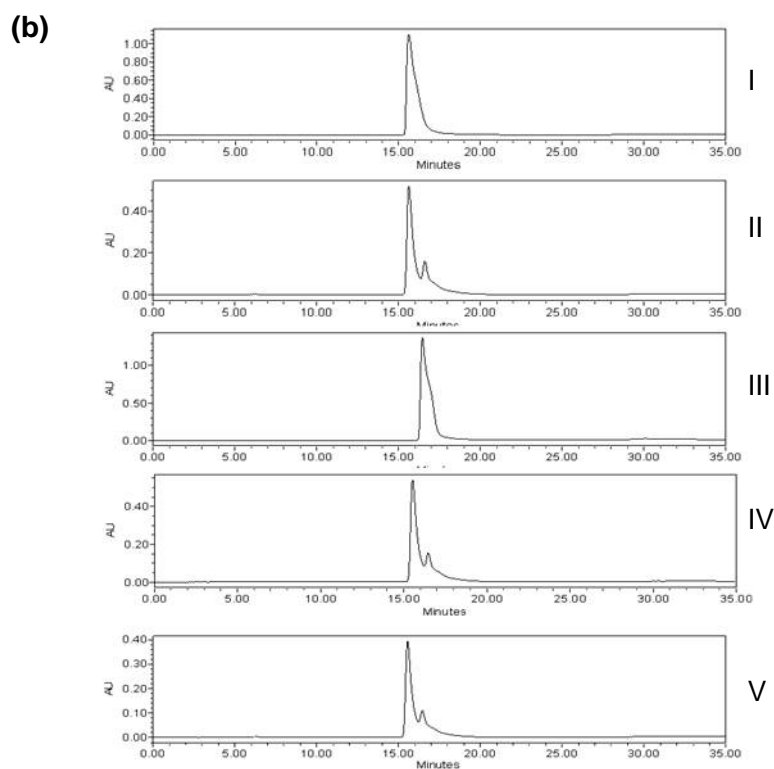


**Figure 3.23.** Characterization of Mra24 with 2'-deoxyUMP. (a) SDS-PAGE analysis of purified His<sub>6</sub>-Mra24 (expected MW of 28 kD). (b) HPLC analysis of the reaction with 2'-deoxyUMP and Mra24 after (I) 1 hr authentic 2'-deoxyUMP without Mra24, (II) 1 hr reaction with Mra24, (III) 1 hr authentic 2'-deoxyuridine (**11**), (IV) 1 hr reaction with Mra24, without  $\alpha$ -KG, (V) 1 hr reaction with Mra24, with EDTA.  $A_{260}$ , absorbance at 260 nm.

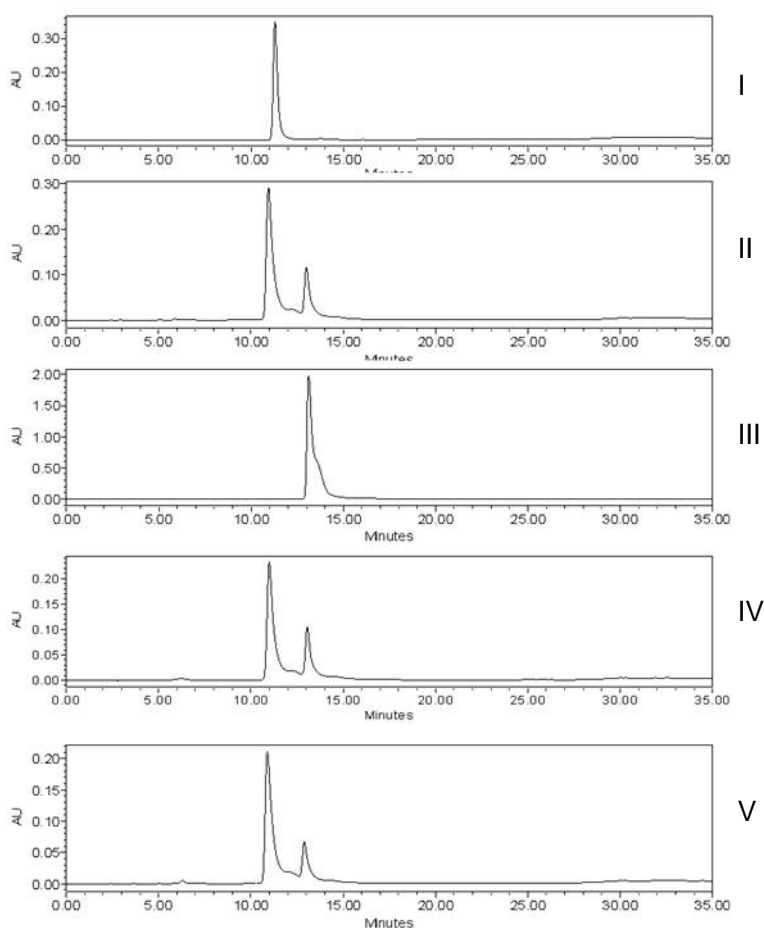


**Figure 3.24.** Characterization of Mra24 with UMP. HPLC analysis of the reaction with UMP and Mra24 after (I) 1 hr authentic UMP without Mra24, (II) 1 hr reaction with Mra24, (III) 1 hr authentic uridine (**3**), (IV) 1 hr reaction with Mra24, without  $\alpha$ -KG, (V) 1 hr reaction with Mra24, with EDTA.  $A_{260}$ , absorbance at 260 nm.

### 3.9.2. Blast and alignment Mra24 with other dioxygenases

Sequence analysis of Mra24 when compared to dioxygenases of the same superfamily showed that Mra24 was lacking ~60 amino acids at the C-terminus. The C-terminus contains a His residue that is critical for activity due to its role in Fe(II) binding that is essential for activity (**Fig 3.25**). Therefore, this might explain why *mra24* does not encode a functional non-heme Fe(II),  $\alpha$ -KG-dependent dioxygenase. Importantly, this suggests that the assembly of the deoxyaminoribose of muraminomicin has significant differences compared to that for A-90289 biosynthesis. These variations are part of our ongoing research efforts.

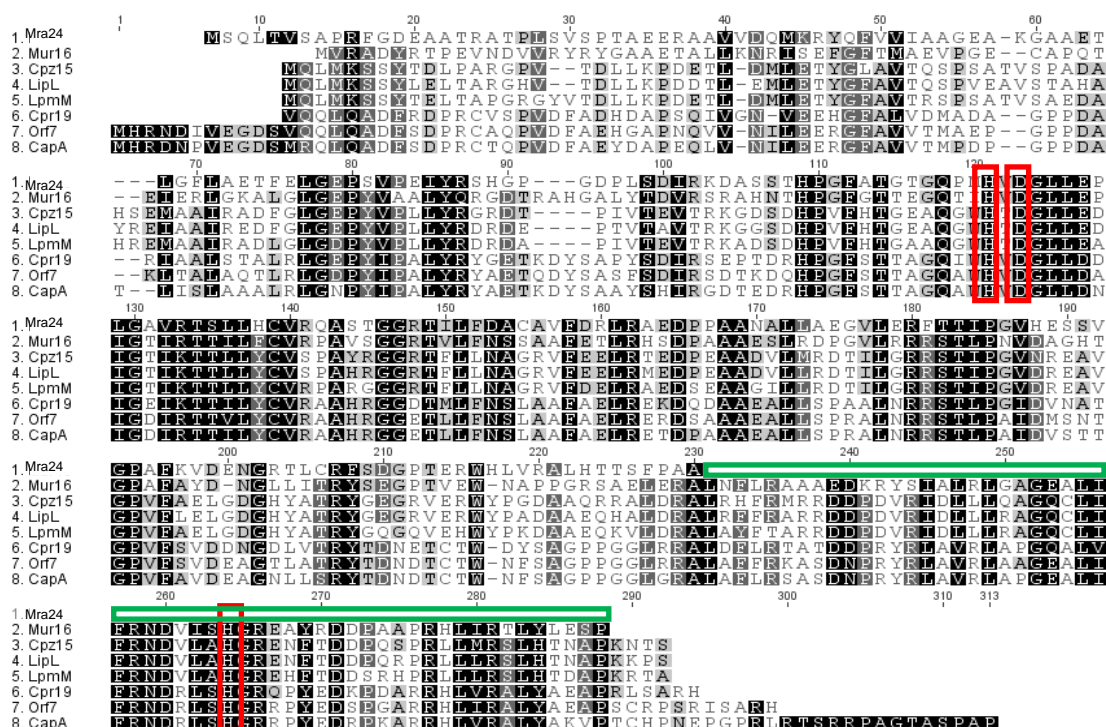


**Figure 3.25.** AlignMra24 with similar dioxygenases from other strains. The three red box stands for the active site for these dioxygenases. Green box showed the miss of amino acids of Mra24 comparing to other dioxygenases.

### 3.9.3. *Streptosporangium amethystogenes* genomic gene library construction

The blast analysis of the whole gene cluster of muraminomicin showed that Mra24 was the only dioxygenase inside the gene cluster. One possibility was that the gene encoding the expected dioxygenase function was located elsewhere in the chromosome. To probe this theory, a *Streptosporangium amethystogenes* genomic library was constructed using pJAZZ-OK vector. The recombinant DNA was transformed into *E.coli* Bigeasy TSA cells, and primers were to amplify dioxygenase-encoding genes from genomic DNA. The expected 520-kb amplified fragment was obtained and labeled with DIG and used to screen the cosmid library. Following colony hybridization and southern blot analysis, four positive colonies were identified and selected for sequencing. Unfortunately, none of the four colonies showed the right gene sequences for a dioxygenase. Thus, we opted to focus on the development of a genetic system within the producing strain to ascertain the significance of individual *orfs* in muraminomicin biosynthesis.

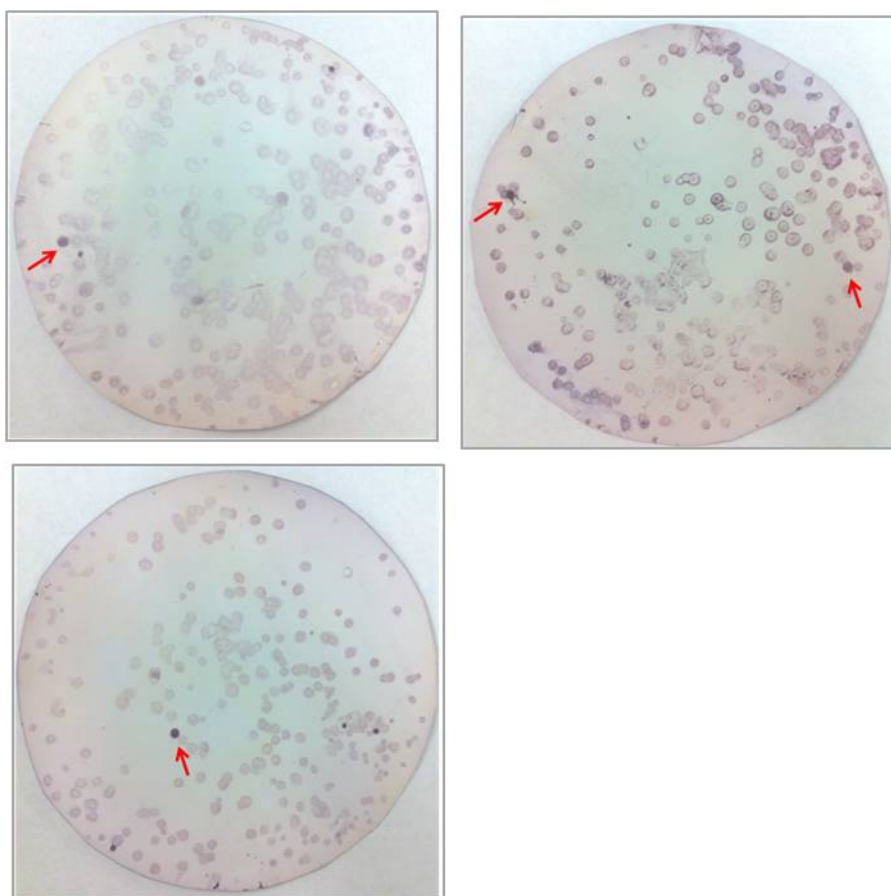


**Figure 3.26.** Colony Hybridization of *Streptosporangiummethystogenes* genomic gene library using dioxygenase gene probes. Four positive colonies were found after hybridization.

### 3.10. Development of a genetic system for *in vivo* muraminomicin studies

We have successfully characterized two enzymes - Mra20 and Mra23 - involved in the assembly of the 5-amino-2,5-dideoxyribofuranoside. As for three other enzymes, their activity and functionality are still unknown – despite the ability to obtain soluble protein. The results suggested Mra20 and Mra23 played a critical role in the identity of the aminoribosyl appendage of muraminomicin, yet several questions remained. We therefore attempted to develop a robust genetic system within the muraminomicin producing strains as a strategy to further delineate muraminomicin biosynthesis. It is expected that a genetic system will (i) reconfirm the reactions catalyzed by enzymes *in vitro*, (ii) establish an essential role for individual *orfs* in muraminomicin

biosynthesis, (iii) verify the identity of the muraminomicin gene cluster, (iv) provide a platform to rationally design and develop muraminomicin analogues. To carry out this strategy, the following procedures were conducted.

First, we explored different growth conditions for muraminomicin strain. Unlike *Streptomyces*, little information is available on the growth conditions for the *Streptosporangium* genus. The limited literature suggest optimal growth may require oatmeal, metal iron and some other nutritional factors [133][134]. Thus, various culture media were tested to obtain the best growth and sporulation conditions for the muraminomicin strain (**Table 9**). The results suggest the best condition for *Streptosporangium* growth was MS medium plus oatmeal, the other medium (ISP2, R2YE, etc) were not as efficient for attaining a dense culture (**Fig 3.27**). Furthermore, the best condition for sporulation was also the oatmeal agar medium, with or without metals supplemented (**Table 9**). This growth condition is now being used with the goal of developing a genetic system.

**Table 9.** Different culture conditions for *Streptosporangium* sp. SNAK 60709.

Strain	Medium	Condition
<b>Growth</b>	MS + Oatmeal	++++ (best)
	MS, M <sub>2</sub> CaO	+++
	ISP2, T-12	++
	R2YE, ISP4, Yeast Starch	+
	R5 medium	-
<b>Sporulation</b>	Oatmeal, Oatmeal + Metal	++++ (best)
	Other medium	+ or -



**Figure 3.27.** *Streptosporangium* sp. SANK 60709strain.

We initially targeted the inactivation of *mra20* gene of *Streptosporangium* sp. using a double-crossover PCR targeting system. Although many conditions were attempted with this strain, a successful mutant strain was not attainable. Thus, the genetic system for *in vivo* muraminomicin studies is still under investigation.

### 3.11. Conclusion

The biosynthetic gene cluster for muraminomicin has been identified. Two enzymes involved in the assembly of the aminoribosyl moiety of muraminomicin have been functionally assigned: Mra20 that catalyzes phosphorolysis to initiate “salvage” of the aminoribose and Mra23 that activates this sugar for subsequent ribosyltransfer. The three other enzymes are still under investigation. The established specificity of Mra20 and Mra23 explains at least in part the incorporation of a 2-deoxy and 5-amino-5-deoxy sugar, respectively, into muraminomicin. The results now set the stage to explore both upstream events, such as the unclear mechanism of 5'-aldehyde formation, and the downstream event of ribosylation. Additionally, the uncovering of the genetic locus for muraminomicin biosynthetic locus provides further information for defining a complete biosynthetic mechanism for lipopeptidyl nucleoside antibiotics.

## Chapter four: Summary

MraY (translocase I), one of the key enzymes involved in peptidoglycan cell wall biosynthesis, is an appealing target for discovering novel bioactive natural products for clinical use. Lipopeptidyl nucleoside antibiotics, inhibitors of MraY, have been recently discovered that have excellent anti Gram-positive bacteria activity. The prominent feature of this family is they all comprise an unusual sugar appendage, a key component for their antibacterial action. Based upon the bioinformatic analysis of A-90289 biosynthetic gene cluster, the biosynthetic pathway for aminoribosyl unit incorporation was firstly proposed and then confirmed by *in vitro* enzyme characterization. Five enzymes participated in the assembly of the sugar moiety and a distinct ribosylation pathway was identified. Uridine-5'-monophosphate was uncovered as the precursor for using sequential catalysis by a dioxygenase, aminotransferase, phosphorylase, nucleotidyltransferase and glycosyltransferase. This distinctive biosynthetic pathway was further confirmed by studies of the biosynthesis of muraminomicin, whose structure is similar to A-90289. Unlike A-90289, however, muraminomicin has a unique 2'-deoxy sugar component. The biosynthetic gene cluster was identified and analyzed by bioinformatics. Two key enzymes, a phosphorylase and a nucleotidyltransferase, were characterized *in vitro* and exhibited highly similar functionality as the homologous enzymes from A-90289. The cumulative results in A-90289 and muraminomicin provide valuable insight into investigating and discovering other lipopeptidyl nucleoside antibiotics and the preparation of their analogues by combinatorial biosynthetic strategies.

## Bibliography

1. Harvey A (2000) Strategies for discovering drugs from previously unexplored natural products. *Drug Discov Today* 5: 294-300.
2. Tulp M, Bohlin L (2002) Functional versus chemical diversity: is biodiversity important for drug discovery? *Trends Pharmacol Sci* 23: 225-231.
3. Walsh CT, Fischbach MA (2010) Natural products version 2.0: connecting genes to molecules. *J Am Chem Soc* 132: 2469-2493.
4. Wender PA, Miller BL (2009) Synthesis at the molecular frontier. *Nature* 460: 197-201.
5. Davies HM (2009) Organic chemistry: Synthetic lessons from nature. *Nature* 459: 786-787.
6. Li JW, Vederas JC (2009) Drug discovery and natural products: end of an era or an endless frontier? *Science* 325: 161-165.
7. Inoki K, Corradetti MN, Guan KL (2005) Dysregulation of the TSC-mTOR pathway in human disease. *Nat Genet* 37: 19-24.
8. Lamb J, Crawford ED, Peck D, Modell JW, Blat IC, et al. (2006) The Connectivity Map: using gene-expression signatures to connect small molecules, genes, and disease. *Science* 313: 1929-1935.
9. Watve MG, Tickoo R, Jog MM, Bhole BD (2001) How many antibiotics are produced by the genus *Streptomyces*? *Arch Microbiol* 176: 386-390.
10. Coppin RJ, Wicke DM, Little PS (2005) Managing nocturnal leg cramps--calf-stretching exercises and cessation of quinine treatment: a factorial randomised controlled trial. *Br J Gen Pract* 55: 186-191.
11. Baltz RH (2006) Marcel Faber Roundtable: is our antibiotic pipeline unproductive because of starvation, constipation or lack of inspiration? *J Ind Microbiol Biotechnol* 33: 507-513.
12. Newman DJ, Cragg GM (2012) Natural products as sources of new drugs over the 30 years from 1981 to 2010. *J Nat Prod* 75: 311-335.
13. Walsh C (2003) Where will new antibiotics come from? *Nat Rev Microbiol* 1: 65-70.
14. Bancroft EA (2007) Antimicrobial resistance: it's not just for hospitals. *JAMA* 298: 1803-1804.
15. Spellberg B, Blaser M, Guidos RJ, Boucher HW, Bradley JS, et al. (2011) Combating antimicrobial resistance: policy recommendations to save lives. *Clin Infect Dis* 52 Suppl 5: S397-428.
16. [www.cddep.org](http://www.cddep.org)
17. Tuberculosis global facts. World Health Organization. 2010/2011, [http://www.who.int/tb/publications/2010/factsheet\\_tb\\_2010.pdf](http://www.who.int/tb/publications/2010/factsheet_tb_2010.pdf).
18. Butler MS, Cooper MA (2011) Antibiotics in the clinical pipeline in 2011. *J Antibiot (Tokyo)* 64: 413-425.
19. Fischbach MA, Walsh CT (2009) Antibiotics for emerging pathogens. *Science* 325: 1089-1093.
20. Walsh, C.T. Antibiotics: Actions, Origins, Resistance. (ASM Press, Washington DC, USA, 2003)



21. Bugg TD, Walsh CT (1992) Intracellular steps of bacterial cell wall peptidoglycan biosynthesis: enzymology, antibiotics, and antibiotic resistance. *Nat Prod Rep* 9: 199-215.
22. Van Heijenoort J (2001) Recent advances in the formation of the bacterial peptidoglycan monomer unit. *Nat Prod Rep* 18: 503-519.
23. T. D. H. Bugg (1999) *Comprehensive Natural Products Chemistry*. ed. M. Pinto, Elsevier Science Ltd, Oxford, vol. 3, pp. 241–294.
24. Park JT, Johnson MJ (1949) Accumulation of labile phosphate in *Staphylococcus aureus* grown in the presence of penicillin. *J Biol Chem* 179: 585-592.
25. Kimura K, Bugg TD (2003) Recent advances in antimicrobial nucleoside antibiotics targeting cell wall biosynthesis. *Nat Prod Rep* 20: 252-273.
26. Winn M, Goss RJ, Kimura K, Bugg TD (2010) Antimicrobial nucleoside antibiotics targeting cell wall assembly: recent advances in structure-function studies and nucleoside biosynthesis. *Nat Prod Rep* 27: 279-304.
27. Lovering AL, Safadi SS, Strynadka NC (2012) Structural perspective of peptidoglycan biosynthesis and assembly. *Annu Rev Biochem* 81: 451-478.
28. T. D. H. Bugg, *Comprehensive Natural Products Chemistry*, ed. M. Pinto, Elsevier Science Ltd, Oxford, 1999, vol. 3, pp. 241–294.
29. Bouhss A, Trunkfield AE, Bugg TD, Mengin-Lecreulx D (2008) The biosynthesis of peptidoglycan lipid-linked intermediates. *FEMS Microbiol Rev* 32: 208-233.
30. Sauvage E, Kerff F, Terrak M, Ayala JA, Charlier P (2008) The penicillin-binding proteins: structure and role in peptidoglycan biosynthesis. *FEMS Microbiol Rev* 32: 234-258.
31. Kahne D, Leimkuhler C, Lu W, Walsh C (2005) Glycopeptide and lipoglycopeptide antibiotics. *Chem Rev* 105: 425-448.
32. Dini C (2005) MraY Inhibitors as Novel Antibacterial Agents. *Curr Top Med Chem* 5: 1221-1236.
33. Ikeda M, Wachi M, Jung HK, Ishino F, Matsushashi M (1991) The *Escherichia coli* mraY gene encoding UDP-N-acetylmuramoyl-pentapeptide: undecaprenyl-phosphate phospho-N-acetylmuramoyl-pentapeptide transferase. *J Bacteriol* 173: 1021-1026.
34. Bugg TD, Brandish PE (1994) From peptidoglycan to glycoproteins: common features of lipid-linked oligosaccharide biosynthesis. *FEMS Microbiol Lett* 119: 255-262.
35. Price NP, Momany FA (2005) Modeling bacterial UDP-HexNAc: polyprenol-P HexNAc-1-P transferases. *Glycobiology* 15: 29R-42R.
36. Pless DD, Neuhaus FC (1973) Initial membrane reaction in peptidoglycan synthesis. Lipid dependence of phospho-n-acetylmuramyl-pentapeptide translocase (exchange reaction). *J Biol Chem* 248: 1568-1576.

37. Struve WG, Sinha RK, Neuhaus FC (1966) On the initial stage in peptidoglycan synthesis. Phospho-N-acetylmuramyl-pentapeptide translocase (uridine monophosphate). *Biochemistry* 5: 82-93.
38. Boyle DS, Donachie WD (1998) *mraY* is an essential gene for cell growth in *Escherichia coli*. *J Bacteriol* 180: 6429-6432.
39. Thanassi JA, Hartman-Neumann SL, Dougherty TJ, Dougherty BA, Pucci MJ (2002) Identification of 113 conserved essential genes using a high-throughput gene disruption system in *Streptococcus pneumoniae*. *Nucleic Acids Res* 30: 3152-3162.
40. Bouhss A, Mengin-Lecreulx D, Le Beller D, Van Heijenoort J (1999) Topological analysis of the *MraY* protein catalysing the first membrane step of peptidoglycan synthesis. *Mol Microbiol* 34: 576-585.
41. Lloyd AJ, Brandish PE, Gilbey AM, Bugg TD (2004) Phospho-N-acetyl-muramyl-pentapeptide translocase from *Escherichia coli*: catalytic role of conserved aspartic acid residues. *J Bacteriol* 186: 1747-1757.
42. Muramatsu Y, Ishii MM, Inukai M (2003) Studies on novel bacterial translocase I inhibitors, A-500359s. II. Biological activities of A-500359 A, C, D and G. *J Antibiot (Tokyo)* 56: 253-258.
43. Al-Dabbagh B, Henry X, El Ghachi M, Auger G, Blanot D, et al. (2008) Active site mapping of *MraY*, a member of the polyprenyl-phosphate N-acetylhexosamine 1-phosphate transferase superfamily, catalyzing the first membrane step of peptidoglycan biosynthesis. *Biochemistry* 47: 8919-8928.
44. Heydanek MG, Jr., Struve WG, Neuhaus FC (1969) On the initial stage in peptidoglycan synthesis. 3. Kinetics and uncoupling of phospho-N-acetylmuramyl-pentapeptide translocase (uridine 5'-phosphate). *Biochemistry* 8: 1214-1221.
45. Tanaka S, Clemons WM, Jr. (2012) Minimal requirements for inhibition of *MraY* by lysis protein E from bacteriophage *PhiX174*. *Mol Microbiol* 85: 975-985.
46. Zheng Y, Struck DK, Bernhardt TG, Young R (2008) Genetic analysis of *MraY* inhibition by the *phiX174* protein E. *Genetics* 180: 1459-1466.
47. Zheng Y, Struck DK, Young R (2009) Purification and functional characterization of *phiX174* lysis protein E. *Biochemistry* 48: 4999-5006.
48. Tanaka H, Oiwa R, Matsukura S, Omura S (1979) Amphomycin inhibits phospho-N-acetylmuramyl-pentapeptide translocase in peptidoglycan synthesis of *Bacillus*. *Biochem Biophys Res Commun* 86: 902-908.
49. Banerjee DK (1989) Amphomycin inhibits mannosylphosphoryldolichol synthesis by forming a complex with dolichylmonophosphate. *J Biol Chem* 264: 2024-2028.
50. Vertesy L, Ehlers E, Kogler H, Kurz M, Meiwes J, et al. (2000) Friulimicins: novel lipopeptide antibiotics with peptidoglycan synthesis inhibiting activity from *Actinoplanes friuliensis* sp. nov. II. Isolation and structural

- characterization. *J Antibiot (Tokyo)* 53: 816-827.
51. Kong F, Carter GT (2003) Structure determination of glycinocins A to D, further evidence for the cyclic structure of the amphomycin antibiotics. *J Antibiot (Tokyo)* 56: 557-564.
  52. Kang MS, Spencer JP, Elbein AD (1978) Amphomycin inhibits the incorporation of mannose and GlcNAc into lipid-linked saccharides by aorta extracts. *Biochem Biophys Res Commun* 82: 568-574.
  53. Kang MS, Spencer JP, Elbein AD (1978) Amphomycin inhibition of mannose and GlcNAc incorporation into lipid-linked saccharides. *J Biol Chem* 253: 8860-8866.
  54. Brandish PE, Kimura KI, Inukai M, Southgate R, Lonsdale JT, et al. (1996) Modes of action of tunicamycin, liposidomycin B, and mureidomycin A: inhibition of phospho-N-acetylmuramyl-pentapeptide translocase from *Escherichia coli*. *Antimicrob Agents Chemother* 40: 1640-1644.
  55. Brandish PE, Burnham MK, Lonsdale JT, Southgate R, Inukai M, et al. (1996) Slow binding inhibition of phospho-N-acetylmuramyl-pentapeptide-translocase (*Escherichia coli*) by mureidomycin A. *J Biol Chem* 271: 7609-7614.
  56. Funabashi M, Baba S, Nonaka K, Hosobuchi M, Fujita Y, et al. (2010) The biosynthesis of liposidomycin-like A-90289 antibiotics featuring a new type of sulfotransferase. *Chembiochem* 11: 184-190.
  57. Igarashi M, Takahashi Y, Shitara T, Nakamura H, Naganawa H, et al. (2005) Caprazamycins, novel lipo-nucleoside antibiotics, from *Streptomyces* sp. II. Structure elucidation of caprazamycins. *J Antibiot (Tokyo)* 58: 327-337.
  58. Ochi, K.; Ezaki, M.; Iwani, M.; Komori, T.; Kohsaka, M. Eur. Patent 333177 A2, 1989.
  59. Igarashi, M.; Takahashi, Y.; Shitara, T.; Nakamura, H.; Naganawa, H.; Miyake, T.; Akamatsu, Y. *J. Antibiot.* 2005, 58, 327-337.
  60. McDonald LA, Barbieri LR, Carter GT, Lenoy E, Lotvin J, et al. (2002) Structures of the muraymycins, novel peptidoglycan biosynthesis inhibitors. *J Am Chem Soc* 124: 10260-10261.
  61. Hirano S, Ichikawa S, Matsuda A (2008) Structure-activity relationship of truncated analogs of caprazamycins as potential anti-tuberculosis agents. *Bioorg Med Chem* 16: 5123-5133.
  62. Dini C, Didier-Laurent S, Drochon N, Feteanu S, Guillot JC, et al. (2002) Synthesis of sub-micromolar inhibitors of MraY by exploring the region originally occupied by the diazepanone ring in the liposidomycin structure. *Bioorg Med Chem Lett* 12: 1209-1213.
  63. Thibodeaux CJ, Melancon CE, 3rd, Liu HW (2008) Natural-product sugar biosynthesis and enzymatic glycodiversification. *Angew Chem Int Ed Engl* 47: 9814-9859.
  64. Blanchard S, Thorson JS (2006) Enzymatic tools for engineering natural product glycosylation. *Curr Opin Chem Biol* 10: 263-271.

65. Kren V, Martinkova L (2001) Glycosides in medicine: "The role of glycosidic residue in biological activity". *Curr Med Chem* 8: 1303-1328.
66. Kren V, Rezanka T (2008) Sweet antibiotics - the role of glycosidic residues in antibiotic and antitumor activity and their randomization. *FEMS Microbiol Rev* 32: 858-889.
67. Hubbard BK, Walsh CT (2003) Vancomycin assembly: nature's way. *Angew Chem Int Ed Engl* 42: 730-765.
68. J.P. Mackay, U Gerhard, D.A. Beauregard, R.A. Maplestone, D.H. Williams. (1994) Dissection of the Contributions toward Dimerization of Glycopeptide Antibiotics. *J. Am. Chem. Soc.* 116: 4573 – 4580.
69. U. Gerhard, J.P. Mackay, R.A. Maplestone, D.H. Williams. (1993) The role of the sugar and chlorine substituents in the dimerization of vancomycin antibiotics. *J. Am. Chem. Soc.* 115: 232-237.
70. Williams DH, Searle MS, Mackay JP, Gerhard U, Maplestone RA (1993) Toward an estimation of binding constants in aqueous solution: studies of associations of vancomycin group antibiotics. *Proc Natl Acad Sci U S A* 90: 1172-1178.
71. Williams DH (1996) The glycopeptide story--how to kill the deadly 'superbugs'. *Nat Prod Rep* 13: 469-477.
72. Stubbe J & Kozarich JW (1987) Mechanisms of DNA degradation. *Chem Rev* 87: 1107–1136
73. Magliozzo RS, Peisach J, Ciriolo MR (1989) Transfer RNA is cleaved by activated bleomycin. *Mol Pharmacol* 35: 428-432.
74. Hecht SM (1994) RNA degradation by bleomycin, a naturally occurring bioconjugate. *Bioconjug Chem* 5: 513-526.
75. Grdadolnik SG, Pristovsek P, Mierke DF (1998) Vancomycin: conformational consequences of the sugar substituent. *J Med Chem* 41: 2090-2099.
76. Natrajan A & Hecht SM (1993) Bleomycin: mechanism of polynucleotide recognition and oxidative degradation. *Molecular Aspects of Anticancer Drug–DNA Interactions* (Neidle S & Waring M, eds), pp. 197–242. MacMillan, London.
77. Thibodeaux CJ, Melancon CE, Liu HW (2007) Unusual sugar biosynthesis and natural product glycodiversification. *Nature* 446: 1008-1016.
78. Kudo F, Fujii T, Kinoshita S, Eguchi T (2007) Unique O-ribosylation in the biosynthesis of butirosin. *Bioorg Med Chem* 15: 4360-4368.
79. Mikusova K, Huang H, Yagi T, Holsters M, Vereecke D, et al. (2005) Decaprenylphosphoryl arabinofuranose, the donor of the D-arabinofuranosyl residues of mycobacterial arabinan, is formed via a two-step epimerization of decaprenylphosphoryl ribose. *J Bacteriol* 187: 8020-8025.
80. Jensen, K. F. *Metabolism of Nucleotides, Nucleosides and Nucleobases in Microorganisms*; Academic, London, UK, 1983; pp 1-25.
81. M. Ubukata, K. Isono, K. Kimura, C. C. Nelson, J. A. McCloskey, J. Am.

Chem. Soc. 1988, 110, pp4416–4417

82. Gust B, Eitel K, Tang X (2013) The biosynthesis of caprazamycins and related liponucleoside antibiotics: new insights. *Biol Chem* 394: 251-259.
83. Hirano S, Ichikawa S, Matsuda A (2008) Synthesis of caprazamycin analogues and their structure--activity relationship for antibacterial activity. *J Org Chem* 73: 569-577.
84. Fujita Y, Kizuka M, Funabashi M, Ogawa Y, Ishikawa T, et al. (2011) A-90289 A and B, new inhibitors of bacterial translocase I, produced by *Streptomyces* sp. SANK 60405. *J Antibiot (Tokyo)* 64: 495-501.
85. Kaysser L, Lutsch L, Siebenberg S, Wemakor E, Kammerer B, et al. (2009) Identification and manipulation of the caprazamycin gene cluster lead to new simplified liponucleoside antibiotics and give insights into the biosynthetic pathway. *J Biol Chem* 284: 14987-14996.
86. Cheng L, Chen W, Zhai L, Xu D, Huang T, et al. (2011) Identification of the gene cluster involved in muraymycin biosynthesis from *Streptomyces* sp. NRRL 30471. *Mol Biosyst* 7: 920-927.
87. Kaysser L, Siebenberg S, Kammerer B, Gust B (2010) Analysis of the liposidomycin gene cluster leads to the identification of new caprazamycin derivatives. *Chembiochem* 11: 191-196.
88. Yang Z, Chi X, Funabashi M, Baba S, Nonaka K, et al. (2011) Characterization of LipL as a non-heme, Fe(II)-dependent alpha-ketoglutarate:UMP dioxygenase that generates uridine-5'-aldehyde during A-90289 biosynthesis. *J Biol Chem* 286: 7885-7892.
89. Barnard-Britson S, Chi X, Nonaka K, Spork AP, Tibrewal N, et al. (2012) Amalgamation of nucleosides and amino acids in antibiotic biosynthesis: discovery of an L-threonine:uridine-5'-aldehyde transaldolase. *J Am Chem Soc* 134: 18514-18517.
90. Winans KA, Bertozzi CR (2002) An inhibitor of the human UDP-GlcNAc 4-epimerase identified from a uridine-based library: a strategy to inhibit O-linked glycosylation. *Chem Biol* 9: 113-129.
91. Hofman-Bang, N. Preparation of lithium azide. *Acta Chem. Scand.* 1957, 11, 581-582.
92. Tozzi MG, Camici M, Mascia L, Sgarrella F, Ipata PL (2006) Pentose phosphates in nucleoside interconversion and catabolism. *FEBS J* 273: 1089-1101.
93. Temmink OH, de Bruin M, Turksma AW, Cricca S, Laan AC, et al. (2007) Activity and substrate specificity of pyrimidine phosphorylases and their role in fluoropyrimidine sensitivity in colon cancer cell lines. *Int J Biochem Cell Biol* 39: 565-575.
94. El Kouni MH, el Kouni MM, Naguib FN (1993) Differences in activities and substrate specificity of human and murine pyrimidine nucleoside phosphorylases: implications for chemotherapy with 5-fluoropyrimidines. *Cancer Res* 53: 3687-3693.

95. Razzell WE, Khorana HG (1958) Purification and properties of a pyrimidine deoxyriboside phosphorylase from *Escherichia coli*. *Biochim Biophys Acta* 28: 562-566.
96. Leer JC, Hammer-Jespersen K, Schwartz M (1977) Uridine phosphorylase from *Escherichia coli*. Physical and chemical characterization. *Eur J Biochem* 75: 217-224.
97. Guyett P, Glushka J, Gu X, Bar-Peled M (2009) Real-time NMR monitoring of intermediates and labile products of the bifunctional enzyme UDP-apiose/UDP-xylose synthase. *Carbohydr Res* 344: 1072-1078.
98. Hove-Jensen B, McSorley FR, Zechel DL (2011) Physiological role of phnP-specified phosphoribosyl cyclic phosphodiesterase in catabolism of organophosphonic acids by the carbon-phosphorus lyase pathway. *J Am Chem Soc* 133: 3617-3624.
99. Simons SS, Jr., Johnson DF (1978) Reaction of o-phthalaldehyde and thiols with primary amines: fluorescence properties of 1-alkyl(and aryl)thio-2-alkylisoindoles. *Anal Biochem* 90: 705-725.
100. Krenitsky TA (1976) Uridine phosphorylase from *Escherichia coli*. Kinetic properties and mechanism. *Biochim Biophys Acta* 429: 352-358.
101. Toney, M. D. PLP-dependent enzymes, chemistry of. In Begley T (ed) *Wiley Encyclopedia of Chemical Biology*. Hoboken, New Jersey: John Wiley & Sons, Inc., 2009; Vol, 3, pp 731-735.
102. Schneider G, Kack H, Lindqvist Y (2000) The manifold of vitamin B6 dependent enzymes. *Structure* 8: R1-6.
103. Rackham EJ, Gruschow S, Ragab AE, Dickens S, Goss RJ (2010) Pacidamycin biosynthesis: identification and heterologous expression of the first uridyl peptide antibiotic gene cluster. *Chembiochem* 11: 1700-1709.
104. Zhang W, Ostash B, Walsh CT (2010) Identification of the biosynthetic gene cluster for the pacidamycin group of peptidyl nucleoside antibiotics. *Proc Natl Acad Sci U S A* 107: 16828-16833.
105. Zhang W, Ntai I, Bolla ML, Malcolmson SJ, Kahne D, et al. (2011) Nine enzymes are required for assembly of the pacidamycin group of peptidyl nucleoside antibiotics. *J Am Chem Soc* 133: 5240-5243.
106. Chapple CC, Glover JR, Ellis BE (1990) Purification and Characterization of Methionine:Glyoxylate Aminotransferase from *Brassica carinata* and *Brassica napus*. *Plant Physiol* 94: 1887-1896.
107. Yang J, Xu H, Zhang Y, Bai L, Deng Z, et al. (2011) Nucleotidylation of unsaturated carbasugar in validamycin biosynthesis. *Org Biomol Chem* 9: 438-449.
108. Billig T, Shepard EM, Ahlert J, Thorson JS (2002) On the origin of deoxypentoses: evidence to support a glucose progenitor in the biosynthesis of calicheamicin. *Chembiochem* 3: 1143-1146.
109. Hofmann C, Boll R, Heitmann B, Hauser G, Durr C, et al. (2005) Genes encoding enzymes responsible for biosynthesis of L-lyxose and

- attachment of eurenate during avilamycin biosynthesis. *Chem Biol* 12: 1137-1143.
110. Bar-Peled M, Griffith CL, Doering TL (2001) Functional cloning and characterization of a UDP- glucuronic acid decarboxylase: the pathogenic fungus *Cryptococcus neoformans* elucidates UDP-xylose synthesis. *Proc Natl Acad Sci U S A* 98: 12003-12008.
  111. Breazeale SD, Ribeiro AA, Raetz CR (2002) Oxidative decarboxylation of UDP-glucuronic acid in extracts of polymyxin-resistant *Escherichia coli*. Origin of lipid a species modified with 4-amino-4-deoxy-L-arabinose. *J Biol Chem* 277: 2886-2896.
  112. Van Lanen SG, Oh TJ, Liu W, Wendt-Pienkowski E, Shen B (2007) Characterization of the maduropeptin biosynthetic gene cluster from *Actinomadura madurae* ATCC 39144 supporting a unifying paradigm for enediyne biosynthesis. *J Am Chem Soc* 129: 13082-13094.
  113. Kotake T, Yamaguchi D, Ohzono H, Hojo S, Kaneko S, et al. (2004) UDP-sugar pyrophosphorylase with broad substrate specificity toward various monosaccharide 1-phosphates from pea sprouts. *J Biol Chem* 279: 45728-45736.
  114. Kotake T, Hojo S, Yamaguchi D, Aohara T, Konishi T, et al. (2007) Properties and physiological functions of UDP-sugar pyrophosphorylase in *Arabidopsis*. *Biosci Biotechnol Biochem* 71: 761-771.
  115. Damerow S, Lamerz AC, Haselhorst T, Fuhring J, Zarnovican P, et al. (2010) *Leishmania* UDP-sugar pyrophosphorylase: the missing link in galactose salvage? *J Biol Chem* 285: 878-887.
  116. Kim JS, Koh S, Shin HJ, Lee DS, Lee SY (1999) Biochemical characterization of a UDP-sugar pyrophosphorylase from *Thermus caldophilus* GK24. *Biotechnol Appl Biochem* 29 ( Pt 1): 11-17.
  117. Fu X, Albermann C, Jiang J, Liao J, Zhang C, et al. (2003) Antibiotic optimization via in vitro glycorandomization. *Nat Biotechnol* 21: 1467-1469.
  118. Jiang J, Biggins JB, Thorson JS (2001) Expanding the Pyrimidine Diphosphosugar Repertoire: The Chemoenzymatic Synthesis of Amino- and Acetamidoglucopyranosyl Derivatives This contribution was supported by the National Institutes of Health (GM58196 and CA84374), a Cancer Center Support Grant (CA-08748), and a grant from the Special Projects Committee of the Society of Memorial Sloan-Kettering Cancer Center. J.S.T. is an Alfred P. Sloan Research Fellow and a Rita Allen Foundation Scholar. *Angew Chem Int Ed Engl* 40: 1502-1505.
  119. Moretti R, Thorson JS (2007) Enhancing the latent nucleotide triphosphate flexibility of the glucose-1-phosphate thymidyltransferase RmlA. *J Biol Chem* 282: 16942-16947.
  120. Kudo F, Kawabe K, Kuriki H, Eguchi T, Kakinuma K (2005) A new family of glucose-1-phosphate/glucosamine-1-phosphate nucleotidyltransferase in the biosynthetic pathways for antibiotics. *J Am Chem Soc* 127:

1711-1718.

121. Mizanur RM, Zea CJ, Pohl NL (2004) Unusually broad substrate tolerance of a heat-stable archaeal sugar nucleotidyltransferase for the synthesis of sugar nucleotides. *J Am Chem Soc* 126: 15993-15998.
122. Timmons SC, Mosher RH, Knowles SA, Jakeman DL (2007) Exploiting nucleotidyltransferases to prepare sugar nucleotides. *Org Lett* 9: 857-860.
123. Y. Muramatsu, F. Yoko, A. Azusa, K. Masaaki, T. Toshio and M Shunichi, Patent WO 2004046368 (Sankyo Co., Ltd.), 2004.
124. Chi X, Pahari P, Nonaka K, Van Lanen SG (2011) Biosynthetic origin and mechanism of formation of the aminoribosyl moiety of peptidyl nucleoside antibiotics. *J Am Chem Soc* 133: 14452-14459.
125. M. Funabashi, S. Baba, W. Cai, S. Barnard-Britson, K. Nonaka, T. Takatsu, Z. Yang, M. Kizuka, M. Sunkara, A. J. Morris and S. G. Van Lanen, manuscript submitted.
126. Kieser, T., Bibb, M., Buttner, M. J., Chater, K. F., and Hoopwood, D. A. (2000) *Practical Streptomyces genetics* The John Innes Foundation, Norwich.
127. Godiska R, Mead D, Dhodda V, Wu C, Hochstein R, et al. (2010) Linear plasmid vector for cloning of repetitive or unstable sequences in *Escherichia coli*. *Nucleic Acids Res* 38: e88.
128. Gust, B.; Kieser, T.; Chater, K. PCR targeting system in *Streptomyces coelicolor* A3(2); John Innes Centre.
129. Noda Y, Yoda K, Takatsuki A, Yamasaki M (1992) TmrB protein, responsible for tunicamycin resistance of *Bacillus subtilis*, is a novel ATP-binding membrane protein. *J Bacteriol* 174: 4302-4307.
130. Pugmire MJ, Ealick SE (2002) Structural analyses reveal two distinct families of nucleoside phosphorylases. *Biochem J* 361: 1-25.
131. Sinha SC, Smith JL (2001) The PRT protein family. *Curr Opin Struct Biol* 11: 733-739.
132. Barton WA, Lesniak J, Biggins JB, Jeffrey PD, Jiang J, et al. (2001) Structure, mechanism and engineering of a nucleotidyltransferase as a first step toward glycorandomization. *Nat Struct Biol* 8: 545-551.
133. Oh YK, Speth JL, Nash CH. Protoplast fusion with *Streptosporangium viridogriseum*. *Dev. Ind. Microbiol.* 1980, 21, 219-226.
134. Mullins PH, Gurtler H, Wellington EM (1995) Selective recovery of *Streptosporangium fragile* from soil by indirect immunomagnetic capture. *Microbiology* 141 ( Pt 9): 2149-2156.



## Vita

### Educational institutions attended and degrees already awarded:

2004-2007	M.S	University of South China	Pharmacology
1999-2004	B.S (MD)	Binzhou Medical University	Medicine

### Professional positions held:

2009.8 - 2011.6 Teaching Assistant, College of Pharmacy, University of Kentucky

2007.7 - 2009.5 Research Scholar Fellow, College of Pharmacy, University of Kentucky

### Scholastic and professional honors:

2012	Graduate School Academic Year Fellowship, University of Kentucky
2005	Outstanding Graduate Award, University of South China, China

### Professional publications:

1. **Chi X**, Baba S, Tibrewal N, Funabashi M, Nonaka K and Van Lanen SG. The muraminomycin biosynthetic gene cluster and enzymatic formation of the 2-deoxyaminoribosyl appendage. *Med. Chem. Commun.*, 2013, 4(1):239-43. This article is part of the collection: New Talent.
2. Barnard-Britson S, **Chi X**, Nonaka K, Spork AP, Tibrewal N, Goswami A, Pahari P, Ducho C, Rohr J, Van Lanen SG. Amalgamation of Nucleosides and Amino Acids in Antibiotic Biosynthesis: Discovery of an L-Threonine: Uridine-5'-Aldehyde Transaldolase. *J Am Chem Soc.* 2012, 134(45):18514-7.
3. Zeng Y, Kulkarni A, Yang Z, Patil PB, Zhou W, **Chi X**, Van Lanen S, Chen S. Biosynthesis of albomycin  $\delta(2)$  provides a template for assembling siderophore and aminoacyl-tRNA synthetase inhibitor conjugates. *ACS Chem Biol.* 2012, 7(9):1565-75.
4. **Chi X**, Pahari P, Nonaka K, Van Lanen SG. Biosynthetic origin and mechanism of formation of the aminoribosyl moiety of peptidyl nucleoside antibiotics. *J Am Chem Soc.* 2011, 133(36):14452-9.
5. Yang Z, **Chi X**, Funabashi M, Baba S, Nonaka K, Pahari P, Unrine J, Jacobsen JM, Elliott GI, Rohr J, Van Lanen SG. Characterization of LipL as a non-heme, Fe(II)-dependent  $\alpha$ -ketoglutarate: UMP dioxygenase that generates uridine-5'-aldehyde during A-90289 biosynthesis. *J Biol Chem.* 2011, 286(10):7885-92.
6. Funabashi M, Yang Z, Nonaka K, Hosobuchi M, Fujita Y, Shibata T, **Chi X**, Van Lanen SG. An ATP-independent strategy for amide bond formation in antibiotic biosynthesis. *Nat Chem Biol.* 2010, 6(8):581-6.

7. Tai HH, **Chi X**, Tong M. Regulation of 15-hydroxyprostaglandin dehydrogenase (15-PGDH) by non-steroidal anti-inflammatory drugs (NSAIDs). *Prostaglandins Other Lipid Mediat.* 2011, 96(1-4):37-40.
8. **Chi X**, Tai HH. Interleukin-4 up-regulates 15-hydroxyprostaglandin dehydrogenase (15-PGDH) in human lung cancer cells. *Exp Cell Res.* 2010, 316(14):2251-9.
9. **Chi X**, Freeman BM, Tong M, Zhao Y, Tai HH. 15-Hydroxyprostaglandin dehydrogenase (15-PGDH) is up-regulated by flurbiprofen and other non-steroidal anti-inflammatory drugs in human colon cancer HT29 cells. *Arch Biochem Biophys.* 2009, 487(2):139-45.

**Typed name of student on final copy:**

Xiuling Chi